Synthesis and Characterization of Amphiphilic Polyamine-based Polymers for Silica Precipitation

Von der Fakultät für Lebenswissenschaften

der Technischen Universität Carolo-Wilhelmina

zu Braunschweig

zur Erlangung des Grades eines

Doktors der Naturwissenschaften

(Dr. rer. nat.)

genehmigte

Dissertation

von Salvador Navarro Navarro
aus Lorca / Spanien

Synthesis and Characterization of Amphiphilic Polyamine-based Polymers for Silica Precipitation

Von der Fakultät für Lebenswissenschaften

der Technischen Universität Carolo-Wilhelmina

zu Braunschweig

zur Erlangung des Grades eines

Doktors der Naturwissenschaften

(Dr. rer. nat.)

genehmigte

Dissertation

von Salvador Navarro Navarro
aus Lorca / Spanien

1. Referentin oder Referent:	Prof. Dr. Henning Menzel
2. Referentin oder Referent:	Prof. Dr. Andreas Taubert
eingereicht am:	18. 12. 2009
mündliche Prüfung (Disputation) am:	23. 03. 2010

Druckjahr 2010

Vorveröffentlichungen der Dissertation

Teilergebnisse aus dieser Arbeit wurden mit Genehmigung der Fakultät für Lebenswissenschaften, vertreten durch den Mentor der Arbeit, in folgenden Beiträgen vorab veröffentlicht:

Publikationen

Navarro, S., Shkilnyy, A., Tiersch B., Taubert A., Menzel H., Preparation, characterization and thermal gelation of amphiphilic alkyl-poly(ethyleneimine). Langmuir 25 (18):10558-10566 (2009).

Tagungsbeiträge

Navarro. S., Menzel, H.: From biomineralization to tailored synthesis: nitrogen-containing polymers for the production of porous silica. (Poster) 3. Berichtskolloquium des Schwerpunktprogramms 1117 der Deutschen Forschungs-Gemeinschaft „Prinzipien der Biomineralisation“, Bad Honnef (2006).

Navarro, S., Menzel, H.: Polyamine-based amphiphilic polymers as template for the production of porous silica. (Poster) 10th International conference of the European Ceramic Society, Berlin (2007).

Navarro, S., Cornelius, F., Menzel, H.: Biomimetic model polymers as template for the synthesis of nanostructured silica. (Poster) European Congress on Advanced Materials and Processes, Nürnberg (2007).

Navarro, S., Menzel, H.: Biomimetic model polymers as template for the synthesis of nanostructured silica. (Vortrag) 4. Jungchemikertag des Jungchemikerforum der TU Braunschweig, Braunschweig (2007).

A mi abuelito Ginés

«Great works are performed, not by strength, but by perseverance.»

Samuel Johnson

«Science is a way of thinking much more than it is a body of knowledge.»

Carl Sagan

Acknowledgements

Without the support of the following people I could not have finished this thesis successfully. For this reason, I would like to express my gratitude to all of them.

It is my great pleasure to thank Prof. Dr. Henning Menzel for giving me the opportunity to do research in this interesting field under his supervision. His immense guidance always motivated me to work hard towards my project. I thank him for his outstanding ideas, discussion, and optimistic approach for my thesis work.

I thank Ass. Prof. Dr. Andreas Taubert for his excellent co-operation and fruitful discussions to publish my results. He gave me valuable ideas for the development of some crucial aspects of this work. In addition, he introduced me to several relevant experts who helped me to solve the research problems in an easier way. I would like also to thank him for his great support. In line with this fruitful collaboration, I thank Ronald Göbbel and Dr. Andriy Shkiny, current and former members, respectively, of the Taubert´s research group for their time, help and attention during my stays in Potsdam. Just as well, I´d also like to thank Dr. Brigitte Tiersch for the obtention of very nice Cryo-SEM images and Dr. Jens Weber from the Max-Planck Institute in Golm for his advice and suggestions when performing the modeling of the SAXS data. In the same way, and also within the framework of this collaboration with Ass. Prof. Dr. Andreas Taubert I am very grateful to some people from other universities. Among those, Prof. Dr. Wolfgang Meier and Dr. Corinne Vebert, both from the University of Basel, are gratefully acknowledged for allowing me to carry out DLS measurements and for taking care of me during my stay in Basel, respectively. Likewise, I´d also like to thank Prof. Dr. Alexander Böker, Dr. Markus Drechsler and Nathalie Mougin, all from the university of Bayreuth, for their help, efforts, and advice to get nice Cryo-TEM images.

I am also thankful to Prof. Dr. Peter Behrens from the university of Hannover for his excellent co-operation at the start of my research. The constructive discussions during the seminars within the graduate school “New materials with tailored properties” as well as those in line with the frequent biomineralization meetings in Hannover and Braunschweig have provided novel and valuable ideas for the development of this thesis. I also want to thank him for the access to some devices of his labs at the university of Hannover. On this regard, I am very grateful to his former co-worker Dr. Falk Heinroth for the performance of the hydrothermal synthesis experiments.

A lot of people which belong to the staff of the technical chemistry department from the university of Braunschweig must also be acknowledged. On this respect, I am especially grateful to Ms. Anita Scherbarth for her patience and effort in the obtention of very nice SEM-images. I thank Dr. Adrian Dobre for his time and attention in the performance of the tensiometry measurements. I thank Ms. Gabi Schirmer and Ms. Christa Vogel for their strong support and caring with bureaucratic work. They had really lots of patience and kindness.

Some of the results shown in this work have been achieved by students who have performed their practical course under my supervision. Therefore, I thank Tareek Cheema and Nils Harmeling for their active co-operation.

Almost last, but not at all least, I´d like to thank all member of the Menzel´s research group for their support, nice working atmosphere and for the unforgettable moments that I have spent with them. For her valuable ideas and constructive criticism in the revision of this work, I am strongly thankful to Dr. Wibke Dempwolf. I thank Dr. Sven Pohle and Sajjad Waraich for their patience, invaluable contributions and tireless enumerable attempts in the performance of DSC measurements. For their timely help to solve my computer problems I thank Uwe Mundil, Ansgar Niehoff and Andreas Bertz. I´d like to thank my office colleagues Dr. Frauke Cornelius, Cornelia Pfaffenroth and Aromita Sen, for their joy, patience, willingness and for the nice work atmosphere. I am grateful to my last office colleague, Dr. Steffen Harling, for his technical and emotional support during the difficult time of writing this thesis. I thank him especially for the time and effort that he has dedicated in teaching me new german words and expressions via the series “Word of the day”. I thank my colleages Dr. Simone Jurjevic and Maria Stern for their co-operation to organize everything in the lab that we shared. To my former neighbor Dr. Olaf Helmecke and to Dr. Sven Pohle I am very grateful for all the football evenings and football matches we have shared these years. I really enjoyed the time I have spent with them in those events and I am very happy to have cooked for them so often. I also thank all other colleagues that have shared this time in the Menzel´s research group with me especially to Dr. Nina Adden, Corinna Lorenz, Magdalena Sluzniak, Bianca Tiedemann, Christian Bork, and El Badawy Kamoun.

I´d like to thank the Science and Culture ministerium of Lower Saxony for the finantial support by means of a Georg Christoph Lichtenberg felowship. I am extremely grateful and proud to have participated in the graduated school “New Materials with tailored properties” of the center for solid state chemistry and new materials (ZFM). On this regard, I thank Prof. Dr. Josef-Christian Buhl for his kindness and help.

Finally, I express my gratitude to my family members, especially to my parents Francisco and Juana, my brother Ginés and my granny Maria for their strong support, motivation and encouragement. They have always inspired me to work hard and to keep on facing this huge challenge, especially in the critical situations.

Table of Contents

Symbols and Abbreviations

a	Radius
ATRP	Atom transfer radical polymerization
α	Degree of hydrolysis
BN	Benzonitrile
β	Experimental geometry factor
c	Concentration
C12E5	Pentaethylene glycol monodecyl ether
c_G	Gelation concentration
CMC	Critical micelle concentration
CROP	Cationic ring-opening polymerization
CRP	Controlled polymerization techniques
Cryo-SEM	Cryogenic scanning electron microscopy
Cryo-TEM	Cryogenic transmission electron microscopy
CTAB	Cetyl trimethyl ammonium bromide
d	Pore volume
d_s	Structural parameter
D	Fractal dimension
D_0	Translational diffusion coefficient
DLS	Dynamic light scattering
D_m	Mutual diffusion coefficient
D_{max}	Maximum dimension
DMF	N,N’-dimethylformamide
DNA	Desoxyribonucleic acid
DSC	Differential Scanning Calorimetry
δ	Bending
ESR	Electron spin resonance
EtOH	Ethanol
EWC	Equilibrium Water Content
FTIR	Fourier Transform Infrared spectroscopy

φ	Volume fraction
$g_1(t)$	Electric field time correlation function
$g_2(\tau)$	Normalized time autocorrelation function
G1PAMAM	Polyamidoamine dendrimer G1
$G(R_g)$	Size distribution
γ	Surface tension
$\gamma(r)$	Correlation function
$\gamma_0(r)$	Function
Γ	Gamma function
Γ	Decay rate
Γ_1	Average decay rate
Γ_2	Variance
HLB	hydrophilic-lipophilic balance
HMWSP	hydrophobically Modified Water Soluble Polymers
η_A	Solvent viscosity
$[I]_0$	Concentration of initiator
$I(q)$	Normalized SAXS intensity
IUPAC	International Union of pure and applied chemistry
κ_b	Boltzmann´s constant
κ_D	Diffusion constant
k_w	ionic product of water
λ	Wavelength
LCPA	Long-chain polyamine
LCT	Liquid crystal templating
M	mass
M	Monomer
$[M]_0$	Initial amount of added monomer
MeOH	Methanol
MeOZI	2-Methyl-5,6-dihydro-4H-1,3-oxazine
MeOZO	2-Methyl-2-oxazoline
M_w	Weight average molecular weight
n	Refractive index

nat-Sil	Native protein of silaffin
N	Number of particles per unit volume
NH^+	Total amount of protonated nitrogen atoms
NMP	Nitroxide-mediated polymerization
NMR	Nuclear Magnetic Resonance
N_{tot}	Total amount of nitrogen atoms
ν	Stretching
OcdOTs	Octadecyl tosylate
OPM	Optical Polarization Microscopy
OZI	Oxazine
p	Pressure
p(r)	Distance distribution function
P	Polydispersity
PAEI	Poly(N-(acetyl)-ethyleneimine)
PAH	Poly(allylamine hydrochloride)
PAPI	Poly(N-(acetyl)-propyleneimine)
PBD	Poly(butadiene)
PDI	Polydispersity index
PEG	Poly(ethylene glycol)
PEI	Poly(ethyleneimine)
PEO	Poly(ethylene oxide)
PFG-SE NMR	Pulse field gradient spin-echo nuclear magnetic resonance
PFPI	Poly(N-(formyl)-propyleneimine)
PI	Poly(isoprene)
PLL	Poly(L-Lysine)
PMEI	Poly(N-(methyl)-ethyleneimine)
PMMA	Poly(methyl methacrylate)
PMPI	Poly(N-(methyl)-propyleneimine)
P_n	Degree of polymerization
PPG	Poly(propylene glycol)
PPI	Poly(propyleneimine)
PPO	Poly(propylene oxide)

P(q)	Particle scattering function
PVP	Poly(N-vinylpyrrolidone)
q	Scattering vector
q_m	Scattering vector at maximum intensity
θ	Scattering angle
r	Vector
R	Spherical radius
RAFT	Reversible addition fragmentation transfer
R_{core}	Radius of the core
R_{eff}	Hard-sphere radius
R_g	Gyration radius
$<R_g>_G$	Average of the gyration radius
R_h	Hydrodynamic radius
R_{shell}	Overall radius of core/shell sphere
ρ	Ratio of shell/core electron densities
ρ_0	Constant density of matrix
$\rho(r)$	Electron density function
s	Unit vector
S	Solvent
S	Surface area
SANS	Small angle neutron scattering
SAXS	Small angle X-ray scattering
SDS	Sodium dodecyl sulfate
SDV	Silica deposition vesicle
SEC	Size exclusion chromatography
SEM	Scanning electron microscopy
SIT	Silicon transporters
SLS	Static light scattering
S_N2	Bimolecular nucleophilic substitution
S(q)	Orientation average effective structure function
STV	Silicon transport vesicles
σ	Relative standard deviation of particle radius

t	Time
t	Twisting
T	Temperature
TEOS	Tetraethylorthosilane
T_g	Glass transition temperature
THF	Tetrahydrofuran
T_{kr}	Krafft temperature
TMAOH	Tetramethyl ammonium hydroxide
TMOS	Tetramethylorthosilane
TMS	Tetramethylsilane
τ	Delay time
v	Particle volume
$\langle v(r) \rangle$	Orientational average
V	Volume
w	weight percentage
ω	Wagging
ω	Weight percentage
ξ	Fractal size parameter

1 Introduction and Aim of this Work

Silica (SiO_2) has become increasingly important within the last decades in chemical, pharmaceutical, and nanotechnological processes. It is produced as a crystalline microporous and mesoporous material (e.g. zeolites used in washing powder, or as molecular sieves) or as amorphous material (e.g., used in car tires) covering a wide range of industrial applications as summarized in Table 1.1.

Table 1.1. Examples for fields of application where silica is used[1].

Silica type	Application	Examples
Zeolites	Catalytic hydrocracking	Oil industries
	Catalytic dewaxing	Improvement of cold flow properties
	Ion-exchange	Washing powders
	(trans)Alkylation of aromatics	Plastic industries
	Isomerization	Plastic industries, fine chemistry
	Drying	Gas industries, water-sensitive products
Amorphous silica	Abrasives	Toothpaste, cleaners
	Absorbents	Flavor (food), detergents (washing powders, soaps, toothpaste), ink (in paper industries)
	Catalysts carrier	Rubber industries, fine chemistry
	Whiteners and/or anti-corrosion	Paints, paper industry, cosmetics
	Fillers	Cosmetics, pharmaceuticals, food
	Clarification and purification	Beer, wine and juice production, food
	Drying	Gasses, flowers, water-sensitive products
	Anti-foam	Pharmaceuticals, food

Nowadays, the industrial production process of those silica-based materials proceeds under high temperature and pressure conditions. Generally, harsh reagents are included to control the pH and surfactants are used as structure directing agents in silica precipitation. From a process technological perspective, silica production under ambient conditions will lead to less cost-demanding production routes and will also be friendlier from an environmental point of view. Because of the increasing demand of well-defined silica structures and novel silica-based materials, new methods have to be developed. Thus, the challenge is to produce a higher number of materials with a complex three-dimensional structure in a cheap and safe way. The novel silica produced under this approach will provide a broad range of applications, especially those in optical sensors, in chemical and biodetectors, in drug-delivery systems, as semiconductors, and in nanodevices[1, 2-4].

When facing up to this challenge of producing highly structured materials under mild operation conditions, biomineralization processes represent a suitable model. In fact, there are highly ordered three-dimensional silica structures in nature. They are found in marine sponges and in microalgae of both continental and marine aquatic habitats. Diatoms are the most prominent of these microalgae. They are able to metabolize silica and to synthesize a very large variety of three-dimensional ordered species-specific structures, ranging in size from 5 µm up to 5 mm[5] as can be observed in Figure 1.1.

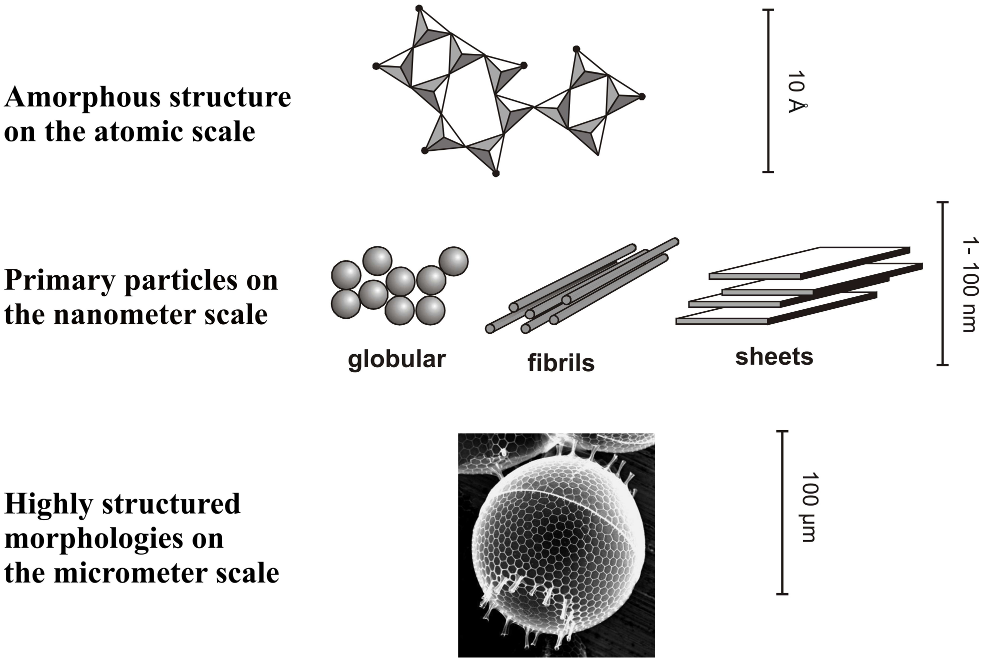

Figure 1.1. Silica structures found in diatoms at different size scales[6].

In contrast to silica produced in the chemical industry, in diatoms the siliceous structures are formed under ambient conditions. Unlike synthetic silica, biosilica is produced under slightly acidic reaction conditions, temperatures ranging from artic to tropic, and at low pressure[7-9]. Because of these mild conditions and also of the hierarchical porosity of the cell walls, diatoms are ideal model organisms to investigate the molecular and physico-chemical processes of silicon biomineralization with purpose of mimicking them in the bioinspired production of highly structured silica. In this respect, similarly to common biominerals like carbonate or phosphate, biosilification processes involve macromolecules such as polypeptides and polyamines[10]. Those macromolecules are supposed to regulate deposition kinetics and mineral morphology[11]. However, while apatite or calcite formation is based on dissolution/precipitation mechanisms, silica builds up via inorganic polymerisation of molecular precursors. This is a complex process since both the nature of these silica precursors and their association strongly depend on reaction conditions such as pH, concentration or salinity[12]. But industrial and biological silica synthesis have also some features in common. The most remarkable aspect is that both require supramolecular aggregates as soft templates to impart structural features to the porous solid formed. Whereas in biosilica synthetic processes structure directing agents are the nitrogen-containing macromolecules mentioned before, in the industrial sol-gel process the templates are usually amphiphilic molecules whose dimensions, shapes and functional groups play an important role on the morphology of the resulting porous structures[13, 14]. This close relation between morphology and dimensions of the template with those of the porous structure requires the production of structure directing agents with tailored dimensions and also the investigation of their aggregation behaviour under the conditions where the silica synthesis will take place. Regarding the dimensions of the template, the production of macromolecules with different architectures and tailored dimensions can be nowadays easily achieved by controlled polymerization techniques[15, 16].

Taking all these concepts into account, polymeric surfactants with tailored dimensions produced by controlled polymerization techniques and with well-defined aggregation behaviour may be suitable templates for the production of highly structured silica. Moreover, the hydrophilic chains of the surfactant can be synthesized in such a way that they bear nitrogen-containing functional groups mimicking those found in the biomolecules associated to diatoms. Amphiphilic templates fulfilling these requirements represent hence a bioinspired strategy within the challenge of producing highly structured silica under milder conditions than those used in industrial processes.

In line with these ideas, the goal of this work is the synthesis and characterization of bioinspired, amphiphilic polymers for the production of highly ordered silica structures. Firstly, amphiphilic alkyl-polyamines with well-defined degrees of polymerization and different nitrogen-containing functional groups in the hydrophilic segment shall be produced. The cationic ring-opening polymerization of cyclic iminoethers with alkyl-bearing initators provides a synthetic route to produce these compounds in high amounts. As has been previously remarked, the aggregation properties of the templates play a crucial role on the final features of the porous structure. For this reason, the aggregation behaviour of the synthesized polymeric surfactants in aqueous solutions shall be tested. Here, together with the determination of some important aggregation parameters such as the critical micelle concentration, investigations on the size and shape of the polymeric aggregates in solution shall be performed. Moreover, the occurrence of some other assembly phenomena of the polymer in other solvents or in the solid state shall also be characterized. Finally, it shall be tested if the polymers possess structure directing properties in the preparation of ordered silica structures as well as the influence of the operation conditions on the morphology of these resulting structures.

2 Theory and Background

2.1 Supramolecular templated inorganic materials

Improvements of properties and synthetic processes of materials has been the driving force for material science and engineering in the last decades. For the preparation of highly structured inorganic materials, the synthesis involving supramolecular aggregates as templates and chemical precursors represents a field of increasing scientific and industrial interest. In fact, products with a broad variety of compositions and properties can be obtained by sol-gel techniques[17]. Nevertheless, the production of highly structured materials is not only limited to these techniques. In this respect, nature has found amazing alternatives to produce high-performance structures at ambient temperatures under physiological conditions: teeth, bone and nacre are evident examples for the capability of biomineralization processes. Even though many aspects of the related *in vivo* mechanisms are not yet fully understood, the utilization of the basic strategies of natural biomineralization has become a challenge for material scientists in an interdisciplinary approach.

2.1.1 Highly structured manufactured materials

According to the classification made by the International Union of Pure and Applied Chemistry IUPAC[18] porous solids can be arranged in three main categories depending on their pore size d, i.e. micro- ($d < 2$ nm), meso- (2 nm $< d <$ 50 nm), or macroporous ($d > 50$ nm). Some illustrative examples are given in Figure 2.1.

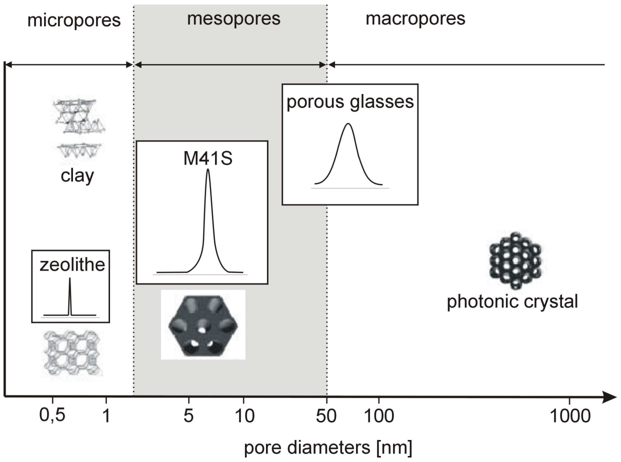

Figure 2.1. Examples of micro-, meso-, and macroporous materials, showing pore size domains and typical pore size distributions[19].

In the field of crystalline microporous solids, zeolites constitute one of the most important groups. In the past 60 years, there has been a sustained interest in the synthesis of these materials, in view of their properties and their applications in catalysis or sorption among others. The original name was initially given to natural aluminosilicates of the tectosilicate type. The latter are built up from a three-dimensional array of tetrahedral units TO_4 (T = Si, Al), with each oxygen atom acting as bridge between two tetrahedra. However, the main difference between zeolites and the other members of the tectosilicate family (feldspat) is the presence of channels and cavities of molecular dimensions which are in contact with the external medium. In order to preserve electroneutrality, alkaline cations and water are present within these cavities. However, in spite of the interesting properties shown by these crystalline materials, their dimensions and accessibility of pores are restrained to the sub-nanometer scale. This limited the application of these pore systems to small molecules. This is the reason why an important effort has been focused on designing molecular sieves showing larger pore size. Research in supramolecular templated materials began in the early 1990´s with the novel synthesis of the mesoporous structure MCM-41 and the related M41´s family of molecular sieves[20] performed by the Mobil Oil company. The mesoporous structures were derived of supramolecular assemblies of surfactants, which acted as templates for the inorganic precursors during the synthetic process[21] as shown in Figure 2.2.

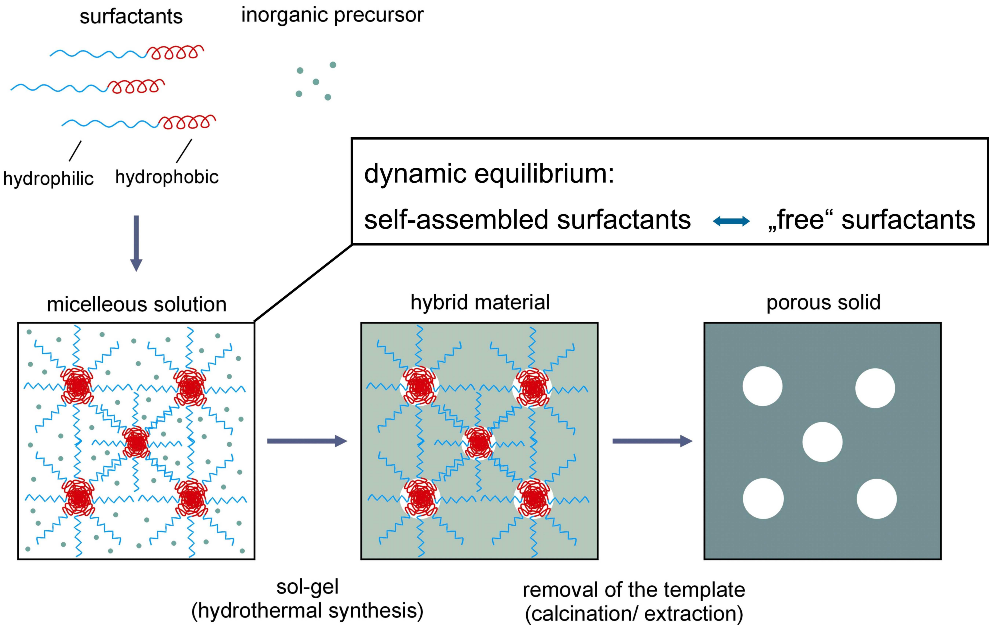

Figure 2.2. Schematic representation of the general synthetic process of M41´s materials from inorganic precursors and organic surfactants[22].

The synthetic process is based on the combination of appropriate amounts of a silica source (e.g. tetramethylorthosilicate (TMOS), dispersions of small silica particles (e.g. Ludox®), fumed silica, sodium silicate), an alkyltrimethylammonium halide surfactant (e.g. cetyltrimethylammonium bromide (CTAB)), a base (e.g. sodium hydroxide or tetramethylammonium hydroxide (TMAOH)) and water. This mixture is then aged at elevated temperatures and pressures ($T \geq 100$ °C and $p \geq 1$ bar) for 24 to 144 hours and results in a solid precipitate. The hybrid mesostructured product is then calcined at about 500 °C under a flowing gas to burn off the surfactant encased within the inorganic framework. The method yields materials with different composition, dimensions and properties and has attracted considerable attention because of the remarkably large surface areas and narrow pore size distributions of the resulting structures.

Different models have been suggested to explain the formation of the mesoporous structure. A common feature in these models is the presence of surfactants in solution to guide the formation of the inorganic mesostructure from the solubilized inorganic precursors (as can be observed in Figure 2.2). Those surfactants are composed of an hydrophilic head group and a long hydrophobic tail group within the same molecule and undergo self-organization to minimize contact between the incompatible ends. The differences between the models arise in the way how the inorganic precursor interacts with the surfactant; the type of interaction between the surfactant and the inorganic precursor represent a significant difference among the various synthetic pathways, the formation models, and hence the resulting classes of mesoporous materials.

In order to explain the formation of M41´s materials a liquid crystal templating (LCT) mechanism was proposed. It is based on the resemblance between liquid crystalline assemblies (lyotropic liquid crystalline phases) of surfactants and the morphology of the M41´s materials[20, 23], whose mesostructure is shown in Figure 2.3.

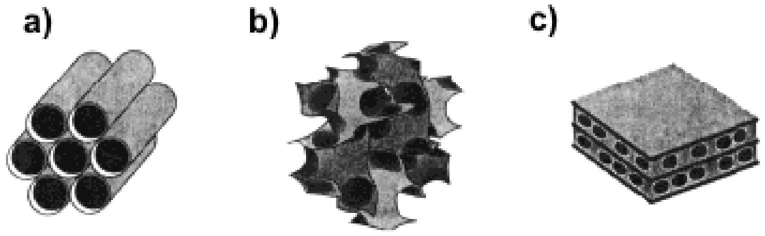

Figure 2.3. Structure of M41´s materials: a) MCM-41 (hexagonal), b) MCM-48 (cubic), and c) MCM-50 (lamellar)[24].

The mechanism includes two main general pathways in which either 1) the lyotropic liquid crystalline phase already exists before the inorganic precursors are added, or 2) the addition of the silicate anions promotes the long-range ordering of the surfactant to build the lyotropic liquid crystalline phase. In both cases the inorganic components, which are negatively charged at the high pH values of the reaction medium, undergo preferential interaction with the positively charged ammonium head groups of the surfactants. As a consequence, they condense into a solid, continuous framework. The resulting hybrid mesostructure can be viewed as a lyotropic liquid crystalline phase of the surfactant entrapped within a silica matrix; the removal of the surfactant produces the open, mesoporous M41´s framework. However, it was proven that route 1 did not take place because the surfactant concentrations used were far below the critical micelle concentration (CMC) required for lyotropic liquid crystalline phase formation[25]. The second mechanistic pathway postulates a cooperative self-assembly of the ammonium surfactant and the silicate precursor species below the CMC. To date, a full agreement over the formation details of M41´s materials has not yet been reached. At this point, several mechanistic models (*Silicate Rod Assembly*[26], *Silicate Layer Puckering*[27] or *Silicate Rod Clusters*[28], among others) have been developed and all of them deal with the ideas that the silicate species promote liquid crystalline phase formation below the CMC and that the interaction between surfactant and inorganic precursors plays a crucial role in the structural morphology of the resulting material.

2.1.2 Biominerals: highly structured materials in nature

Hierarchically structured materials can not only be manufactured but also found in nature. Shells, bone and teeth, among others (see Table 2.1), are good examples. Biomineralization covers all processes that lead to the formation of these organic-inorganic composites. The mechanical, optical, and magnetic properties of these materials are exploited by the organisms for a variety of purposes. Those properties are often optimized for a given function if compared to the properties of biological materials of similar composition. Materials scientists are fascinated by the exceptional control that organisms exert over the composition, crystallography, morphology, and materials properties of biominerals and the mild conditions (physiological temperature, pressure, and pH) required for their production. Therefore, in recent years the field of biomineralization has emerged as a suitable model in the production of synthetic materials. This huge impact of biomineralization is reflected in the application of strategies adapted from biology, i.e.

bioinspired strategies. Those strategies are by definition a multidisciplinary field that leans on researchers from biology, chemistry, geology, materials science, etc.

Table 2.1. Summary of the most important biominerals found in nature[29].

Mineral	Form	Function
calcium carbonate ($CaCO_3$)	calcite, aragonite, vaterite, amorphous	exoskeleton, eye lens, gravity device, calcium storage
calcium phosphate ($Ca_2(OH)PO_4$)	apatite, brushite, octacalcium phosphate, amorphous	endoskeleton, calcium store, ionic storage
calcium oxalate ($CaC_2O_4 \cdot 2H_2O$)	whewellite, weddelite	calcium storage, deterrent
iron oxide (Fe_3O_4)	magnetite	magnet, teeth
iron hydroxide FeO(OH)	goethite, lepidocrocite, ferrihydrite	iron storage, teeth
Silica (SiO_2)	amorphous	skeleton (plants, diatoms), deterrent
alkaline earth sulfates ($CaSO_4 \cdot H_2O$, $SrSO_4$, $BaSO_4$)	gypsum, celestine, barite	gravity device, skeleton

Chemistry impacts the field of biomineralization in different ways, the characterization of composition and biochemistry of the biological materials, the design of *in vitro* model systems used to test hypothesis about interaction between inorganic and organic components or the development of new synthetic methods based on the biological systems in order to control materials properties. These efforts lead to new classes of organic-inorganic composites. Biomineralization processes are often under strict biological control and involve the interactions of biological macromolecules. In recent years, much progress has been made towards determining the sequences and solution-state structures of these biomacromolecules as well as establishing structure-function relationships for them.

2.1.2.1 Biosilification: highly structured silica in nature

Diatoms are unicellular, eukaryotic microalgae that constitute one of the most common types of phytoplankton. They make a composite cell wall of silica and organic material and are recognized as useful model systems for understanding silica biomineralization. They generally range in size from a few up to several hundred µm, with typical average sizes of 15-30 µm. Diatom species are classified according to their silica structures, and the total number of species is estimated in more than 10.000. Thus, an enormous variety of structures exists (see Figure 2.4).

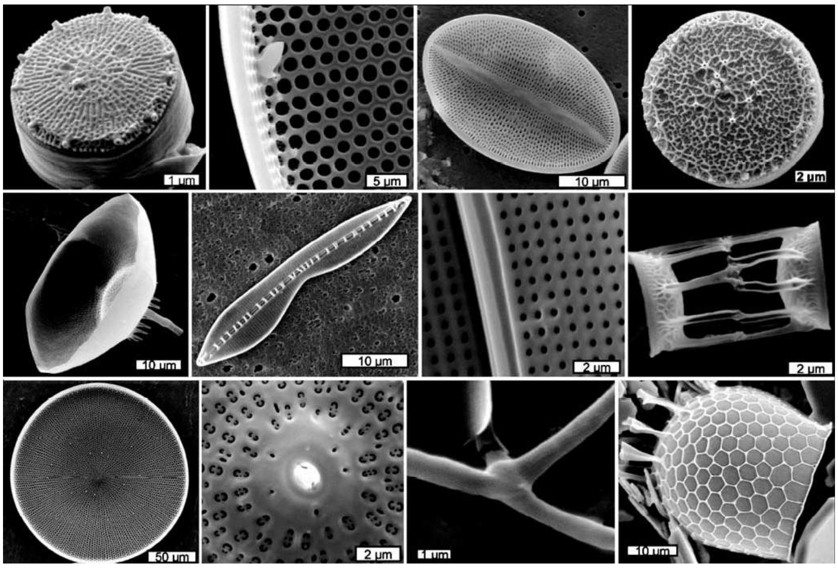

Figure 2.4. Diversity of diatom silica structures. Samples of acid-clean silica from a variety of diatom species imaged by SEM[30].

Diatoms possess rigid cell walls (exoskeletons) which are composed of amorphous silica[31]. These cell walls consist of 2 valves linked by one or more girdle bands. This whole box is known as the ‘frustule’[32-34]. The mineral parts are each enclosed within a thick mucilaginous organic layer, composed of polysaccharides and glycoproteins[7, 35-38], which interconnects the siliceous frustule components[33, 34, 38, 39]. The proposed function of the layer is to protect the silica of the frustule against dissolution in the aqueous environment[34, 39, 40]. Indeed, when diatoms die, many frustules remain quite well protected from dissolution and grazing, and sink to the bottom of oceans and lakes where they form the so-called diatom ‘ooze’. Over time this ooze has been built up, forming massive geological fossil deposits, which currently are known as diatomaceous earth. This material has been recognized as being useful in a variety of applications, such as filter, abrasive, filler, absorbent and decolouring agent[7, 41, 42]. Diatomaceous earth is characterized as mesoporous silica with a low specific surface area[1, 7, 9]. In comparison to artificially synthesized silica, application is quite limited because of loss of detailed nanostructural features due to the long period (over hundreds of millions of years) of aging and dissolution. In addition, diatomaceous earth contains impurities by contamination with elements such as aluminum, iron and cadmium that limit the use [7].

An interesting fact is that each one of the over 10.000 different diatom species has its own characteristic frustule morphology[33, 34]. Besides the diverse morphology of the frustule, their mineral silica-based parts are composed of pores in a broad size range, from dimensions of only a few nm up to some of over 300 nm. These pore dimensions, and also the shape of the pores, vary among species and can be classified according to the definitions of the IUPAC into micropores (< 2 nm), mesopores (2 - 50 nm), and macropores (> 50 nm), as mentioned in the previous section dealing with porous manufactured materials. In general, the pore dimensions in diatomaceous silica are much larger than those found in artificially produced silica and silica-based materials. Even within the frustule of a single species different pore types are present, which are hierarchically ordered with respect to size[1, 33, 43]. In diatoms, the frustule morphology remains after cell division, replicating the nanostructural details in descendants from generation to generation. Obviously, diatom cell wall formation is controlled genetically[34]. Some data are available of the physico-chemical, biochemical, and molecular mechanisms of silica cell wall formation, although much remains to be discovered. In this respect, the synergy between these processes remains unknown and needs to be elucidated in order to enable meaningful biomimicking of frustule formation in industrial production processes and hence the design of improved and innovative artificial silica.

In order to understand some aspects of diatom silicon biomineralization, a detailed description of the diatom cell wall is required. The siliceous exoskeleton of the diatom cell wall is composed of two overlapping parts that fit together like a petri-dish (see Figure 2.5). The lid is called epitheca and consists of an epivalve and an epicingulum. The epitheca overlaps the bottom part of the dish, the hypotheca. This hypotheca is composed of a hypovalve and a hypocingulum. The epicingulum and hypocingulum, also known as girdle bands, are interconnected, keeping the valves together[33, 34].

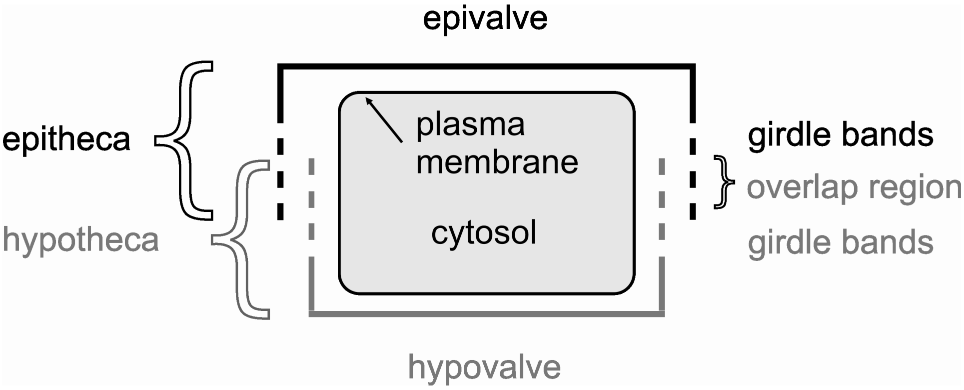

Figure 2.5. Structure of a diatom cell wall showing its different components.

During cell division (Figure 2.6) each parental cell forms two daughter cells within its own exoskeleton (a). Subsequently, each daughter cell develops a new hypovalve inside a silica deposition vesicle (SDV), which is formed in the center of each daughter cell at the side of the cleavage groove[32-34]. During valve formation and silica deposition (b-d), the SDV expands continuously in the second dimension until the optimal size of the new hypovalve is reached[44]. Simultaneously with completion of two-dimensional expansion, the frustule thickens in the third dimension and finally is completed by its coverage with an organic layer just prior to cell separation (e)[32, 39, 45, 46].

Proteins play a relevant role in diatom cell wall formation. However, only a few of them have been extracted and partially characterized. The species *Cylindrotheca fusiformis* has been studied for identification of these proteins. HILDEBRAND *et al.*[47, 48] were the first to isolate genes involved in silicon transport. Diatoms are the first and so far only organisms in which silicon transporters (SITs) have been identified. SITs are assumed to play a key role in the regulation of silicon uptake from the environment and transporting it across cellular membranes. In total 5 SIT genes have been identified with a distinct expression pattern during cell wall synthesis and their own affinities and capacities for transport. Their specific roles, however, have not been yet determined[4, 48, 49]. For intracellular silica transport[44] it has been proposed that silica transport vesicles (STVs) are involved in transporting silicic acid and/or silicon precursors through the cell in order to release their contents inside the SDV. However, the presence of silicon or silica precursors inside the STVs has never been confirmed and therefore their function is still under debate[50, 51]. Frustulins, calcium-binding cell wall associated glycoproteins, belong to a different class. They were also first identified in *C. fusiformis* and were located in the organic casing[52, 53]. Apparently, they are not directly involved in the silification process and it is more likely that they have a structural function in the organic casing that covers the silica. Pleuralins are hydrogen fluoride (HF) extractable proteins of *C. fusiformis* that appeared to be specifically associated with the pleural (girdle) bands after completion of silica deposition[54, 55]. Pleuralins are also not involved in silica formation itself, but they may interconnect the pleural bands.

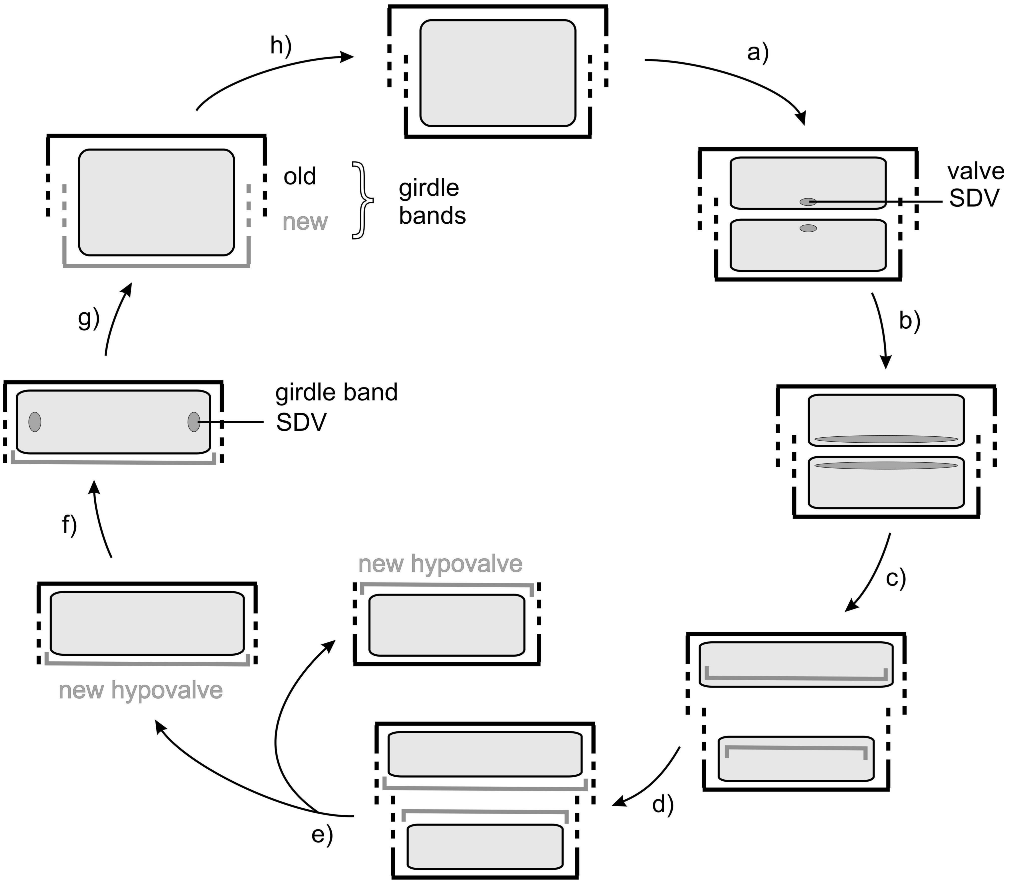

Figure 2.6. Schematic representation of valve morphogenesis of a diatom, showing the various stages of valve formation from cytokinesis of the parental cell until separation of the daughter cells.

Other HF-extractable macromolecules that were identified in *C. fusiformis* are silaffins and long-chain polyamines (LCPAs) (see Figure 2.7). They both are able to precipitate silica *in vitro*[56]. The native silaffin-1 protein (natSil-1) is highly post-translationally modified and heavily phosphorylated with phosphate groups bound to all the serine residues[10]. The functionality of silaffin-1 itself in silica precipitation depends on the presence of modified lysine residues, since heterologously expressed silaffin-1, without the characteristic post-translational modifications, does not precipitate silica[56]. In particular, natSil-1A and LCPAs can be used together at different ratios to create a variety of silica structures *in vitro* when they are combined with natSil-2[10, 57-59]. Although natSil-2 contains the same lysine modifications as silaffin, it is not capable of precipitating silica itself because of auto-inhibition of the polyamine moieties caused by other modifications such as sulfation and glycosylation[57]. Furthermore, each diatom may well possess species-specific LCPAs and silaffins, which are most likely involved in the formation of the species-specific biosilica structures[38, 60, 61].

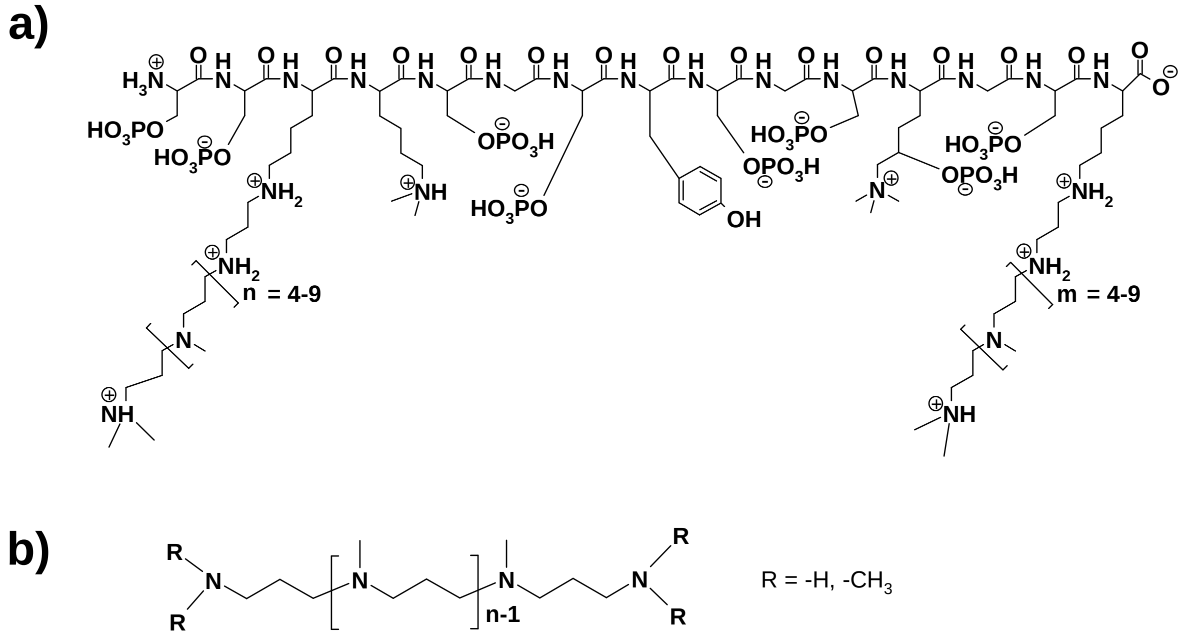

Figure 2.7. a) Chemical structure of native silaffin-1 (natSil-1) from *Cylindrotheca fusiformis*[10]. **b)** Structures of long-chain polyamines (LCPAs) associated with biosilica in diatoms[62].

The identification of silaffins and LCPAs has resulted in two different conceptual models of how structure direction in diatoms may proceed. The first model is based on computer simulations and postulates a mechanism in which LCPA rich phases (‘emulsion droplets’) work as templates for the formation of silica structures via a so-called phase separation process[63].

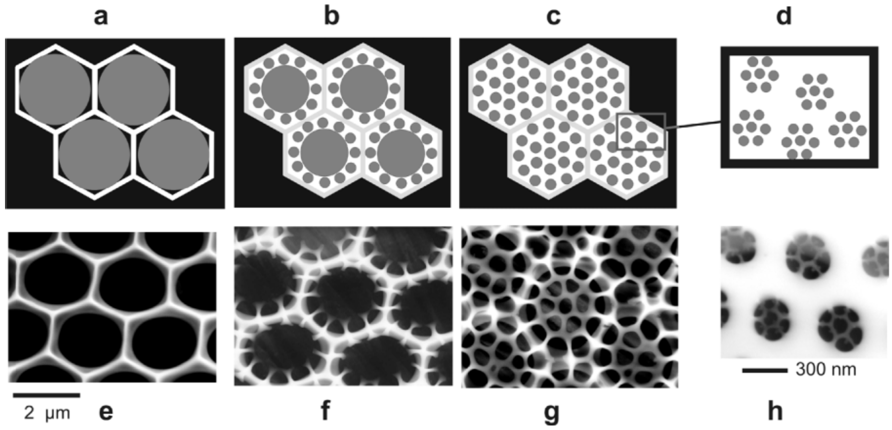

Figure 2.8. Schematic representation of the templating mechanism by the phase-separation model (a–d) and comparison with the stages of the developing cell wall of *C. wailesii* (e–h)[63].

As can be observed in Figure 2.8, the monolayer of polyamine-containing droplets in close-packed arrangement within the silica-deposition vesicle directs silica deposition (a). Consecutive segregations of smaller (about 300 nm) droplets lead to new routes for silica precipitation (b,c). Dispersion of 300 nm droplets into 50 nm ones guides the final stage of silica deposition (d). Silica precipitation only occurs within the water phase (white areas). The repeated phase separations produce a hierarchy of self-similar patterns. This model has been referred to as the down-scaling approach. Within the development of this model it was found that silica precipitation promoted by both silaffins and long-chain polyamines depends respectively on the phosphorylation of the silaffins and on the presence of phosphate in the polyamine solution. The most likely reason for these phenomena leans on the fact that long chain polyamines are positively charged polymers (in the pH range where condensation of silicic acid takes place). Therefore, they are able to form aggregates in the presence of multivalent anions like phosphate acting as crosslinkers. Increasing concentrations of these anions produce emulsion droplets of increasing size with macroscopic phase separation at high concentrations of the multivalent anion. Microscopic phase separation is then supposed to play a crucial role for the polyamine-induced precipitation of silica nanospheres[64].

The other model that describes frustule morphogenesis is based on experimental results[65]. In contrast to the downscaling model, it implies an up-scaling mechanism[66], in which again phase separation processes occur. Here phase separation is induced by organic molecules other than silaffins and/or LCPAs, being present in the SDV. Silaffins and LCPAs are small organic molecules which as remarked before effectively initiate silica precipitation, but because of their size are expected to become fully encapsulated in the forming silica spheres[65]. Encapsulation of such small organic molecules (< 17 kDa) is common in silica formation[67].

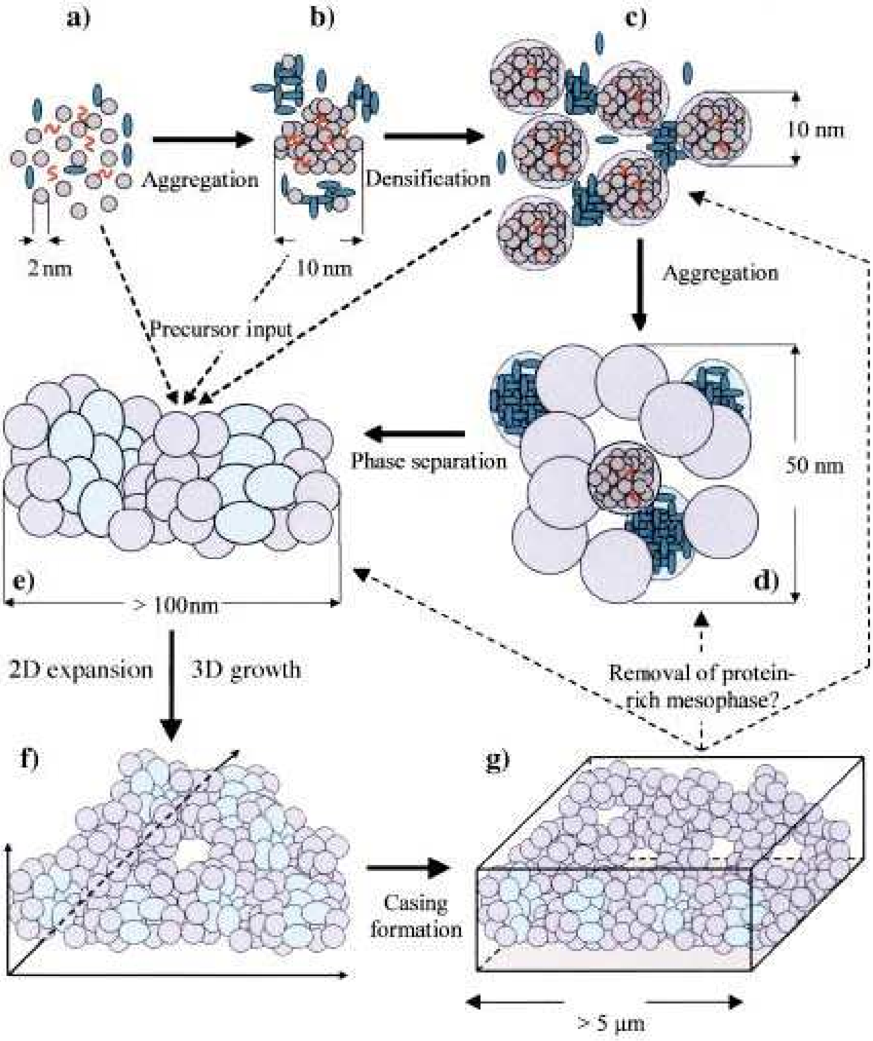

Figure 2.9. Schematic model of mesophase silica polymerization in diatoms proposed by VRIELING *et al.*[65].

According to Vrieling [65] (Figure 2.9), silaffins and/or polyamines (curved structures), larger organic molecules (ellipsoids), and silica precursors are present in the immature silica deposition vesicle (SDV). The latter forms small silica sols (spheres) (a). Silaffins and polyamines in combination with the environmental pH and continuous import of silica precursors into the SDV, induce fast aggregation of silica. In this process the small organic molecules become completely encapsulated, while larger peptides interact with the silica and each other (b). Hybrid aggregates of silica and silaffins/polyamines collide into larger silica structures (circles) and interact with growing aggregates of the larger peptides (the mesophase precursors) (c). Subsequent aggregation results in larger silica/silica and silica/peptide aggregates (ovals) with structures of about 50 nm in size (d). Densified mesophase particles grow to sizes larger than 100 nm (e). Following continuous input of peptides and silica precursors into the SDV results into two-dimensional expansion and three-dimensional growth of the hybrid mesophase (f). Although those peptides acting as inducers of phase separation are so far unknown, they are expected to be involved in pore formation since they do not remain in the final cell wall. In fact, they have never been found inside. At this point, it should be also remarked that the mature silica exoskeletons contain very low amounts of organic matter[65]. Therefore, it was suggested that the peptide-rich phases enclosed within the silica matrix should somehow be removed during valve formation in diatoms, finally leaving cavities in the silica (g). However, the mechanism that would be involved in such a peptide removal has not been yet clarified.

2.1.2.2 Silica chemistry

The chemistry of silicic acid is a very important topic when dealing with silica formation and must be therefore summarized within this work.

The most simple soluble form of silica is the monomer orthosilicic acid $Si(OH)_4$. It shows a weak acidity with a pKa value around 9.8[12]. $Si(OH)_4$ solutions are stable within a range of pH between 2 and 9 as long as its concentration remains below 1 mM. At higher concentrations silicic acid undergoes autopolymerization reactions. This process can be divided in three different stages:

1. Polymerization of monomers towards stable nuclei of critical size.
2. Growth of these nuclei towards spherical particles.
3. Aggregation of these particles towards precipitates or gels.

This polymerization process starts with the dimerization of the silicic acid (Figure 2.10-a). Subsequent polymerization of the dimeric species yields higher molecular weight oligomers of the silicic acid such as trimers, tetramers, etc. Those oligomers strongly tend to further polymerize in such a way that maximizes the number of siloxane bonds (Si-O-Si) and minimizes the number of remaining silanol groups (Si-OH). For this reason after the first reaction phase, highly branched polysilicic acid species are predominant in the medium. After the total consumption of the monosilicic acid, the highly branched polysilicic acids transform into bigger spherical particles by Ostwald ripening. In this process, smaller particles, which are more soluble, dissolve and release silicic acid that redeposits onto the larger ones. At pH values close to neutrality the particles bear a negative charge on their surface and can grow as isolated sol particles with final diameters ranging from 1 to 50 nm depending on the conditions (pH and temperature).

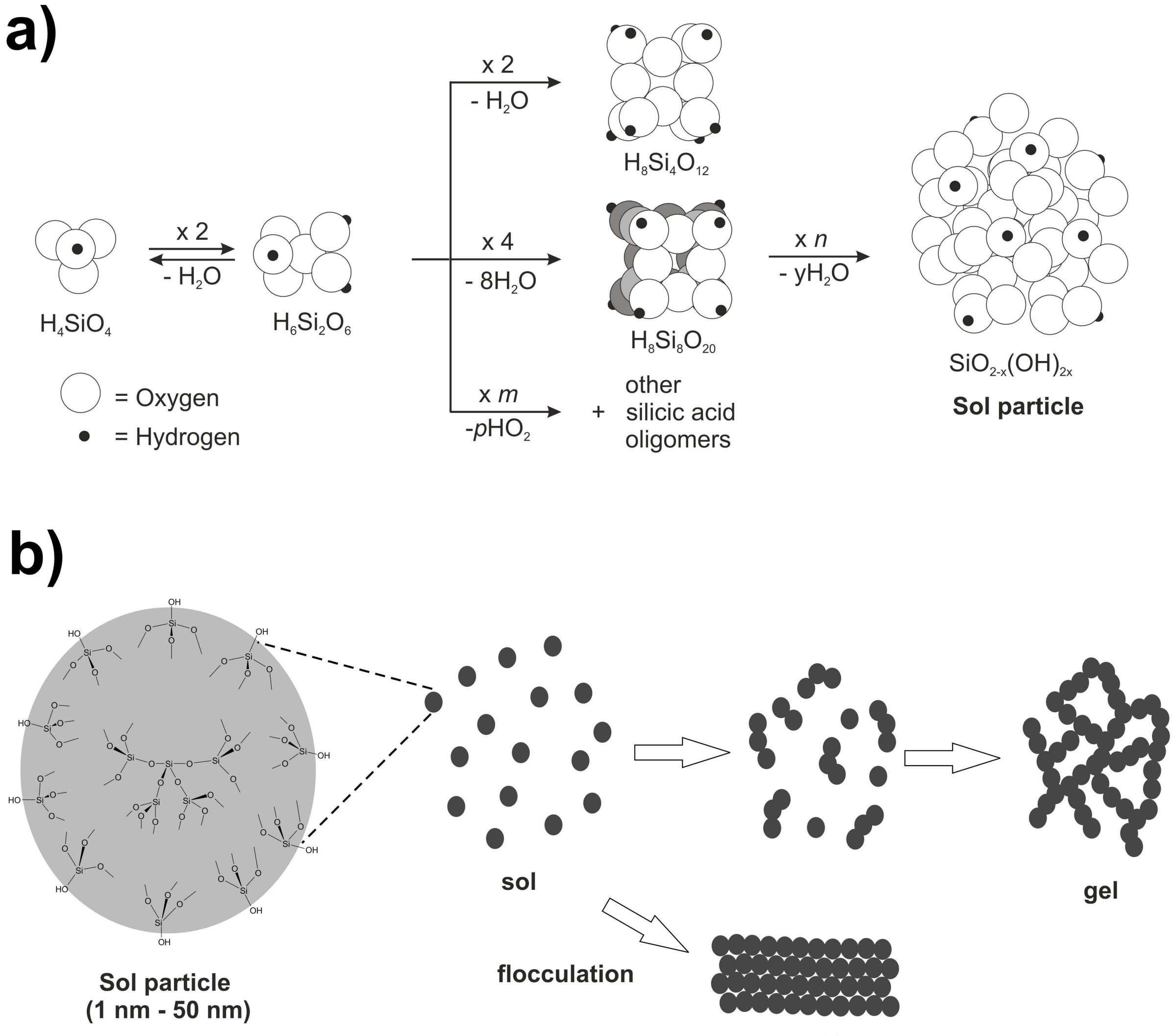

Figure 2.10. Schematic representation of **a)** polymerization of monosilicic acid into disilicic acid and further cyclic oligomers with subsequent condensation into spherical polysilicic acid particles and, **b)** formation of silica gels and precipitates from a silica sol.

The presence of salts or acidic conditions (i.e. pH 6) in the medium reduces or even eliminates the negative surface charge responsible for individual repulsion among the particles and make them aggregate into dense three-dimensional silica gels (Figure 2.10-b). However, in the presence of polycationic polymers (e.g. polyamines) silica sols tend to precipitate instead of gelling. This process is known as flocculation and is based on the interaction of polycationic polymeric chains with the negative surface charge on adjacent sol particles. As a result the polymeric cationic chains interconnect these sol particles and build compact and dense silica networks which rapidly precipitate (Figure 2.10-b).

2.2 Supramolecular aggregation of surfactants in aqueous media

2.2.1 Introduction

As mentioned in the previous section when dealing with the production of porous materials by liquid crystal template mechanisms, the aggregation behaviour of amphiphilic molecules in aqueous media represents a crucial aspect within those mechanisms. That is due to the strong influence of the properties of the aggregates on the morphology of the final porous structure.

Generally, a surfactant molecule consists of two parts with different properties: a headgroup (hydrophilic) with a strong affinity for the solvent and a tail (hydrophobic) repelling the solvent (Figure 2.11-a). The head group may carry a negative or positive charge, giving rise to anionic or cationic surfactants, respectively. Alternatively, it may contain ethylene oxide chains or even saccharide type groups, as is the case of non-ionic surfactants. Another type are known as zwitterionic or amphoteric surfactants which alter their ionic behaviour according to the pH value of the solvent. The tail part of the molecule is usually a hydrocarbon chain, but may as well contain aromatic groups. Depending on the molecular structure and type, a balance between hydrophilicity and hydrophobicity exists in the surfactant molecule. This is called hydrophilic-lipophilic balance or HLB, which is important in categorizing surfactants as emulsifiers, detergents, wetting agents, solubilizing agents, micelle forming types, etc[68].

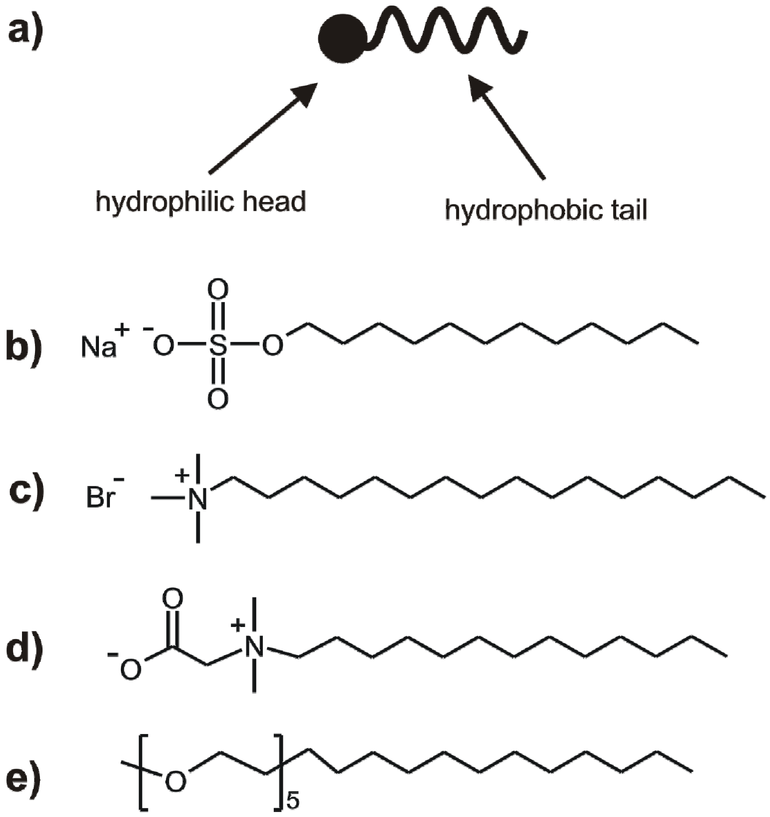

Figure 2.11. (a) Sketch of a surfactant showing its hydrophilic head and hydrophobic tail. Examples of **(b)** anionic surfactant: sodium dodecyl sulphate (SDS), **(c)** cationic surfactant: cetyltrimethylammonium bromide (CTAB), **(d)** zwitterionic or amphoteric surfactant: alkyl-betaine and **(e)** non-ionic surfactant: pentaethylene glycol monododecyl ether.

When the head group of the surfactant molecule bears an anion, the molecule is referred to as an anionic surfactant. Anionic surfactants are most widely used for laundering or dishwashing liquids and shampoos because of their excellent cleaning properties. Important examples of anionic surfactants are carboxylates, sulfonates, sulfates and phosphates. Sodium dodecyl sulphate (SDS) is a well-known surfactant that belongs to this type and has been used in a wide range of applications (Figure 2.11-b). Surfactants which carry a cationic head group are referred to as cationic surfactants. They play an important role as antiseptic agents in cosmetics, as general fungicides and germicides, corrosion inhibitors, fuel and lubricating oil additives and in a number of bulk chemical applications. Two common types of cationic surfactants are long chain amines and quaternary amine salts. Alkyl amines with chain-length C_8 to C_{18} are the most important ones in this category. In the pharmaceutical area, cationic surfactants with pyridinium and piperidinium groups are also used. Cetyltrimethylammonium bromide (CTAB) (Figure 2.11-c) is also a well-known example of cationic surfactant and have been extensively studied. The last type of charged surfactants are zwitterionic or amphoteric. They are very mild, making them particularly suitable for use in personal care and household cleaning products. Zwitterionic surfactants are compatible with all other classes of surfactants and are soluble and effective in the presence of high concentrations of electrolytes, acids and alkalies. They exhibit cationic behaviour near or below their isoelectric points and anionic behaviour at higher pH. The isoelectric point depends on their structure. This type of surfactants usually contains two charged groups of different sign. Whereas the positive charge is almost always ammonium, the source of the negative charge may vary (carboxylate, sulfate, sulfonate). They have excellent dermatological properties and are hence frequently used in shampoos and other cosmetic products, and also in hand dishwashing liquids because of their good foaming properties. One example for this kind of surfactants is alkyl-betaine (Figure 2.11-d).

Pentaethylene glycol monododecyl ether (C12E5) is an example for a non-ionic surfactant (Figure 2.11-b). These surfactants do not carry any electrical charge and are more stable over the entire pH range. They show lower sensitivity to the presence of electrolytes in the system and are compatible with other surfactants. They are excellent grease removers used in laundry products, household cleaners, and hand dishwashing liquids. The amphiphilic nature of these surfactants is expressed in terms of an empirical hydrophilic-lipophilic balance (HLB)[68]. Water-soluble surfactants have an HLB above 13 and those with poor or no dispersibility in water have HLB below 6.

2.2.2 Self-assembly of surfactants

Surfactant molecules can associate in aqueous media to build large aggregates. This remarkable phenomenon can be explained in terms of the tendency of non-polar groups to avoid contact with water, while the polar parts show strong affinity to be hydrated. The primary driving force for this aggregation lies in the hydrophobic effect[69]. The origin of this effect stems from the fact that hydrocarbon-water interactions are unfavourable in comparison to water-water and hydrocarbon-hydrocarbon ones. In this respect, Figure 2.12 shows how, because of these interactions, surfactants undergo cooperative association leading to aggregates of define size and shape.

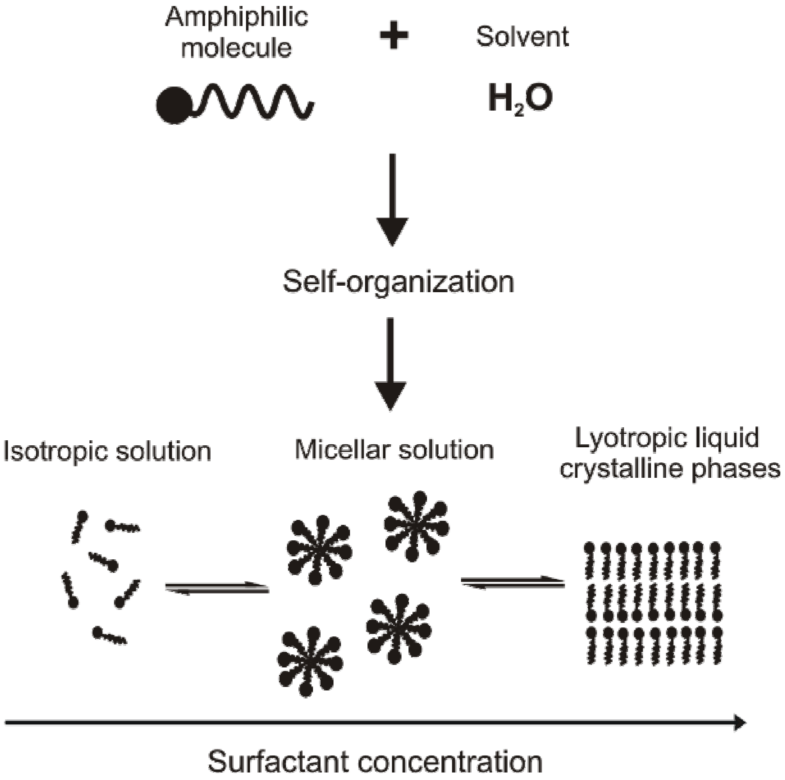

Figure 2.12. Amphiphilic molecules and their aggregates in aqueous media[70].

As can be observed, when mixing a surfactant with water at low concentrations it dissolves and behaves like an isotropic solution. As the concentration of the surfactant increases above a certain value (the critical micelle concentration, CMC), the amphiphilic molecules self-assemble to create aggregates in which the hydrocarbon chains are packed inside and the polar head groups form the surface surrounded by the aqueous medium. These structures are called micelles and they are stable as long as the surfactant concentration is above the CMC. The shape and size of the micelles are strongly dependent upon the dimensions and type of hydrophilic and hydrophobic parts. Typical shapes for the micellar aggregates are disks, spheres or cylinders[70]. Further increase of the surfactant concentration promotes arrangement of the micelles into lyotropic liquid crystalline phases. The main feature of these complex phases is that the micellar aggregates are forced to be disposed regularly within a latter.

Micelle formation or micellization is an important parameter due to the fact that several important interfacial phenomena, such as detergency and solubilization, depend on the existence of micelles in solution. Furthemore, micelles have become a subject of great interest in biochemistry and organic chemistry because of their similarity to biological membranes and globular proteins[71]. The concentration of surfactants at which micelle formation begins is called the critical micelle concentration (CMC) as mentioned previously. This parameter can be determined by many different techniques since at this concentration value many physical properties exhibit abrupt changes as illustrated in Figure 2.13.

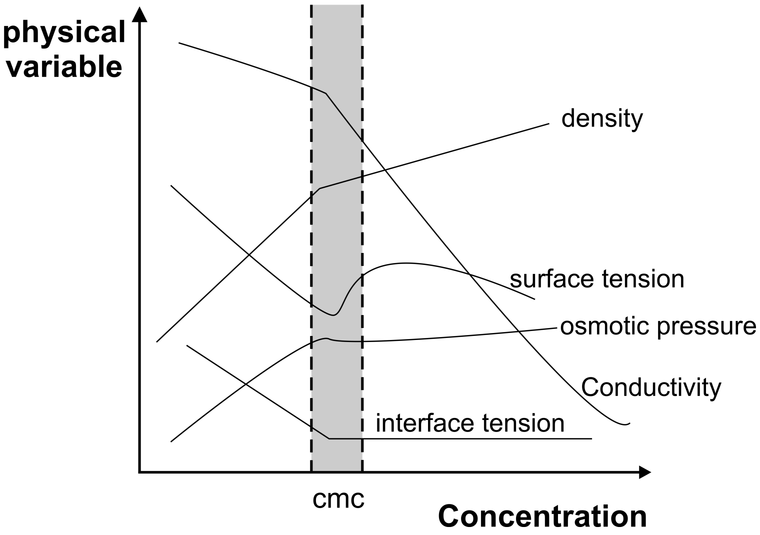

Figure 2.13. Illustration of the dramatic changes undergone by some physical properties beyond the critical micellar concentration[72].

Surface tension, turbidity, conductivity and osmotic pressure are among those properties. As seen in Figure 2.13 all of these methods involve plotting the measured value of the variable as a function of the surfactant concentration. The breakpoint in the plot represents the CMC. Since the surfactant molecules are in continuous motion, the nature of micelles is dynamic. There is a constant interchange between micelles and solution. The lifetime of a surfactant molecule in a micelle is in the order of 10^{-7} seconds, and the half-life for micelle formation or breakdown is usually in the region of 10^{-3} to 1 seconds[68]. Typical CMC values[73] at room temperature are:

Anionic surfactants: 10^{-3} – 10^{-2} mol/l
Cationic surfactants: 10^{-3} – 10^{-1} mol/l
Zwitterionic surfactants: 10^{-3} – 10^{-1} mol/l
Non-ionic surfactants: 10^{-5} – 10^{-1} mol/l

The CMC is afected by several factors like hydrophobic and hydrophilic groups, temperature and addition of salts and organic solvents[71]. Among those variables, the important role of the temperature on the behavior of surfactant molecules is especially remarkable as depicted in Figure 2.14.

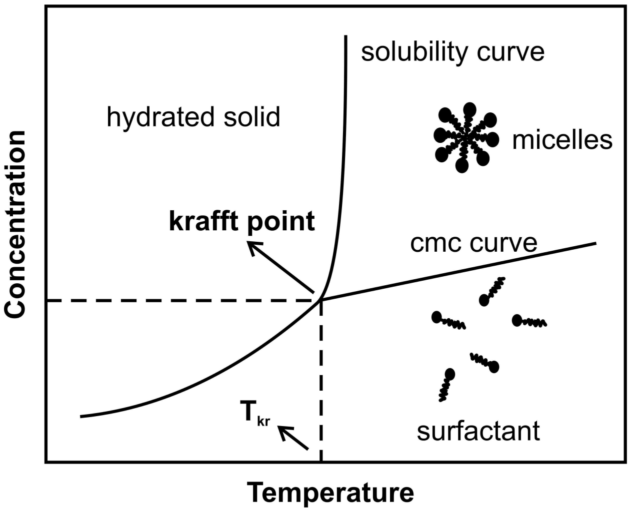

Figure 2.14. Schematic phase diagram of surfactant solubility in the region of the Krafft point[74].

At lower temperature surfactants often precipitate from the solution as hydrated crystals instead of forming micelles. This results in a different surface behaviour because of the changing of temperature[75]. The temperature at which the solubility equals the CMC is called the *Krafft temperature* (T_{kr}). The solubility of micelle-forming surfactants shows a strong increase above T_{kr} and a solution of any composition becomes a single homogeneous phase. The Krafft temperature increases strongly along with the alkyl chain length. The head group and the counterion of the surfactant have also been proven to strongly influence the Krafft temperature. Generally, the addition of salt makes the Krafft temperature increase[76]. Non-ionic surfactants do not exhibit Krafft points. Their solubility typically decreases with increasing temperature. These surfactants even may begin to lose their surface activity above a transition temperature referred to as the cloud point[73].

Further increase of the surfactant concentration in the micellar solutions results in lyotropic liquid crystalline phases. These type of surfactant aggregates share properties which are normally associated to both liquids and crystals. In this respect, it should be mentioned that the fundamental difference between crystals and liquids is the fact that ordered arrays of molecules are found in crystals in contrast to the random arrangement of molecules in liquids. The order in a crystal is normally positional and orientational while the molecules in liquids diffuse randomly throughout the sample container. In lyotropic liquid crystalline phases the order of the molecules is less than in crystals and more pronounced than in liquids. From that point of view, surfactants forming liquid crystals self-assemble into organized mesophases as intermediate between the crystalline solids and the isotropic liquids depending on the ambient conditions such as temperature (thermotropic liquid crystals) and concentration of the molecules in a solvent such as water (lyotropic liquid crystals)[70]. Surfactant molecules in these mesophases aggregate dynamically and collectively into a viscous phase with a high degree of organization. Different lyotropic liquid crystalline phases can be found depending on the temperature and the ratio of surfactant to water in the liquid crystalline media. The most common phases are micellar, hexagonal, cubic and lamellar[77, 78]. It is possible to extend this range to the inverse phases such as the inverse hexagonal and inverse cubic phase. These phases correspond to the most stable equilibrium existing at a certain concentration between all the chemicals present.

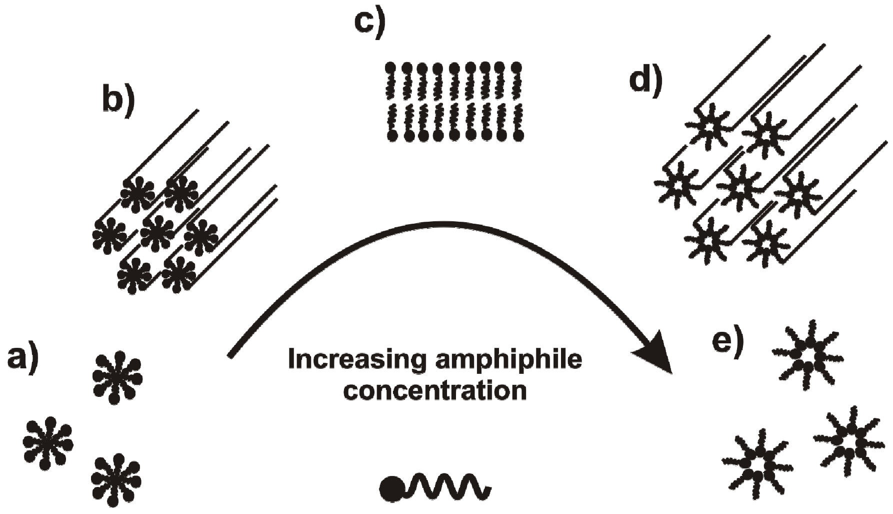

Figure 2.15. Various supramolecular building blocks obtained when the ratio surfactant to water was increased from a) to e).

As can be recognized in Figure 2.15-a, the first type of assemblies build by the surfactants at concentrations beyond the CMC are the micellar aggregates. The formation of these micellar aggregates continues up to a concentration where they are forced to be disposed within the solution volume and combine to form larger structures. Figure 2.15-b corresponds to an arrangement in which the ratio of surfactant to water increases with respect to a micellar solution. The surfactant is ordered in cylinders of indefinite length surrounded by the aqueous medium. The head groups of the molecules constitute the surface and the hydrocarbon chains are packed inside. This arrangement can be found in the two-dimensional hexagonal and the three-dimensional cubic phases.

In Figure 2.15-c the ratio surfactant to water increases. The surfactant molecules are arranged in bilayers separated by the aqueous medium. From such an arrangement the lamellar phase can be obtained. Figure 2.15-d represent a phase where the amount of surfactant is much higher and the surfactant molecules are arranged in cylinders as in Figure 2.15-b. However, unlike the arrangement given in Figure 15-b, the surface of the cylinders is formed by surfactant molecule head groups packed inside and surrounded by the aqueous solution which is now trapped inside the cylinders. From such an arrangement the inverse hexagonal and inverse cubic phases can be obtained. In Figure 2.15-e the concentration of surfactant in water increases so dramatically that the aqueous medium is trapped inside the spheres formed by the surfactant molecule head group. This arrangement represents the inverse micellar phase. It is interesting to note that if comparing all the supramolecular building blocks, the arrangement given in Figure 15-a and 15-b is the opposite to that of respectively Figure 15-d and 15-e regarding the position of the surfactant molecule head groups.

2.2.3 Characterization methods for surfactant aggregation

In order to understand the physico-chemical properties of the surfactant aggregates, a great variety of methods has been used. Among those, physico-chemical, spectroscopic and scattering techniques have become nowadays very useful.

Binding isotherms, phase equilibrium, potentiometry, surface tension, viscometry, dye solubilization, calorimetry, chromatography and other separation techniques or micellar relaxation kinetics are important physico-chemical methods to characterize surfactant aggregation[79, 80]. The determination of binding isotherms is useful to know the amount of bound surfactant as function of the free surfactant concentration. It allows to explore the nature of the binding process and the structure of aggregates. As discussed in the previous section, the measurement of the surface tension is useful to determine the critical micelle concentration (CMC). The dye solubilization method can also be used to determine this parameter. Separation methods such as electrophoresis[81, 82], size exclusion chromatography (SEC)[83] and ultracentrifugation can be also applied for studying surfactant aggregates.

In addition, spectroscopic methods are very useful to determine local structure and environment of the components in the system, aggregation numbers, diffusion coefficients, and kinetic parameters in surfactant aggregation. The methods within this type include pulsed field gradient spin-echo nuclear magnetic resonance (PFG-SE NMR)[84-86], electron spin resonance (ESR)[87, 88], infrared, Raman and UV-visible spectroscopy. It must be also remarked that each technique has its own limitations and advantages and that the selection of the most suitable one depends on the system under investigation.

Finally, important aspects dealing with the characterization of surfactant aggregates in aqueous media can be investigated with scattering methods. Light scattering, small-angle neutron scattering (SANS) and small-angle X-ray scattering (SAXS) have been employed for the characterization of different materials with a relatively broad dimensional range. This versatility in the materials that can be characterized with these methods stems from the different wavelengths that they use as shown in Figure 2.16. As a result of employing such different wavelengths, a specific contrast can be achieved[89].

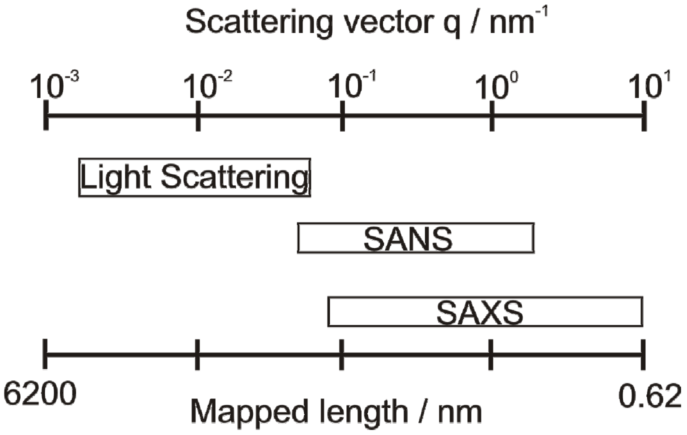

Figure 2.16. Representation of the scattering vector (q) and the mapped length ranges which are covered by light scattering, small-angle neutron scattering (SANS) and small-angle X-ray scattering (SAXS) methods[90].

Dynamic light scattering (DLS) and SAXS represent two important methods in the characterization of surfactant aggregation performed within this work. For this reason, both methods will be described more in detail in order to understand their basic principles as well as their potential application in the field of surfactant aggregation.

2.2.3.1 <u>D</u>ynamic <u>L</u>ight <u>S</u>cattering (DLS)[91, 92]

Dynamic Light Scattering (DLS) (also known as Photon Correlation Spectroscopy or Quasi-Elastic Light Scattering) is one of the most used methods in the determination of the particle size. It uses the time dependence of the intensity of the scattered light to observe the dynamic behaviour of the particles and to determine their translational diffusion coefficient. The method works well for sub-micron particle dimensions, sometimes with particles up to a few μm in diameter. The smallest particle size, that can be determined using dynamic light scattering, depends on the scattering properties of the particles (relative refractive index of particle and medium), the incident light intensity (laser power and wavelength) and the detector/optics configuration.

Although the principles of DLS are similar to those of SLS (Static Light Scattering), in case of DLS, detected fluctuations are measured within time intervals as short as 100 ns. These fluctuations in the scattered intensity arise from the constantly varying distances between particles due to thermal (Brownian) motion. Constructive and destructive interference of light scattered by neighbouring particles within the illuminated zone causes the intensity fluctuations at the detector plane. Those intensity fluctuations contain information about the particle motion. Thus, in a dynamic light scattering experiment, a laser beam is scattered by a small volume of the sample and light is collected by a photomultiplier at an angle θ with respect to the incident beam. The scattered light presents intensity fluctuations that can be related to the mutual diffusion coefficient D_m of the particles present in solution. The normalized time autocorrelation function of the intensity of the scattered light for a given delay time τ is:

$$g_2(\tau) - 1 = \beta \cdot |g_1(\tau)|^2 \qquad (1)$$

where β is a factor that depends on the experimental geometry and $g_1(t)$ is the electric field time correlation function. For a monomodal, monodisperse system this field correlation function decays exponentially:

$$g_1(t) = \exp(-\Gamma \cdot t) \tag{2}$$

with a decay rate $\Gamma = D_m \cdot q^2$, where D_m is the mutual diffusion coefficient and $q = (4\pi n/\lambda) \cdot \sin(\theta/2)$ is the magnitude of the scattering vector, n, λ and θ being the refractive index, wavelength and scattering angle in the medium, respectively. Thus, the translational diffusion coefficient D_m at a concentration c can be calculated from the plot $\ln(g_1(t))$ vs. t, whose slope is the decay rate $\Gamma = D_m \cdot q^2$. Mostly, however, the plot of $\ln(g_1(t))$ vs. t shows deviations from a straight line, but the initial slope, ascribed to a fast diffusion mode is still given by $\Gamma_1 = D_m \cdot q^2$. In order to find this initial slope Γ_1, a so-called cumulant fit is applied. Here, the curve is fitted by a cubic:

$$\ln(g_1(t)) = \ln(\Gamma_0) - \Gamma_1 \cdot t + \left({}^{\Gamma_2}\!/_{2} \right) \cdot t^2 - \left({}^{\Gamma_3}\!/_{6} \right) \cdot t^3 \tag{3}$$

where Γ_1 is the average decay rate and Γ_2 is the variance of the distribution. With both values, the polydispersity index can be defined as:

$$P = \frac{\Gamma_2}{\Gamma_1^2} \tag{4}$$

At infinite dilution the ratio Γ/q^2 becomes the translational diffusion coefficient D_o, and the hydrodynamic radius R_h can be calculated with the Stokes-Einstein relationship:

$$R_h = \frac{k_b \cdot T}{6 \cdot \pi \cdot \eta_A \cdot D_0} \tag{5}$$

being k_b the Boltzman's constant, T the absolute temperature in Kelvin and η_A the solvent viscosity. At this point it must be remarked that the hydrodynamically effective radius R_h defined by this expression correspond to a monodisperse material with a well-defined molar mass. In general, the diffusion coefficient depends on concentration and often can be described in a wide range of concentrations by a linear equation:

$$D_m = D_0 \cdot (1 + k_D \cdot c) \qquad (6)$$

The deviations of the time field correlation function from a straight line can be caused by polydispersity, and in the case of very large particles, also by internal modes of motion. Sometimes this distribution is very broad, and in such cases it makes more sense to plot the linear function $g_1(t)$ against the logarithm of time.

2.2.3.2 Small Angle X-ray Scattering (SAXS)[90]

Small Angle X-ray Scattering (SAXS) has become a powerful technique in colloidal science for determining size, shape and internal structure of polymer particles in the size range from a few nanometers up to about 100 nm. SAXS is mainly applied to systems of randomly oriented and statistically distributed structures of colloidal dimensions, such as latexes[93-95], supramolecular aggregates (e.g. micelles[96]), proteins[90], natural and synthetic high molecular weight polymers dispersed in solutions[97-99] or precipitates in amorphous materials[100, 101].

Apart from the structural analysis of single particles, the spatial and orientational arrangement of those particles in colloidal suspensions, determined by the interaction between them and by their form and symmetry, can also be studied by SAXS. SAXS is also suitable for analysis of supramolecular aggregates (such as micelles or self-assembling systems) and the origin of the aggregation. In fact, the intermolecular forces that hold small molecules together and arise from weak van der Waals, hydrophobic, hydrogen-bonding and screened electrostatic interactions[102], can be studied by SAXS. These investigations allow the determination of the internal structures of aggregates, e.g., the (in)homogeneity (distribution of electron density) inside micelles.

The physical principles of SAXS, SANS (small-angle neutron scattering) and light scattering (LS) are the same[90]. The electric field of the incoming wave induces dipole oscillations in the atoms. The accelerated charges generate secondary waves that add at large distanced (far field approach) to the overall scattering amplitude. All secondary waves have the same frequency but may have different phases caused by different path lengths.

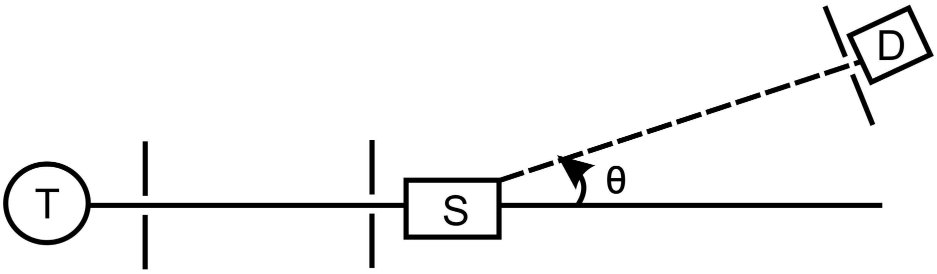

Figure 2.17. The essential parts of a small angle scattering system. The drawing shows the X-ray source T, the sample S, the scattering angle θ, the slits used to define the incident and scattered beams, and the detector D.

A schematic description of the scattering principle is shown in Figure 2.17. X-rays (or neutrons or light) from the source T are formed into a fine beam, often by slits, and strike the sample S. A small fraction of this beam is scattered in other directions (e. g., in Figure 2.17 an angle θ with the direction of the incoming beam). D is a detector, used to record the scattering intensity (the square of the scattering amplitude) and its dependence on the scattering angle. Information about the sample structure can often be obtained from the analysis of the scattering intensity at a sequence of scattering angles. The X-ray scattering intensity is experimentally determined as a function of the scattering vector q (as defined in Figure 2.18) whose modulus is given by $q = (4\pi/\lambda)\cdot \sin(\theta/2)$, where λ is the X-ray wavelength and θ is the scattering angle, the angle between the directions of the scattered and transmitted beams.

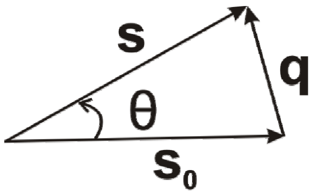

$$\mathbf{q} = \mathbf{s} - \mathbf{s}_0$$

$$q = |\mathbf{q}| = 2 \cdot |\mathbf{s}| \cdot \sin(\theta/2) = (4\pi/\lambda)\cdot \sin(\theta/2)$$

Figure 2.18. Definition of the scattering vector q. s and s_0 are unit vectors in the directions of the scattered or incident beam, respectively. θ denotes the scattering angle.

Macroscopically isotropic systems produce a scattering intensity which only depends on the modulus of q. In the special case of isotropic systems composed of isolated and identical particles embedded in a matrix with a constant electronic density (e.g. silica spheres in water), the normalized SAXS intensity I(q) is usually approximated by the product:

$$I(q) = N \cdot P(q) \cdot S(q) \tag{7}$$

where N is the number of particles per unit volume and P(q) is the scattering function of a single isolated particle given by:

$$P(q) = \int_0^\infty 4\pi \cdot r^2 \gamma(r) \frac{\sin qr}{qr} dr \tag{8}$$

where γ (r) is the correlation function given by:

$$\gamma(r) = \langle \int_V [\rho(r') - \rho_0][\rho(r + r') - \rho_0] dr' \rangle \tag{9}$$

where ρ(r) is the electronic density function inside the particle, ρ_0 is the constant density of the matrix and < > indicates an averaging for all particle orientations. S(q) is the orientation averaged effective structure function that accounts for the short range spatial correlation between them. Equation 7 is strictly valid for systems of not very concentrated spheres. It is also generally used as an approximation for anisotropic particles provided that the interparticle short range order and the orientational order of each particle are independent. This occurs in real cases when the particles are not very close one to each other. If the system is "dilute", i.e. the particles are far away from each other and without spatial correlation, then S(q) = 1 over the whole q range. On the other hand, is S(q) = 1 in the high q limit for any system of particles with short-range spatial correlation. Under these conditions, Equation 7 simplifies:

$$I(q) = N \cdot P(q) \tag{10}$$

For "two-electronic density systems" consisting of homogeneous particles with a constant electronic density ρ_1 (except the short wavelength modulation associated to individual atoms), and an also homogeneous matrix with a constant density ρ_0, the scattering function for a single particle is given by:

$$P(q) = (\rho_1 - \rho_0)^2 v \int_0^{D\max} 4\pi r^2 \gamma_0(r) \frac{\sin qr}{qr} dr \tag{11}$$

where v is the particle volume, D_{max} its maximum dimension and γ_0(r) is a function defined by <v(r)>/v, being <v(r)> the orientational average of the intersection between the volume of the particle and the same volume displaced by a vector r. The value of the integral only depends on the shape and size of the particle. Equation 11 implies that the function P(q) associated to particles embedded in a homogeneous matrix is equivalent to the same function corresponding to pores of same size and shape as the particles embedded in a homogeneous material, on condition that the difference in electronic density between both phases $\Delta\rho$ is in both cases the same (Babinet principle). The distance distribution function of the particle, $p(r) = \gamma_0(r) \cdot r^2$, can be determined from the scattering function of a single particle by:

$$p(r) = \frac{1}{\left[2\pi^2 (\rho_1 - \rho_0)^2 v\right] \cdot \int_0^\infty P(q) qr \sin qr \cdot dq} \tag{12}$$

For dilute systems, the function p(r) has positive nonzero values up to a maximum one, D_{max}, corresponding to the largest dimension of the particle. The function P(q) (Equation 11) has as asymptotic behaviour at small q given by:

$$P(q) = (\rho_1 - \rho_0)^2 v \cdot e^{-\frac{\langle Rg \rangle_G{}^2 q^2}{3}} \quad (q \to 0) \tag{13}$$

where v is the particle volume and R_g the radius of gyration of the particles defined by:

$$R_g = \left(\frac{1}{v} \int_V r^2 dV\right)^{1/2} \tag{14}$$

Equations 10 and 13 lead to the low-q asymptotic scattering function, I(q), corresponding to an isotropic dilute system of N identical particles per unit volume, given by Guinier´s law:

$$I(q) = N(\rho_1 - \rho_0)^2 v^2 e^{-\frac{\langle Rg \rangle_G{}^2 q^2}{3}} \quad (q \to 0) \tag{15}$$

Guinier’s law also applies to a dilute system of identical particles with a size distribution. In this case, the parameter $<R_g>_G$ corresponds to an average of the radius of gyration to which large particles contribute the most, given by:

$$\langle R_g \rangle_G = \left[\frac{\int [v(R_g)]^2 R_g{}^2 G(R_g) dR_g}{\int [v(R_g)]^2 G(R_g) dR_g} \right]^{1/2} \tag{16}$$

where $G(R_g)$ is the function that defines the size distribution of the particles. For any isotropic two-electronic density systems, dilute or concentrated (or even for a more general two-phase geometry), the asymptotic behaviour of I(q) at high q is given by Porod’s law:

$$I(q) = \frac{2\pi(\rho_1 - \rho_0)^2 S}{q^4} \quad (q \to 0) \tag{17}$$

where S is the surface area of the interface between the two phases. Equation 17 holds for all two-phase systems, provided that particles are not very thin disks or cylinders. In the particular case of a dilute solution of spherical particles with radius R, the scattering function P(q) (Equations 10 and 11) is given by:

$$I(q) = N(\rho_1 - \rho_0)^2 v^2 [\Phi(q)]^2 \tag{18}$$

with $\Phi(q) = \left[3(\sin qR - qR \sin qR)/(qR)^3\right]$. This function is characterized by a primary maximum at q = 0 and by oscillations at high q with weak secondary maxima located at $q \cdot R = 5.78, 9.05, \ldots$. In the case of identical spherical particles, the asymptotic scattering function at high q oscillates around a curve $I(q) \propto q^{-4}$, as predicted by Equation 17. These oscillations are damped for systems of spheres having a radius distribution with a small non-zero width and vanish for systems with a wide size distribution.

The scattering function of a dilute set of spherical particles with a radius distribution defined by G(R) is given by:

$$I(q) = \int_0^\infty G(R)P(q)dR = (\rho_1 - \rho_0)^2 \int_0^\infty G(R)\left[(4/3)\pi R^3\right]^2 [\Phi(qR)]^2 dR \qquad (19)$$

The function G(R), whose integral is equal to the number of particles per unit volume, N, can be determined from the experimental scattering functions by solving the integral Equation 19 using a numerical procedure. An integral property of scattering function that applies to two-density systems is given by:

$$Q = \int_0^\infty q^2 I(q)dq = 2\pi^2 (\rho_1 - \rho_0)^2 \phi(1-\phi)V \qquad (20)$$

where φ and (1-φ) are the respective volume fractions of both phases and V the irradiated volume. For a dilute system of N particles of volume v, Equation 20 becomes:

$$Q = 2\pi^2 N(\rho_1 - \rho_0)^2 V \qquad (21)$$

The scattering functions of very concentrated or strongly correlated particle systems exhibit a peak, which is more pronounced and shifts to higher q for increasing particle concentration. For concentrated systems, Equation 10 does not apply. Instead Equation 7 can be used to fit experimental results and so to determine the relevant structural parameters. Generally, the analysis of the results of scattering measurements of spatially correlated systems is rather difficult, particularly when both, the single particle scattering function P(q) and structure function S(q), are not known. One of the difficulties arising in data analysis is to establish the actual origin of the peak. The question to be answered is: Does the maximum correspond to P(q) (particles with a complex non-constant electron density), to S(q) (concentrated system of correlated particles) or to both functions?

In the particular case of nearly homogeneous particles, the peak shape of I(q) corresponds to the structure function S(q). Semiquantitative analysis of scattering data yields a structural parameter, d_s, corresponding to the average distance between particles, given by:

$$d_s = \frac{2\pi}{q_m} \qquad (22)$$

where q_m is the q value corresponding to the maximum of scattering intensity. Equation 22 is not exact for disordered systems because the average distance also depends on the particular type of arrangement around each particle. Nevertheless it can be applied as a useful semiquantitative estimation in order to characterize trends in structural transformations. A particular case of a correlated particle system is that in which primary particles build up a so-called fractal object. The structure function associated to this system is given by:

$$S(q) = 1 + \frac{1}{(qa)^D} \cdot \frac{D\Gamma(D-1)}{\left(1 + \frac{1}{q^2\zeta^2}\right)^{\frac{D-1}{2}}} \cdot \sin\left[(D-1)\tan^{-1}(q\zeta)\right] \qquad (23)$$

where a is the radius of the (assumed spherical) primary particles, ξ is the correlation length or size parameter of the fractal object, D is the fractal dimension of the structure and Γ is the gamma function. If the primary particles that build up the fractal object are very small (a << ξ), the single particle scattering function P(q) of Equation 13 can be approximated by a constant value:

$$P(q) = (\rho_1 - \rho_0)^2 v^2 \qquad (24)$$

Assuming the composite material consisting of N fractal objects per unit of volume, without spatial correlation between them, and that each fractal aggregate is composed of very small primary particles (a << ξ) of volume v, the scattering intensity (Equation 7) is given by:

$$I(q) = N(\rho_1 - \rho_0)^2 v^2 S(q) \propto S(q) \qquad (25)$$

where S(q) is the intra-aggregate structure function defined by Equation 23 and N is the number of fractal objects per unit volume. Within the range 1/ξ < q << 1/a, Equation 25 becomes a simple power law:

$$I(q) \propto q^{-D} \qquad (26)$$

For q values close to or larger than 1/a, the assumption of a constant value for the scattering function of a primary particle (Equation 24) is not acceptable. Using a better approximation for the single particle scattering function P(q), the scattering intensity eventually reaches the asymptotic Porod range and so becomes proportional to q^{-4} (Equation 17).

At small q ($q \leq 1/\xi$), I(q) exhibits a Guinier-type behaviour (Equation 15) and therefore the radius of gyration of the isolated fractal aggregates, R_g, can easily be determined from experimental results. This parameter is related to the correlation length ξ of the fractal objets by:

$$R_g = \left[\frac{D(D+1)}{2} \right]^{\frac{1}{2}} \zeta \tag{27}$$

The equations mentioned in this section can be considered as the basic background needed to understand procedures often used to infer low-resolution (superatomic) structural information from experimental scattering data. The procedure of data evaluation corresponding the scattering patterns obtained within this work will be explained in section 3 more in detail.

2.3 Synthesis of polymers with tailored dimensions and shapes

A particularly challenging aspect of polymer synthesis concerns the development of techniques for the preparation of macromolecular materials with well defined structures. An essential requirement for many applications is the precise control of copolymer structure in terms of composition, molecular weight, molecular weight distribution (polydispersity index), or balance between hydrophilic and hydrophobic segments, e. g. in the synthesis of polymeric surfactants for the production of porous frameworks. Additionally, it is well known that solution and bulk properties of a polymer are drastically influenced by its architecture and differ significantly for linear and non-linear structures with similar molecular weight. Synthetic strategies leading to these tailored macromolecules depend strongly on the target architecture.

2.3.1 Controlled Polymerization Techniques (CPT)

As mentioned before, one of the main goals in modern synthetic polymer chemistry is to prepare polymers and copolymers with predictable, well-defined molecular weights, narrow molecular weight distribution, desired architecture and functional groups or active molecules at well-defined locations of the polymeric chain. A polymerization process is based on a repetitive reaction in which a monomer is converted into a polymer segment. For this purpose, it is possible to choose from a variety of synthetic processes. Each method has its strengths and weaknesses. Therefore, many factors have to be taken into account before starting the synthesis. However, the ambitious goals mentioned before can only be fulfilled via controlled/living polymerization techniques. SZWARC *et al.*[104] proposed the term living polymers for those macromolecules which spontaneously continue their growth whenever fresh monomer is supplied to the system. Thus, all active centres generated upon initiation step remain active and the polymer chains grow until all monomers are consumed, and continue their linear growth, whenever fresh monomer is added to the system. Two conditions have to be fulfilled so that such behaviour could be observed. First, no side reactions such as termination or chain transfer should occur in the system. Secondly, the rate of initiation of the polymerization has to be faster or at least comparable to the rate of propagation. Under those conditions any single initiator molecule initiates simultaneously polymerization, and all chains start growing at the same time.

In practice the term living is applied to polymerization systems, in which the rates of side reactions and of termination caused by presence of impurities are sufficiently slow to permit successful completion of a desired task. Under such conditions, polymers with controlled molecular weights and narrow molecular weight distributions can be obtained. Taking these facts into account, ideal controlled polymerizations fulfil the following criteria:

- ***The molecular weight can be adjusted via the monomer to initiator ratio.*** Since in living systems initiation is quantitative, tailoring of the molecular weight of the products is based on the variation of the amount of added initiator. As side reaction are suppressed, all molecules are allowed to grow under the same conditions and hence the degree of polymerization (P_n) of the product formed by this technique is given as the ratio of the total number of added monomer $[M]_0$ to the total number of active centres. Taking into account the quantitative initiation (i.e. one living polymer chain per initiator molecule), the total number of active centres corresponds to concentration of initiator $[I]_0$ and at full conversion of the monomer the P_n of the product can be then described as presented in equation:

$$P_n = \frac{[M]_0}{[I]_0}$$

with:
P_n – degree of polymerization of the polymer
$[I]_0$ – concentration of initiator
$[M]_0$ – the initial amount of added monomer

- ***The degree of polymerization increases with the conversion in a linear way.*** The degree of polymerization of polymers obtained by controlled polymerization techniques increases linearly with conversion since all macromolecules grow proportionally to the amount of monomer consumed. At given period of time P_n of the product can be thus calculated according to the equation:

$$P_n = \frac{[M]_0 - [M]_t}{[I]_0}$$

- The polymerization reaction shows a ***first order kinetic*** with respect to the concentration of monomer. Thus, if plotting the term $\ln[M]_0/[M]_t$ versus the reaction time (t), the dependence is linear.

- Another common criterion used for polymer characterization is the polydispersity index (M_w/M_n), which refers to the unity of polymer chains length in the sample. For living polymerizations with fast initiation the ***polydispersity index decreases with increasing conversion***. This is due to the fact that at the beginning of the process the equilibrium between the active propagating intermediates and their complexes has not been yet properly established. As soon as this equilibrium has been achieved, uniform chain growth can take place.

- The lowest value for the ***polydispersity index*** that can be achieved by conventional radical polymerization is around 1.5[105]. Thus, if dealing with controlled radical polymerizations, polydispersity indexes are clearly below this value.

The field of controlled polymerizations was opened in 1956 by SZWARC *et al.*[104] with the discovery of the living anionic polymerizations. This technique was proven to ensure the control over molecular weight, molecular weight distribution as well as the architecture of the synthesized products. However, the demanding conditions such as high purity of monomers, exclusion of oxygen and moisture, and requirements of highly sophisticated equipment made these techniques difficult. Thus, the discovery of this method was followed by several attempts to find analogous living cationic systems. SAWAMOTO *et al.*[106] proved in 1984 that polymerization with carbocations also can take place under a controlled mechanism yielding products with similar properties to those obtained by living anionic polymerizations. Control of the free radical polymerization by a fast established dynamic equilibrium between active free radicals and their dormant complexes was proposed by OTSU *et al.*[107] in 1982. Further investigations on this topic have crystallized in the widely used today living/controlled free radical polymerization systems. These systems include methods such as the nitroxide-mediated polymerization (NMP), the atom transfer radical polymerization (ATRP) and the reversible addition-fragmentation transfer (RAFT). The methods differ from each other in the way how the concentration of radicals is diminished. Finally, the living character of ring-opening polymerizations, which was firstly proven by PENCZEK *et al.*[108], must be pointed out. On this regard, the cationic ring-opening polymerization of cyclic iminoethers will be treated within the following section. As will be shown, the controlled character of this polymerization depends on the suitable establishment of a dynamic equilibrium between ionic propagating species and covalent intermediates. The adjustment of the reactivity of both, monomer and initiator plays a crucial role in the achievement of this equilibrium.

2.3.2 Cationic Ring-Opening Polymerization (CROP) of oxazolines

A large variety of heterocyclic monomers can be polymerized by a cationic ring-opening polymerization (CROP) mechanism[108]. However, only a limited number of these polymerizations provide the possibility to prepare well-defined polymers, i.e. with predictable molecular weights and polydispersities, known micro- or macrostructures, and having known functional end groups. Whether a polymerization leads to such well-defined polymers or not, depends on the reaction mechanism of polymerization and more particularly on the occurrence of chain transfer and / or termination reactions.

As explained in the section dealing with diatoms, besides silaffins, polyamines have also been found attached to the silica-based framework. Hyperbranched polyethyleneimine (PEI) is a commercially available polyamine which can be easily synthesized via cationic ring-opening polymerization of aziridine as shown in Figure 2.19.

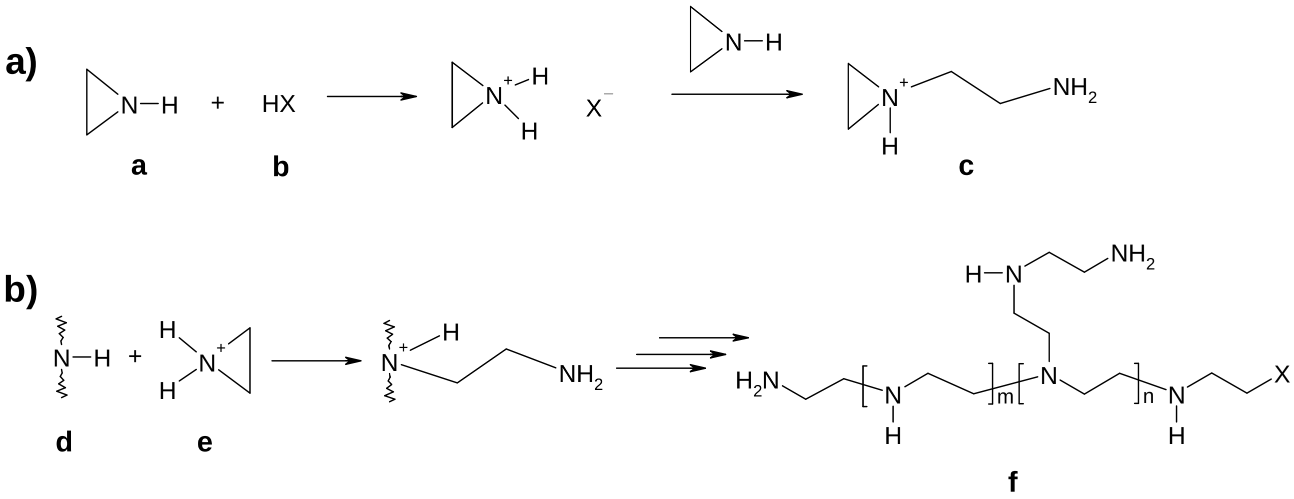

Figure 2.19. Mechanistic pathway of the Cationic ring-opening polymerization of aziridine to hyperbranched PEI[109].

As can be observed, the initiation step (Figure 2.19-a) involves the nucleophilic attack of the monomer **a** by a protic acid **b** resulting in the formation of a dimer **c**. Subsequent addition of monomer leads to the formation of a linear polymer. Moreover, the transfer of protons between the dimers and other amino groups is also possible and leads to the formation of uncharged alkylenediamines. Further chain growth (Figure 2.19-b) enables the formation of secondary amino groups **d** which can react with aziridinium cations **e**. Subsequent chain transfer results in the formation of branching points. As a result, the final product **f** possesses 20-30 % of branching points.

However, the structure of these hyperbranched polyamines differs considerably from those isolated in diatoms. As mentioned before, SUMPER *et al.* and KRÖGER *et al.* have reported the isolation of linear polyamines with low molecular weights from these marine organisms[58, 110-112]. For this reason, another synthetic pathway different from the CROP of aziridines has to be chosen in order to produce polyamines resembling those isolated in diatoms. In this respect, the cationic ring-opening polymerization of cyclic iminoethers (which bear O-C-N bonds) represents a suitable synthetic route towards the linear low molecular weight polyamines[113]. Many of these compounds have been successfully polymerized, oxazolines (Figure 2.20-a) and 1,3-oxazines

(Figure 2.20-b) play a crucial role within this work, since subsequent modification reactions (e.g. hydrolysis and methylation) of the produced polymers yield linear polyamines similar to those found in diatoms[109, 113-120].

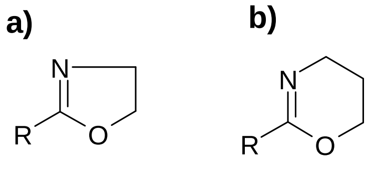

R = H, methyl, ethyl, phenyl, etc.

Figure 2.20. Oxazoline (a) and 1,3-oxazine (b) monomers used in cationic ring-opening polymerizations.

The cationic ring-opening polymerization (CROP) of 2-oxazolines (Figure 2.21) was firstly established in the sixties of the last century[109, 113]. Different chemicals such as Lewis acids (e.g. BF_3OEt_2, $AlCl_3$, $TiCl_4$), strong protic acids and related salts, esters and anhydrides (e.g. $HClO_4$, $CF_3SO_3CH_3$, HBr), alkylhalogenides (e.g. CH_3I, $C_6H_5CH_2Cl$) and even electron acceptor functionalities (e.g. tetracyanoethylene) have been used as initiators in this process. The resulting macromolecules range from the hydrophilic poly(N-formylethylene)imine ($R^1 = H$) to the increasingly hydrophobic poly(N-acylethylene)imine (R^1 = alkyl). The longer the alkyl chain, the more hydrophobic the resulting polymer.

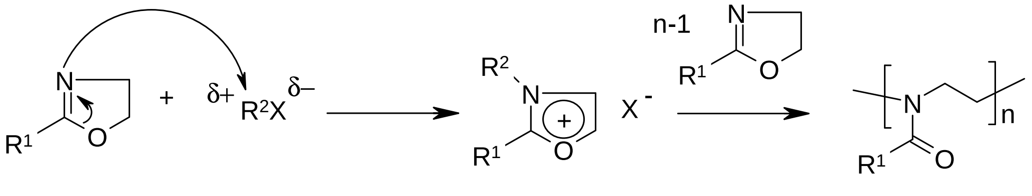

R1 = H, methyl, ethyl, phenyl, etc.

Figure 2.21. Cationic ring-opening polymerization of 2-oxazolines[116].

Concerning the mechanism of the CROP of cyclic iminoethers, two different pathways for the propagation step have been proposed[109, 113]. The occurrence of those propagation pathways depends on different variables such as nucleophilic character of the initiator counterion (X^-), substituent in the monomer (R[1]), solvent and temperature[116]. Both propagating routes are shown in Figure 2.22.

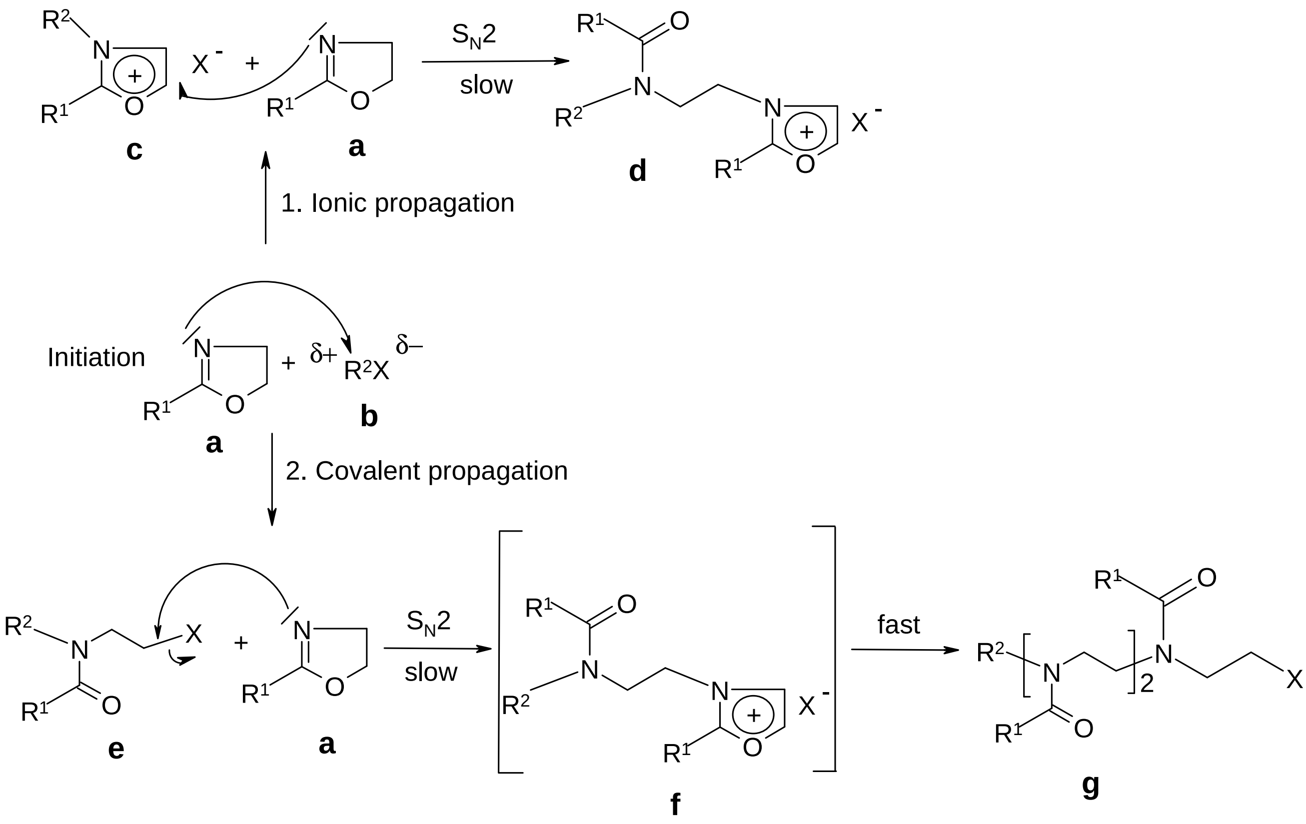

Figure 2.22. Mechanistic pathway of the cationic ring-opening polymerization of 2-oxazolines showing ionic and covalent propagating species[116].

As can be observed in route 1 of Figure 2.22, if the propagation step consists of a S_N2-ion-dipole reaction, an ionic propagating intermediate is formed. In the initiation step, the free electronic pair at the nitrogen atom in the oxazoline **a** attacks the positively polarized carbon atom in the initiator molecule **b** yielding the cationic oxazolinium intermediate **c** and the nucleophilic counterion of the initiator X^-. Further addition of monomer takes place in the subsequent propagating steps via nucleophilic attack of the cationic oxazolinium intermediate **c** by the free electronic pair in the oxazoline **a**. This nucleophilic attack causes the ring-opening and as a consequence the formation of the carbonyl group in the intermediate **d**.

On the contrary, if the propagation step consists of a S_N2-dipole-dipole reaction, a covalent propagating intermediate is formed (see route 2 in Figure 2.22)[113]. The propagating intermediate

e is not positively charged but bears the counterpartner X of the initiator attached to a carbon atom. This carbon atom is positively polarized and hence can be attacked by the free electronic pair of the nucleophilic monomer **a**. The resulting cationic oxazolinium intermediate **f** is very unstable and reacts with the strong nucleoplilic counter anion X^-, which builds the carbonyl group of the final molecule **g** via ring-opening.

As remarked previously, the occurrence of each propagation pathway depends on different variables. The nucleophilic character of the initiator counter anion (X^-), the substituent in the monomer (R^1), solvent and temperature are those variables which have been investigated intensively[116]. In this respect, the relative nucleophilic reactivities of monomer and counter anion of the initiator seem to play a crucial role and have been therefore established as shown in Figure 2.23.

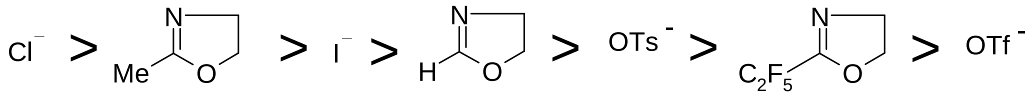

Figure 2.23. Comparison of nucleophilic reactivities of monomers and counter anions used in CROP[121].

Based on kinetic and spectroscopic studies, the nature of the propagating intermediates in the ring-opening polymerization of a family of 2-oxazoline monomers with different cationic initiators was investigated by SAEGUSA *et al.* as summarized in Table 2.2[121].

Table 2.2: Type of propagating species in the CROP of oxazolines[121].

M X⁻			← Nucleophilicity			
	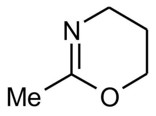	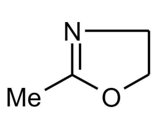	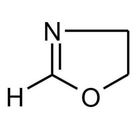	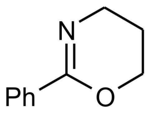	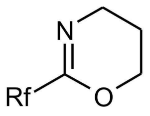	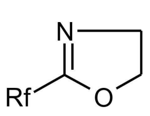
Cl⁻	C	C	C	-	-	-
I⁻	I	I	C	C	C	C
OTs⁻	I	I	I	I	C	C
OTf⁻	I	I	I	I	I	I

I = ionic species, C = covalent species.
R_f = fluorocarbon chain.

It can be easily recognized that the nucleophilicity of the monomer is strongly dependent on the substituent at the 2-position. Electron-donating groups (e.g. methyl) increase the nucleophilicity, while electron-accepting ones (e.g. fluorocarbon chains, aromatic groups) tend to stabilize the ring and hence reduce its opening tendency. As a general conclusion it was found that if the monomer possesses a higher nucleophilic character than the initiator counterion (e.g. unsubstituted-2-oxazoline and methyl tosylate[113]) the propagating species are predominantly ionic. On the contrary, if the nucleophilic reactivity of the initiator counter anion is higher than that of the monomer, the polymerization occurs under a covalent propagating mechanism (e.g. unsubstituted-2-oxazoline and methyl iodide). Futhermore, it is important to note that in some polymerizations (5-methyl-2-oxazoline initiated with methyl iodide[113] and 2-methyl-2-oxazoline initiated by benzyl bromide[122]) both, covalent and ionic propagating species have been found to be present in equilibrium. The reason for this coexistence of the propagating species may be related to the comparable nucleophilic character of monomer and initiator counter anion in those cases (as can be seen in Figure 2.23 with 2-methyl-2-oxazoline and iodide). Within some of these investigations[122] it was also proven that the ionic propagating species are those which mostly contribute to the chain growth. This fact could explain the controlled character observed in CROP of 2-oxazolines via kinetic measurements[109, 113, 114, 123], which allows the production of polyamine chains with well defined dimensions and narrow molecular weight distributions. The controlled character is then provided by the establishment of an equilibrium between ionic species, which are active in terms of chain growth, and covalent species, which hardly contribute to chain growth.

The reaction conditions (initiator counter anion, temperature, solvent) must be chosen so that this equilibrium is shifted towards the covalent (non-active) centers. Further investigations on this topic performed by HOGENBROOM *et al.*[124] have also proven that the controlled character of the CROP of 2-oxazolines depends not only on the initiator counter anion but also on the temperature. This fact would explain the occurrence of controlled polymerizations of monomers with higher nucleophilic character than that of the initiator counter anion. From the experimental point of view, as any controlled polymerization, CROP is extremely sensitive to impurities. In order to keep the controlled character, the polymerization must be carried out with high purity reagents and in the absence of oxygen and water since any traces of moisture lead to termination of the growing chains.

The polymerizability of the monomer has been found to be governed by two factors, i.e. the nucleophilicity of the monomer (listed in Table 2.2) and the ring-opening tendency of the propagating species[113]. The ring-opening tendency of the propagating species seems to exert a stronger influence[113] and is related to both, the 2-substituent and the number of members in the ring. The presence of electron-donating groups (e.g. alkyl chains) as 2-substituents tend to stabilize the positively charged onium species and reduces the ring-opening tendency. Monomers with a high number of members in the ring undergo lower hoop stress and stronger steric effects and therefore show a lower ring-opening tendency. For these reasons, the polymerization of oxazoline (5-membered ring) proceeds faster than that of oxazine (6-membered ring) in the presence of the same initiator, in spite of the higher nucleophilic reactivity of the second one[125].

3 Results and Discussion

3.1 Synthesis and modification of amphiphilic polymers

3.1.1 Introduction

The interest in the synthesis and characterization of amphiphilic block copolymers has increased within the last decades due to their unique molecular structure consisting of two polymeric chains with different chemical nature. This coexistence of chains with different chemical affinities within the same molecule enables self-assembly in solution resulting in different types of supramolecular aggregates. As a consequence, these structures have become a valuable polymeric material playing an important role in a great variety of technical applications such as hydrogels, stabilizers, structure directing agents or emulsifiers, among others[126, 127]. Several synthetic strategies leading to the production of linear block copolymers have been reported, including those based on the use of bifunctional- and macroinitiators[128]. Furthermore, several attempts have been performed to produce linear polymeric surfactants. SAEGUSA *et al.* reported the synthesis of amphiphilic poly(N-(acyl)-alkyleneimine)-based AB diblock copolymers[129] by CROP of cyclic iminoethers. The hydrophilic or hydrophobic character of each poly(N-(acyl)-alkyleneimine) segment is determined by the 2-substituent R^1 in the monomer as shown in Figures 2.19 and 2.20. In this regard, methyl for the hydrophilic block and phenyl for the hydrophobic one are the usual choices for the R^1 substituent. Other synthetic strategies towards the production of non-ionic surfactants from cyclic iminoethers are the initiator and end-capping methods and have been reported by SAEGUSA *et al.* too[130, 131]. Here, the hydrophobic segment is usually a long alkyl chain which can be introduced as a group attached to the initiator –“initiator method”–, or by a termination reaction of the living chain end –“end-capping method”–. The hydrophilicity of the poly(N-(acyl)-alkyleneimine), which depends on the 2-substituent R^1, in combination with the hydrophobicity of alkyl chains provides easy access to amphiphilic structures. The resulting amphiphilic non-ionic prepolymers can be then easily converted into polyamines via alkaline hydrolysis[132]. The polyamine-based surfactants produced in this way represent a biomimetic approach as silica precipitating polymers since they bear functional groups similar to those of the biomolecules isolated from diatoms. Moreover, as reported in section 2.3.1, the controlled character of these cationic ring-opening polymerizations enables the synthesis of poly(N-(acyl)-alkyleneimine) chains with tailored dimensions.

Taking all these ideas into account, the CROP of cyclic iminoethers with an alkyl-bearing cationic initiator along with different modification reactions has been chosen within this work as the synthetic strategy towards the target linear polymeric surfactants. Figure 3.1 shows the steps and compounds of this synthetic strategy in a more detailed way.

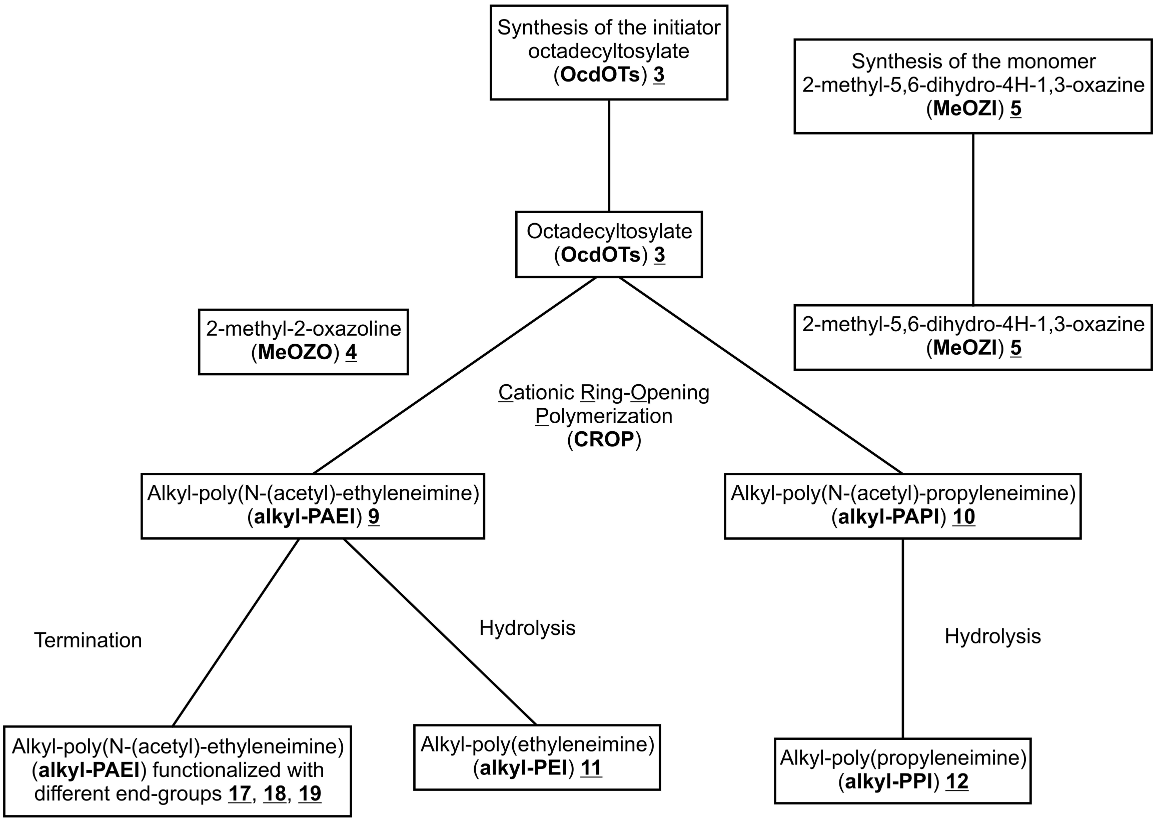

Figure 3.1. Synthetic scheme leading to the production of different linear polymeric surfactants.

As can be observed, it involves the synthesis of both, initiator and monomer as well as the cationic ring-opening polymerizations and the following modification reactions. The development of these steps is reported within this section.

3.1.2 Initiators

As commented previously, the initiator represents an important element and must be hence carefully chosen. It must provide both the hydrophobic segment of the surfactant and a suitable group for the CROP of 2-oxazolines. Regarding the initiating group, kinetic investigations performed by HOGENBROOM *et al.*[124] have proven the living character of the polymerization of

2-methyl-2-oxazoline (MeOZO) with methyltosylate as initiator at 80 and 100 °C. Its controlled character allows to tailor the chain-length by adjusting the monomer to initiator ratio and the reaction time. It can be therefore expected that other alkyl- tosylates behave in similar way, yielding amphiphilic polyamines with well-defined chain lengths for the hydrophilic segment. Under this approach, 1-octadecyltosylate (OcdOTS) would be a suitable choice as initiating system. Furthermore, VOLET *et al.* have reported the synthesis of the target amphiphilic n-octadecyl-poly(N-(acetyl)-ethyleneimine) via ring-opening polymerization of MeOZO with the cationic initiator n-octadecyliodide, which is commercially available[117]. Some other alkyliodides are also commercially available[117]. However, the synthetic route suggested within this work possesses a more versatile character since it allows the production of suitable initiating systems with any chain-length for the hydrophobic alkyl substituent. As a result, the synthesis of amphiphilic alkyl-polyamines with any chain-length for both, hydrophilic and hydrophobic segments can be achieved.

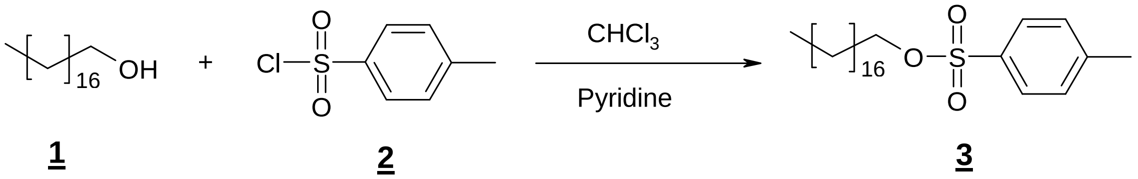

Figure 3.2. Synthesis of the alkyl-bearing initiator 1-octadecyltosylate (**OcdOTs**) **3** via esterification of 1-octadecanol **1** with tosyl chloride **2**.

As can be observed in Figure 3.2, 1-octadecyltosylate **3** was synthesized by esterification of 1-octadecanol **1** with tosyl chloride **2** following a procedure of HORSTMANN[6]. Esterifications usually take place in excess of the alcohol[133]. However, in this case the reaction was optimized to take place in excess of the other main reagent, tosyl chloride, since 1-octadecanol was extremely difficult to remove from the reaction solution. A complete removal of 1-octadecanol was necessary because small traces of alcohol can interrupt cationic ring-opening polymerizations. Unlike 1-octadecanol, non-reacted tosyl choride could be easily removed from the reaction solution by recrystallization, giving pure, white 1-octadecyltosylate with 44 % yield referred to the initial amount of 1-octadecanol.

3.1.3 Monomers

The cationic ring-opening polymerization (CROP) of cyclic iminoethers with subsequent modification reactions represents a suitable synthetic route leading to macromolecular templates for silica precipitation, as already mentioned. The resulting polymers bear functional groups resembling those found in the biomolecules associated to diatoms. In fact, Saegusa *et al.*[132] and Tanaka *et al.*[134] synthesized linear poly(ethyleneimine) (PEI) and poly(propyleneimine) (PPI) via CROP of 2-methyl-2-oxazoline (MeOZO) and unsubstituted-5,6-dihydro-4H-1,3-oxazine (OZI), respectively and a subsequent hydrolysis reaction. Within those investigations, the modification of the prepolymers via a reductive methylation reaction yields the derivates poly(methylethyleneinime) (PMEI) and poly(methylpropyleneimine) (PMPI).

In this work, 2-methyl-2-oxazoline (MeOZO) **4** and 2-methyl-5,6-dihydro-4H-1,3-oxazine (MeOZI) **5**, both shown in Figure 3.3, have been chosen as monomers for cationic ring-opening polymerization with the alkylinitator 1-octadecyltosylate (ocdOTs) **3**.

4 **5**

Figure 3.3. Chemical structure of the monomers 2-methyl-2-oxazoline (**MeOZO**) **4** and 2-methyl-5,6-dihydro-4H-1,3-oxazine (**MeOZI**) **5**.

The choice of 2-methyl-5,6-dihydro-4H-1,3-oxazine (MeOZI) instead of unsubstituted-5,6-dihydro-4H-1,3-oxazine (OZI) as monomer for the CROP is based on several considerations. Within this work, not only alkyl-PEI and alkyl-PPI are going to be characterized regarding their aggregation behaviour, but also the corresponding non-ionic prepolymers (alkyl-poly(N-(acyl)-alkyleneimines). Along with the fact that alkyl-PEI and alkyl-PPI only differ in the alkyl spacing group, the corresponding prepolymers can also differ in the substituent R^1 attached to the carbonyl group of the repeting unit. This substituent R^1 is determined by selection of the monomer, OZI or MeOZI. As already mentioned in section 2.3.1, the hydrophilic or hydrophobic character of the poly(N-(acyl)-alkyleneimine) depends strongly on this substituent. Therefore, in order to compare the prepolymers regarding their aggregation behaviour, they should bear the same substituent R^1 so that the expected differences originate only from the spacing group, as in case using alkyl-PEI and alkyl-PPI. From that point of view, the analogue molecular structure of alkyl-poly(N-(acetyl)-ethyleneimine) (alkyl-PAEI) is alkyl-poly(N-(acetyl)-propyleneimine) (alkyl-PAPI) and not alkyl-poly(N-(formyl)-propyleneimine) (alkyl-PFPI).

Another aspect that should be taken into account when selecting the monomer is the synthetic procedure for both OZI and MeOZI. HORSTMANN[6] performed the synthesis of OZI via cyclization of 3-amino-1-propanol with *tert.*-butylisocyanide by the method of SAEGUSA *et al.*[135]. However, during the course of reaction, *tert.*-butylamine, which could not be completely removed from the reaction solution, formed as side product. The remaining amount of this compound acted as termination reagent in the subsequent CROP, interrupting the chain growth. On the contrary, the synthesis of MeOZI **5** performed by CORNELIUS[125] using the procedure of LEE *et al.*[136] did not include those problems. As can be observed in Figure 3.4, it involved the reaction of 3-amino-1-propanol **6** with acetonitrile **7** in the presence of zinc chloride as catalyst.

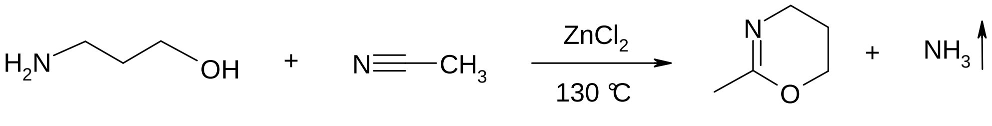

6 **7** **5** **8**

Figure 3.4. Synthesis of 2-methyl-5,6-dihydro-4H-1,3-oxazine (**MeOZI**) **5** according to LEE *et al.*[136].

Ammonia **8** formed in the course of reaction as side product but it can be completely removed by vacuum distillation. Apart from that, no further side products, which could act as termination reagents in the subsequent CROP, are formed. The reaction gives pure MeOZI **5** in 62 % yield.

3.1.4 Cationic Ring-Opening Polymerization (CROP)

The following step towards the production of the target amphiphilic alkyl-polyamines consists of the CROP of the monomers MeOZO **4** and MeOZI **5** with the alkyl-bearing initiator 1-octadecyltosylate **3** as it is shown in Figure 3.5. The resulting prepolymers are the non-ionic alkyl-poly(N-(acetyl)-ethyleneimine) (alkyl-PAEI) **9** and alkyl-poly(N-(acetyl)-propyleneimine) (alkyl-PAPI) **10**.

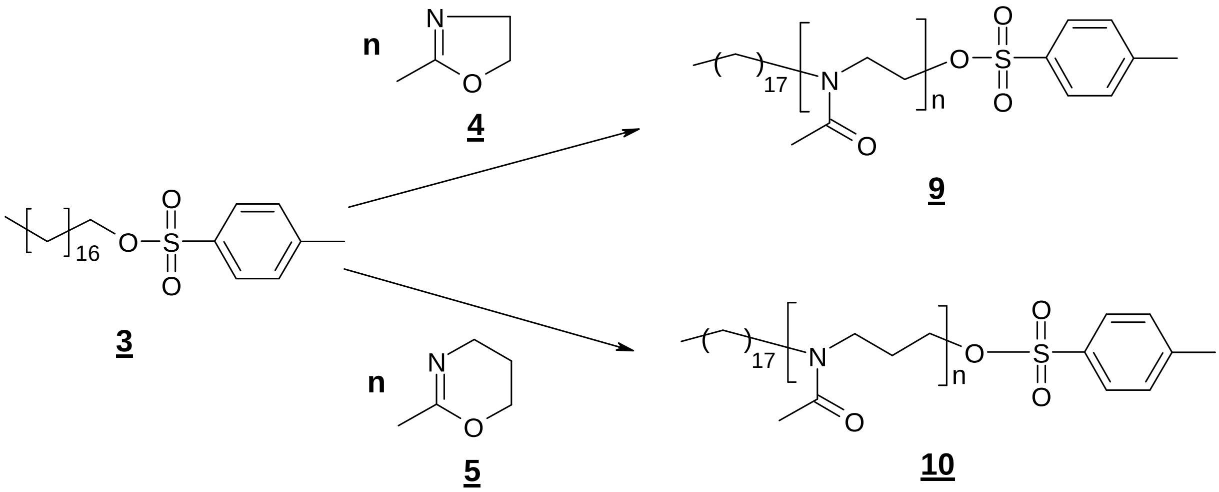

Figure 3.5. Cationic ring-opening polymerization of **MeOZO** **4** and **MeOZI** **5** with 1-octadecyltosylate (**OcdOTs**) **1** yielding the prepolymers alkyl-poly(N-(acetyl)-ethyleneimine) (**alkyl-PAEI**) **9** and alkyl-poly(N-(acetyl)-propyleneimine) (**alkyl-PAPI**) **10**.

Table 3.1 lists the results and experimental conditions for a set of polymerizations of the monomers MeOZO **4** and MeOZI **5** with 1-octadecyltosylate **3** as cationic initiator. Regarding the temperature, kinetic investigations have proven that the cationic ring-opening polymerization of MeOZO **4** with different initiators like methyltosylate, methyltriflate, benzyl bromide and methyl iodide were controlled and with high polymerization rates at temperatures between 80 °C and 100 °C[137]. Therefore the polymerizations with MeOZO as monomer were initially carried out at 80 °C in benzonitrile (BN) or N,N-dimethylformamide (DMF) and for 22 h (samples **9.1**, **9.2** and **9.3** in Table 3.1). Under those conditions the reaction solution became solid, even in sample **9.3** where a higher volume of BN was used. The resulting material was soluble neither in polar nor in non-polar solvents. Such a physical crosslinking of block copolymers by self-association in solution has already been described in the literature[138, 139] and seems to be the most likely reason for the gelation observed during the polymerization.

Table 3.1. Results and experimental conditions corresponging the CROP of the monomers **MeOZO** **4** and **MeOZI** **5** with 1-octadecyltosylate (**OcdOTs**) **3** as initiator.

Sample	Monomer (M)	Solvent (S)	M/S, V/V	T, °C	t, h	P_n[a]	P_n[b]	T_g[c], °C
9.1[d]	MeOZO	BN	1/1	80	22	20	21	61-66
9.2[d]	MeOZO	DMF	1/1	80	22	20	19	61-65
9.3[d]	MeOZO	BN	1/2	80	22	20	22	54-56
9.4	MeOZO	DMF	1/2	90	8	20	21	63-66
9.5	MeOZO	DMF	1/1	80	8	10	11	54-59
9.6[d]	MeOZO	BN	1/1	80	4	10	11	55-58
9.7	MeOZO	DMF	1/2	90	16	40	26	64-69
9.8	MeOZO	DMF	1/2	90	24	40	39	63-67
10.1	MeOZI	DMF	1/1	80	24	10	11	7-11
10.2	MeOZI	DMF	1/1	80	24	20	19	16-20

a, fixed with the monomer to initiator ratio.
b, calculated from ^{1}H-NMR analysis by comparing the integrals corresponding the signals of the aliphatic protons in the monomer and the aromatic ones in the initiator.
c, first and second heating curve, respectively.
d, reaction solution became solid.

In order to prevent the solidification of the reaction solution, the polymerization time was decreased. It can be observed that samples **9.4** and **9.5**, where polymerization was carried out in DMF for 8 h, did not undergo any solidification. On the contrary, sample **9.6**, where BN was employed as solvent, became solid after 4 h. These facts confirm that both, solvent and reaction time, are the most important aspects to be controlled in order to prevent the solidification of the polymerization media. Thus, by using DMF instead of BN as solvent, the solidification of the reaction media takes places after longer reaction times. However, too long reaction times, as can be observed in samples **9.1**, **9.2** and **9.3**, can also cause solidification of the system while too short ones make it impossible to reach the required degree of polymerization P_n. Therefore, there is an optimum reaction time depending on the desired degree of polymerization. Samples **9.4**, **9.5** and **9.8** fulfill these requirements since solidification of the reaction medium did not take place and the degree of polymerization determined by ^{1}H-NMR is in good agreement with the one calculated from the monomer to initiator ratio. It can be then concluded that reaction times of 8 hours are sufficient to obtain polymer chains with 10 and 20 repeating units. However, to reach a degree of polymerization of 40 units, 24 h are required. Such a long reaction time is also required for the CROP of MeOZI yielding alkyl-poly(N-acetyl-proplymeimine), which corresponds to samples **10.1** and **10.2**, with degrees of polymerization 10 and 20. For those samples, the polymerization was carried out at 80 °C in DMF as solvent. The degrees of polymerization determined by ^{1}H-NMR were in good accordance with those fixed from the monomer to initiator ratio. This agreement between theoretical and experimental P_n values was also reported by CORNELIUS[125] and HORSTMANN[6] in the CROP of MeOZI and OZI with methyl tosylate. Those polymerizations were carried out under the same reaction conditions as for samples **10.1** and **10.2**, i. e. DMF as solvent, 80 °C and 24 h.

The thermal properties of the produced alkyl-poly(N-(acetyl)-alkyleneimine)s have also been investigated. For this purpose, their glass transition temperature T_g (Table 3.1) was measured by differential scanning calorimetry (DSC). The alkyl-PAEI samples, **9.1** to **9.8** in Table 3.1, showed T_g values between 54 and 69 °C. The differences between the samples can be ascribed to the different length of the polymer chains. In fact, except for sample **9.3**, it can be observed that T_g increases by increasing the degree of polymerization P_n of the chain. However, the T_g values reported in the literature for poly(N-(acetyl)-ethyleneimine) are around 80 °C[140]. It can be envisioned that the deviation in the T_g values obtained within this work may be caused by the presence of the long alkyl group attached to the polymer chain. However, pol(N-(acetyl)-ethyleneimine) samples with P_n between 8 and 43 synthesized by HORSTMANN[6] showed similar T_g values, concretely between 57 and 63 °C, to those of alkyl-PAEI. Hence, the alkyl chain does not seem to exert a substantial influence on T_g. The reason for this deviation may be then found in the fact that the T_g value reported in the literature was obtained by dynamic mechanical methods and not by DSC as in this work and in the work of HORSTMANN[6]. A similar behaviour was observed for alkyl-poly(N-(acetyl)-propyleleimine) (alkyl-PAPI) (samples **10.1** and **10.2**). Here, the T_g values obtained by DSC are between 7 and 20 °C. As can be recognized, they are slightly lower than those reported in the literature[140], which are around 30 °C. Furthermore, as for alkyl-PAEI, T_g increases with increasing P_n.

3.1.5 Modification reactions: hydrolysis and termination

SAEGUSA *et al.* reported the production of linear poly(ethyleneimine) (PEI) and poly(propyleneimine) (PPI)[115, 120]. The synthetic route described within those investigations involved the CROP of cyclic iminoethers with subsequent alkaline hydrolysis. This method provides relatively high amounts of polymers with functional groups resembling those of the biomolecules found in diatoms. In a similar way, the alkyl-PAEI **9** and alkyl-PAPI **10** prepolymers are subsequently converted into the amphiphilic alkyl-poly(ethyleneimine) (alkyl-

PEI) **11** and alkyl-poly(propyleneimine) (alkyl-PPI) **12** via alkaline hydrolysis as shown in Figure 3.6.

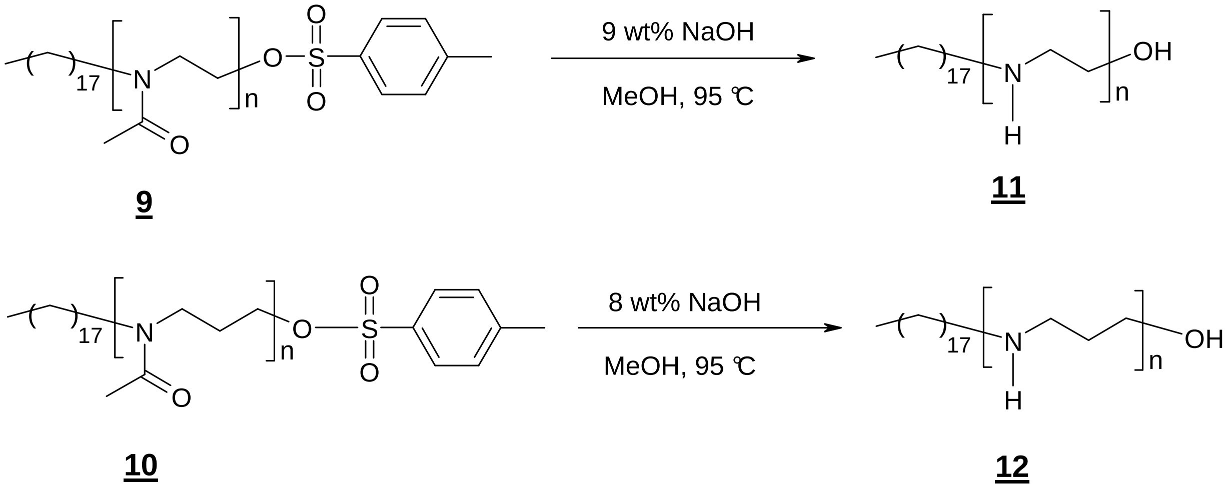

Figure 3.6. Alkaline hydrolysis of the prepolymers **alkyl-PAEI** 9 and **alkyl-PAPI** 10 yielding **alkyl-PEI** 11 and **alkyl-PPI** 12, respectively.

As described in section 4.2.4, the corresponding prepolymer, alkyl-PEI or alkyl-PAPI, is dissolved in methanol. Then, an aqueous solution of NaOH is added and the resulting mixture is heated under nitrogen atmosphere. After the desired reaction time, the solution is cooled down to room temperature and dialyzed against deionized water. The final product is obtained by freeze-drying.

The results are summarized in Table 3.2. The degree of hydrolysis strongly depends on temperature and reaction time. High conversions (~ 98 %) of alkyl-PAEI **9** into alkyl-PEI **11** are only possible by increasing the temperature to 95 °C and the reaction time to 72 hours as it was the case for samples **11.5**, **11.7** and **11.8**. As can be observed, those samples show higher degrees of hydrolysis than other ones subjected to lower temperature and shorter reaction time, e.g. **11.1**, **11.2** or **11.3**, in spite of the fact that the concentration of the alkaline solution is slightly lower. SAEGUSA *et al.* reported conversions around 87 % for the alkaline hydrolysis of poly(styrene)-g-PAEI[141] but in that case reaction time was only 22 hours. Although the reaction does not proceed quantitatively, since ^{1}H-NMR spectra of the product show the presence of N-(acetyl)-ethyleneimine groups, the polymer is predominantly composed of free secondary amino groups in its hydrophilic chain. Regarding the purification process of the reaction solution, alkyl-polyamines are slightly soluble in pure water because of their amphiphilic character. Purification by filtration and subsequent washing (sample **11.4**) leads to lower yields and, for this reason, dialysis of the reaction solution against deionized water has been carried out.

Table 3.2. Alkaline hydrolysis of **alkyl-PAEI 9** and **alkyl-PAPI 10** to **alkyl-PEI 11** and **alkyl-PPI 12**, respectively.

Sample	Polymer	P_n[a]	Purification method	c_{NaOH}, wt%	T, °C	t, h	Degree of hydrolysis, % [b]
11.1	alkyl-PAEI	10	dialysis	12.4	85	40	61
11.2	alkyl-PAEI	20	dialysis	10.7	85	40	58
11.3	alkyl-PAEI	40	dialysis	11.3	85	70	81
11.4	alkyl-PAEI	10	washing	6.3	95	46	95
11.5	alkyl-PAEI	10	dialysis	9	95	70	98
11.6	alkyl-PAEI	20	dialysis	9.3	95	64	95
11.7	alkyl-PAEI	20	dialysis	9	95	70	99
11.8	alkyl-PAEI	40	dialysis	9	95	72	98
12.1	alkyl-PAPI	10	dialysis	4.2	95	72	52
12.2	alkyl-PAPI	20	dialysis	4	95	72	60
12.3	alkyl-PAPI	20	dialysis	8.1	95	72	98

[a], adjusted value, experimentally is ± 1
[b], determined by ^{1}H-NMR

In a similar way, the hydrolysis of alkyl-PAPI **10** into alkyl-PPI **12** was carried out. From the results listed in Table 3.2, it can be recognized that not only temperature and reaction time, but also the concentration of the alkaline solution c_{NaOH} play a role in the degree of hydrolysis of the resulting product. In fact, high conversions, around 98 % for sample **12.3**, of PAPI into PPI can be reached under similar conditions to those used with alkyl-PAEI, i.e. 95 °C, 72 h and $c_{NaOH} \sim 8$ wt%. On the contrary, in samples **12.1** and **12.2**, where reaction takes also place at 95 °C for 72 h but in the presence of an alkaline solution with a lower concentration $c_{NaOH} \sim 4$ wt%, the complete transformation of PAPI into PPI can not be achieved.

Apart from hydrolysis, termination reactions have been performed in order to provide alkyl-PAEI chains with different end groups. Such an end-functionalization is required since the tosyl group provided by the alkylinitiator remains attached to the alkyl-PAEI chains, as can be observed in Figure 3.5. The tosyl group is removed in the hydrolysis step of the synthesis resulting in a hydroxyl group. As already remarked in section 2.1.2.1, the organic silaffin and LPA´s templates associated to the inorganic framework in diatoms possess well-defined functional groups. Among those, tosyl has not been found. For this reason, different moieties must be introduced in the chain ends in order to keep the resemblance with those biomolecules found in diatoms. In this respect, the removal of the tosyl can be achieved by terminating the living end of the propagating polymer with different reagents.

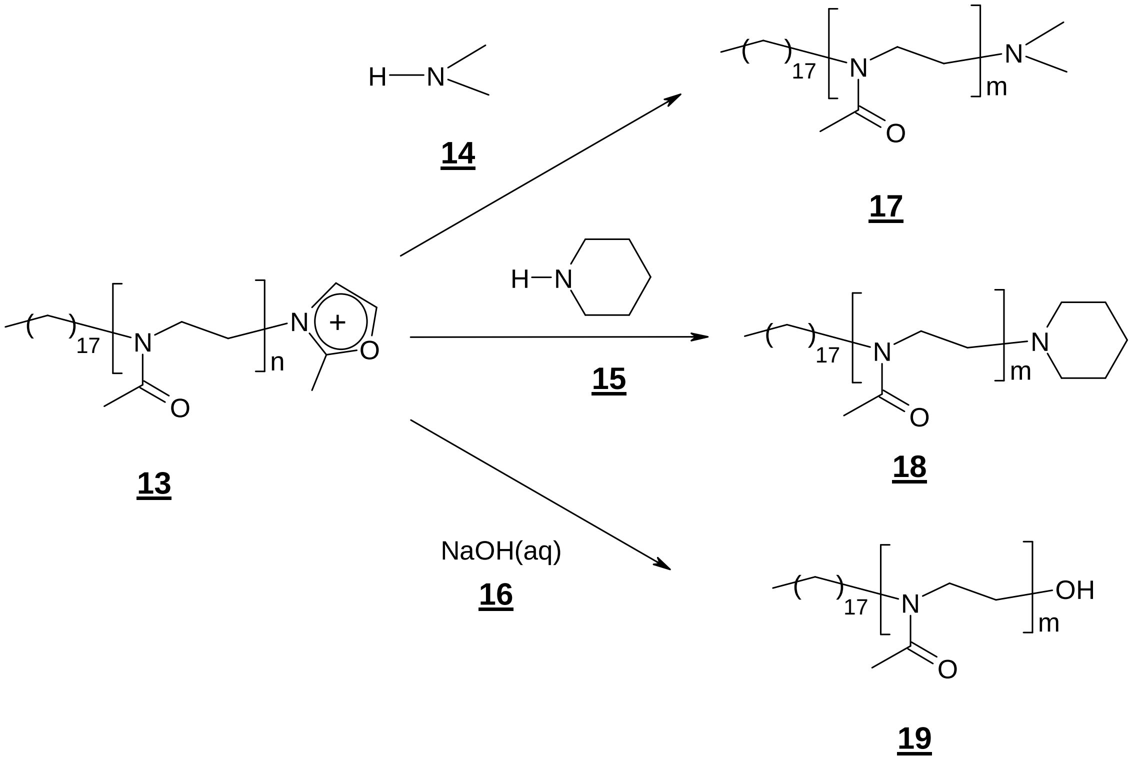

Figure 3.7. Termination reaction of the **alkyl-PAEI** living ends13 with **dimethylamine** 14, **piperidine** 15 and an **alkaline solution** 16, respectively.

Among those reagents, the use of secondary amines is especially advantageous. SAEGUSA *et al.* reported the use of primary and secondary alkylamines as termination reagents in the CROP of 2-oxazolines[130]. Within those investigations, the goal of the termination reaction was to provide hydrophobic segments in the synthesis of non-ionic polyoxazoline-based surfactants. Subsequent ionic exchange of the reaction product yielded the resulting amine-terminated deionized product. Removal of the tosyl group via hydrolysis of the polyoxazoline living ends with NaOH and KOH aqueous solutions, respectively, has also been performed by SAEGUSA *et al.*[130] and NUYKEN *et al.*[142]. In both cases, together with an amine-ester structure, the reaction yields the OH-terminated polyoxazoline as main product. Another reagent used by NUYKEN *et al.* to terminate oxazoline polymerizations started with tosyl-bearing initiators was piperidine[142]. According to those investigations, piperidine reacts with oxazolinium salts very fast and quantitatively, in spite of the fact that complete conversion can be reached just by using excess of the termination reagent. Taking all these results into account, the termination of the polymer living ends produced via CROP of MeOZO **4** with the alkylinitiator **3** (OcOTS) was carried out in this work with different reagents as schematized in Figure 3.7.

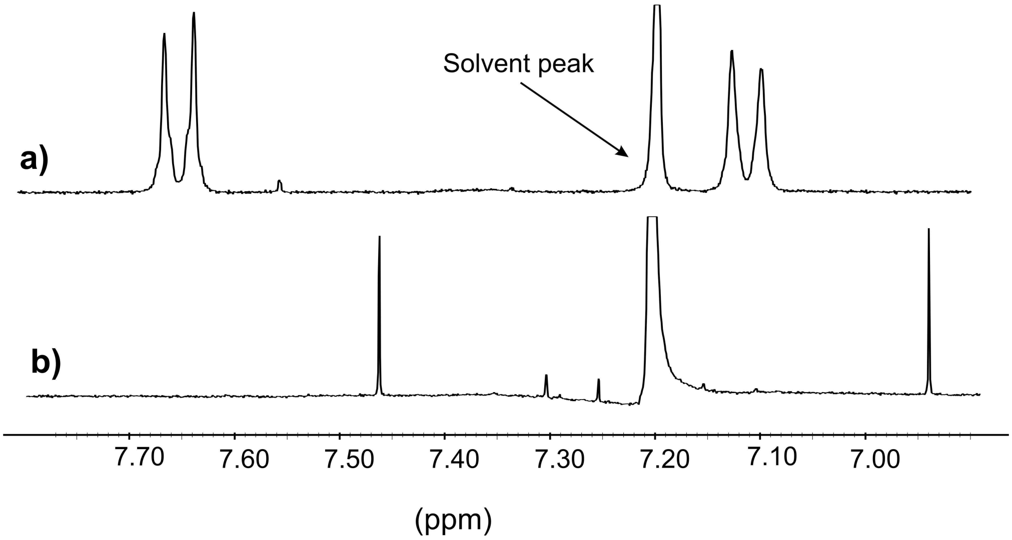

Figure 3.8. Aromatic region in the ^{1}H-NMR spectra of **alkyl-PAEI** **18** terminated with **dimethylamine** **14** before **(a)** and after **(b)** ion exchange.

Termination by using a solution of dimethylamine **14** (2 mol/l) in methanol was performed under different time and temperature experimental conditions listed in Table 4.3 (experimental section). Figure 3.8 shows the aromatic region in the ^{1}H-NMR spectra of the product obtained by termination reaction with dimethylamine at room temperature for 16 hours before (3.8-a) and after (3.8-b) ion exchange. As can be observed, the doublets at 7.10 and 7.65 ppm ascribed to the aromatic protons in the tosyl group are present in the reaction product before the ion exchange (Figure 3.8-a). After the ion exchange (Figure 3.8-b), both doublets can no longer be detected suggesting the complete removal of the tosyl group. However, two new singlets at 6.95 and 7.48 ppm appear. A similar result is obtained when the reaction takes place with dimethylamine as termination reagent and at higher temperatures. The presence of those singlets in the ^{1}H-NMR spectra of the product after ion exchange has not been reported by SAEGUSA *et al.* when carrying out the reaction with alkylamines as termination reagents[130]. Furthermore, similar signals in the aromatic region of the ^{1}H-NMR spectra before and after ion exchange are obtained when the reaction is performed with piperidine **15**. Proton signals corresponding to piperidine can not be separated in the ^{1}H-NMR sprectra due to overlapping with those produced by the aliphatic protons of the alkyl chain. Nevertheless, NUYKEN *et al.*[142] have proven that oxazolinium salts react quantitatively with an excess of piperidine within 10 minutes. Therefore, even when the doublets produced by the tosyl aromatic protons are present in the spectrum of the product before ion exchange, it can be concluded that the reaction was quantitative. NaOH aqueous solutions can be used as termination reagent, too. In this case the same signals can be identified in the aromatic region of the ^{1}H-NMR spectra of the product before and after ion exchange as it was the case with methylamine and piperidine. That is, while tosyl is present in the samples before ion exchange, the ^{1}H-NMR spectrum of the product after deionization does not show tosyl signals but two new singlets appear in the aromatic region. The presence of the tosyl group in the product before ion exchange has not yet been clarified. CORNELIUS[125] ascribed it to the fact that in the CROP of MeOZO with tosyl-bearing initiators, the polymer chain growth takes place via propagating ionic species. According to this hypothesis, the termination reagent may be covalently bound to the polymer chain-end whereas the tosylate anion would remain in the sample due to its electrostatic interaction with the polymer chain. The absence of the doublets produced by the aromatic protons of the tosyl group in the ^{1}H-NMR spectrum of the deionized product corroborates this hypothesis. Concerning the presence of the singlets in the aromatic region of the ^{1}H-NMR spectrum of the deionized product, they could be caused by impurities contained in the ion exchange resin. The reason for this assumption is that, as mentioned before, they appear in the ^{1}H-NMR spectra of all the deionized products, regardless of the employed termination reagent.

3.1.6 Concluding remarks on synthesis and modification

Within this section the production of the bioinspired polymeric surfactants alkyl-poly(N-(acetyl)-ethyleneimine) (alkyl-PAEI), alkyl-poly(ethyleneimine) (alkyl-PEI) and their analogous molecular structures with a propylene spacing group, alkyl-PAPI and alkyl-PPI, has been reported. The first step of the synthetic pathway has been the production of the alkyl-bearing initiator 1-octadecyltosylate and of the monomer 2-methyl-5,6-dihydro-4H-1,3-oxazine (MeOZI). Subsequent cationic ring-opening polymerization (CROP) of 2-methyl-2-oxazoline (MeOZO) and of the synthesized MeOZI with the alkyl-bearing initiator yielded alkyl-PAEI and alkyl-PAPI, respectively. Because of the controlled character of this process it is possible to tailor the length of the hydrophilic segment. Thus, the synthesis of polymers with well-defined degree of polymerization is feasible. Furthermore, other variables such as solvent and reaction time have to be properly adjusted to reach the desired chain-length and also to prevent the solidification of the reaction medium. Finally, different reactions have been performed in order to modify the functional groups located along the polymer chain. Hydrolysis of alkyl-PAEI and alkyl-PAPI yielded the related compounds alkyl-PEI and alkyl-PPI. It was shown that the conversion of N-(acetyl)-ethyleneimine groups into ethyleneimine groups depends not only on the reaction time but also on the concentration of the alkaline solution used for the reaction. Moreover, the combination of both elements allows achieving high degrees of hydrolysis. The other modification performed on the hydrophilic segment of the surfactant has been the removal of the tosyl end group. Terminations reactions with different reagents providing different end-groups have been carried out. ^{1}H-NMR spectra of the reaction products reveal the presence of the tosyl group. Subsequent ion exchange of the reaction product removes the peaks ascribed to this group. However, new signals can be identified in the spectra regardless the employed termination reagent. The origin of these signals has not yet been identified unambiguously, but could be related to impurities from the ionic exchange resin.

3.2 Supramolecular aggregation of amphiphilic polymers

3.2.1 Alkyl-poly(N-(acetyl)-ethyleneimine) (alkyl-PAEI)

3.2.1.1 Introduction

Amphiphilic polymers, also known as polymeric surfactants, are a class of macromolecules that consist of hydrophobic and hydrophilic segments linked by a covalent bond. Because of the coexistence of these two kinds of segments within the same molecule, these polymers are expected to possess interesting properties as for instance surface activity and to undergo different phenomena in the aqueous medium such as supramolecular aggregation. This ability of polymeric surfactants to organize into micelles or other complex aggregates in selective solvents above a certain critical micelle concentration (CMC) has been studied for the last decades[143]. In particular, block copolymers with hydrophilic and hydrophobic segments have become a rich field of research due to the structural diversity of the assemblies that they can build in solvents selective for one block. In fact, they can aggregate into various supramolecular assemblies such as spherical micelles, vesicles, cylindrical micelles, and other complex aggregates in solution[144, 145]. Furthermore, their micellar characteristics depend on the nature of each block. On this regard, in an aqueous medium, the surface properties of the micellar aggregates are highly dependent on the structure of the hydrophilic block, whereas those of the micellar core are determined by the structure of the hydrophobic segments[146-148]. The reason behind the keen interest in the self-association phenomena of these copolymers has been their potential applications in different fields such as biomedicine, pharmacy and technology[149-151].

An interesting variation of these molecular structures is represented by the amphiphilic polymers with a long hydrophilic block attached to a small hydrophobic block at one or both ends. They are known as “hydrophobically modified water soluble polymers” (HMWSP) and have been proven to exhibit unusual rheological properties. For this reason, they are widely used as thickening agents[152, 153]. Furthermore, HMWSP have also been used to solubilize reactants in micellar catalysis[154]. In line with this application, the synthesized alkyl-poly(N-(acetyl)-ethyleneimine) (alkyl-PAEI) is expected to undergo self-assembly phenomena in the aqueous medium and may be a good candidate as structure directing agent in the production of structured silica. In addition, other macromolecular structures containing hydrophilic PAEI segments have also been proven to self-assembly in aqueous solution[155, 156].

Within this section, the characterization of the aggregation behaviour of alkyl-PAEI is reported. As will be described, this characterization includes not only investigations on the micellization phenomena but also on the determination of size and shape of the surfactant aggregates.

3.2.1.2 Optical Polarization Microscopy (OPM)

As already mentioned in section 2.2.2, surfactants self-assemble in pure water to build different kinds of aggregates. Among those, lyotropic liquid crystalline phases occur at high surfactant concentrations and their optical properties reflect the symmetry of their structure. Specifically, anisotropy of the refractive index, or birefringence, is one of the characteristic physical properties of liquid crystals since it allows the visualization of the macroscopic molecular orientation. In liquid crystal samples placed between two crossed polarizers under an optical microscope, a variety of textures and birefringence colors can be observed. These textures and colors can provide valuable information about the macroscopic structure of the liquid crystalline phases. Thus, although there are many experimental techniques available to investigate the structure and physical properties of these phases, microscopic observations represent an important method. They offer a proof of the aggregation properties of the surfactant and can even offer enough information to determine the structure of the studied mesophases provided that well-aligned domains are obtained.

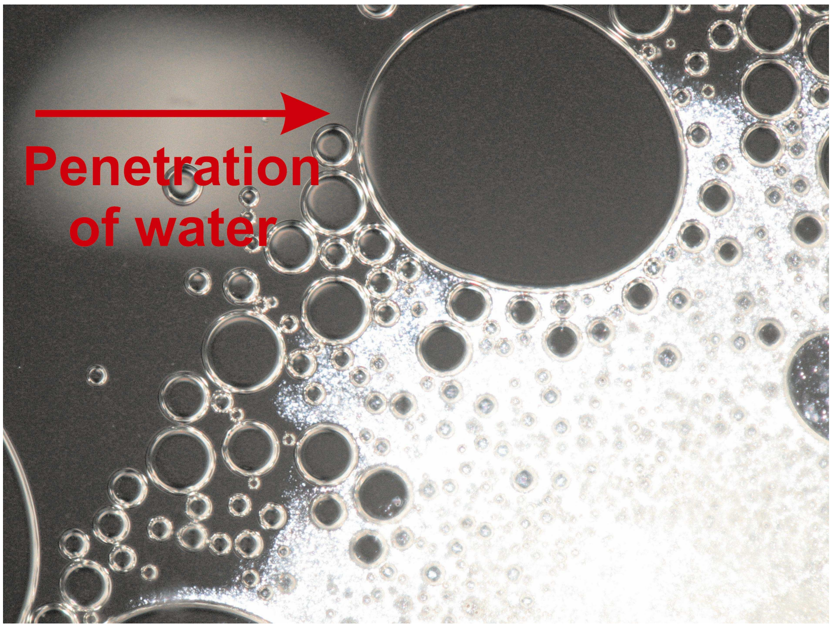

Figure 3.9. Optical microscope image of a water penetration scan for alkyl-PAEI ($P_n = 40$) held at room temperature and observed under cross-polarized light.

In Figure 3.9 an optical microscope image with crossed polarized light of a water penetration scan for alkyl-PAEI ($P_n = 40$) is shown. In this experiment, the surfactant is placed in contact with water, which penetrates from left to right, and the interdiffusion region is examined under crossed polarizers. It is usually performed to determine whether lyotropic liquid crystalline phases can form. As can be observed, apart from the spherical air bubbles trapped between the glass slides, two different regions can be recognised in the micrograph. At the left top side a dark region is found, where no interaction between cross-polarized light and the studied material takes place. That region corresponds to isotropic media where either the polymer is completely dissolved in water or there is just water in absence of polymeric material. On the other hand, a birefringent region is found at the right bottom side of the micrograph. Here, interaction between cross-polarized light and the observed material takes place indicating the presence of anisotropic domains. Thus, the polymer forms lyotropic liquid crystalline phases. However, the textures are rather non-clarifying, which makes it difficult to determine the mesophase composition in the birefringent region.

3.2.1.3 Fluorescence of pyrene

Spectroscopic techniques, based either on optical absorption or on emission of light of probe molecules, are well-established for investigating a wide range of properties of micellar solutions[157]. The ability of the supramolecular aggregates for solubilizing relatively large amounts of sparingly water-soluble compounds has been used to prove surfactant self-assembly and even to determine the onset of micelle formation, i.e. the critical micelle concentration (CMC)[158]. Pyrene is one of those compounds commonly used as a fluorescence probe to monitor micropolarity[159]. It is a condensed aromatic hydrocarbon, highly hydrophobic and sensitive to the polarity of the surrounding environment. Below the CMC, pyrene will exist mainly in an aqueous medium, whereas above the CMC it is incorporated into micelles. The transfer of pyrene from a polar to a non-polar environment results in a sharp increase of its fluorescence efficiency.

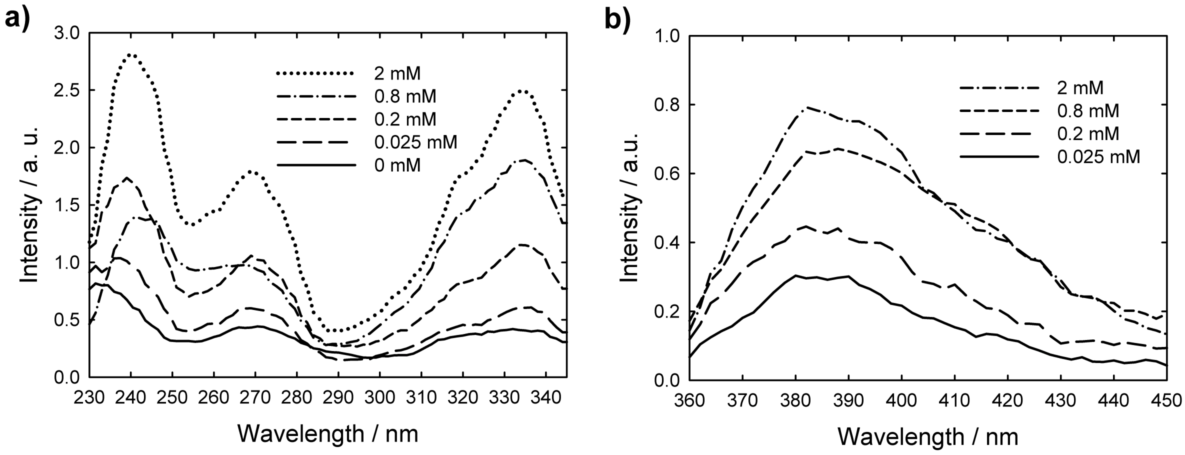

Figure 3.10. (a) Fluorescence excitation spectra of pyrene in aqueous solutions ($6 \cdot 10^{-7}$ M), monitored at λ_{em} = 392 nm, in the presence of different concentrations of alkyl-PAEI (P_n = 10). (b) Fluorescence emission spectra of pyrene in aqueous solutions ($6 \cdot 10^{-7}$ M), monitored at λ_{ex} = 336 nm, in the presence of different concentrations of alkyl-PAEI (P_n = 40).

In Figure 3.10-a, fluorescence excitation spectra of pyrene ($\lambda_{em} = 392$ nm) in alkyl-PAEI ($P_n = 10$) aqueous solutions are shown. As can be observed, in the absence of polymer, the intensities of the fluorescence absorption peaks of pyrene in water at 275 nm and 339 nm show low values, which are typical in polar environments. On the contrary, solutions containing alkyl-PAEI present larger intensities. This is due to the formation of supramolecular aggregates with hydrophobic domains. The transfer of pyrene into the non-polar microenvironment causes the enhancement of the absorption peaks. That is, a significant increase of the intensity is observed when the alkyl-PAEI ($P_n = 10$) concentration of the solution increases from 0.025 to 0.2 mM. As will be reported in section 3.2.1.4, the critical micelle concentration of alkyl-PAEI with $P_n = 10$ in pure water has been found to be 0.18 mM. For this reason, alkyl-PAEI solutions with $c = 0.2$ mM, which is above the CMC, show significantly higher intensities than those with $c = 0.025$ mM. Whereas at the former concentration value hydrophobic domains have already formed, at the latter one the solution is still isotropic. Further increase of the intensities with increasing surfactant concentrations is also observed above the CMC. This is because the increase of the surfactant concentration results in a higher concentration of aggregates and hence of non-polar domains in the solution.

A similar situation can be recognized in the emission spectra of pyrene ($\lambda_{ex} = 336$ nm) in alkyl-PAEI ($P_n = 40$) aqueous solutions (Figure 3.10-b). The fluorescence intensity increases substantially with the concentration of polymer in solution indicating the presence of aggregates with hydrophobic domains into which pyrene transfers. This gives clear evidence of the ability of alkyl-PAEI to undergo supramolecular aggregation in aqueous solution.

3.2.1.4 Critical Micelle Concentration (CMC)

As already remarked in section 2.2.2, the critical micelle concentration (CMC) is one of the most important physical parameters of surfactants, especially in sol-gel processes involving supramolecular aggregation of amphiphilic molecules. Therefore, when dealing with the characterization of silica-precipitating amphiphilic polymers, the CMC represents a crucial parameter since it indicates the minimum amount of the amphiphilic macromolecule required in the aqueous medium to produce supramolecular aggregates. According to the liquid crystal template model previously commented in section 2.1.1, those aggregates act as scaffolds in the formation of the mineral structure from the inorganic precursors dissolved in the aqueous medium. Concerning the determination of the CMC, a variety of methods has been reported thus far. In the most common ones, the CMC can be obtained from breaks in the plots of different physical variables versus the concentration of the surfactant solutions. Within this work, the critical micelle concentration of the synthesized amphiphilic polymers has been determined via surface tension measurements. As it is well-known, adsorption of surface active-agents such as amphiphilic polymers causes a reduction in the surface tension at the air/water interface. Thus, the ability of these compounds for reducing the surface tension of aqueous solutions is used to determine the CMC.

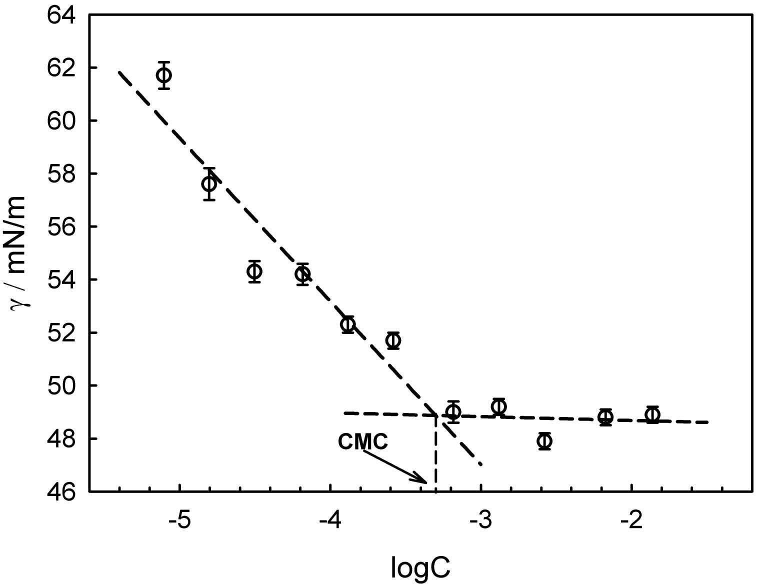

Figure 3.11. Semilogarithmic plot of surface tension (γ, mN/m) versus concentration (mM) for an alkyl-PAEI (P_n = 40) aqueous solutions at 25 °C showing the break of the surface tension at the CMC.

Figure 3.11 depicts a semilogarithmic plot of the surface tension values measured for aqueous solutions containing alkyl-PAEI (P_n = 40) versus the concentration. As can be observed, with increasing polymer concentration the surface tension decreases almost linearly and then becomes constant above a certain concentration value. Such a break point in the surface tension of the solutions implies surfactant aggregation and corresponds to the CMC.

Table 3.3. Critical micelle concentration (CMC) values of alkyl-PAEI samples with different degree of polymerization in pure water at 25 °C.

Degree of polymerization, P_n [a]	**CMC, mM**	**CMC, wt%**	**γ_{CMC}, mN/m**	**$\omega_{hydrophobic}$, wt%**	**$\omega_{hydrophilic}$, wt%**
10	0.18	0.023	44.5	23	77
20	0.45	0.095	47.5	13	87
40	0.5	0.19	48.4	7	93

[a], adjusted value, experimentally is ± 1

Table 3.3 summarizes the CMC values for alkyl-PAEI with different degree of polymerization obtained from the semilogarithmic representation of the surface tension (γ) versus the concentration as already shown in Figure 3.11. It can be recognized that the critical micelle concentration (CMC) increases by increasing the degree of polymerization of the poly(N-(acetyl)-ethyleneimine) block, i.e. when the length of the hydrophilic segment of the surfactant increases. This trend is in good accordance with previous investigations dealing with the aggregation behaviour of different amphiphilic block-copolymers[160, 161]. Furthermore, the obtained values are lower than those reported for low molecular weight surfactants used in sol-gel processes, e.g. 0.9 mM for cetyltrimethylammonium bromide[162], but higher than those obtained for other polymeric surfactants[163-165]. They are even higher than the CMC values obtained by VOLET *et al.*[117] for octadecyl-poly(2-methyl-2-oxazoline), $2.2 \cdot 10^{-3}$ mM when $P_n = 30$, and those reported by OBEID *et al.*[166] for the analogous octadecyl-poly(2-ethyl-2-oxazoline) and octadecyl-poly(2-n-isopropyl-2-oxazoline). Unlike this work, in those investigations the CMC values were determined via fluorescence spectroscopic measurements. This may be the most likely reason for the observed deviations since the addition of hydrophobic dyes can induce micelle formation at lower concentrations[167, 168].

The surface activity of alkyl-PAEI can be evaluated from the surface tension values at concentrations above the CMC (γ_{CMC}, see Table 3.3). According to those values, the ability to reduce the surface tension increases with a decrease in the length of the hydrophilic segment. This is in good agreement with previous results reported in the literature[129-131, 169]. In fact, when the ratio of the hydrophilic segment decreases, a higher amount of hydrophobic chains can be oriented on the surface since the hydrophilic coils dissolved in the aqueous solution became less bulky. Consequently, the surface tension diminishes.

Table 3.4. Critical micelle concentration (CMC) values of alkyl-PAEI with $P_n = 20$ in buffer solutions with different pH values at 25 °C.

Buffer	**pH**	**CMC, mM**	**CMC, wt%**	γ_{buffer}, **mN/m**	γ_{CMC}, **mN/m**
Water	7	0.45	0.095	72.1	47.5
Malonate	5.6	0.11	0.023	26.0	22.5
Phosphate	5.5	0.089	0.019	28.7	22.3
Acetate	4.5	0.009	0.002	30.6	23.2
Citrate	3.5	0.052	0.011	29.4	22.5

Another important aspect regarding the micellization of alkyl-PAEI in aqueous medium is the influence of pH on the critical micelle concentration. As the subsequent silica precipitation experiments in the presence of alkyl-PAEI will be carried out in different pH buffers (see section 3.3.2), the CMC of alkyl-PAEI with $P_n = 20$ in those buffers has been determined and the results are shown in Table 3.4. As a general remark, it can be said that the CMC values in the buffers are lower than in pure water. However, a clear dependence upon the pH value of the solution can not be identified. Previous investigations[170] have proven the influence of pH on the micellization of amine-based surfactants. In fact, an influence of pH on the micellization of alkaline surfactants can be expected since it is well-known that the degree of protonation of polyelectrolytes is strongly affected by pH[171]. This may be the reason why the CMC values of alkyl-PAEI, which is a non-ionic surfactant, do not show such a close dependence from pH. The differences between the CMC values in the buffers with the one obtained in pure water may then result from the presence of different anions in the solution such as malonate or acetate. Concerning the surface activity of the surfactant in the buffers, it must be remarked that the buffer solutions without any surfactant gave surface tension values between 26 and 30 mN/m (see Table 3.4), which are much lower than that of pure water (72.1 mN/m). As can be observed, the reduction of the surface tension by alkyl-PAEI is much higher in pure water (24.6 mN/m) than in the buffers. The highest decrease reached 7.4 mN/m in citrate. In addition, this mild decay of the surface tension with the surfactant concentration in the buffers makes it difficult to determine the CMC in the former. However, it is obvious that the CMC values are lower in the buffers than in pure water. Furthermore, in all buffers the CMC is lower than 0.1 wt%, which is the lowest polymer concentration used in the silica precipitation experiments. This ensures that the alkyl-PAEI solutions used in those precipitation experiments are not isotropic but they contain supramolecular aggregates.

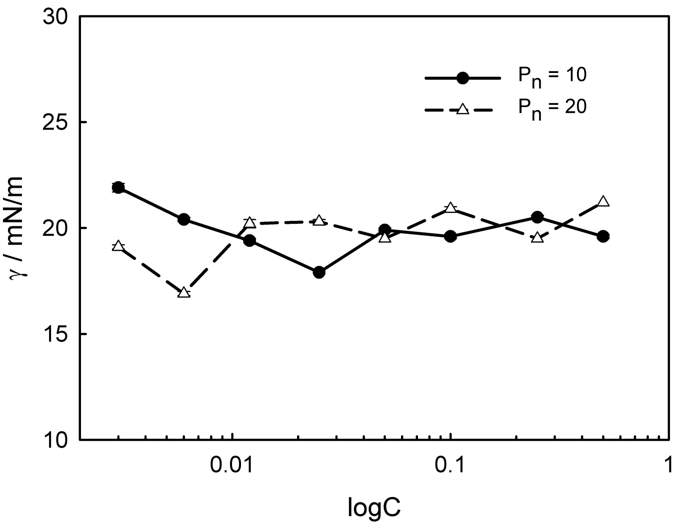

Figure 3.12. Semilogarithmic plot of surface tension (γ, mN/m) versus concentration (mM) for alkyl-PAPI aqueous solutions with P_n = 10 and 20, at 25 °C.

In the same way, surface tension of aqueous solutions containing alkyl-poly(N-(acetyl)-propyleneimine) (alkyl-PAPI) with different degree of polymerization (P_n = 10 and 20) has been measured as shown in Figure 3.12. Unlike alkyl-PAEI, a linear decay of the surface tension can not be recognized, but it decreases dramatically at very low concentration. In fact, solutions containing 0.003 wt% of alkyl-PAPI with P_n = 10 yields surface tensions around 21.9 mN/m. This value is much closer to those of the solutions with higher polymer concentrations, e.g. 0.05 wt% gives 19.9 mN/m, than to the one obtained for pure water (~ 72 mN/m). This means that the lowest polymer concentration represented the plot (0.003 wt%) is higher than the CMC. Therefore, accurate CMC values can not be obtained from the available data. Moreover, the determination of those values would involve the production of solutions with lower concentrations, which results in high experimental errors. Anyway, even when accurate values can not be offered, it can be concluded that alkyl-PAPI possesses lower CMC values than alkyl-PAEI.

The surface activity of the alkyl-PAPI solutions has been found to give higher values than that of alkyl-PAEI. While alkyl-PAEI with P_n = 10 can decrease the surface tension of pure water from 72.1 mN/m to 44.5 mN/m, alkyl-PAPI with the same degree of polymerization reaches a final value around 19.5 mN/m. The surface tensions reported by SAEGUSA *et al.*[131] for n-octyl-PAEI and n-octyl-PAPI with P_n = 5, i.e. having the same hydrophilic-lipophilic balance as alkyl-PAEI and alkyl-PAPI with P_n = 10, were 29.5 and 33.5 mN/m, respectively. As can be observed, the reported values are not in accordance with those obtained in this work. The values obtained for alkyl-PAEI are higher than those reported by SAEGUSA for n-octyl-PAEI. Yet, the surface tension values measured for alkyl-PAPI solutions are lower than those reported by SAEGUSA for n-octyl-PAPI. Furthermore, n-dodecyl-PAEI with P_n between 16 and 48 and which was produced by Saegusa in that work via initiation with alkyl-oxazolinium salts yielded surface tensions between 48.1 and 48.9 mN/m. These values are close to those obtained for alkyl-PAEI within this work, i.e. between 44.5 and 48.4 mN/m. Taking these observations into account, it may be concluded that the surface activity of the surfactants depends not only on the hydrophilic-lipophilic balance, but also on the length of each single segment. Concerning the low surface tension values obtained for alkyl-PAPI, an explanation has not been found so far.

3.2.1.5 Dynamic Light Scattering (DLS)

Dynamic light scattering (DLS) measurements have been performed in order to determine the size and shape of the aggregates that alkyl-PAEI builds in aqueous solution. The mean apparent hydrodynamic radius R_h of polymer assemblies can be determined with this method as was already described in section 2.2.3.1. For this purpose, the time autocorrelation function $g_1(t)$ of solutions containing different alkyl-PAEI concentrations, depending on P_n, have been measured at scattering angles of 30, 60, 90, 100, 120 and 150°. Figure 3.13-a depicts the time correlation function for a solution containing 15 mg/ml of alkyl-PAEI (P_n = 20) at 90°. The presented experimental data (filled triangles) fit in well with an exponential decay of the type $g_1(t) = \exp(-\Gamma \cdot t)$ (red line). That kind of profile for the autocorrelation function has already been reported to correspond to systems which are monomodal, monodiperse distributions of aggregates[172, 173]. Likewise, all the measured autocorrelation functions $g_1(t)$ corresponding alkyl-PAEI aqueous solutions within the concentration ranges 4-40, 3-30, and 2-20 mg/ml, for P_n = 10, 20 and 40, respectively, can be fitted to an exponential profile. Thus, within that concentration range, alkyl-PAEI forms a monomodal, monodisperse distribution of aggregates in aqueous solution. Furthermore, the polydispersity indexes $PDI = \Gamma_2/\Gamma_1^2$, with Γ_1 the decay of the autocorrelation function and Γ_2 the second moment of the cumulant analysis, are between 0.1 and 0.2. Those values confirm the monodisperse character of the distribution[174].

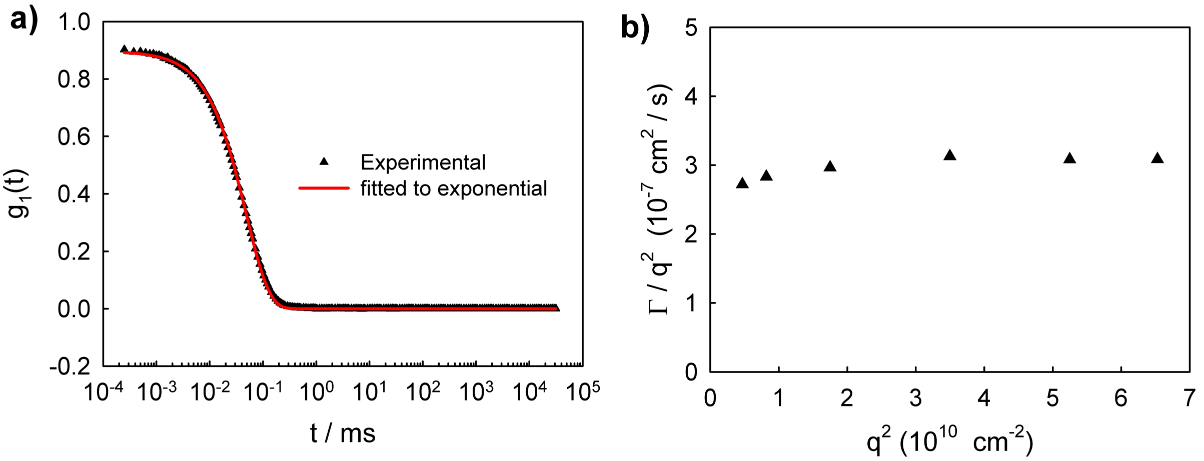

Figure 3.13. (a) Plot of the experimental (triangle) and exponential-fitted (red line) first-order electric field correlation function versus time at a scattering angle of 90° for an aqueous solution containing 15 mg/ml alkyl-PAEI ($P_n = 20$) at 25 °C. (b) Plots of the q^2-scaled average characteristic decay rate Γ (Γ/q^2) versus q^2 for an aqueous solutions containing 15 mg/ml alkyl-PAEI ($P_n = 20$) at 25 °C.

To obtain information about the shape of the alkyl-PAEI aggregates, the angular dependence of the scattering data has been estimated. Figure 3.13-b shows the dependence of the scaled decay rate (Γ/q^2) on the scattering vector (q^2), for an aqueous solution containing 15 mg/ml alkyl-PAEI ($P_n = 20$). Isotropic scattering objects such as spherical micelles show no angle dependence of the scaled decay rate on the scattering vector[175, 176]. As shown in Figure 3.13-b, the value of Γ/q^2 is almost constant against q^2, indicating that the aggregates in dilute solution are indeed spherical micelles. Furthermore, the dependence of decay rate Γ on q^2 has been examined and is depicted in Figure 3.14-a. As can be observed, a linear dependence of Γ on q^2 is found, which indicates that the decay of the autocorrelation function is related to translational diffusion of the scattering objects in solution[177]. The translational diffusion coefficient D_m can be determined from the slopes of the plot Γ vs. q^2. In order to determine the concentration dependence of the diffusion coefficient D_m, DLS measurements have been carried out on alkyl-PAEI aqueous solutions with different concentrations.

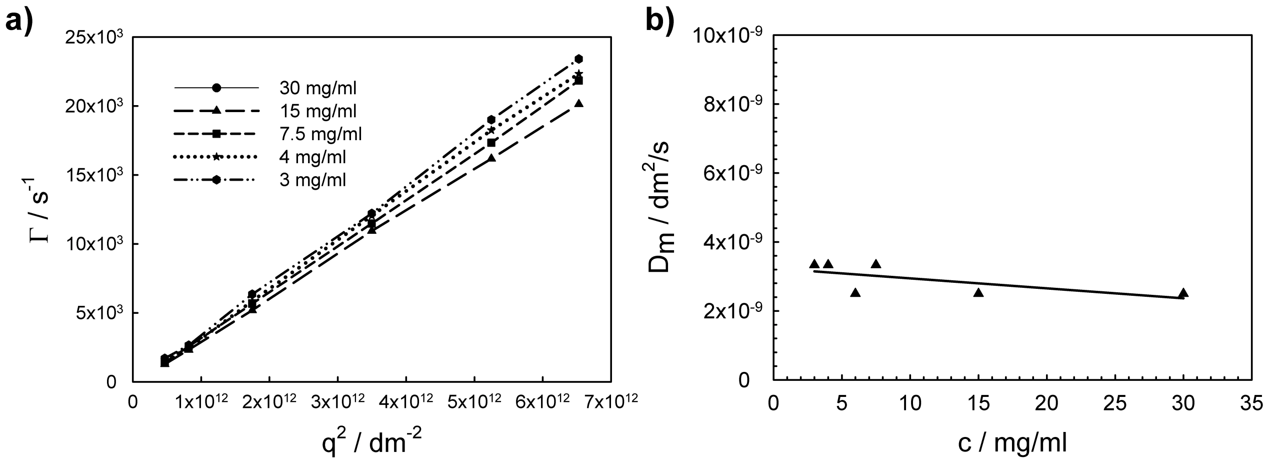

Figure 3.14. (a) Relationship between the decay rate Γ and q^2 for alkyl-PAEI ($P_n = 20$) aqueous solutions with different concentrations at 20 °C. (b) Concentration profile of the diffusion coefficient of alkyl-PAEI with $P_n = 20$ in dilute aqueous solution.

Figure 3.14-b shows the concentration profile of the translational diffusion coefficient D_m obtained from aqueous solutions containing alkyl-PAEI with $P_n = 20$. It is evident that in spite of slight deviations, due to experimental errors, the diffusion coefficient remains constant within that concentration range (3-30 mg/ml). Similar results have also been obtained for aqueous solutions containing alkyl-PAEI with $P_n = 10$ and 40. The fact that the diffusion coefficients are independent on the polymer concentration indicates that alkyl-PAEI spherical micelles do not undergo any interactions with each other[177, 178]. In fact, the DLS measurements have been performed in a dilute concentration regime. Under those conditions, the amount of alkyl-PAEI micelles in the system is relatively low and they are so far from each other that no interactions take place. This also explains the exponential decay rate of the autocorrelation function. At a dilute concentration regime, the aggregates are far from each other and the formation of bigger clusters, which results in more complex decay rates of the autocorrelation function[179, 180], does not occur. Under these conditions, the translational diffusion is the only contribution to the scattering phenomena in the sample as has already been commented.

As already reported in section 2.2.3.1, the diffusion coefficient depends on the concentration and can be described by a linear equation in a wide range of concentration:

$$D_m = D_0 \cdot (1 + k_D \cdot c)$$

Hence, by extrapolating the diffusion coefficients to zero concentration in the plot D_m vs. c (Figure 3.14-b), the diffusion coefficients in the infinite dilute solution D_0 have been calculated. Subsequently, the hydrodynamic radii of the scattering objects have been obtained using the Stokes-Einstein relationship:

$$R_h = \frac{k_b \cdot T}{6 \cdot \pi \cdot \eta_A \cdot D_0}$$

where k_b is the Boltzman's constant, T the absolute temperature in Kelvin and η_A the solvent viscosity. The results of these calculations are summarized in Table 3.5.

Table 3.5. Dynamic Light Scattering (DLS) results for alkyl-PAEI with different degrees of polymerization in aqueous solution at 20 °C.

P_n [a]	$D_{0,app} \times 10^9$, dm^2/s	κ_D, ml/g	R_h, nm
10	3.87	-15.5	6.22
20	3.23	-9.24	7.56
40	2.18	22.94	11.06

[a], adjusted value, experimentally is ± 1

It can be clearly seen that the hydrodynamic radius of the alkyl-PAEI micelles increases by increasing the degree of polymerization of the hydrophilic chain, but not linearly. Taking the DLS results into account, it can be concluded that in dilute solution alkyl-PAEI builds monodisperse, non-interacting spherical micelles with sizes that increase by increasing the degree of polymerization of the hydrophilic chain. These conclusions are in good agreement with those reported by OBEID *et al.*[166] for the DLS characterization of amphiphilic alkyl-polyoxazolines with ethyl and isopropyl, respectively, as 2-substituent in the oxazoline ring. In fact, according to those investigations, alkyl-poly(2-ethyl-2-oxazoline) and alkyl-poly(2-isopropyl-2-oxazoline) build monodisperse distributions of non-interacting, spherical micelles in the dilute concentration regime. A non-linear increase of the hydrodynamic radius is also observed by increasing the degree of polymerization of the polyoxazoline chain. In addition, the hydrodynamic radius of the aggregates strongly depends on the 2-substituent of the oxazoline ring. The finding of these common features in the aggregates built by polyoxazolines different substituents highlights the potential applicability of these compounds in the production of supramolecular aggregates with tunable, well-defined dimensions.

3.2.1.6 Small Angle X-ray Scattering (SAXS)

Further characterization of the alkyl-PAEI aggregates has been performed by small angle X-ray scattering (SAXS). The aim of these measurements is to investigate the internal structure of the aggregates and also to provide additional information about the aggregates size. For this purpose, the SAXS profiles I(q) vs. q of aqueous solutions containing alkyl-PAEI (P_n = 10, 20 and 40) with concentrations ranging from 5 to 15 wt% (~ 53-176 mg/ml) have been measured. It should be noted that the concentration range for the SAXS measurements, between 53 and 176 mg/ml, is higher than for the DLS investigations. The reason is that for polymer concentrations below 5 wt% the scattered intensity is too low. As a consequence, SAXS profiles with prominent features can not be obtained. On the other hand, solutions with concentrations above 15 wt% become extremely viscous, making it difficult to introduce them into the capillary sample holders. The modelling of the experimental data has been performed with the software SCATTER, developed by FÖRSTER *et al.*[181, 182]. This modelling procedure is based on the introduction of the experimental profiles I(q) vs. q in the software. Subsequently, the geometry, morphology and mutual interaction model of the aggregates have to be estimated. With all these variables, SCATTER simulates SAXS profiles, which can be compared with the experimental data. This process has to be carried out until both profiles, experimental and simulated, fit with each other in terms of their scattering features such as peaks, minima or shoulders. The coincidence between both profiles indicates that the chosen model describes reasonably well the structural properties of the aggregate solution. Therefore, different parameters useful for the characterization of the aggregate dimensions and internal structure can be extracted from the simulated profile.

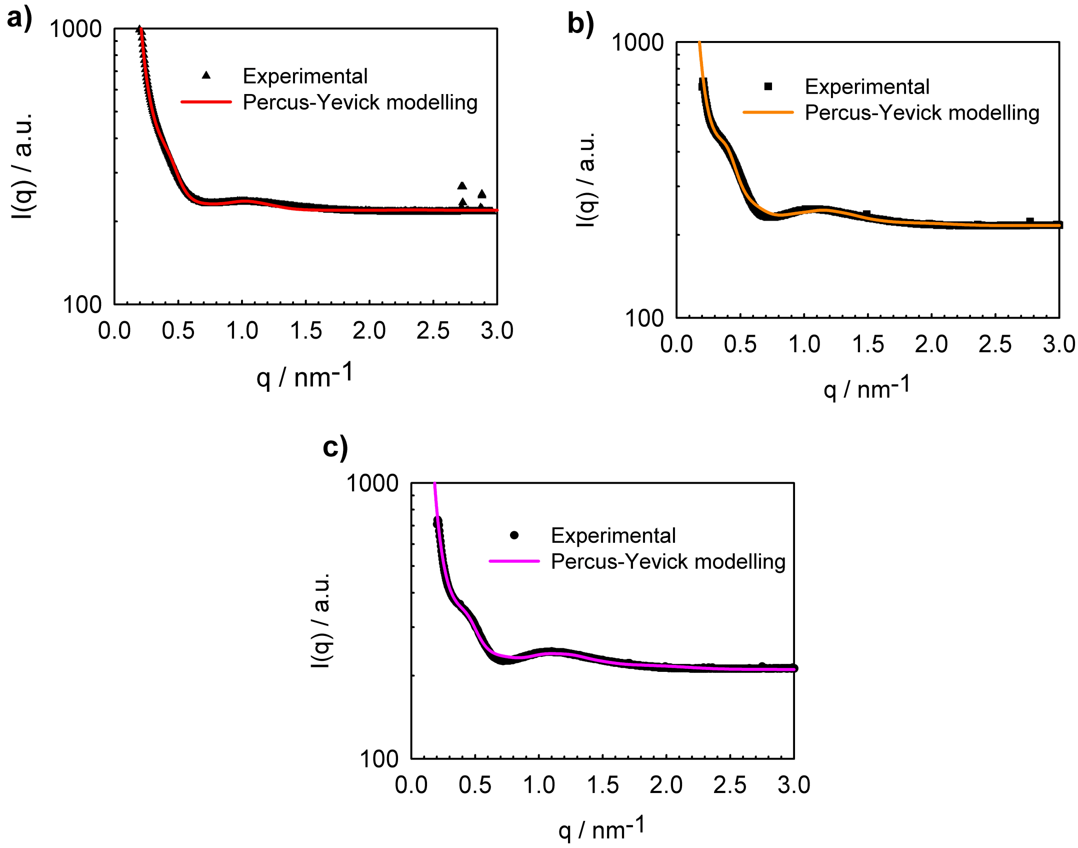

Figure 3.15. Experimental and modelled SAXS profiles of aqueous solutions containing (a) 5, (b) 10 and (c) 15 wt% alkyl-PAEI ($P_n = 10$) at 20 °C obtained with SCATTER[181, 182].

Figure 3.15 shows both, experimental and simulated SAXS profiles of aqueous solutions containing 5 wt% (Fig. 3.15-a), 10 wt% (Fig. 3.15-b) and 15 wt% (Fig. 3.15-c) alkyl-PAEI ($P_n = 10$) at 20 °C. The geometry, morphology and interaction model of the aggregates in the simulated profiles have been estimated by considering the results offered by the DLS investigations. Here, the aggregates built by alkyl-PAEI in water have been found to be monodisperse, non-interacting, spherical micelles. Therefore, in the SAXS modeling the aggregates have been assumed to be spherical micelles composed of an alkyl-based, hydrophobic core and a PAEI-based, homogeneous, hydrophilic shell. Furthermore, they have also been assumed to undergo weak, hard-sphere interactions corresponding to the Percus-Yevick model[183]. This interaction model has been chosen because the SAXS experiments have been performed at higher concentrations than the DLS. Under those conditions, the hypothesis of non-interacting aggregates is not plausible any more. As can be observed in Figure 3.15, the experimental and simulated profiles fit in reasonably well with each other. In order words, the simulated profile describes faithfully the features observed in the experimental one. These features arise from the scattering properties of the sample. It can be recognized that the increase of the alkyl-PAEI concentration affects the features observed in the profiles. The shoulder at 0.3 nm^{-1} (low q region), which originates from the Percus-Yevick structure factor[184], becomes sharper when the polymer concentration increases. This increase of the alkyl-PAEI concentration results in a higher number of micelles, and hence of scattering objects in the solution. As a consequence, they become closer to each other and an enhancement of the interactions between them takes place[185]. Such an influence of the polymer concentration in the features of the SAXS patterns can be appreciated not only in the experimental profiles but also in the simulated ones. This fact confirms that the established model describes faithfully the behaviour of the aggregates within the investigated concentration range (5-15 wt%). Thus, according to this model, the aggregates built by alkyl-PAEI in water are spherical micelles composed of hydrophobic core and homogeneous, hydrophilic shell. In addition, they undergo hard-sphere interactions. Figure 3.16 shows schematically how the described aqueous solutions of alkyl-PAEI look like.

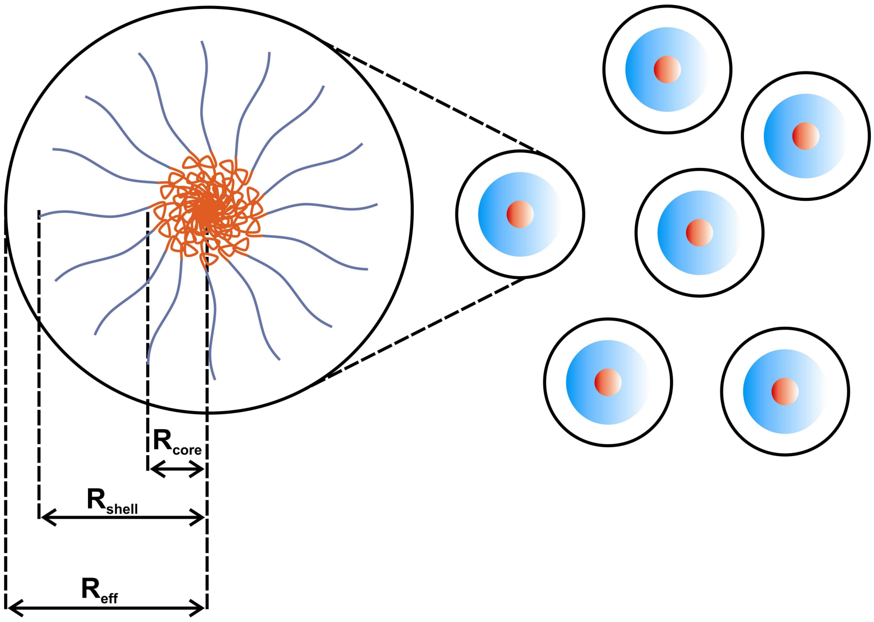

Figure 3.16. Schematic model of spherical alkyl-PAEI micelles in aqueous solution undergoing hard-sphere interactions.

It can be observed that together with the dimensions of the spherical micelles, R_{core} and R_{shell}, an effective hard-sphere radius R_{eff} has been defined. According to the Percus-Yevick theory, this parameter results from the interactions among the aggregates[183]. Those interactions can be regarded as a hard-sphere pair potential. From this point of view, the solution can be seen as a disordered, liquid-like arrangement of the micelles in the aqueous phase similar to that of the metal atoms in the melt state[184]. The effective hard-sphere radius R_{eff} represents the separation at which the micelles are just beginning to interact[186]. A similar kind of interaction has been reported for other amphiphilic systems, which also build spherical micelles in selective solvents[187-189].

Aqueous solutions containing hydrophobically-modified polyoxazolines have also been characterized by scattering methods. OBEID *et al.*[166] have investigated solutions containing telechelic and semitelechelic n-octadecyl-poly(N-(ethyl)-ethyleneimine) and n-octadecyl-poly(N-(isopropyl)-ethyleimine) via SAXS measurements. Furthermore, VOLET *et al.*[190] have recently reported Small Angle Neutron Scattering (SANS) investigations in aqueous solutions containing semitelechelic n-octadecyl-poly(N-(acetyl)-ethyleneimine) similar to that characterized within this section. In both studies, the polymers have been proven to aggregate in pure water forming spherical micelles composed of hydrophobic alkyl-based core and hydrophilic polyoxazoline-based shell. In addition, OBEID *et al.*[166] have chosen an exponential density profile for the shell whereas VOLET *et al.*[190] have assumed the aggregates to be star-like micelles. However, according to their investigations, the micelles built by the semitelechelic polymers undergo long-range repulsive interactions, while those built the telechelic ones act more like hard-spheres. The reason for these deviations with respect to the results reported in this work for the micelles built by alkyl-PAEI may arise in the concentration range at which the SAXS experiments have been performed. Whereas OBEID *et al.* and VOLET *et al.*[166, 190] have investigated solutions with a polymer concentration between 10 and 20 mg/ml, those characterized in this work contained between 53 and 176 mg/ml. At those high polymer concentrations, different phenomena like interpenetration of the hydrophilic shells can take place and a different kind of interaction between the micelles is possible. The occurrence of hard-sphere interactions between spherical, interpenetrable domains of diblock copolymers reported by KINNING *et al.*[187] supports this hypothesis. It is also worth mentioning that organic coatings such as poly-12-hydroxystearic acid (PHSA) has been used on colloidal spheres to provide a ‘‘hard-sphere type’’ interaction[191]. Thus, not only the concentration but also the type of functional groups on the shell-forming block can exert an influence on the type of interaction among the aggregates.

As already mentioned, as soon as the experimental and simulated profiles fit in reasonably well with each other, important parameters that describe the morphology and interactions of the aggregates can be extracted. Table 3.6 summarizes the parameters yielded by the modeling of the SAXS data for alkyl-PAEI aqueous solutions with concentrations from 53 to 176 mg/mL at 20 °C.

Table 3.6. Modelling of the SAXS data obtained for alkyl-PAEI in aqueous solution at 20 °C using the Percus-Yevick hard-sphere theory[183]a.

P_n [b]	c, wt%	c, mg/mL	R_{core}, nm	R_{shell}, nm	ρ	σ	R_{eff}, nm
10	5	52.6	2	8.4	0.048	0.158	12.30
	10	111.1	1.65	7.34	0.028	0.03	13.45
	15	176.5	1.52	7.44	0.019	0.03	12.02
20	5	52.6	2.64	10.04	0.072	0.24	12.3
	10	111.1	1.79	7.33	0.043	0.08	13.45
	15	176.5	1.92	7.81	0.040	0.14	10.53
40	5	52.6	2.8	14.78	0.02	0.29	14.79
	10	111.1	1.98	9.72	0.03	0.27	13.83
	15	176.5	1.74	8.74	0.025	0.21	12.93

[a], represented modelling parameters are: R_{core}, radius of the core; R_{shell}, overall radius of the core/shell spheres; ρ, ratio of shell/core electron densities; σ, relative standard deviation of particle radius; R_{eff}, hard-sphere radius.

[b], adjusted value, experimentally is ± 1

As a general conclusion it can be stated that the samples containing alkyl-PAEI with $P_n = 10$ show the most prominent features. At every concentration it is possible to identify the distinct minima, which are related to the size of the micelles[90]. For the higher polymerization degrees ($P_n = 20$ and 40), the prominent minima can be identified but less clearly. It can be expected that the phase boundary between the hydrated oxazoline shell and the surrounding water gets less defined for materials of higher P_n. With increasing P_n of the oxazoline block the polymers become more hydrophilic and micelle formation is shifted to higher concentrations. However, under the conditions of the SAXS measurements, it seems to be clear that all samples form micelles. For the solutions with 5 wt% of polymer the first shoulder, which originates from the Percus-Yevick factor, is still not completely developed. The fact that the overall shape of the patterns does not change much upon increasing concentration means that the micelle shape is not affected by higher concentrations, i.e. a phase transition does not take place but a closer packing of the micelles. From the modeled data it seems as if compression of the micelles occurs. This effect is pronounced in the solutions containing alkyl-PAEI with $P_n = 40$. As can be observed the radius of the hydrophilic shell R_{shell} decreases from 14.78 to 8.74 nm when the polymer concentration increases from 5 to 15 wt%. A similar but not so pronounced effect can be observed when the solutions contain alkyl-PAEI with $P_n = 10$ and 20. Regarding the dimensions of the micelles, solutions with 5 wt% of polymer yield values for R_{shell} that increase with the degree of polymerization of the hydrophilic chain, but not linearly. A similar effect has been observed in the dynamic light scattering (DLS) experiments. However, the values for the hydrodynamic radius R_h found by DLS are slightly lower than those obtained for R_{shell} via SAXS measurements. This effect may be again ascribed to the fact that the DLS experiments have been carried out at a dilute concentration regime. Another important aspect expressed by the values in Table 3.6 is that the increase of R_{shell} with the degree of polymerization of the hydrophilic block becomes less prominent at higher concentrations. In fact, at 5 wt% R_{shell} reaches values of 8.4 and 14.78 nm for $P_n = 10$ and 40, respectively. At 15 wt% R_{shell} becomes 7.44 and 8.44 nm, respectively, for the same P_n values. It can be also detected that generally the radius of the hydrophobic core R_{core} slightly decreases by increasing the polymer concentration. Both observations support the hypothesis that a compression of the micelles takes place at higher polymer concentrations. The values obtained for R_{core} are quite similar for polymers with different degree of polymerization at a given concentration. This observation is in accordance with the fact that the polymers only differ in the length of their hydrophilic chains. However, the length of the alkyl chain, which builds the hydrophobic micelle core, remains constant.

Another important parameter useful for the characterization of the aggregate morphology is the ratio of shell/core electron densities ρ. As can be seen in Table 3.6, for $P_n = 10$ and 20 this parameter decreases with increasing polymer concentration. This may be a consequence of the already mentioned compression of the micelles. Because of this compression some of the surrounding water gets into the micelles and the interface between core, shell and solvent becomes less sharp. Therefore, the difference of electron densities is lower. On the contrary, for the samples containing alkyl-PAEI with $P_n = 40$ ρ remains relatively constant over the whole concentration range. Here, the compression already takes place at the lowest concentration because of the higher length of the hydrophilic segment.

Regarding the polydispersity of the micelles, solutions containing alkyl-PAEI with $P_n = 10$ and 20 yield σ values below 0.2. This is typical for monodisperse distributions as was already commented in section 3.2.1.4 when dealing with DLS measurements. For solutions containing alkyl-PAEI with $P_n = 40$ the values for the polydispersity factor σ are slightly above 0.2. Nevertheless, they are quite close to this value indicating a relatively monodisperse distribution of micelles.

The values for the hard-sphere interaction radius (R_{eff}) of the alkyl-PAEI spherical micelles are also listed in Table 3.6. As can be detected, for $P_n = 10$ and 20 R_{eff} reaches a maximum at c = 10 wt%. In addition, R_{eff} at c = 5 wt% is higher than at c = 15 wt%. Furthermore, the difference between both values is higher for $P_n = 20$ than for $P_n = 10$. This finding provides another clear evidence of the already described compression phenomena at higher polymer concentrations. In fact, the increase of R_{eff} by increasing the polymer concentration from 5 to 10 wt% originates the appearance of stronger interactions between the micelles. The subsequent decrease of R_{eff} by increasing the polymer concentration from 10 to 15 wt% is caused by the compression of the micelles. For this reason solutions with c = 5 wt% possess higher interaction distances than those with c = 15 wt%, in spite of the fact in the latter the interactions between the aggregates are stronger. Contrary to $P_n = 10$ and 20, it can be observed that for $P_n = 40$ R_{eff} does not reach a maximum but it decreases by increasing the polymer concentration in accordance with the trend reported for R_{shell}. Here, owing to the higher size of the alkyl-PAEI aggregates, compression phenomena take place at lower concentration values in comparison to the previous cases.

Taking all these observations into consideration, another aspect that should be discussed is why the micelles are compressed but do not merge. This phenomenon could be related to the increase of the osmotic pressure which has been reported to take place in micellar solutions of ionic[192, 193] and non-ionic surfactants[194]. Such an increase of the osmotic pressure is caused by the appearance of interactions between the micelles and prevents the collapse of those. Along with the increase of the osmotic pressure, the presence of a hydration shell surrounding the hydrophilic corona of the micelles may be as well another reason why the micelles do not merge. Such a hydration shell has been found to surround the hydrophilic corona of the micelles formed by different surfactants[195, 196], including several PEO-containing amphiphilic polymers[197-200]. Furthermore, strong hydrogen bondings between water molecules and functional groups that compose the hydrophilic shell have been described in protein-based micelles[201]. Alkyl-PAEI contains functional groups similar to those of a protein, i.e. amino and carbonyl groups. Therefore, hydrogen bondings between water and those functional groups located on the corona are likely to take place. Due to these multiple hydrogen bondings, a high energy barrier has to be overcome in order to destroy the hydration shell. As a consequence the micelles can not merge.

3.2.1.7 Cryo-Transmission Electron Microscopy (Cryo-TEM)

Electron microscopy techniques are frequently used to directly visualize macromolecular structures. Among those, cryo-transmission electron microscopy (cryo-TEM), which has been widely used in the case of biological objects, has given promising results in surfactant sciences[202, 203]. Within this field, cryo-TEM has become increasingly popular for investigating the shape of surfactant aggregates, such as micelles, vesicles, or lamellae[204, 205]. Although it is hard to go beyond an observation of the aggregate shape and perform a quantitative analysis of the micrographs, cryo-TEM gives a direct visualization of the aggregate structure. This visualization can complement the results provided by different scattering techniques such as DLS and SAXS. Moreover, in contrast to the traditional solvent evaporation method, the application of the cryo-TEM technique allows the visualization of the aggregates as they are present in solution[206, 207]. As it is well-known, evaporation of the solvent can generate artifacts in the samples. As a result the morphologies of the aggregates in the TEM images may be different from those in the solution.

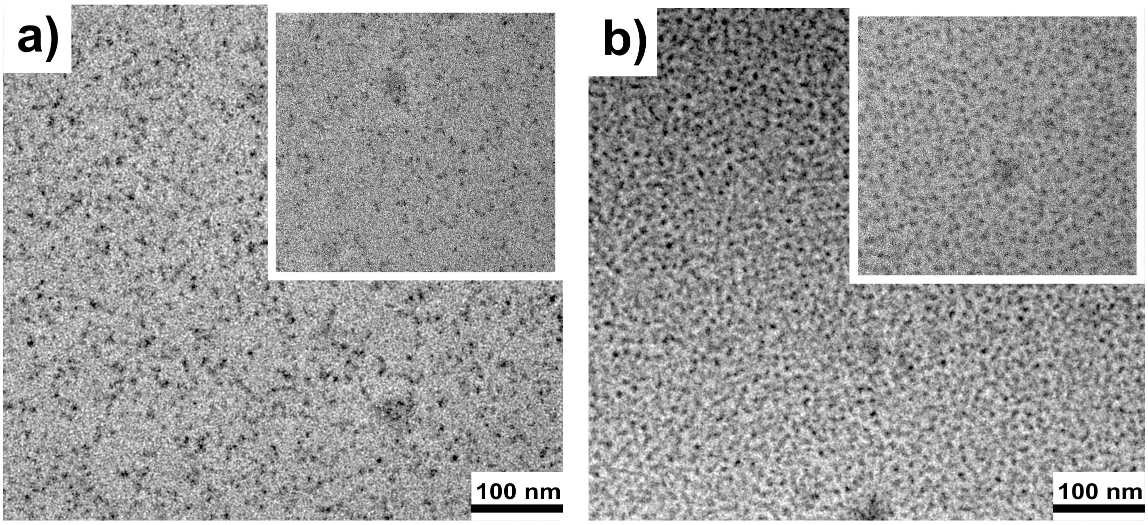

Figure 3.17. Cryo-TEM images corresponding alkyl-PAEI ($P_n = 10$) aqueous solutions with concentrations (a) 1 wt% (10 mg/ml) and (b) 5 wt% (50 mg/ml) at 25 °C.

In line with those considerations, cryo-TEM has been used within this work in order to confirm the results obtained by the scattering methods reported previously, i.e. DLS and SAXS. For this purpose, cryo-TEM images of solutions containing polymer concentrations similar to those investigated by DLS and SAXS have been taken. Figure 3.17-a shows the cryo-TEM image of an aqueous solution containing 1 wt% (10 mg/ml) of alkyl-PAEI with $P_n = 10$. As has already been reported in section 3.2.1.5, the DLS experiments for alkyl-PAEI with $P_n = 10$ have been performed within a concentration range from 4 to 40 mg/ml. Thus, the cryo-TEM image depicted in Figure 3.17-a offers information about the aggregate solution within the concentration range at which the DLS experiments have been performed. In fact, the presence of spherical micelles (dark dots) with a size around a few nanometers can be identified in the polymer solution (light background). However, a more accurate value for the size of the micelles can not be determined from these images. Likewise, Figure 3.17-b shows the cryo-TEM image of an aqueous solution of alkyl-PAEI ($P_n = 10$) but with a concentration around 5 wt% (50 mg/ml). This value corresponds to the lowest concentration of the solutions which the SAXS profiles have been obtained for. Therefore, Figure 3.17-b can give visual information of the aggregate solution within the concentration range at which the SAXS measurements have been performed. Spherical micelles with a size around a few nanometers can also be observed in this image. Similarly, the determination of a more accurate value is hard as in the previous case. However, further comparison between both images reveals a higher density of micelles (dark dots) and hence a closer packing of them at the higher polymer concentration (Figure 3.17-b). This is in agreement with the conclusions provided by both, DLS and SAXS investigations. Both scattering methods have revealed the existence of alkyl-PAEI spherical micelles in aqueous solution. However, whereas in the dilute concentration regime studied via DLS (Figure 3.17-a) the micelles possess a non-interacting character, at higher concentrations (Figure 3.17-b) the SAXS results have revealed that they undergo hard-sphere interactions. In fact, as can be observed in Figure 3.17 the increase of the alkyl-PAEI concentration results in a higher density of micelles. As a consequence, they become closer to each which explains the appearance of interactions among them.

3.2.1.8 Concluding remarks on alkyl-PAEI characterization

Within this section the aggregation behaviour of alkyl-PAEI in water has been studied. Optical microscope images with cross-polarized light of water penetration scan for the polymer prove the formation of lyotropic liquid crystalline domains. The micellization of the polymer in pure water has been investigated via fluorescence spectroscopy in the presence of pyrene. The substantial enhancement of the fluorescence intensity by increasing the concentration of polymer in solution indicates the presence of aggregates with hydrophobic domains into which pyrene transfers. The critical micelle concentration, which has been determined by measuring surface tension, increases with the degree of polymerization of the hydrophilic segment. Besides, the CMC values measured in different acid buffers are extremely lower than those obtained in pure water.

The size, shape and internal structure of the aggregates in water have been investigated via scattering methods. Dynamic light scattering (DLS) and small angle X-ray scattering (SAXS) experiments show the presence of alkyl-PAEI spherical core-shell micelles in pure water with sizes ranging from 6 to 11 nm depending on the degree of polymerization of the hydrophilic chain. These micelles are monodisperse and non-interacting at a low concentration regime (1 wt%) and undergo hard-sphere interactions at higher concentration values (5-15 wt%).

Finally, cryo-TEM images of alkyl-PAEI solutions in pure water confirm the presence of spherical micelles and show that with increasing polymer concentration the aggregates become closer to each other.

3.2.2 Alkyl-poly(ethyleneimine) (alkyl-PEI)

3.2.2.1 Introduction

Poly(ethylenimine) (PEI) is a partially water-soluble polymer, which is widely used in paper industry**.** It is commercially available in linear and hyperbranched forms. Moreover, oligomers with tailored chain-lengths can be also produced via cationic ring-opening polymerization (CROP) of aziridines[109] or cyclic iminoethers with subsequent hydrolysis[132]. As it is relatively easy to attach a variety of organic groups to PEI, several PEI-based macromolecular structures with different architectures have been developed[115, 208, 209]. Its chelating properties have been used to form complexes with molecules bearing organic functionalities[210, 211] and with metal ions such as gold[212]. This ability to form complexes and the low cytotoxicity of low molecular weight PEI are why PEO-PEI-PEO triblock copolymers have been suggested as efficient polymeric carriers for DNA delivery[213]. Another important property of PEI is its ability to undergo thermoreversible gelation, yielding opaque ice-cream-like hydrogels, which have been used as soft sacrificial template in the production of porous metal frameworks[214].

PEI-based polymers have been also used in bioinspired mineralization. Homopolymers and double-hydrophilic block copolymers containing PEI segments can modify the growth of calcium phosphate crystals[215, 216]. It is also well known that PEI resembles the polyamines found in silica biominerals[217, 218]. These polymers seem to play a crucial role in the formation of highly ordered silica structures in nature under ambient conditions. In this regard, silica nanospheres with tunable size have been produced in the presence of dendritic templates bearing PEI and PPI blocks[38, 219]. Thus, combining the ability of PEI or PPI to promote silicic acid condensation with functional groups which enable self-assembly of polymers into well-defined structures may be a suitable approach for the biomimetic production of tailored silica structures. In this context, there are some examples where PEI, linear or branched, has been hydrophobically modified in different ways, which promotes its self-association into aggregates with tailored shapes and dimensions[58, 220, 221].

Here, hydrophobically modified alkyl-PEI is interesting, because it exhibits different properties than pure PEI because of its amphiphilic character. This section describes how the combination of the unique properties of PEI with the amphiphilic character provided by the alkyl chain leads to modifications in its behaviour.

3.2.2.2 Critical Micelle Concentration (CMC)

In a similar way to alkyl-PAEI, the critical micelle concentration of alkyl-PEI in pure water and in buffers of different pH has been determined by measuring surface tension. First of all it must be mentioned that, as already reported by TANAKA *et al.*[134] for linear poly(ethyleneimine) (lin-PEI), alkyl-PEI dissolves in hot water but shows low solubility in cold aqueous media. Therefore, for the production of alkyl-PEI aqueous solutions, the polymer was suspended in water, subsequently heated up to 80 °C and finally cooled down to room temperature. Figure 3.18 shows alkyl-PEI ($P_n = 40$) aqueous solutions with different concentrations prepared in this way.

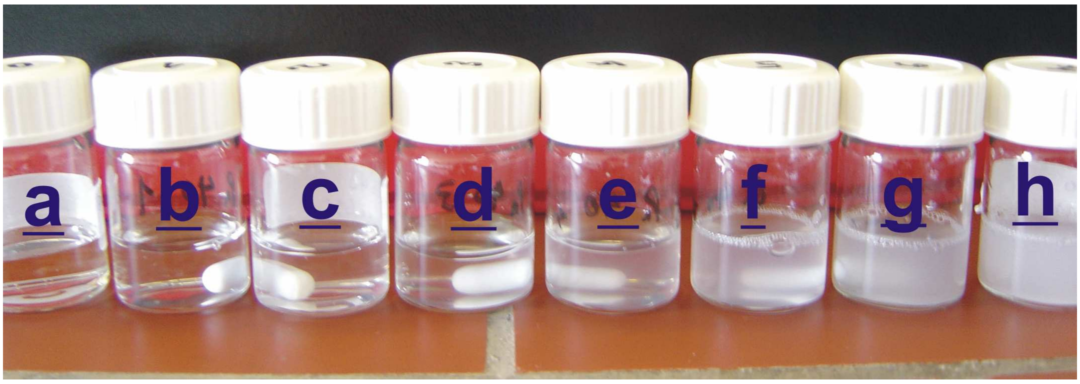

Figure 3.18. Aqueous solutions containing (a) 0, (b) 0.003, (c) 0.006, (d) 0.012, (e) 0.025, (f) 0.05, (g) 0.1, and (h) 0.25 wt% of alkyl-PEI ($P_n = 40$) after heating to 80 °C and subsequent cooling to room temperature.

As can be observed, the solutions are clear at concentrations below 0.025 wt%, solution **e** in Figure 3.18, but become turbid at higher concentrations. This turbidity increases by increasing the polymer concentration and according to YUAN *et al.*[222] this is caused by the formation of nanofiber-based three-dimensional aggregates. It has also been observed[222] that the concentration at which the turbidity appears increases by decreasing the degree of polymerization of the PEI chain. Nevertheless, a linear decay of the surface tension with the polymer concentration can be measured for the clear solutions as can be seen in Figure 3.19. In fact, the surface tension values obtained for aqueous solutions of alkyl-PEI with $P_n = 10$ decrease linearly and then show a break at 0.34 mM, remaining relatively constant at concentrations above this value. It is worth to mention that the turbidity appears at a concentration value around 1.17 mM (0.082 wt%), which is above the CMC. Thus, at 25 °C the solubility of alkyl-PEI in pure water is higher than its critical micelle concentration. In other words, the Krafft temperature (section 2.2.2) for this polymeric surfactant is lower than 25 °C. For this reason, the production of alkyl-PEI clear aqueous solutions containing aggregates is feasible at this temperature. The CMC values determined for alkyl-PEI with different degree of polymerization in pure water and in different pH buffers are summarized in Table 3.7.

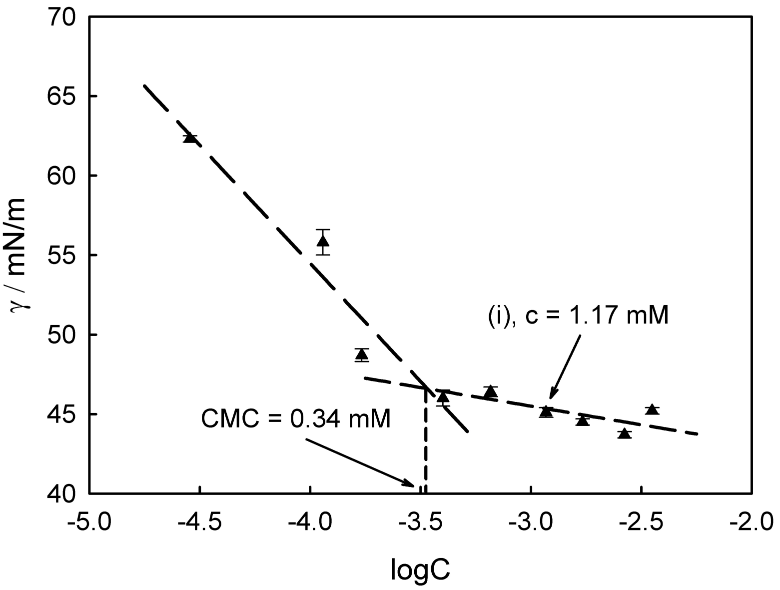

Figure 3.19. Semilogarithmic plot of surface tension (γ) versus concentration (mM) of aqueous solutions containing alkyl-PEI ($P_n = 10$) at 25 °C showing both, the CMC and the concentration at which turbidity appears (i).

Table 3.7. Critical micelle concentration (CMC) values of alkyl-PEI samples with different degree of polymerization in pure water and in different pH buffers at 25 °C.

P_n [a]	Buffer	pH[b]	CMC, wt%	CMC, mM	γ_{cmc}, mN/m
10	water	7	0.023	0.34	46
20	water	7	0.056	0.51	48
40	water	7	0.005	0.024	49
40	citrate	3.5	0.008	0.034	22
40	acetate	4.5	0.005	0.024	21
40	malonate	5.5	0.0018	$8.64 \cdot 10^{-3}$	21
40	phosphate	5.6	0.007	0.034	25

[a], adjusted value, experimentally is ± 1. [b], the pH values of the medium after dissolution of the polymer were slightly higher (~ 0.5) than that of the buffer.

Unlike the CMC values reported for alkyl-PAEI (section 3.2.1.4), those determined for alkyl-PEI in pure water (pH = 7) do not increase with increasing degree of polymerization of the hydrophilic segment but they show a maximum at $P_n = 20$. The low CMC value (CMC = 0.005 wt%) obtained for the alkyl-PEI sample with $P_n = 40$, in comparison to those with $P_n = 10$ and 20, 0.023 and 0.056 wt%, respectively, is especially remarkable. Further comparison of the values obtained for alkyl-PAEI (section 3.2.1.4) and alkyl-PEI reveals that for $P_n = 20$ both polymers present the same CMC in wt%, CMC = 0.023 wt%. A subsequent increase of the degree of polymerization in the hydrophilic chain results in higher CMC values for alkyl-PAEI than for alkyl-PEI. Moreover, the difference between the values found for both polymers becomes higher as the degree of polymerization increases. This behavior may be again ascribed to the lower solubility of alkyl-PEI in pure water, which decreases dramatically by increasing the degree of polymerization of the PEI segment as described previously.

Regarding the influence of the pH in the micellization process, the CMC values of alkyl-PEI in the different buffers are also shown in Table 3.7. At this point, it is important to highlight the alkaline properties of alkyl-PEI. They are due to the presence of amino groups in its structure. As a consequence, a slight increase of the pH, around 0.5, takes place after dissolving the polymer in the buffer solution. Taking these alkaline properties into account, it could be expected that both, the solubility and CMC of alkyl-PEI in the acidic buffers increases in comparison to those in pure water. Regarding the solubility, it is slightly higher in acetate buffer (pH = 4.5). As will be explain in the section dealing with the production of polymer-mediated silica precipitates (see section 3.3.2), clear solutions of alkyl-PEI (P_n = 10, 20 and 40) in acetate buffer can be produced but with concentrations up to 0.1 wt% only. In malonate buffer (pH = 5.5), the highest concentration for alkyl-PEI clear solutions is 0.01 wt%. Thus, as expected, the lower is the pH of the medium, the more soluble is the polymer. However, in citrate (pH = 3.5) and phosphate buffers (pH = 5.6) a different behavior has been observed. Here, alkyl-PEI becomes less soluble than in pure water showing turbidity at very low concentrations, e.g. 0.009 wt% for alkyl-PEI with $P_n = 40$ in phosphate and citrate buffers, even in spite of the fact that in the citrate buffer the pH value (3.5) is lower than in acetate (4.5). Such a turbidity in aqueous solutions containing linear PEI at very low concentration, within a pH range between 3 and 8 and in the presence of phosphate and citrate has already been reported by MANZUR *et al.*[223]. According to these investigations, the turbidity is caused by formation of insoluble PEI complexes under the previously mentioned conditions. That precipitation ability of PEI combined with its affinity for proteins makes it a suitable material in the field of protein purification[224]. Within this work, the solutions containing alkyl-PEI insoluble complexes in citrate and phosphate buffers have been used to produce silica precipitates as will be reported in section 3.3.2.

Regarding the influence of pH on the CMC, the values obtained for alkyl-PEI with $P_n = 40$ in citrate, acetate and phosphate, 0.008, 0.005 and 0.007 wt%, respectively, are comparable to that obtained in pure water with 0.005 wt%. Yet, the CMC value determined in malonate buffer (pH = 5.5) is slightly lower, 0.0018 wt%. Thus, a similar trend to that observed for the solubility of alkyl-PEI in acetate and malonate has not been identified for the CMC. Moreover, the CMC values in citrate and phosphate buffers are slightly higher than that obtained in pure water, even when the solubilities are much lower. In this respect, it must be remarked that, as already explained in section 2.2.2, the CMC of a surfactant depends upon many factors. In this case, the presence of the different anions (citrate, acetate, malonate or phosphate) provided by the buffers may play an important role in the final values.

Finally, the surface activity of alkyl-PEI in pure water and in the different buffers is similar to that shown by alkyl-PAEI under the same conditions. In fact, in pure water alkyl-PEI yields surface tension values between 46 and 49 mN/m, depending on P_n. These values are close to those obtained for alkyl-PAEI, between 44 and 48 mN/m (see Table 3.4). In the different buffers a same situation is found and both, alkyl-PEI and alkyl-PAEI give surface tensions between 21 and 25 mN/m. This observation involves that, at low concentrations, both surfactants show a similar behaviour in aqueous solution apart from the fact that alkyl-PAEI has been proven to be more soluble than alkyl-PEI. Therefore, alkyl-PAEI can be regarded as an acetyl-modified alkyl-PEI. This modification does not affect its surface activity but modifies its solubility and CMC values in pure water. Furthermore, as discussed in section 3.2.1.4, SAEGUSA *et al.*[131] have proven that the surface activity of polyoxazoline-based surfactants strongly depends on the length of both, hydrophilic and hydrophobic segments as well as on the nature of the functional groups contained in those segments. That is the reason why the surface activities of alkyl-PEI and alkyl-PAEI are so similar. Their functional groups resemble and they both have been produced with the same degrees of polymerization (P_n = 10, 20 and 40).

3.2.2.3 Potentiometric titration

As already mentioned in section 2.1.2.2, the condensation of silicic acid is strongly influenced by the pH value of the reaction medium. Therefore, the acid-base behavior of any substances, such as polyamines, taking part in the silica precipitation process should be investigated. For this purpose, potentiometric titrations represent a suitable method. They have been used to study the influence of pH on different phenomena shown by polyelectrolytes, like aggregation[225], interaction with other macromolecules[226] or even adsorption on surfaces[227].

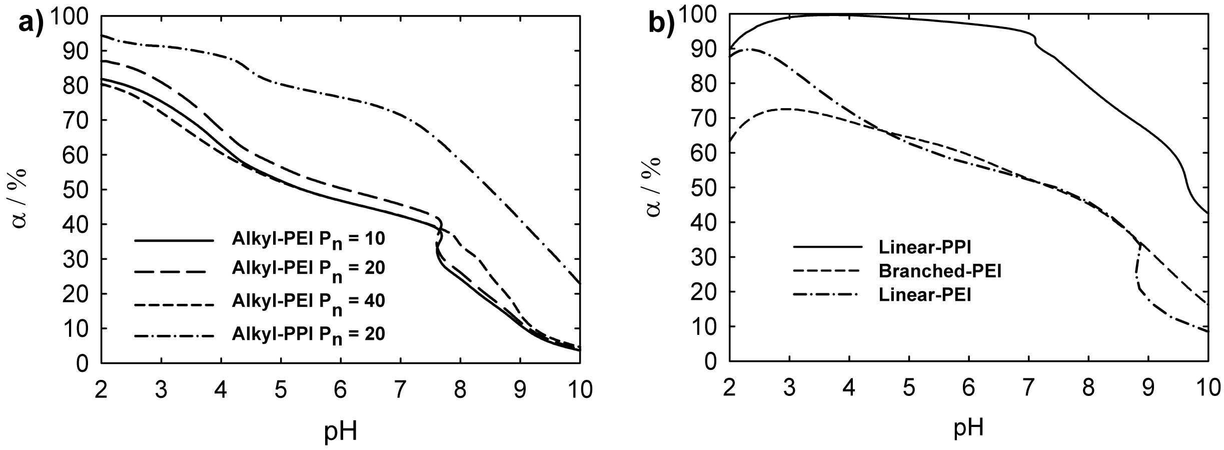

Figure 3.20. Degree of protonation of (a) synthesized alkyl-PEI and alkyl-PPI and (b) linear and branched PEI and linear PPI[218] as a function of pH at 25 °C.

Figure 3.20-a shows the degree of protonation α of alkyl-PEI samples with different degrees of polymerization (P_n = 10, 20 and 40) and of alkyl-poly(propyleneimine) (alkyl-PPI) with P_n = 20 as a function of the solution pH. SHKILNYY *et al.*[218] performed potentiometric titration of linear PEI (M_w ca. 22000 g/mol), branched PEI (M_w ca. 25000 g/mol) and linear PPI (M_w ca. 3700 g/mol) (Figure 3.20-b). It is well-known that the ionic strength of the medium does not affect the shape of the titration curves but can shift them towards different pH values[228, 229]. Thus, within all these titrations the polymer solutions possess the same concentration of NaCl (0.5 M) in order to ensure constant ionic strength.

Figure 3.20 shows that the degree of protonation of alkyl-PPI is higher than that of the alkyl-PEI samples at any pH value. The reason is the lower electrostatic repulsion between neighboring groups upon replacing ethylene by propylene as spacer.

The titration curves of alkyl-PEI with P_n = 10 and 20 are similar to that of linear PEI. First, two steps with a less pronounced drop beginning at about α 50 % and pH 4.5 can be distinguished. At this pH value, in average every second amino group is protonated. Further protonation has to take place between two neighboring, already positively charged, sites[218]. As result of the electrostatic repulsion the binding constants for this process become lower and it is not possible to completely protonate alkyl-PEI at pH 2. The maximum degree of protonation α is around 80 %. On the other hand, the conformation of polyamines strongly depends on the solution pH[230]. With increasing pH, charge repulsion diminishes and the polymer chains fold into coils becoming insoluble at pH values higher than 8 as indicates the mirrored S-shape of the curves. At this point (α ~ 30 %), the electrostatic energy barrier, which inhibits the formation of aggregates in solution, becomes smaller than the thermal energy. Alkyl-PEI chains collapse and the excess of protons, which prevent the aggregation, are forced out into solution. In the case of linear PEI the precipitation (mirrored S-shape of the curve) takes place at higher pH values (around 9). This effect is also observed in the titration curves of linear PPI and alkyl-PPI (precipitation at pH 5 and 7, respectively) and is caused by the hydrophobic interaction of alkyl chains, which promotes the polymer aggregation at lower pH values.

Finally, the titration curves of alkyl-PEI with $P_n = 40$ and branched PEI are similar at high pH values. Unlike linear PEI and alkyl-PEI with $P_n = 10$ and 20, the most important feature is the absence of polymer precipitation at high pH. This fact can be ascribed to the low tendency of branched PEI macromolecules to precipitate readily. The relatively high length ratio between PEI block and alkyl chain in the alkyl-PEI with $P_n = 40$ (in comparison to those with $P_n = 10$ and 20) could make a spherical aggregation of the PEI blocks around an hydrophobic core of the alkyl chains possible[225, 231]. This conformation hinders the precipitation since collapse of PEI chains is less probable. In both cases -the branched PEI and the spherical aggregates of alkyl-PEI with $P_n = 40$ -the electrostatic repulsion occurs in three dimensions in contrast to alkyl-PEI with $P_n = 10$ and 20 and linear PEI, where the repulsion takes place only in one dimension (along the polymer chain).

3.2.2.4 Solid state characterization

XRD investigations by CHATANI *et al.* have proven that the hygroscopic character of poly(ethyleneimine) is directly related to the formation of crystalline hydrates containing stoichiometrical amounts of water[232-234]. Whereas in the anhydrate state (which contains zero water molecules per each PEI unit and is hence represented as (0)) PEI chains fold into double-stranded helices, in the different hydrates (which contain 0.5, 1.5 and 2 water molecules per PEI unit and are hence represented as (0.5), (1.5) and (2), respectively) the chains adopt a planar zig-zag conformation as a consequence of intermolecular hydrogen bonds with water molecules. The existence of one or more of these crystalline species in PEI samples depends on the water vapour pressure of the atmosphere. The transition mechanism between these hydration states has been studied spectroscopically (IR, Raman) by HASHIDA *et al.*[235, 236].

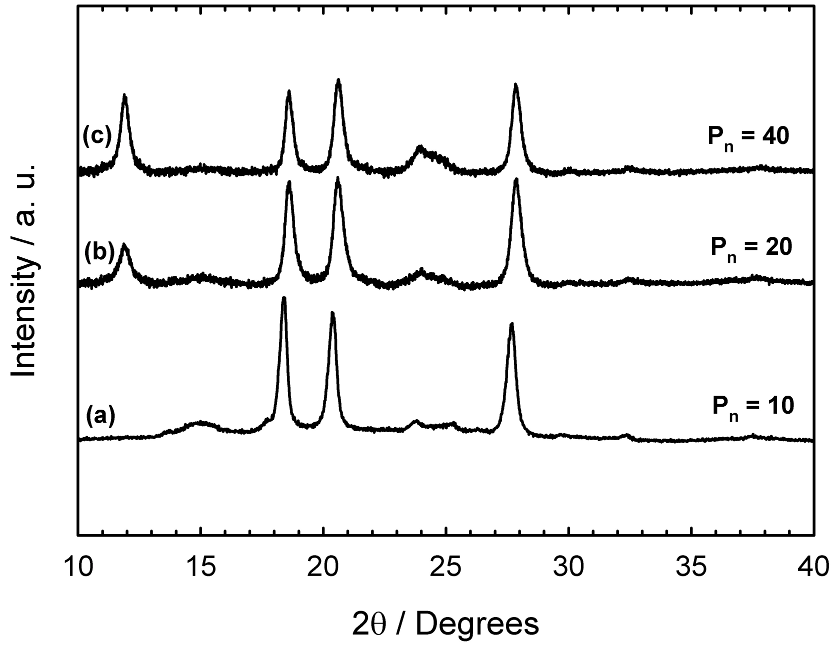

Figure 3.21. X-ray diffraction patterns of alkyl-PEI samples with degrees of polymerization P_n = 10 (a), 20 (b) and 40 (c) measured at 25 °C.

Figure 3.21 shows the XRD patterns of alkyl-PEI samples with different degrees of polymerization. A reflection at 11.89° corresponds to the anhydrate (0)[232] in the samples with P_n = 20 (b) and 40 (c). However, the sample with P_n = 10 (a) does not show this characteristic reflection of the anhydrate (0).

Table 3.8. Water content of alkyl-PEI samples determined by Karl-Fischer titration.

Degree of polymerization, P_n ^{a}	**Water content, wt%**
10	5.02
20	2.81
40	2.08

^{a}, adjusted value. Experimentally is ± 1.

Table 3.8 shows the water content of the alkyl-PEI samples determined by Karl-Fischer titration[237]. The sample with P_n = 10 contains a higher amount of water (5.02 wt%) than those with P_n = 20 and 40 (2.81 and 2.08 wt%, respectively). This explains the absence of reflections corresponding to the anhydrate (0) (Figure 3.21). Further reflections at 18.4°, 20.3°, 24.5° and

27.7° can be identified in each sample. The reflection at 24.5° is broader in the patterns b ($P_n = 20$) and c ($P_n = 40$) than in the a ($P_n = 10$) where it is composed of two small twin reflections (24° and 25.4°) corresponding those found in samples containing the sesquihydrate (1.5). In pattern b and c these two reflections can not be recognized because of overlapping with another one characteristic of the anhydrate state[232] (0). The combination of the other three sharp reflections (18.4°, 20.3° and 27.7°) observed in each sample was found by CHATANI in mixtures of sesquihydrate (1.5) with hemihydrate (0.5) or dihydrate (2)[232], making it difficult to determine the composition of the samples. However, the low water content of the samples (PEI can uptake over 50 % its weight of water[232]) together with the identification of the anhydrate (0) in two of them (P_n = 20 and 40) indicates that hemihydrate (0.5) and sesquihydrate (1.5) is the most probable mixture of phases composing alkyl-PEI samples. This statement is also supported by the fact that the samples were kept under dry storage conditions (vacuum, silica gel orange), where the existence of the dihydrate (2) is less probable because of the low water content in the surrounding atmosphere. Considering these observations, alkyl-PEI with P_n = 20 and 40 consists of a mixture where anhydrate (0), hemihydrate (0.5) and sesquihydrate (1.5) coexist while alkyl-PEI with $P_n = 10$ is composed of hemihydrate (0.5) and sesquihydrate (1.5).

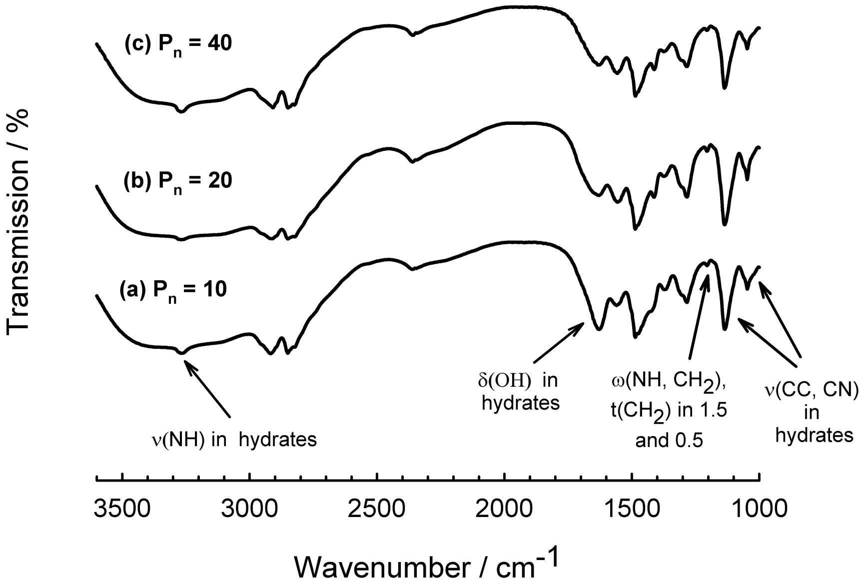

Figure 3.22. FTIR spectra of alkyl-PEI samples with degrees of polymerization P_n = 10 (a), 20 (b), and 40 (c) measured at 25 °C showing stretching (υ), wagging (ω), twisting (t) and bending (δ) bands of different bonds in the alkyl-PEI hydrates.

FTIR spectra of alkyl-PEI samples are shown in Figure 3.22. Characteristic bands related to stretching, bending, wagging or twisting modes of different bonds in the hydrates can be identified. The higher intensity of the band at 1652 cm^{-1} (related to the bending of the OH groups in the hydrates) for the sample with $P_n = 10$ in comparison to those with $P_n = 20$ and 40 is obvious. This may be caused by the higher water content of the sample with $P_n = 10$. Broad bands at 3000-3600 cm^{-1} and 1000-1600 cm^{-1} from vibration modes of absorbed water can be also observed in each spectrum. However, characteristic groups of sharp tiny bands found in anhydrate PEI samples[235] do not appear in spectra of alkyl-PEI with $P_n = 20$ and 40, which contain the anhydrate crystalline state as shown before in its XRD patterns. The overlapping of the bands useful for identification of hydrates with each other or with broad water bands is the reason for the absence of anhydrate bands in the spectra of alkyl-PEI with $P_n = 20$ and 40 and represents a limitation in the detection of PEI hydration states by FTIR spectroscopy. HASHIDA *et al.* have solved this problem by performing the hydration process of PEI in atmospheres with heavy water (D_2O) and by complementing FTIR spectroscopy with Raman spectroscopy[236]. Replacing H_2O by D_2O can shift overlapped characteristic bands crucial for identification of hydrated species and Raman spectroscopy can detect bands which in FTIR spectra are hidden by the broad water absorption bands.

3.2.2.5 Thermal characterization

XRD, FTIR and DSC studies by HASHIDA *et al.* have also proven that PEI (M_w ca. 500000 g/mol) undergoes water-induced and thermally-induced phase transitions among crystalline hydrates[238, 239]. According to these investigations almost perfectly dried anhydrate melts at about 60 °C. Anhydrate containing a small amount of water shows a phase transition into a mixture of hemihydrate (0.5) and sesquihydrate (1.5) at around 40 °C. The hemihydrate (0.5) transfers into the sesquihydrate (1.5) at around 60 °C, and the latter melts above 80 °C. When the starting PEI sample contains a greater amount of water and consists of a mixture of hemihydrate (0.5) and sesquihydrate (1.5), the hemihydrate (0.5) transfers into the sesquihydrate (1.5), and the latter melts at around 75 °C. For a sample of dihydrate (2) containing a high amount of water, it transfers into the sesquihydrate (1.5) at around 65 °C, and the latter melts above 90 °C. A sample of dihydrate (2) with a much higher water content melts at about 110 °C; during this period, no transition into the sesquihydrate (1.5) is observed. These results highlight the complex thermal behaviour of linear PEI.

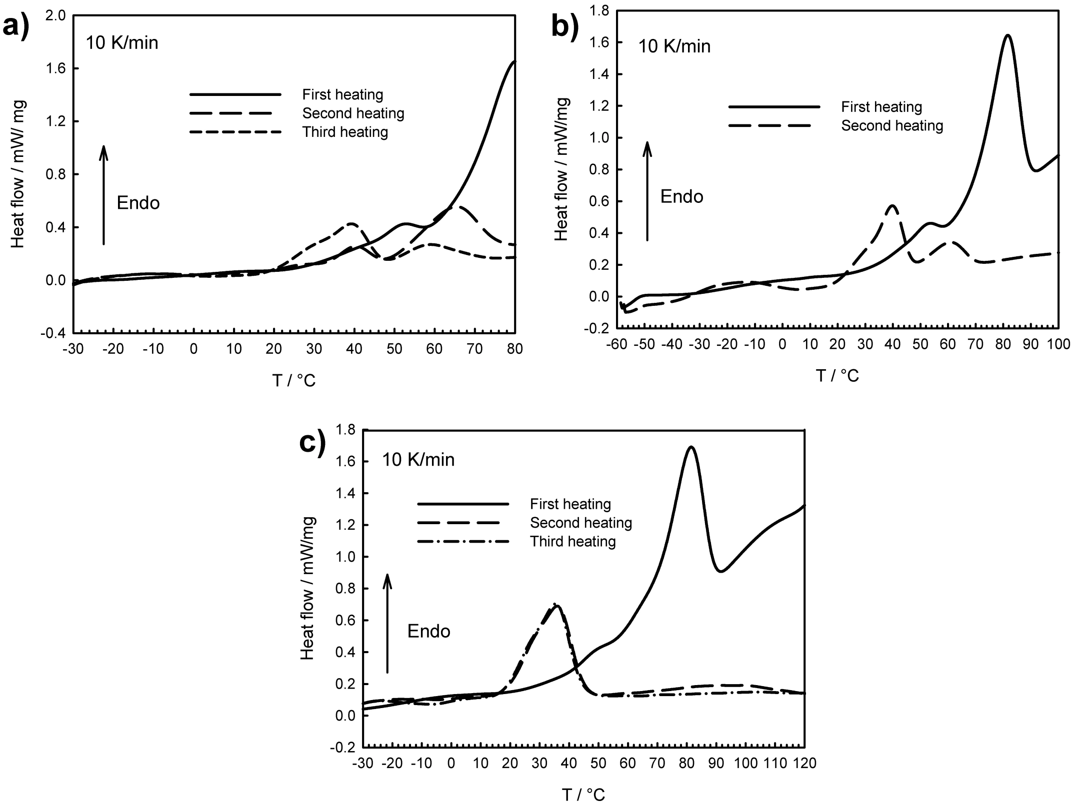

Figure 3.23. DSC thermograms of alkyl-PEI with P_n = 10 showing heating scans of the sample to 80 °C (a), 100 °C (b) and 120 °C (c).

In order to identify thermal transitions in alkyl-PEI samples, DSC investigations have been performed. Figure 3.23-a shows DSC thermograms of an alkyl-PEI sample with P_n = 10 heated to 80 °C. In the first heating curve, a small peak at 53 °C and a half-developed peak at 80 °C can be recognized. From XRD experiments it was previously concluded that the alkyl-PEI sample with P_n = 10 consisted of a mixture of hemihydrate (0.5) and sesquihydrate (1.5). The peak at 53 °C may be ascribed to the transition of hemihydrate (0.5) into sesquihydrate (1.5) and the half-developed peak at 80 °C to the melting of the sesquihydrate (1.5). The second and third heating curves each show two peaks (40 °C and 65 °C, 39 °C and 59 °C, respectively) shifted to lower temperatures with respect to those found in the first heating curve. This can be due to the fact that the sample loses some water by heating it to 80 °C. As a consequence the starting material for the second heating may not have the same amount of water as for the first one. The first peak found in these curves (~ 40 °C) may be produced by transition of anhydrate containing a small amount of water into a mixture of hemihydrate (0.5) and sesquihydrate (1.5) whereas the second one may be ascribed to the hemihydrate (0.5) to sesquihydrate (1.5) transition. Further heating of the sample shows the melting of the sesquihydrate (1.5), which as seen from thermal data of PEI[238] is strongly dependent on the sample water content.

Figure 3.23-b shows the DSC thermogram of an alkyl-PEI sample with $P_n = 10$ heated to 100 °C. The first heating curve does not reveal any variations with that obtained by heating to 80 °C (hemihydrate (0.5) to sesquihydrate (1.5) transition at 50 °C and melting at 80 °C). The second heating curve shows two peaks at around the same temperatures (40 °C, 61 °C) as those found in the second and third curves when heating to 80 °C. Finally, alkyl-PEI with $P_n = 10$ was heated to 120 °C (Figure 3.23-c). The first heating curve shows transitions at 50 °C and 80 °C as already reported in first heating scans with 80 °C or 100 °C as maximum temperature, respectively. On the contrary, the second and third heating curves show a single broad peak centered at 39 °C. This single peak may be caused by the melting of the anhydrate (0) since no more peaks are observed at higher temperatures. The heating of the sample to 120 °C seems to produce completely dehydrated alkyl-PEI after just one heating scan.

The DSC thermal data of alkyl-PEI samples with $P_n = 20$ and 40 are summarized in Table 3.9. The first heating curve of the sample with $P_n = 20$ shows three endothermic peaks. Besides those also found in the first heating curve of alkyl-PEI with $P_n = 10$ and which correspond to transition of hemihydrate (0.5) to sequihydrate (1.5) (around 50 °C) and melting of the sesquihydrate (1.5) (around 80 °C), an additional peak at around 34 °C for $P_n = 20$ and around 40 °C for $P_n = 40$ is observed. XRD investigations prove that these alkyl-PEI samples ($P_n = 20$ and 40) consist of a mixture of anhydrate (0), hemihydrate (0.5) and sesquihydrate (1.5). Hence, the peak at around 40 °C could be ascribed either to the melting of the anhydrate or to the transition of the anhydrate containing a small amount of water into a mixture of hemihydrate (0.5) and sesquihydrate (1.5). Subsequent heating cycles prove that both phenomena take place simultaneously. The broad melting peaks of the anhydrate suggest they could overlap with those ascribed to the transition of anhydrate with small of water into a mixture of hemihydrate (0.5) and sesquihydrate (1.5). The starting material would then be composed of hemihydrate, sesquihydrate, and additional anhydrate domains with less water. The second heating curve of alkyl-PEI with $P_n = 20$ supports this statement. Peaks at 45 °C, which correspond to transition of anhydrate with small amounts of water to a mixture of hemi- (0.5) and sesquihydrate (1.5), and at 69 °C produced by transition of hemihydrate (0.5) to sesquihydrate (1.5) can be observed. The absence of peaks at lower temperatures in the second heating curve is due to the fact that, after the melting of the latter observed in the first heating curve (peak at 80 °C), the material becomes homogeneous.

Table 3.9. Thermal transition data of alkyl-PEI hydrates obtained from DSC analysis.

Degree of polymerization, P_n	**Final temperature, °C**	**Heating scan**	**Thermal transition, °C**
10	80	1st	53[a], 80[b]
		2nd	40[c], 65[a]
		3rd	39[c], 59[a]
	100	1st	53*[a], 81[b]
		2nd	40[c], 61[b]
	120	1st	50*[a], 80[b]
		2nd	39[d]
		3rd	39[d]
20	80	1st	34[d,c], 50*[a], 80[b]
		2nd	45*[c], 69[a]
		3rd	36[c], 60[a]
	100	1st	35[d,c], 50*[a], 80[b]
		2nd	35[d]
	120	1st	35[d,c], 50*[a], 80[b]
		2nd	35[d]
		3rd	30[d]
40	80	1st	38[d,c], 55*[a], 79[b]
		2nd	40[d]
		3rd	35[d]
	100	1st	40[d,c], 60*[a], 83[b]
		2nd	32[d]
	120	1st	40[d,c], 60*[a], 80[b]
		2nd	30[d]
		3rd	25[d]

*, shoulder [a], hemihydrate (0.5) to sesquihydrate (1.5) transition, [b], 1.5 melting, [c], Anhydrate (0) with small amount of water to mixture of sesquihydrate (1.5) and hemihydrate (0.5) transition, [d], anhydrate (0) melting.

In addition, the heating to 80 °C makes the material lose some water as explained in the previous case. Consequently, pure anhydrate domains as detected in XRD disappear. The resulting, more homogeneous, material is composed of anhydrate with a small amount of water. Upon heating to

100 °C or 120 °C the melting of the anhydrate can be observed already in the second heating curve. Finally, in the case of alkyl-PEI with $P_n = 40$ the melting of the anhydrate can already be observed in the second curve when heating to 80 °C. Those differences in the distribution of the endotherm peaks during heating scans of the samples results from the different water contents (5.02, 2.81 and 2.08 wt% for $P_n = 10$, 20 and 40, respectively). Concerning the difference in the anhydrate melting temperature between the alkyl-PEI samples (around 35 °C) and with the linear PEI (M_w ca. 500000 g/mol) investigated by HASHIDA[239] (around 60 °C), previous investigations[240, 241] on the thermal properties of amphiphilic polymers have proven that both, the degree of polymerization of each block and the ratio of hydrophilic to hydrophobic length, can play a role in its thermal properties.

3.2.2.6 Thermoreversible gelation

Thermally reversible gelation of aqueous polymer solutions has attracted interest because of its potential application in different fields, such as drug delivery, tissue engineering, or cell encapsulation[242]. In this process polymers are loaded with bioactive molecules or additives in an aqueous solution which subsequently transforms into a physically cross-linked hydrogel by the action of temperature, pH, or radiation. Typical examples of polymers which can undergo thermal gelation are triblock copolymers composed of poly(ethyleneoxide) and poly(propyleneoxide) (PEO-PPO-PEO)[243] or hydrophobically modified cellulose derivates[244]. Poly(ethyleneimine) (PEI) with different molecular architectures has also been reported to form thermoreversible physical hydrogels[222]. XRD and DSC experiments performed within these investigations revealed that the main driving force for PEI thermal gelation is the formation of crystalline dihydrate states.

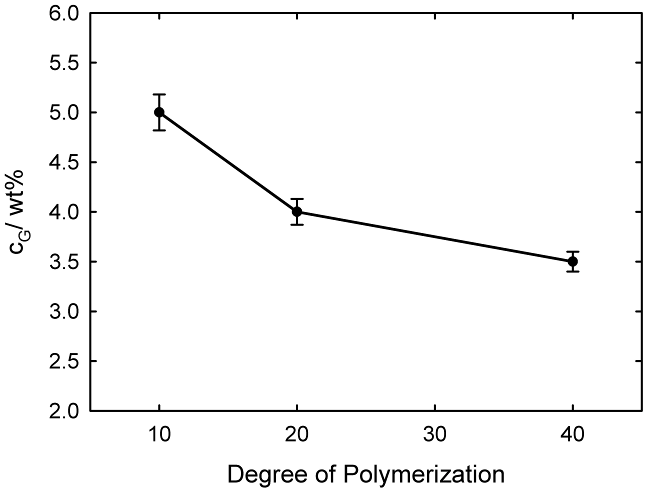

Figure 3.24. Gelation concentration (c_G) values of alkyl-PEI as a function of the degree of polymerization.

In the current study aqueous solutions of alkyl-PEI were heated to 80 °C and cooled down to room temperature resulting in opaque, ice-cream like hydrogels. The gel state was established by the vial-inversion test. Figure 3.24 shows the gelation concentration (c_G) for alkyl-PEI determined as a function of its degree of polymerization P_n. The gelation concentration decreases with the degree of polymerization of the PEI chain, although the decrease is not linear. This fact involves that longer PEI chains are more effective in terms of the water amount that they can gelate. This trend was also observed in thermal PEI-containing hydrogels produced by YUAN *et al.*[222]. In that case the gelation concentration of hydrogels produced with linear PEI reached c_G values of 0.31 wt% and 0.25 wt% for degrees of polymerization P_n = 290 and 1470, respectively. Such a strong dependence of the gelation concentration on the molecular structure and dimensions of the gelator is also well known for other polymers[245, 246].

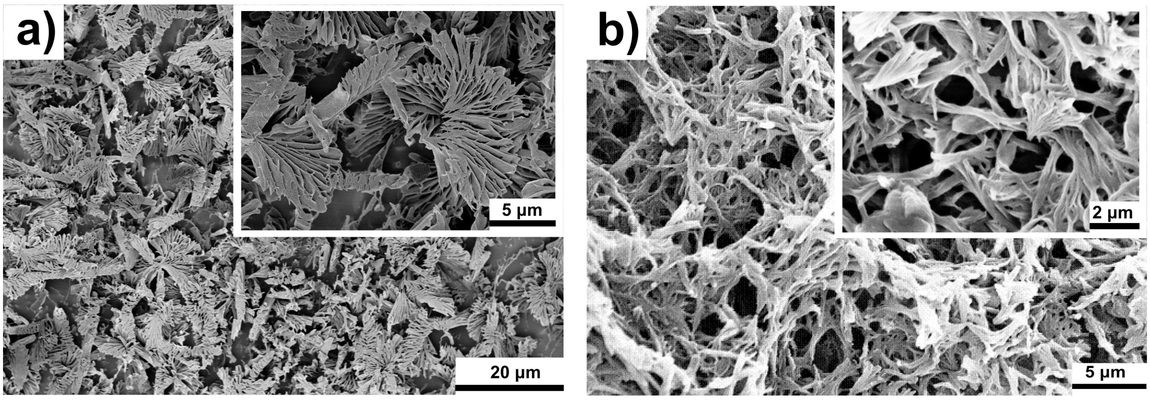

Figure 3.25. (a) Cryo-SEM image of alkyl-PEI ($P_n = 20$) thermal hydrogel and (b) SEM image of alkyl-PEI ($P_n = 20$) thermal hydrogel cross-linked with glutaraldehyde (1 wt%, 72 h) and subsequently freeze-dried.

Figure 3.25-a shows a cryo-SEM image of an alkyl-PEI ($P_n = 20$) hydrogel in the swollen state. The morphology of the hydrogel consists of fibrous bundles with fan-like shape in the micrometer range. Further cross-linking of the hydrogels with glutaraldehyde improves its mechanical stability enabling the production of thin slices, useful for the observation of the hydrogel interior. Figure 3.25-b shows a SEM image of one of these cross-linked hydrogel slices. Alkyl-PEI organizes into a fibrous network. The differences between the morphologies of the hydrogel observed in both figures result from the sample preparation. In fact, the image shown in Figure 3.25-a was obtained by cryo-SEM whereas that in Figure 3.25-b required cross-linking, freeze drying, which can generate artefacts, and SEM. Thus, these hydrogels seem to consist of a fibrous alkyl-PEI network composed of fan-like units. The formation of hydrogels with a similar morphology was observed by YUAN[222] when gelling aqueous solutions of a unimolecular star with six PEI arms ($P_n = 100$ each) attached to a benzene core. Those investigations concluded that PEI is present in the hydrogels in the dihydrate crystalline state and that the morphology of the hydrogels is determined by the molecular architecture of the polymer. Even in solution PEI with various architectures can aggregate into different shaped morphologies modulated by the media conditions[247]. Therefore, the fan-like shape of the fibrous bundles composing the alkyl-PEI hydrogel may be ascribed to supramolecular aggregates promoted by hydrophobic interactions of the alkyl groups. Those aggregates can be assumed to resemble the geometry of the unimolecular star with six PEI arms and benzene core. This finding is in accordance with the similarity between the aggregates and the branched PEI reported in the titration experiments.

Another important aspect of hydrogels is the state of the water entrapped within the polymeric network. NMR, FTIR and DSC are the most common methods to determine the states of water in hydrogels[248-250]. Several studies carried out in recent years suggest that water in polymer hydrogels can be found in three different states[251]:

a) Free-freezing water, which does not undergo any interaction with the surrounding polymeric network and hence shows transition temperature and melting enthalpy similar to those of pure water.
b) Freezable bound water also known as interstitial water, which is weakly bound to the polymeric network and shows phase transition at temperatures lower than 273 K.
c) Non-freezing water, which shows stronger interaction with the polymer and does not show any thermal transitions along the temperature range where bulk water usually shows melting/freezing phenomena (200 to 273 K).

States of water in alkyl-PEI thermoreversible hydrogels were determined by DSC measurements.

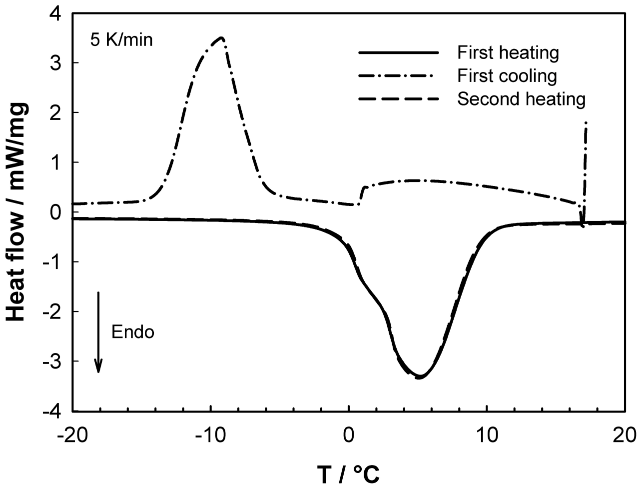

Figure 3.26. DSC thermogram of alkyl-PEI ($P_n = 10$) thermal hydrogel. Heating and cooling scans were performed at 5 K / min.

Figure 3.26 shows a DSC thermogram of an alkyl-PEI ($P_n = 10$) hydrogel. The endotherm peak in the heating curves represents the melting of the total freezing water contained in the hydrogel, that is free-freezing and freezable bound water. The shoulder observed at the beginning of the melting process suggests overlapping of peaks corresponding to the melting of weakly bound water (which melts at lower temperatures) and free-freezing water. In principle it should be possible to separate the two fractions, however AHMAD *et al.* reported that the separation of the peaks corresponding to the melting of these two kinds of water depends on the total water content of the hydrogel[251]. Thus, from the DSC results obtained for alkyl-PEI hydrogels it is only possible to differentiate between freezing water (free and weakly bound) and non-freezing water (bound).

Table 3.10. Water states of alkyl-PEI thermal hydrogels determined by DSC analysis.

Degree of polymerization, P_n	EWC, wt%[a]	Free water (freezing), wt%	Bound water (non-freezing), wt%	C_{NH}, mol/l
10	89.6±0.2[b]	72.6±0.1	17.0±0.1	1.81±0.03
20	91.2±0.3	78.7±0.5	12.4±0.2	1.59±0.01
40	94.0±0.2	81.0±0.6	13.1±0.4	1.38±0.05

[a] Equilibrium water content.

[b] Standard deviation was calculated based on three replicates.

Table 3.10 shows the corresponding distribution of water states in our hydrogels. For each alkyl-PEI sample (P_n = 10, 20 and 40) three different hydrogels with similar polymer concentrations were prepared. Integration of the endotherm peak area yields the amount of freezing water in the hydrogel. The amount of non-freezing water is calculated by difference between the total water content of the swollen hydrogel (EWC) and the freezing water. At a first look it can be observed that with increasing degree of polymerization of the alkyl-PEI, the total water content of the hydrogel (EWC) and the free water fraction (freezable water) increase. As discussed before the increase of the total amount of water in the hydrogel (EWC) with increasing degree of polymerization (P_n) of the gelator is related with the effectiveness of longer polymer chains in terms of water immobilization. It involves that the amount of alkyl-PEI required for hydrogel formation and hence the concentration of amino groups available to interact with water molecules become lower. This may be the reason why the percentage of free water in the hydrogel increases. Such an increase of the free water fraction by decreasing the concentration of polar groups in the hydrogel was reported in the literature when reducing the amount of chitosan in chitosan-polyacrylonitrile hydrogels[249].

Finally, the percentage of bound water (non-freezing) is calculated as the difference between the equilibrium water content (EWC) and the percentage of free water. It shows a higher value (17.0 ± 0.1 wt%) when the hydrogel is composed of alkyl-PEI with P_n = 10 and then decreases

(12.4 ± 0.2 wt%) if composed of alkyl-PEI with $P_n = 20$. Finally, it remains at a similar value (13.1 ± 0.4 wt%) when the hydrogel is composed of alkyl-PEI with $P_n = 40$ in spite of the fact that the concentration of the amino group decreases. Taking this observation into account, the percentage of bound water depends not only on the concentration of polar amino groups in the hydrogel but also on other factors like the total water content of the hydrogel or interaction with hydrophobic moieties. Those interactions of water with hydrophobic groups have been already reported[252, 253] and may play an important role in these hydrogels due to the presence of the long alkyl chain attached to the PEI block.

3.2.2.7 Alkyl-poly(propyleneimine) (alkyl-PPI)

In a similar way to alkyl-PEI, alkyl-PPI ($P_n = 20$) has been characterized. Regarding its alkaline properties, the titration curve of alkyl-PPI has already been described in section 3.2.2.3. As already commented for alkyl-PEI, -PAEI and -PAPI, another important parameter related to the aggregation properties of the polymer in aqueous solution is the critical micelle concentration (CMC). In order to determine this parameter, surface tension of alkyl-PPI solutions with different concentrations in pure water have been measured.

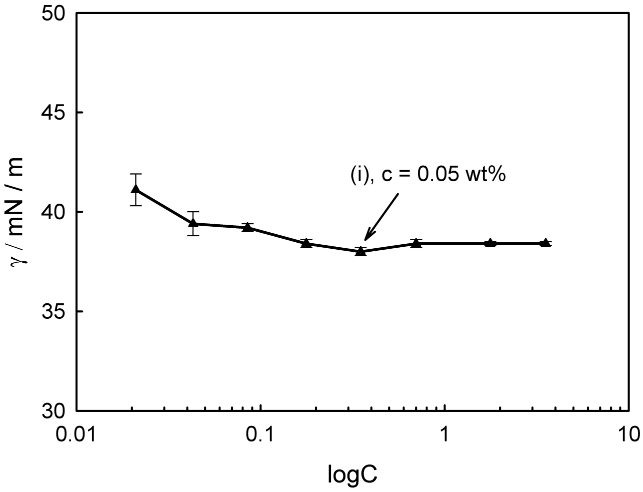

Figure 3.27. Semilogarothmic plot of surface tension (γ) versus concentration for alkyl-PPI ($P_n = 20$) in pure water at 25 °C showing the concentration (i) at which turbidity appears.

Figure 3.27 shows the semilogarithmic plot of the measured surface tension values versus the concentration of the alkyl-PPI solutions. As for alkyl-PAPI (section 3.2.1.4), the surface tension decreases dramatically at very low concentration. Solutions containing 0.003 wt% of alkyl-PPI yield surface tensions around 41 mN/m, which are closer to those of the solutions with much higher concentrations, e.g. 0.05 wt% gives 38.4 mN/m, than to the value for pure water (72 mN/m). This means that the lowest polymer concentration of the plot is higher than the CMC, i.e. aqueous solutions with 0.003 wt% of alkyl-PPI (P_n = 10 and 20) are not isotropic but already contain polymer aggregates. Thus, an accurate value for the CMC can not be obtained from the available data. Moreover, the determination of those values involves the production of solutions with lower concentrations, which results in high experimental errors. Regarding the solubility of the samples, it must be said that clear aqueous solutions of alkyl-PPI (P_n = 20) can be produced up to concentrations around 0.05 wt% (point i in Figure 3.27). In that concentration range, the surface tension remains constant, i.e. alkyl-PPI micelles form. This fact indicates that at 25 °C, temperature at which surface tension was measured, the solubility of alkyl-PPI in pure water is higher than the critical micelle concentration. Therefore, similarly to alkyl-PEI, 25 °C is a higher temperature than the Krafft temperature of alkyl-PPI in water.

Furthermore, a characterization of alkyl-PPI in the solid state has been carried out. Figure 3.28 show the XRD pattern of alkyl-PPI (P_n = 20).

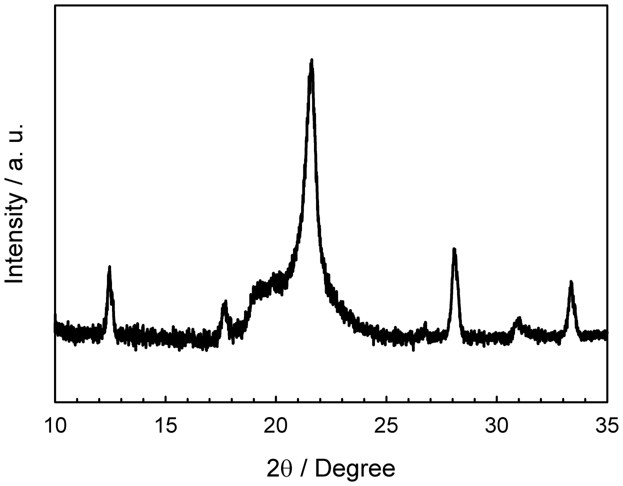

Figure 3.28. X-ray diffraction pattern of alkyl-PPI with a degree of polymerization P_n = 20 measured at 25 °C.

As can be observed, the XRD pattern of alkyl-PPI is different from that of alkyl-PEI (Figure 3.21). It is composed of sharp peaks, at 12.5 °, 17.5 °, 28.2 ° and 34.5 °, resembling those found in alkyl-PEI samples and which were ascribed to hydrates. However, it also shows a very broad peak between 19 ° and 24 °, crowned by a sharp, prominent tip at 21.5 °. SAEGUSA *et al.* synthesized linear PPI via CROP of unsubstituted 5,6-dihydro-4H-1,3-oxazine with cationic initiators and subsequent alkaline hydrolysis[120]. Within that work, the resulting linear poly(N-propyleneimine) was shown to contain water of crystallization and to be slightly crystalline in spite of the fact that a detailed physical characterization similar to that performed for PEI has not been reported. Concerning the water of crystallization, Karl-Fischer titration of the alkyl-PPI (P_n = 20) sample did not offered reproducible values. The reason could be that the upper limit for that method is around 10 wt% and the sample may possess a higher water content.

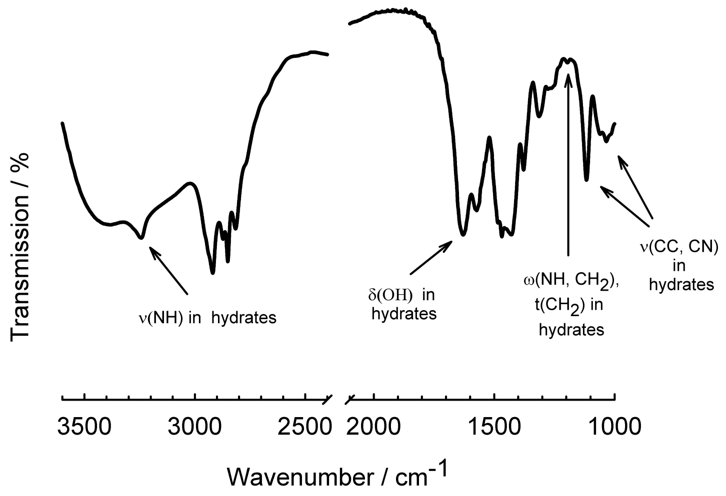

Figure 3.29. FTIR spectra of an alkyl-PPI sample with a degree of polymerization P_n = 20 measured at 25 °C showing stretching (υ), wagging (ω), twisting (t) and bending (δ) bands similar to those found in alkyl-PEI hydrates .

In fact, the FTIR spectrum depicted in Figure 3.29 reveals the presence of a typical broad water absorption band between 3000 and 3600 cm^{-1}, which confirms the high hygroscopic character of alkyl-PPI. Furthermore, some bands similar to those ascribed to the presence hydrates in alkyl-PEI samples can be found. Since alkyl-PEI and alkyl-PPI differ only in the length of the alkylene spacing group, those bands represent a proof of the existence of alkyl-PPI hydrates. However, the presence of the broad peak in the XRD pattern of alkyl-PPI suggests that another type of chain conformation apart from the planar one reported before for alkyl-PEI hydrates[232-234] takes place. In fact, XRD studies[254] carried out with different types of starch show the presence of such broad peaks with sharp, prominent tips, like those observed for alkyl-PPI. According to these investigations that kind of peak distribution is usually caused by packing of the molecules into stranded helices. Taking this idea into account, the alkyl-PPI chains would be packed into stranded helices in the solid state in spite of the fact that the sample also contains some water of crystallization which tends to build planar hydrates, as observed with alkyl-PEI. However, alkyl-PPI seems to show as well a tendency for chain folding into stranded helix apart from the interaction with water. This different behaviour with respect to alkyl-PEI may be ascribed to the higher length of the alkylene spacing group. The presence of propylene instead of ethylene moves the amine neighboring groups away and makes the interaction with water molecules more difficult. In line with this influence of the spacing group, SASANUMA *et al.*[288] proved via molecular simulations that PPI possesses a higher mobility than PEI. This is because PPI can build C-H···N and N-H···N intra- and intermolecular bonds while PEI can just build the second ones. Within these investigations it was highlighted that although that kind of hydrogen bonds are very weak, they play a crucial role in the conformation, crystal structure and solution properties of the polymers. Taking these observations into account, the material would be composed of planar hydrate domains promoted by alkyl-PPI-water interactions, coexisting with alkyl-PPI regions where the polymer chains are folded into stranded helices. Such a coexistence of hydrates and anhydrate domains in the solid state has been previously reported concerning the thermal behaviour of alkyl-PEI with $P_n = 20$ (see Table 3.9).

As for alkyl-PEI, the thermal behaviour of alkyl-PPI has been investigated by scanning differential calorimetry (DSC). Figure 3.30-a shows DSC thermograms of alkyl-PPI ($P_n = 20$) heated to 80 °C. As can be observed, in the first heating curve a narrow peak appears at around 48 °C. A subsequent increase of the heat flow until the end of the curve (80 °C) can be also observed. In the second heating curve, the first peak broadens and shifts to 36 °C, while the following increasing of the heat flow is also observed. Finally, in the third heating curve, the first peak remains at 36 °C, as in the second heating curve, and a new broad peak centered at 72 °C appears. According to the investigations performed by SAEGUSA *et al.* and which were mentioned before, linear PPI was observed to melt at 74 °C if the water content is around 9 wt%. For a crystallization water content around 17 wt% it was reported to melt at 84 °C. Such a dependence of the melting point of linear PPI upon the water content has already been described with regard to the thermal behaviour of alkyl-PEI. Taking these values into account, the increase of the heating flow observed during the first and second heating cycles and the peak at 74 °C observed in the third one may be ascribed to the melting of alkyl-PPI in the hydrated state. Moreover, the melting peak that appears at 74 °C during the third heating curve involves a crystallization water content around 9 wt% if considering the results of SAEGUSA *et al.*. Thus, because of the loss of water undergone by the sample after the first and second heating cycles, even when the final temperature is 80 °C, the initial water content is higher than 9 wt%. This is in accordance with the poor reproducibility of the values obtained by Karl-Fischer titration, since the maximum amount of water which can be detected with this method is 10 wt%. Concerning the first peak observed when heating the sample to 80 °C, at 48 °C in the first and at 36 °C in the second and third ones, it can be ascribed to the melting of anhydrate domains.

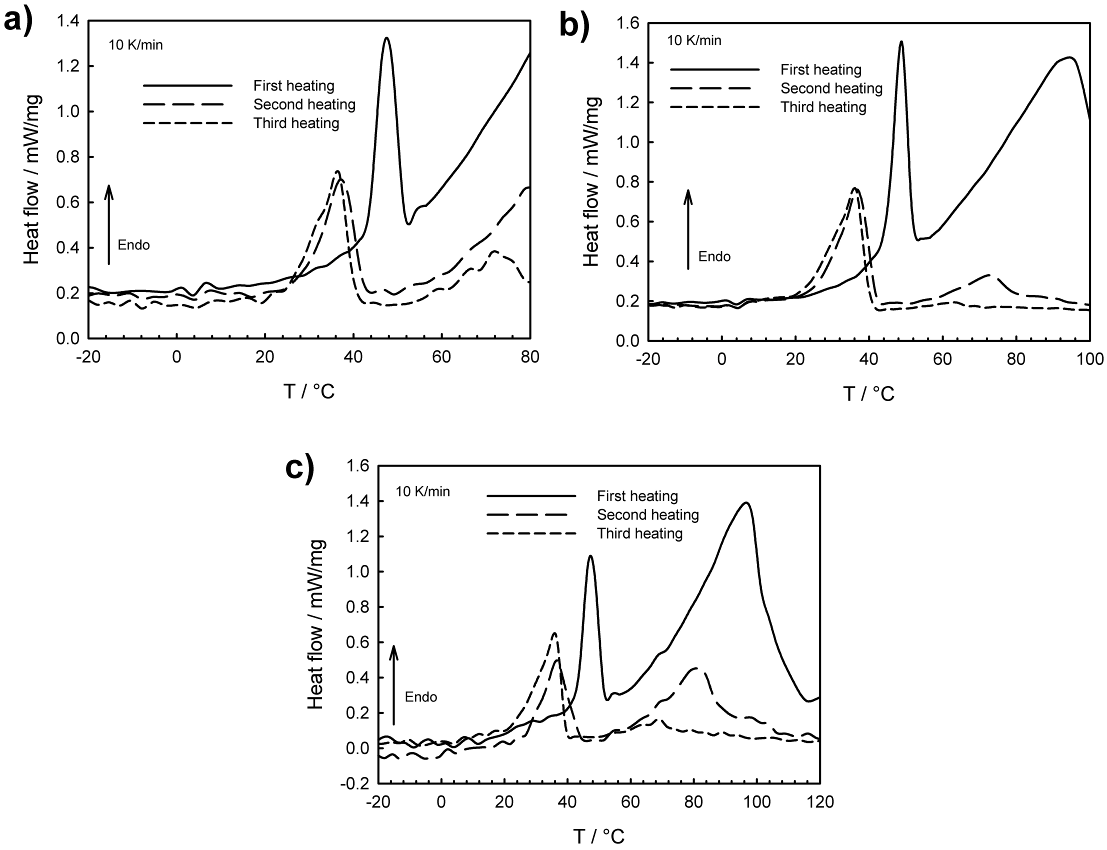

Figure 3.30. DSC thermograms of alkyl-PPI with $P_n = 20$ showing heating scans of the sample to 80 °C (a), 100 °C (b) and 120 °C (c).

The presence of these anhydrate domains has already been identified in the XRD pattern of the sample. The assignment of this peak to the melting of the anhydrate is also supported by the fact that, as commented in section 3.2.2.4, alkyl-PEI samples with $P_n = 20$ in the anhydrate state were found to melt within a similar temperature range (see Table 3.9). A similar distribution of peaks can be observed when heating alkyl-PPI samples to 100 °C and 120 °C (Figures 3.30-b and 3.30-c, respectively). It can be recognized that the peak ascribed to the melting of the anhydrate at around 48 °C in the first heating curve broadens and shifts to lower temperatures (~ 36 °C). Likewise, the broad peak centered at 90 °C in the first curve and ascribed to the melting of hydrated alkyl-PPI also shifts to lower temperatures in the second curve and even vanishes in the third one. When heating up to 80 °C, the peak can be observed at 72 °C. The shift of both peaks as well as the enhancement of the first (~ 36 °C) and the disappearance of the second (~ 80 - 90 °C) may be caused by the loss of crystallization water during the heating process.

In light of these results, it can be concluded that, unlike alkyl-PEI, alkyl-PPI does not show such a complex thermal behaviour. In fact, whereas the former can build different kinds of planar hydrates apart from the helicoidal anhydrate state, the latter may possess only two conformational states, i.e. anhydrate and hydrated. This statement is supported by the fact that in the DSC thermograms of alkyl-PEI, a higher number of peaks appear. Moreover, the distribution of those peaks changes depending on the final heating temperature since the amount of water of crystallization and hence of the different hydrates also changes. On the contrary, the DSC thermogram of alkyl-PPI just shows two peaks produced by the melting process of anhydrate and hydrated fractions of the sample. The shift, enhancement and disappearance of those peaks indicate that conversion of hydrated into anhydrate alkyl-PPI takes place. This conversion occurs also because of the water loss during the heating cycles, as observed with alkyl-PEI. These differences in the thermal behaviour of alkyl-PEI and alkyl-PPI may arise, as explained before, from the alkylene spacing group. In contrast to the ethylene spacing group of alkyl-PEI, the propylene spacing unit of alkyl-PPI makes it difficult the interaction of neighboring amino groups with water molecules, and hence the formation of hydrates. The consequence is that while alkyl-PEI tends to build planar hydrates, in alkyl-PPI the chain folding into stranded helices is favoured.

Finally, as well as for alkyl-PEI, the thermoreversible gelation of alkyl-PPI ($P_n = 20$) has been investigated. For this purpose, aqueous solutions of the polymer with concentrations up to 17 wt% have been heated to 80 °C and then cooled down to room temperature. However, unlike alkyl-PEI, alkyl-PPI solutions do not form hydrogels. The resulting material is composed of polymer lumps mixed with a milky, liquid suspension. At this point, it should be mentioned that alkyl-PEI aqueous solutions with polymer concentration lower than c_G (see Figure 3.23) do not show any polymer lumps after cooling them down to room temperature but they are milky, homogeneous suspensions of the polymer in the aqueous medium. Furthermore, the minimum gelation concentration for aqueous solutions containing alkyl-PEI with P_n = 20 was found to to be c_G = 4.0 wt% (Figure 3.24). However, even when similar c_G values could be expected for alkyl-PPI with P_n = 20, solutions with polymer concentration up to 17 % do not yield any hydrogels, as described before. The reason for this behaviour may be once more ascribed to the different alkylene spacer of the polymer chain. In section 3.2.2.6, it was mentioned that XRD and DSC studies performed by YUAN *et al.*[222] have proven that linear-PEI-based hydrogels arise from the formation of dihydrated crystalline states (2). Thus, replacing the ethylene spacing group by propylene increases the distance between neighboring amino groups and hinders the interaction with water molecules and hence formation of crystalline hydrated states. As a consequence, alkyl-PPI does not build crystalline hydrated states at the same extent as alkyl-PEI and hydrogelation does not take place.

3.2.2.8 Concluding remarks on alkyl-PEI and alkyl-PPI characterization

Within this section, alkyl-PEI has been characterized. The behaviour of the polymer in aqueous solution has been investigated. As for alkyl-PAEI, surface tension measurements have been performed in order to determinate the critical micelle concentration (CMC). Unlike alkyl-PAEI, the CMC values obtained for alkyl-PEI in water do not increase with the degree of polymerization of the hydrophilic segment but they show a maximum at P_n = 20. In addition, the solubility of alkyl-PEI in pure water has been found to be lower than that of alkyl-PAEI. Solutions with polymer concentrations above 0.082 wt% are not clear but turbid. The acid-base behaviour of the polymers has been characterized via potentiometric titration. The titration curves of alkyl-PEI with P_n = 10 and 20 show that the hydrophobic interaction by the alkyl chains shifts polymer precipitation to lower pH values than for linear PEI. On the contrary, alkyl-PEI with P_n = 40 shows a titration curve similar to that of the branched PEI, which suggests the formation of spherical aggregates without precipitation at high pH.

The solid-state behaviour of alkyl-PEI has also been studied. XRD and FTIR show that even under dry storage conditions alkyl-PEI samples take up water from the atmosphere and form different hydrates. The presence of these hydrates is directly related to the water content of the alkyl-PEI samples. DSC measurements prove that thermal transitions between the different hydrates take place. Besides, cooling down hot aqueous solutions of alkyl-PEI yields opaque, ice-cream-like hydrogels. The gelation concentration decreases with increasing degree of polymerization of the alkyl-PEI sample used as gelator. Scanning electron microscopy (SEM and cryo-SEM) of the hydrogels reveal that they consist of a fibrous polymeric network forming fan-like bundles. The presence of water in different states in the hydrogels has been proven by DSC measurements. The percentages of free (freezing) water and bound (non-freezing) water depend not only on the concentration of hydrophilic amino groups, but also on the total amount of water (EWC).

Finally, a similar characterization has been performed for alkyl-PPI. Here, micellization phenomena take place at lower concentrations than for alkyl-PEI. Regarding the acid-base behaviour, alkyl-PPI possesses a higher degree of protonation than alkyl-PEI over the whole pH range. The reason is the lower electrostatic repulsion between neighboring groups upon replacing ethylene by propylene as spacer. Solid state characterization has also been performed. FTIR measurements indicate that water uptake occurs and XRD reveals the existence of crystalline domains in alkyl-PPI samples but to a lower extent than for alkyl-PEI. Moreover, thermal transitions have been detected by DSC. However, alkyl-PPI solutions did not undergo any thermal gelation phenomena similar to those observed for alkyl-PEI. Solutions with concentrations up to 17 wt% remained liquid after heating up to 80 °C and subsequent cooling to room temperature. The reason for this behaviour could be found in the presence of the propylene group as spacer between the imine units. Unlike alkyl-PEI, the propyl spacer may hinder interactions between imine groups and water, which have been proven to play a crucial role in the gelation process.

3.3 Production of polymer-mediated silica precipitates

3.3.1 Introduction

Among other biomineralization processes, biosilicification has attracted the interest in nanotechnology and materials sciences in the last few decades[111, 255], as has been highlighted in section 2.1.2.1. The process has been reported to take place in diatoms[33] and glass sponges[256] under ambient conditions and at slightly acidic pH. The resulting silica structures are precisely controlled at the nanometer scale and their formation is achieved by specific interactions between silicic acid derivatives and biopolymers. Among those, in diatoms the crucial role is played by cationic polypeptides (silaffins) containing long-chain polyamines. The self-assembled structure of the silaffins is thought to act as a template for the *in vivo* polycondensation of silicic acid derivatives[257, 258]. Within this process, the long-chain polyamines promote the aggregation of the negatively charged primary particles[10, 63, 110].

With the goal of producing tailored nanostructures based on the silica biomineralization, silica nanospheres have been produced *in vitro* with several types of polyamines, such as poly-L-lysine[259], poly(allylamine hydrochloride)[260, 261], amine-terminated dendrimers[221], and others[262]. From the reported investigations, it seems to be clear that the condensation of silicic acid is promoted by the amine groups borne by the polymer, leading to the formation of silica precipitates. Furthermore, the influence of different variables, such as pH, molecular weight and concentration of polyamine or concentration of the silica precursors, on the morphology of the silica precipitates has been tested within those investigations.

Likewise, it can be expected that the previously described alkyl-PAEI- and alkyl-PEI-based supramolecular aggregates will also be active in terms of promoting silicic acid condensation. In this regard, the production of silica precipitates under different experimental conditions in the presence of these supramolecular assemblies has been performed. The influence of the experimental conditions on the morphology of the silica precipitates, investigated by Scanning Electron Microscopy (SEM), is reported within this section.

3.3.2 Polymer-mediated silicic acid condensation

PATWARDHAN *et al.*[263, 264] reported a detailed study on the condensation of silicic acid in the presence of polyallylamine hydrochloride (PAH). Within those investigations, the influence of different factors, e.g. buffer, polymer concentration, polymer molecular weight, or silicic acid precursor concentration, was tested. Similarly, taking this approach into account, the morphology of the silica precipitates produced in aqueous solutions containing alkyl-PAEI, alkyl-PAPI and alkyl-PEI has been investigated by SEM. Furthermore, the effect of different variables such as functional groups on the polymer chain, buffer, polymer concentration or degree of polymerization, on the morphology of the silica precipitates has been studied. A summary of the experimental conditions under which these experiments have been performed can be found in Table 3.11.

Table 3.11. Summary of experimental conditions under which the condensation of silicic acid has been investigated.

Polymer	Type of solution	Buffer (pH)	P_n	Concentration (wt%)
Alkyl-PAEI	Clear	Phosphate (5.6) Malonate (5.5) Acetate (4.5) Citrate (3.5)	10, 20, 40	0.01,0.1, 0.25
Alkyl-PAPI	Clear	Malonate (5.5) Acetate (4.5)	20	0.1
Alkyl-PEI	Clear	Malonate (5.5) Acetate (4.5)	10, 20 40	0.01 0.1
	Turbid	Malonate (5.5) Phosphate (5.6) Citrate (3.5)	10, 20, 40	0.05, 0.1, 0.25

For this purpose, solutions containing different concentrations of alkyl-PAEI, alkyl-PAPI and alkyl-PEI in different buffers have been produced (see section 5.3.1). In addition, fresh silicic acid solutions have also been prepared just before each condensation experiment by hydrolysis of tetramethylorthosilane (TMOS) with hydrochloric acid. The subsequent step in the condensation experiment consists of mixing both solutions and stirring the resulting mixture for 40 minutes. Within that time, the reaction medium becomes turbid provided that the investigated polymer promotes silicic acid condensation. Finally, the silica precipitates have been washed with water and methanol, centrifuged, dried in vacuo and investigated by SEM.

• Alkyl-PAEI

In order to test the effect of alkyl-PAEI (P_n = 10, 20 and 40) in the condensation of silicic acid, a set of aqueous solutions containing 0.01, 0.1 and 0.25 wt% of the polymer in phosphate (pH = 5.6), malonate (pH = 5.5), acetate (pH = 4.5) and citrate (pH = 3.5) buffers have been prepared. Subsequently, the condensation experiments have been carried out with those solutions as described above, which allows to investigate the effect of the different variables in the process. As a first remark, it must be said that all solutions containing alkyl-PAEI have been found to promote the condensation of silicic acid as they become turbid within the 40 minutes that takes the condensation experiment. However, solutions containing just the buffer in the absence of polymer do not undergo any precipitation or gelling phenomena. In this respect, it is worth mentioning that in contrast to the amine group, N-(acetyl)ethyleneimine units do not posses alkaline properties. In the same way, Polypeptides[262] and other polymers such as the dendrimer G1PANAM[221], which do not posses alkaline properties and also bear amid groups, have been found to promote silica precipitation. At this point, the fact that poly(N-vinylpyrrolidone) (PVP) can also promote the silica precipitation[265] is worth to be mentioned. According to previous investigations[110], the promoting effect of polymers bearing alkaline groups such as polyethyleneimine (PEI)[266], polyallylamine (PAH)[261] or poly-L-lysine (PLL)[261], in the condensation of silicic acid at neutral pH conditions results from their polyelectrolyte character. Under those conditions, the amine groups are positively charged and can interact with the negatively charged siloxyl (SiO^-) groups (see section 2.1.2.2) located on the surface of the silica particles[12]. As a consequence, the polymer chains can shield the superficial charge on the surface of the silica particles and promote their aggregation. Since alkyl-PAEI can not act as a polyelectrolyte at any pH value, it seems to be clear that another type of interaction with the negatively charged surface of the silica particles takes place. As can be observed, the carbon atom in the polymer repeating unit $N\text{-}CO\text{-}CH_3$ is bound to both, oxygen and nitrogen atoms. Their high electronegativity may polarize the carbon atom positively[267], which would enable interactions with the oxygen atoms of the negatively charged siloxyl (SiO^-) groups. Another possible explanation for the activity of alkyl-PAEI regarding the silicic acid condensation may be found in the mesomeric effect of amino and carbonyl groups[268]. According to this hypothesis, the positively charged nitrogen atoms of the resonance structures built by alkyl-PAEI interact with the oxygen atoms of the negatively charged siloxyl (SiO^-) groups and promote particle aggregation. The mechanistic pathway leading to the promoting effect of the N-(acetyl)ethyleneimine group on the silicic acid condensation has not yet been completely clarified. However, the interaction mechanisms proposed here seem to be both plausible.

Another aspect that has to be considered within these condensation experiments is the time until the turbidity appears in the solution. In this regard, the solutions prepared with malonate (pH = 5.6), phosphate (pH = 5.5) and acetate (pH = 4.5) as well as those with concentrations above c = 0.01 wt% developed the turbidity within five minutes after mixing silicic acid and polymer solutions. On the contrary, those solutions prepared with citrate (pH = 3.5) and those containing c = 0.01 wt% polymer developed the precipitate around 20 minutes after mixing. The observation that solutions containing c = 0.01 wt% alkyl-PAEI show the presence of a precipitate only after longer times than those containing higher concentrations is in accordance with previous results reported by CORNELIUS[125]. Within that work the kinetics of the particle growth in silica colloids produced in the presence of linear PEI and PPI have been investigated via time-resolved static light scattering. According to those investigations, the induction time required to start a noticeable particle growth increases by decreasing the concentration of active groups, and hence of polymer, in the solution. Furthermore, a minimum concentration of active sites is required to observe the particle growth.

Regarding the observation that the development of the turbidity in citrate (pH = 3.5) occurs at longer times than in the other buffers, it can be ascribed to the high tendency of citrate groups to form multiple hydrogen bonding with the N-(acetyl)ethyleneimine units. These interactions of the citrate groups with the polymer active units may prevent the aggregation of the silica nuclei. This conclusion is supported by the fact that citrate groups have been reported by PATWARDHAN *et al.* to hold together polyallylamine (PAH) chains preventing the polymer dissolution[264].

As mentioned before, in order to investigate the effect of different variables in the morphology of the silica precipitates, silicic acid condensation assays have been carried out under different experimental conditions. SEM images of the resulting silica precipitates have been taken in order to establish the effect of those experimental conditions in the morphology.

Influence of P_n and c:

Figure 3.31 depicts SEM images of silica precipitates prepared in solutions containing 0.1 wt% alkyl-PAEI with $P_n = 10$, 20 and 40 (Figures 3.31-a, -b and -c, respectively) and, 0.01 and 0.25 wt% of alkyl-PAEI with $P_n = 20$ (Figures 3.31-d and -e, respectively) in malonate (pH = 5.5) at room temperature. As can be observed, the morphology of all samples is characterized by fused spheres with non-uniform size around several hundred nanometers. A more accurate estimation of the particle size can not be achieved because of the fact that the spheres are fused and also that they do not have a uniform size. However, it can be noticed that the size of the spheres increases by increasing the degree of polymerization of the used alkyl-PAEI (Figures 3.31-a, -b and -c). The same trend has been reported by CORNELIUS[125] and PATWARDHAN *et al.*[264, 269] for the silica precipitates obtained in the presence of different polymers. This may be due to the fact that the higher the chain-length of the used polymer, the bulkier will be their coils in the solution and hence the silica particles. For alkyl-PAEI such a result could also be expected. As reported in section 3.2.1.4, at pH values similar to those of the buffers used for the condensation experiments, alkyl-PAEI has been found to possess extremely low CMC values. According to those results, alkyl-PAEI solutions with concentrations around

0.01 wt% contain supramolecular aggregates. Consequently, the polymer solutions used here for the silica precipitation assays contain alkyl-PAEI aggregates. In addition, the DLS results reported in section 3.2.1.5 have proven that the size of the spherical micelles built by alkyl-PAEI in aqueous solution strongly depends on the degree of polymerization of the polymer chain. Thus, these findings provide support for the observed dependence of the silica particle size on the degree of polymerization of the template.

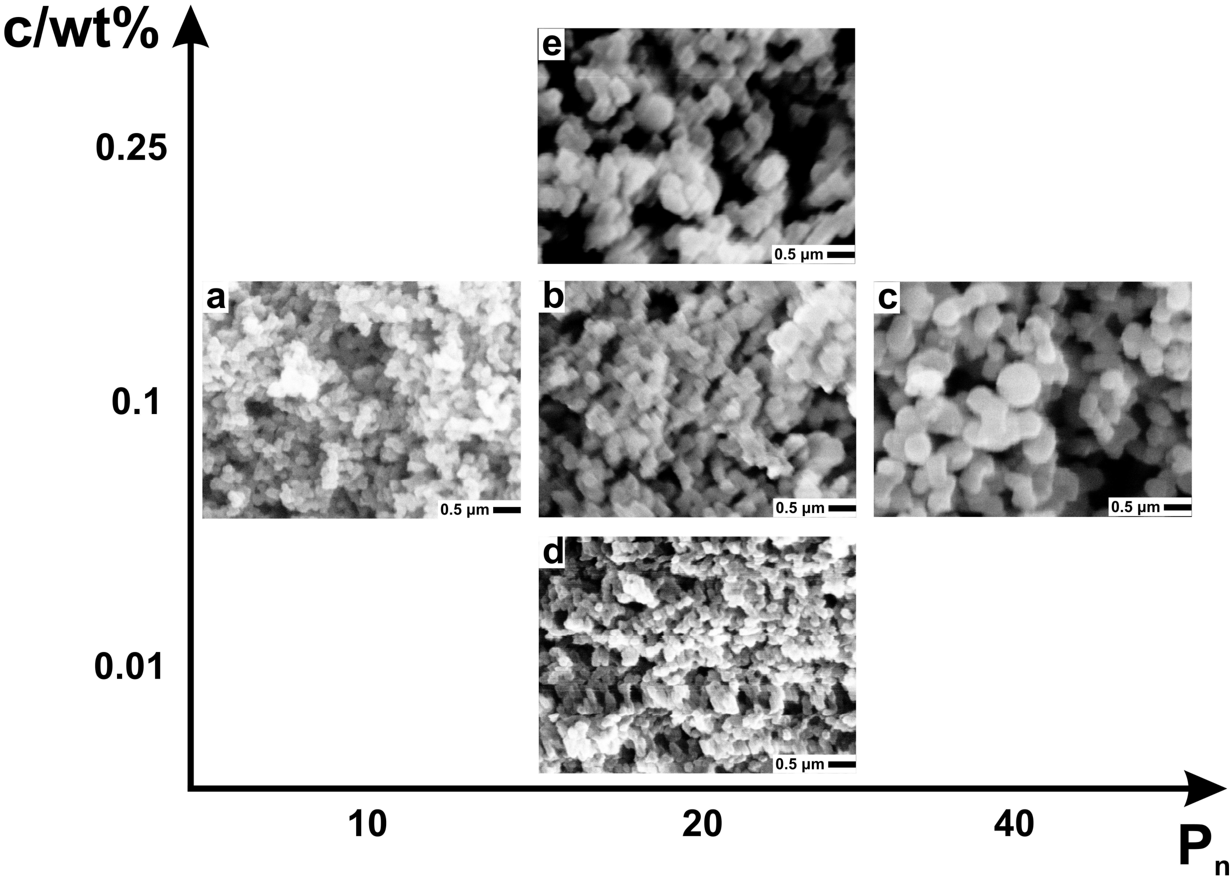

Figure 3.31. SEM images of the silica precipitates produced in the presence of alkyl-PAEI, dissolved in malonate buffer (pH = 5.5) with: (a) $P_n = 10$, c = 0.1 wt%; (b) $P_n = 20$, c = 0.1 wt%; (c) $P_n = 40$, c = 0.1 wt%; (d) $P_n = 20$, c = 0.01 wt%; and (e) $P_n = 20$, c = 0.25 wt%, at room temperature.

Another clear trend that can be identified in Figure 3.31 is that the overall size of the spheres increases by increasing the concentration of alkyl-PAEI in the solution (Figures 3.31-d, -b and -e). A similar result was obtained in the already mentioned work of PATWARDHAN *et al.*[264] when performed silicic acid condensation in solutions containing 10 and 50 mg/ml of polyallylamine (PAH), respectively. These observations are also in accordance with those reported by JAHNS[265] with respect to the condensation of silicic acid in solutions containing different concentrations of poly(N-methyl-propyleneimine) with $P_n = 20$ ($PMPI_{20}$). Within that work, it was remarked that the silica spheres tend to adhere to each other and that their surface becomes smoother by increasing the polymer concentration. Unfortunately, the SEM images available within this work do not allow clarifying if the silica particles produced in the presence of alkyl-PAEI also possess those structural features.

Influence of pH:

Another important variable when dealing with the condensation of silicic acid is the pH of the reaction medium. In order to test its influence, alkyl-PAEI has been dissolved in buffers with different pH values and the condensation of silicic acid has been performed in those solutions.

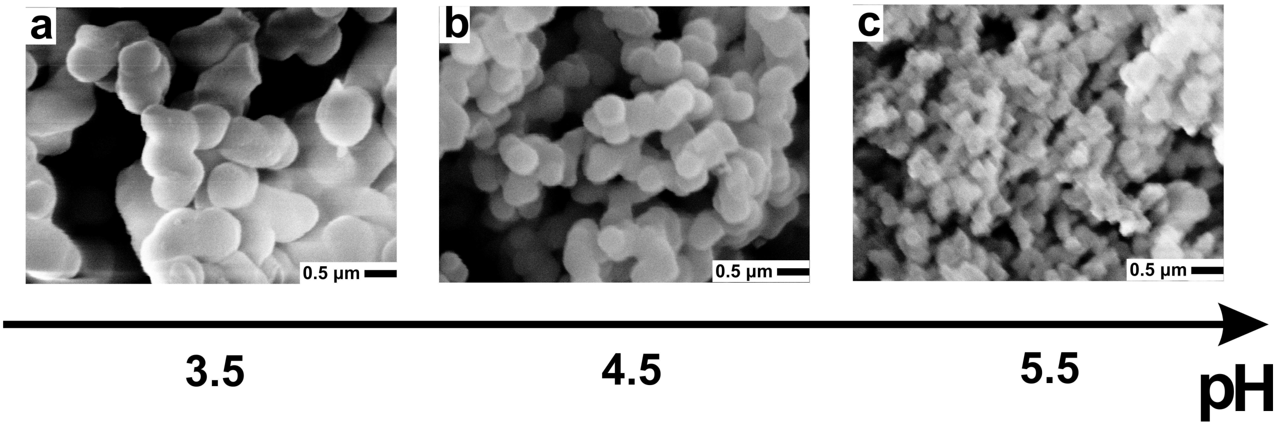

Figure 3.32. SEM images of the silica precipitates produced in the presence of alkyl-PAEI ($P_n = 20$) dissolved in: (a) citrate buffer (pH = 3.5); (b) acetate buffer (pH = 4.5); and (c) malonate buffer (pH = 5.5), at room temperature. The alkyl-PAEI concentration in each sample is 0.1 wt%.

As can be recognized in Figure 3.32, the size of the silica spheres prepared with alkyl-PAEI containing aqueous solutions increases dramatically by decreasing the pH of the buffer used to prepare the polymer solution. This effect has also been described by KRÖGER *et al.*[110] in the production of sphere-like silica precipitates in the presence of the long-chain polymines isolated from diatoms. Moreover, investigations performed by BELTON *et al.*[270] have proven that methylated, long-chain polyamines can form emulsion droplets in the aqueous medium with sizes up to 1 μm, strongly depending on the pH of the medium. However, the polyamine-based oligomers used within the studies performed by KRÖGER *et al.* and BELTON *et al.* as template for the condensation of silicic acid possess alkaline properties. Therefore, the detected influence of the pH of the medium in the size of the silica spheres produce within those studies can be ascribed to the alkaline properties of the polymers. On the contrary, as remarked previously, alkyl-PAEI does not possess alkaline character and hence its solution properties are not strongly influenced by pH. Thus, the dependence of the particle size in the silica precipitates on the pH of the reaction medium may be related to the effect of pH on the growing species. In fact, the isoelectric point for silica has been found to be between pH 1–3[12] and therefore the growing species in the silica precipitation assays are expected to be negatively charged. Furthermore, the negative charge on the surface of the growing species increases by increasing the pH of the solution. For this reason, at the lower pH values (e.g. in citrate, pH = 3.5, Figure 3.32-a) the particles are less charged than at the higher pH values (e.g. in malonate, pH = 5.5, Figure 3.32-c). As a consequence, at the lower pH values repulsion between the growing particles diminishes and aggregation takes place resulting in larger agglomerates than at higher pH.

Influence of phosphate:

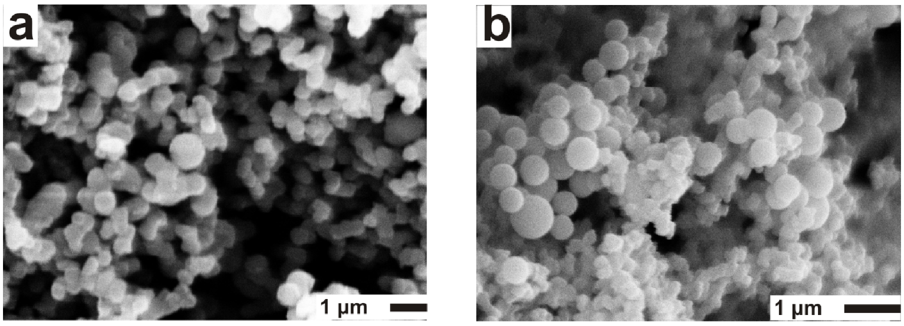

Figure 3.33. SEM images of the silica precipitates produced in the presence of alkyl-PAEI ($P_n = 40$) dissolved in: (a) malonate buffer (pH = 5.5); and (b) phosphate buffer (pH = 5.6, 15 mM), at room temperature. The alkyl-PAEI concentration is 0.1 wt% in both samples.

As has been mentioned in section 2.1.2.1, the native silaffin-1 protein (natSil-1) is highly post-translationally modified and heavily phosphorilated with phosphate groups bound to all the serine residues. In addition, it has been proven that long-chain polyamines dissolved in a phosphate buffer are able to precipitate silica nanospheres in the same way as silaffins[271]. Taking into account the crucial role of phosphate in the biomineralization of silica, a phosphate buffer (pH = 5.6, 15 mM) has been used to perform the condensation of silicic acid. Figure 3.33 shows the SEM pictures of the silica precipitates produced in the presence of alkyl-PAEI ($P_n = 40$) dissolved in malonate (pH = 5.5, Figure 3.33-a) and phosphate (pH = 5.6, Figure 3.33-b). As can be observed, both silica precipitates are composed of fused spheres with sizes around some hundred nanometers. In addition, the silica precipitate produced in phosphate exhibits some bigger spherical particles with well-defined shape. In other words, in the precipitate prepared in phosphate buffer the spheres are not that much fused to each other as in that produced in malonate but they keep their individual character. It is well known that phosphate anions can induce self-assembly of polyamines and subsequent macroscopic phase separation[64]. In this respect, investigations on the production of silica precipitates in the presence of phosphate anions have revealed that the size and unity of the spheres composing the precipitate are directly related to the concentration of phosphate in the reaction medium[221, 58]. Taking into account these results, the interactions of phosphate anions with alkyl-PAEI seem to be the most likely reason for the presence of bigger individual spheres in the SEM image of Figure 3.33-b. As described previously, alkyl-PAEI does not possess alkaline character and at low pH does not behave as a polyelectrolyte. For this reason, electrostatic interactions with phosphate anions can not take place. However, the high electronegativity of the nitrogen and oxygen atoms could polarize the carbon atom positively. This polarization of the carbon atom would enable interaction with phosphate anions. Another hypothesis, already mentioned, is the mesomeric effect of carbonyl and amino groups in the polymer repeating unit. Here, the presence of resonance structures where the nitrogen atom of the repeating unit would be positively charged would enable interactions with phosphate anions. The mechanism leading to the interaction of N-acetyl-ethyleneimine units with phosphate anions has not been clarified yet. However, the interaction mechanisms proposed here seem to be both plausible.

- ### Alkyl-PAPI

As for alkyl-PAEI, the activity of alkyl-PAPI regarding the condensation of silicic acid has been tested within this work.

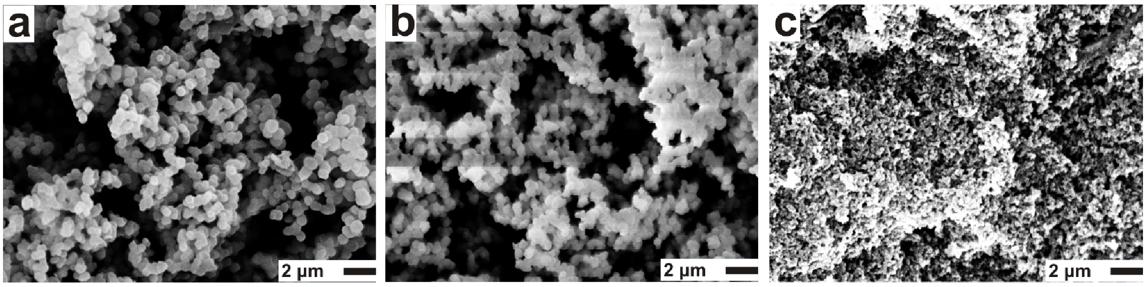

Figure 3.34. SEM images of the silica precipitates produced in the presence of: (a) alkyl-PAEI ($P_n = 20$), (b) alkyl-PAPI ($P_n = 20$), both dissolved in acetate buffer (pH = 4.5); and (c) alkyl-PAPI ($P_n = 20$) dissolved in malonate buffer (pH = 5.5), at room temperature. The polymer concentration in each sample is 0.1 wt%.

Figure 3.34 shows SEM images of silica precipitates prepared in aqueous solutions containing either alkyl-PAEI or alkyl-PAPI. As can be observed, similar to the precipitates produced in alkyl-PAEI-containing aqueous solutions, those prepared in the presence of alkyl-PAPI are composed of fused spheres with sizes around several hundred nanometers in diameter. Figures 3.34-a and 3.34–b correspond to silica precipitates prepared in acetate buffer (pH = 4.5) containing 0.1 wt% of, alkyl-PAEI and alkyl-PAPI, respectively, both with $P_n = 20$. Comparing both SEM images, there is no significant increase of the sphere size for the alkyl-PAPI-containing solution (Figure 3.34-b) with respect to that containing alkyl-PAEI (Figure 3.34-a). An explanation for this behaviour may be found in the size of the supramolecular aggregates built by both polymeric surfactants in water, which act as template in the condensation of silicic acid. As previously commented in section 3.2.1.5, the DLS investigations carried out in alkyl-PAEI-containing aqueous solutions revealed the presence of spherical micelles. The size of those micelles has been found to increase with the degree of polymerization of the hydrophilic chain, but not in a linear way. In fact, in Table 3.5 (section 3.2.1.5) it can be recognized that an increase of the degree of polymerization from 10 to 40 in the PAEI chain, results in an increase of the hydrodynamic radius of the spherical micelles just from 6.52 to 11.56 nm. Thus, by increasing the degree of polymerization of the hydrophilic segment three times, the hydrodynamic radius of the aggregates increases only twice. According to these results, the replacement of ethylene (alkyl-PAEI) by propylene (alkyl-PAPI) in the spacing group of the polymer repeating unit may not result in a significant increase of the aggregate size provided that the polymers possess a relatively low degree of polymerization. This is the case of alkyl-PAEI and alkyl-PAPI with

$P_n = 20$. Consequently, that may be the reason why the spheres of the silica precipitates prepared in the presence of both polymers show a similar size.

Regarding the effect of pH, Figures 3.34-b and 3.34-c show silica precipitates produced in aqueous solutions containing 0.1 wt% alkyl-PAPI ($P_n = 20$) dissolved respectively in acetate (pH = 4.5) and malonate (pH = 5.5) buffers. Here, a similar trend to that reported for alkyl-PAEI can be detected. As can be observed, the spheres composing the silica precipitate produced in acetate (pH = 4.5) are considerably bigger than those corresponding to the precipitate yielded by alkyl-PAPI in malonate (pH = 5.5), i.e. the size of the spheres increases by decreasing the pH of the reaction medium. The reason for this behaviour has already been discussed within this section.

- **Alkyl-PEI**

Clear solutions:

Similarly to alkyl-PAEI and alkyl-PAPI, silicic acid condensation experiments have been carried out in aqueous solutions containing alkyl-PEI. At this point, it is important to remark that, unlike alkyl-PAEI and alkyl-PAPI, the solubility of alkyl-PEI in pure water at room temperature is extremely low. In fact, as mentioned in section 3.2.2.2, clear, aqueous solutions containing alkyl-PEI only can be prepared up to concentrations below 0.025 wt% only. On the contrary, solutions with higher concentrations can be produced in slightly acidic buffers because of the alkaline properties of alkyl-PEI. In this regard, clear solutions containing up to 0.1 wt% alkyl-PEI in acetate buffer (pH = 4.5) can be prepared. In malonate buffer (pH = 5.5), which is less acidic than acetate, the highest polymer concentration resulting in a clear solution is around 0.01 wt%. It is also worth mentioning that, unlike alkyl-PAEI, alkyl-PEI does not dissolve completely in the buffers immediately but only after 12 hours under stirring.

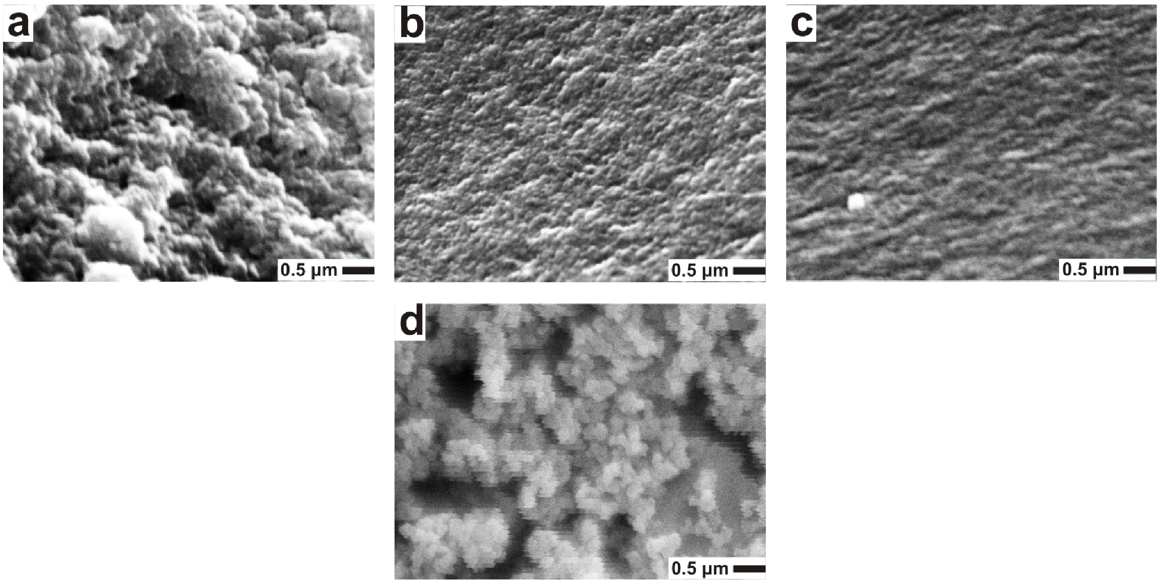

Figure 3.35. SEM images of the silica precipitates produced in the presence of alkyl-PEI with: (a) P_n = 10, (b) P_n = 20 and (c) P_n = 40 dissolved in acetate buffer (pH = 4.5) to a concentration of 0.1 wt%, at room temperature. Picture (d), which unfortunately does not possess a high quality, corresponds to a silica precipitate produced in the presence of alkyl-PEI (P_n = 20) dissolved in malonate buffer (pH = 5.5) to a concentration of 0.01 wt%.

Nevertheless, Experiments on the condensation of silicic acid in these alkyl-PEI-containing solutions have been performed.Within these experiments, it has been found that solutions containing 0.1 wt% alkyl-PEI (P_n = 10, 20 and 40) dissolved in acetate buffer (pH = 4.5) do not promote silica precipitation but they yield silica gels. However, solutions containing polymer concentrations around 0.01 wt% in acetate buffer (pH = 4.5) yield neither silica gels nor silica precipitates. This may be a consequence of the fact that, as reported by CORNELIUS[125], the polymer solution has to provide a minimum concentration of active amino groups in order to obtain any silica precipitate or gel. In contrast to this acceleration of the gelation by alkyl-PEI in acetate buffer (pH = 4.5), solutions containing alkyl-PEI dissolved in malonate (pH = 5.5) result in silica precipitates looking like those obtained in the presence of alkyl-PAEI. Figure 3.35 shows SEM images of both, silica gels produced in solutions containing 0.1 wt% alkyl-PEI (P_n = 10, 20 and 40) dissolved in acetate (Figures 3.35-a, -b and- c) and a silica precipitate produced in a solution with 0.01 wt% alkyl-PEI (P_n = 20) dissolved in malonate buffer (Figure 3.35-d). As can be observed, the silica gels obtained (Figures 3.35-a, -b and -c) exhibit a smooth, dense surface resembling that of the acid- and polymer-catalyzed silicas reported by ADAMSON *et al.*[272].

Within that work, silica-based solid materials have been produced with acidic, basic and polymeric additives. Tetraethylorthosilane (TEOS) was the silica precursor and, as polymeric template, a block copolymer of poly(2-vinylpyridine-*b*-1,2-butadiene), functionalized by the formation of hydroxyl groups via hydroboration chemistry was used. According to those investigations, the different morphology of the obtained silica-solids arise from the fact that hydrolysis and condensation of the silica precursor takes place to a different extent depending on the reaction conditions. While under acidic and polymeric additives, hydrolysis of the silica precursor is favored over condensation, under basic conditions the condensation is favoured. As a result, acid- and polymer-promoted silica formation yields dense, smooth surfaces, whereas base-promoted silica formation results in larger voids. However, the silica gels depicted in Figure 3.35-a, -b and –c are produced by using tetramethylortosilane (TMOS), which becomes hydrolyzed much faster than TEOS[273], as silica precursor. Furthermore, here TMOS was prehydrolyzed with HCl providing fresh silicic acid and subsequently the polymer-containing solution was added. Thus, within this work the polymer is supposed to affect the condensation of silicic acid and not the hydrolysis of the silica precursor. Therefore, the reasons for the formation of the gels depicted in Figure 3.35 must be rather different to those reported by ADAMSON *et al*. Here, the charge of both, silica growing species and alkyl-PEI may play a crucial role. In fact, as discussed in section 3.2.2.3, the degree of protonation of alkyl-PEI strongly depends on the pH of the medium. In Figure 3.20-a (section 3.2.2.3) it can be appreciated that alkyl-PEI with $P_n = 20$ possess a degree of protonation around 60 % at pH = 4.5 (acetate buffer), while it decreases to around 55 % at pH = 5.5 (malonate buffer). Nevertheless both values are quite similar. On the other hand, the isoelectric point for silica has been found to be between pH 1–3[12, 273] and therefore the growing sol species in the silica precipitation assays are expected to be negatively charged. Concretely, at pH = 4.5 (acetate buffer) the silica sol growing particles are expected to be less negatively charged than at pH = 5.5 (malonate buffer). Furthermore, it has to be pointed out that acetate is a monovalent anion, whereas malonate is divalent. As a consequence, bigger alkyl-PEI aggregates are formed in the presence of malonate. Taking all these aspects into account, the reason why alkyl-PEI yields silica gels in acetate (pH = 4.5) and silica precipitates in malonate (pH = 5.5) may be found in its interaction with the silica sol growing species and with the anions provided by the buffer. As mentioned previously the degree of protonation of alkyl-PEI at pH = 4.5 does not differ too much from that at pH = 5.5. However, this is not the case for the superficial, negative charge of the silica sol growing species. It has already been discussed that in the presence of alkyl-PAEI, the size of the spheres increases by decreasing the pH of the reaction medium. Figures 3.32-b and 3.32-c depict the silica precipitates produced in solutions containing alkyl-PAEI dissolved respectively in acetate (pH = 4.5) and malonate (pH = 5.5) buffers. It can be appreciated that the size of the spheres decreases considerably by increasing the pH of the solution from 4.5 to 5.5. Thus, the effect of pH on the superficial charge of the silica sol growing species seems to be stronger than on the degree of protonation of alkyl-PEI. Therefore, as the degree of protonation of alkyl-PEI at pH values 4.5 and 5.5 is very similar, the surface negative charge of the silica sol growing species may be higher at the latter pH value. Another aspect that has to be considered is that alkyl-PEI forms bigger aggregates in the presence of multivalent anions such as malonate than with monovalent anions like acetate. Those may be the main reasons for the different behaviour regarding the condensation of silicic acid in both pH buffers. At pH = 4.5 the silica sol growing species are less charged than at pH = 5.5, while the degree of protonation of the polymer does not vary considerably. Furthermore, in the presence of malonate (pH = 5.5) alkyl-PEI forms bigger aggregates than in the presence of acetate (pH = 4.5). As a consequence, interactions between the elements involved in the process, namely alkyl-PEI, sol growing species and anion of the buffer, take place to a high extent at pH = 5.5, promoting particle aggregation and subsequent precipitation. On the contrary, at pH = 4.5 those elements undergo weaker interactions. For this reason the silica sols can grow without undergoing aggregation phenomena until they collide, becoming a gel and not a precipitate. PATWARDHAN *et al.* have also reported the formation of silica gels in the presence of different polymers such as polyvinyl alcohol (PVA), polyanetholesulfonic acid, and polyacrylic acid and polymethacrylic acid[262]. According to these investigations, silica gelation in the presence of those polymers might be related to the fact that, at slightly acidic conditions, they bear negative charges that repel the growing silica sol species, which are also negatively charged. Thus, in spite of the fact that the interactions between polymer and silica sol species described within that work are different to those taking place between alkyl-PEI and silica sol species, the described gelation mechanism is analogous.

Turbid suspensions:

Samples where alkyl-PEI does not dissolve completely in the buffer at room temperature after 12 hours under stirring have to be heated up to 80 °C and subsequently cooled down to room temperature. As a result, turbid suspensions of the polymer in the buffer similar to those depicted in Figure 3.18 (section 3.2.2.2) have been obtained. Here, it has to be also remarked that samples containing alkyl-PEI suspended in either citrate or phosphate buffers become very turbid, almost opaque, already at polymer concentrations around 0.056 wt%. In malonate buffer the suspensions show a considerable turbidity at 0.1 wt% and become intensively turbid at 0.25 wt%. As has already been mentioned in section 3.2.2.2., according to MANZUR *et al.*[223], the turbidity developed by PEI-containing solutions in the presence of phosphate and citrate anions at pH values between 3 and 8 is caused by formation of insoluble PEI complexes under those conditions. Hence, the formation of these complexes together with the low solubility at room temperature may be the reason why alkyl-PEI aqueous solutions in citrate and phosphate buffers become almost opaque at very low polymer concentrations. Similarly to alkyl-PEI-containing clear solutions, the described turbid suspensions have been used to produce silica precipitates.

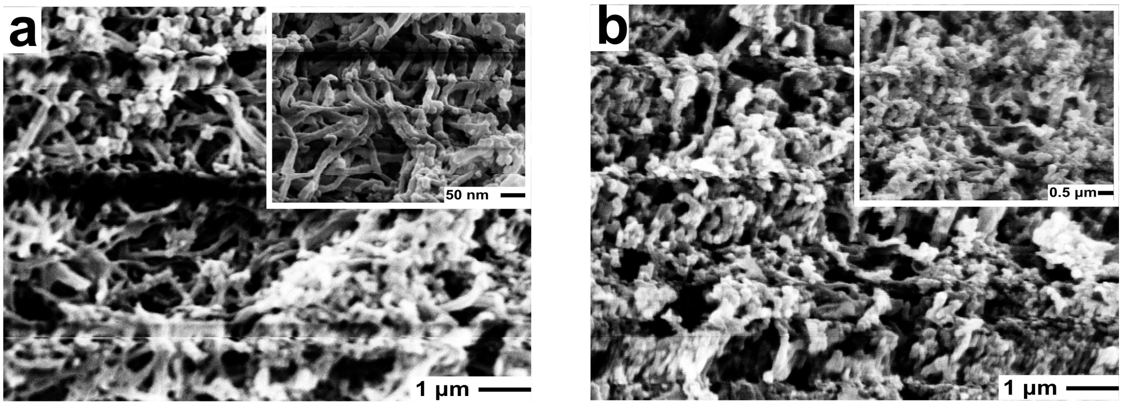

Figure 3.36. SEM images of the silica precipitates produced in the presence of alkyl-PEI suspended in malonate buffer (pH = 5.5), heated to 80 °C till complete polymer dissolution and cooled down to room temperature with: (a) $P_n = 20$, c = 0.1 wt%, and (b) $P_n = 40$, c = 0.25 wt%.

In this respect, Figure 3.36 depicts the silica precipitates produced in turbid alkyl-PEI solutions, in which the polymer has been suspended in malonate buffer (pH = 5.5), subsequently heated up to 80 °C and finally cooled down to room temperature. Here, unlike the gelation that has taken place in clear solutions containing alkyl-PEI dissolved in acetate buffer, the reaction medium becomes even more turbid within twenty minutes after adding the silicic acid solution. This increase in the turbidity of the solution indicates silica precipitation.

Figures 3.36-a and 3.36-b show the silica precipitates obtained in solutions containing alkyl-PEI suspended in malonate buffer (pH = 5.5) with, $P_n = 20$ and c = 0.1 wt% (3.36-a), and, $P_n = 40$ and c = 0.25 wt% (3.36-b), respectively. As can be observed, all SEM images show the existence of network-like structure, together with some fused spheres resembling those found in alkyl-PAEI-mediated silica precipitates. YUAN *et al.*[222] have proven that linear poly(ethyleneimine) (PEI) can self-organize into fibrous aggregates with a crystalline core and a brushlike shell of ethyleneimine (EI) segments. Besides, silicic acid condensation mediated by solutions containing PEI aggregates easily produces silica nanofibers with a core of axial, crystalline PEI filaments and a shell of silica. Taking these observations into account, it seems to be clear that the network-like component of the silica precipitates depicted in Figure 3.36 results from the presence of organized PEI fibrous aggregates, which act as scaffolds in the subsequent condensation of silicic acid. On the contrary, the presence of fused spheres in the silica precipitates could be ascribed to the fact that the amount of polymer in the turbid suspension has not been sufficient to convert completely the silicic acid into a silica network. As a consequence, non-reacted silicid acid condensates into fused spheres, as it occurs without the influence of any polymer. Another possible reason for the presence of fused spheres could be that presence of alkyl-PEI spherical micelles in the solution. In fact, despite the low solubility of alkyl-PEI in water and in slightly acidic buffers, small amounts of polymer have been found to be dissolved in the buffer. As mentioned in section 3.2.2.2, the CMC value yielded by alkyl-PEI (P_n = 40) in malonate buffer was found to be 0.0018 wt%. According to this value, solutions containing 0.25 wt% of alkyl-PEI (P_n = 40) (Figure 3.36-b) have developed, along with the alkyl-PEI fibrous aggregates, spherical micelles. These spherical micelles, together with the alkyl-PEI fibrous aggregates, act as templates in the subsequent silicic acid condensation. Those may be the reasons why the resulting precipitate is composed, not only of the network-like structure promoted by the fibrous aggregates, but also of fused spheres.

Likewise, silicic acid condensation has also been performed in turbid alkyl-PEI solutions, in which the polymer has been suspended in phosphate buffer (pH = 5.6), subsequently heated up to 80 °C and finally cooled down to room temperature. Figure 3.37 depicts the silica precipitates obtained under those conditions.

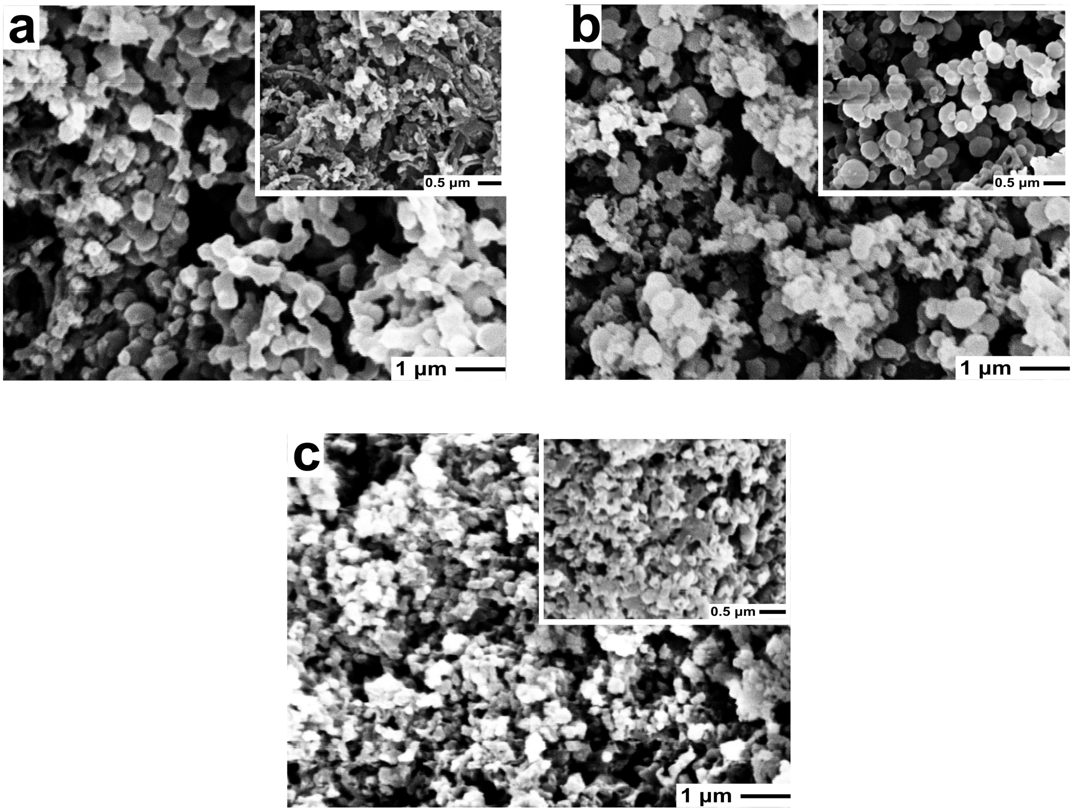

Figure 3.37. SEM images of the silica precipitates produced in the presence of alkyl-PEI suspended in phosphate buffer (pH = 5.6), heated to 80 °C till complete polymer dissolution and cooled down to room temperature with: (a) $P_n = 10$, $c = 0.05$ wt%; (b) $P_n = 40$, $c = 0.05$ wt%; and (c) $P_n = 20$, $c = 0.25$ wt%.

Here, as in the previous case, i.e. alkyl-PEI suspended in malonate buffer, the reaction medium becomes even more turbid within twenty minutes after adding the silicic acid solution. This increase in the turbidity of the solution indicates silica precipitation. Figures 3.37-a, -b and-c show SEM images of the silica precipitates obtained in solutions containing alkyl-PEI suspended in phosphate buffer (pH = 5.6) with $P_n = 10$ and $c = 0.05$ wt% (3.37-a), $P_n = 40$ and $c = 0.05$ wt% (3.37-b), and, $P_n = 20$ and $c = 0.25$ wt% (3.37-c), respectively. As can be observed, Figures 3.37-a and 3.37-b show the presence of some fused spheres resembling those found in alkyl-PAEI-mediated silica precipitates. Furthermore, it is hard to identify a network-like structure similar to that observed in the silica precipitates produced in malonate buffer. However, it can be appreciated that the fused spheres arrange into small, randomly-orientated bundles. Again, both phenomena take place simultaneously. On the one hand, Alkyl-PEI fibrous bundles act as scaffolds in the condensation of silicic acid, which results in the formation of the network-like structure. On the other hand, the presence of fused spheres in the silica precipitates could be related to the fact that the amount of polymer in the turbid suspension has not been sufficient to convert completely the silicic acid into a silica network. As a consequence, subsequent condensation of non-reacted silicic acid results in fused spheres, as it occurs without the influence of any polymer. As mentioned before, another reason for the formation of fused spheres could be the presence of alkyl-PEI spherical micelles which can also promote silicic acid condensation. It is well-known that, unlike malonate anions, phosphate can promote polyamine aggregation and macroscopic separation[64]. Therefore, it can be thought that in the presence of phosphate anions, aggregation of the dissolved alkyl-PEI molecules around the brush-like alkyl-PEI segments which compose the fibrous bundles may take place. As a result, the subsequent silicic acid condensation onto the alkyl-PEI aggregates surrounding the fibrous bundles yields spheres which make it difficult to identify the network-like structure of the precipitate. Yet, in malonate (Figure 3.36), interactions between dissolved and brush-like alkyl-PEI are not plausible and the network-like structure of the precipitate can be easily identified.

Figure 3.37-c shows the SEM image of a precipitate prepared with the solution containing the highest alkyl-PEI concentration in phosphate buffer (0.25 wt%). As can be appreciated, the silica precipitate possesses a denser and more compact structure than those produced in the presence of less concentrated solutions (Figures 3.37-a and -b). In addition, the presence of fused spheres is less visible than in the precipitates prepared in the presence of less concentrated alkyl-PEI solutions (Figures 3.37-a and -b). The formation of such a compact structure may be ascribed to the fact that at high alkyl-PEI concentrations, the fibrous bundles with the surrounding alkyl-PEI-phosphate aggregates become closer to each other.

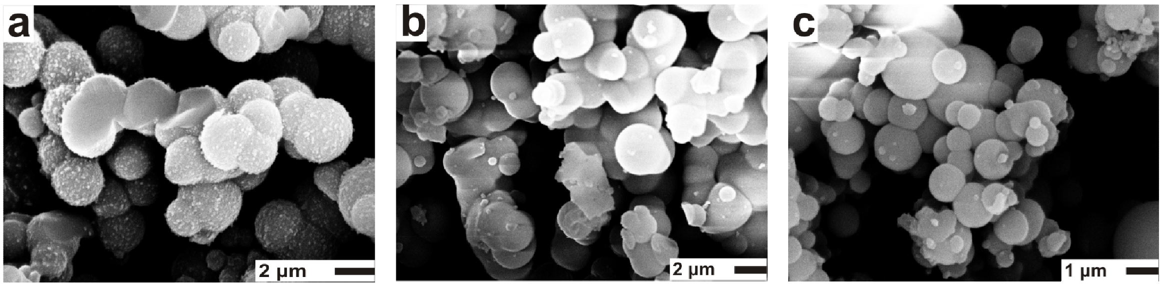

Figure 3.38. SEM images of the silica precipitates produced in the presence of alkyl-PEI suspended in citrate buffer (pH = 3.5), heated to 80 °C till complete polymer dissolution and cooled down to room temperature with: (a) P_n = 10, c = 0.1 wt%; (b) P_n = 20, c = 0.25 wt%; and (c) P_n = 40, c = 0.25 wt%.

Finally, silicic acid condensation has also been performed in turbid alkyl-PEI aqueous solutions, in which the polymer has been suspended in citrate buffer (pH = 3.5), subsequently heated up to 80 °C and finally cooled down to room temperature. Figure 3.38-a, -b and-c depicts SEM images of the silica precipitates obtained in those solutions containing alkyl-PEI suspended in citrate buffer with (a) P_n = 10, c = 0.1 wt%; (b) P_n = 20, c = 0.25 wt%; and (c) P_n = 40, c = 0.25 wt%. As can be observed, the structure of all silica precipitates is composed of fused spheres with diameters around 2 μm. Furthermore, the morphology resembles that of the silica precipitates produced in alkyl-PAEI-containing aqueous solutions. However, in those alkyl-PAEI-mediated silica precipitates (Figures 3.31, 3.32 and 3.33) the size of the spheres is smaller, around some hundreds of nanometers, depending on the reaction conditions. This resemblance between the morphology of both precipitates suggests a similar formation mechanism. Nevertheless, the size of spheres in alkyl-PAEI-mediated silica precipitates is around ten times smaller than that in silica precipitates produced in the presence of alkyl-PEI suspended in citrate. As mentioned in section 2.1.1, the morphology of silica precipitates produced via sol-gel methods strongly depends on the dimensions of the template. Therefore, the different size of the spheres in both silica precipitates may result from the different size of the supramolecular aggregates built by the polymers, i.e. alkyl-PAEI in the different buffers and alkyl-PEI in citrate. In this respect, it has been found via DLS measurements (section 3.2.1.5) that alkyl-PAEI builds spherical micelles in pure water with sizes between 6.22 and 11.06 nm (see Table 3.5) depending on its degree of polymerization. As commented regarding Figure 3.31 within this section, the degree of polymerization of the alkyl-PAEI chains exerts an influence on the size of the spheres composing the silica precipitate obtained from solutions containing this polymer. For alkyl-PEI, DLS measurements on the aggregation of this polymer in citrate buffer have not been performed because of the poor solubility and formation of turbid suspension. However, CHEN *et al.*[274] have proven that mono- and dialkylated-PEI (C9, P_n = 10) can aggregate into respectively poly- and monodisperse spherical micelles with sizes around 170 nm at pH = 3. Thus, taking this result into account and in spite of the low solubility, the presence of such spherical alkyl-PEI aggregates with sizes around 170 nm in citrate buffer (pH = 3.5) is plausible. Furthermore, this hypothesis is also supported by the fact that at pH = 3.5, alkyl-PEI has been shown to possess a degree of protonation α around 80 % (see Figure 3.20-a). Under those conditions, the repulsion between the hydrophilic PEI segments may enable their stretching and build spherical aggregates which may act as template in the silicic acid condensation. At this point, it is also worth mentioning that the micellar aggregates undergo a further level of aggregation under the influence of the silica oligomers. The combination of these different levels of aggregation for alkyl-PEI at pH = 3.5 may be the reason for the presence of μ-spheres in the silica precipitates. Another remarkable aspect of the SEM images depicted in Figure 3.38 is the total absence of a network-like morphology comparable to that observed in silica precipitates produced in solutions containing alkyl-PEI suspended in malonate and citrate buffers (Figures 3.36 and 3.37). In fact, because of the strong turbidity developed by alkyl-PEI solutions in citrate, which has been ascribed to the formation of insoluble complexes[223], the presence of a network-like morphology in the precipitates produced within these turbid solutions could be expected. However, only fused spheres can be identified in the SEM images shown in Figure 3.38. A reason for the absence of a network-like component within the structure of the precipitate has not been found so far and hence further investigations should be carried out on this topic.

3.3.3 Alkyl-PEI-hydrogel-mediated silicic acid condensation

In addition to the clear and turbid aqueous solutions/suspensions of alkyl-PEI in different buffers reported in the previous section, the thermoreversible alkyl-PEI-based hydrogels described in section 3.2.2.6 have been used as template in the hydrolytic condensation of TMOS. YUAN *et al.*[222] have reported TMOS silification templated by hydrogels from linear and star shaped architectures bearing linear PEI segments. Within that work, it has been proven that silification takes place around PEI-brushes on the surface of the crystalline fibers which compose the hydrogel. Furthermore, PEI-based hydrogels have been applied not only in silification experiments, but also as soft sacrificial templates in the production of porous silver framework[275].

Under this approach, the hydrolytic condensation of TMOS has been examined in the presence of alkyl-PEI hydrogels. For this purpose, a mixture of TMOS/ethanol (1/1, v/v) has been poured over non-crosslinked alkyl-PEI hydrogels in the swollen state for 24 h in order to ensure reactants diffusion and silica deposition. During this process, the hydrogels become white, hard, and brittle silica hybrid monoliths. As mentioned in section 3.2.2.6, cross-linking of alkyl-PEI hydrogels with glutaraldehyde improves their mechanical properties. As a result, alkyl-PEI hydrogels cross-linked with glutaraldehyde in both, swollen state and freeze-dried, have been cut into thin slices which have been subsequently immersed into TMOS/ethanol (1/1, v/v) for 24 h. As for the non-cross-linked hydrogels, the slices become white, hard, and brittle silica hybrid monoliths.

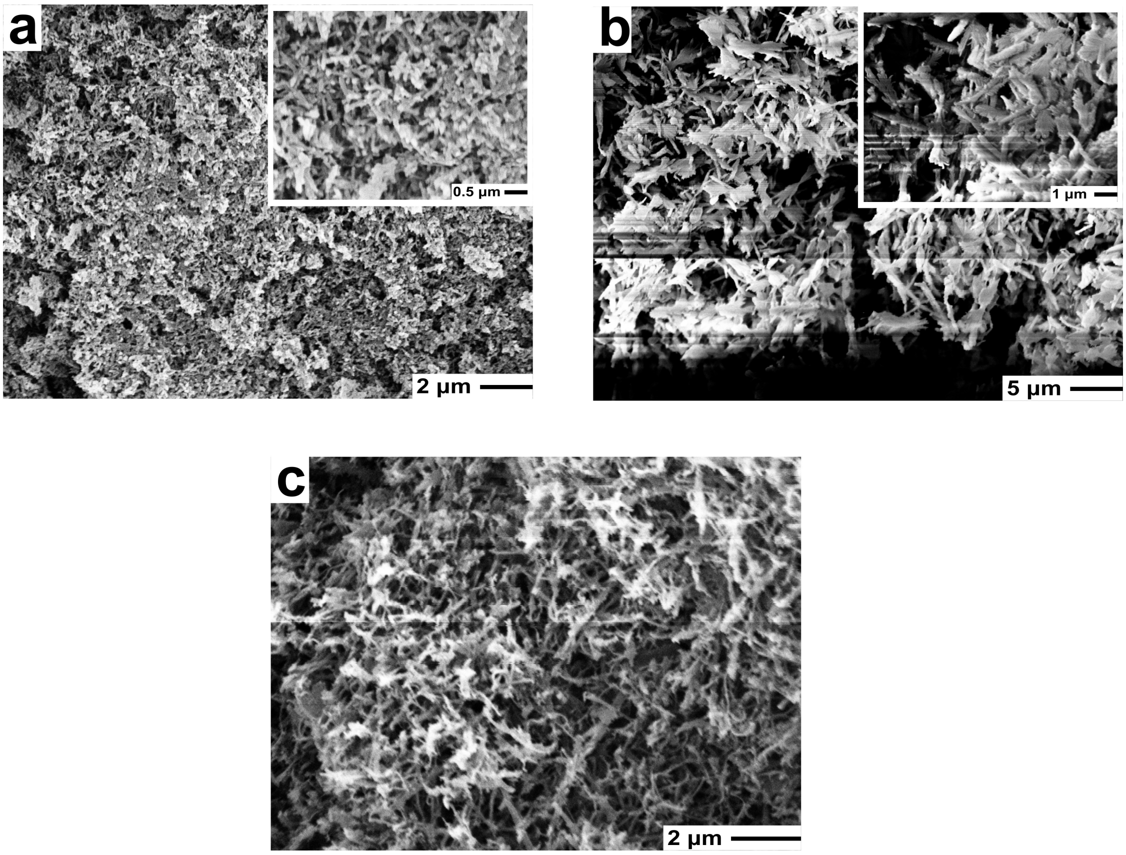

Figure 3.39. SEM images of the silica monoliths produced via: (a) diffusion of TMOS/ethanol into a non-cross-linked alkyl-PEI ($P_n = 40$) hydrogel in the swollen state; (b) dipping a slice of a cross-linked alkyl-PEI ($P_n = 20$) hydrogel in the swollen state into TMOS/ethanol; and (c) dipping a slice of a cross-linked and subsequently freeze-dried alkyl-PEI ($P_n = 10$) hydrogel into TMOS/ethanol, at room temperature.

Figure 3.39 shows the representative SEM images of the silica/PEI hybrid monoliths. As can be observed for all samples, the structure of the silica monolith consists of a dense, fibrous network resembling that of the PEI-mediated hybrid silica monoliths described by YUAN *et al.*[222]. Nevertheless, such a coincidence between the morphologies of the monoliths could be expected since the formation mechanism is the same. Here, as with the PEI-based hybrid silica monoliths described by YUAN *et al.*, TMOS condensation takes place around the active PEI-brushes on the surface of the fibrous aggregates composing the hydrogel, which act as scaffolds. That is the reason why the silica hybrid monolith captures the morphology of the hydrogels acting as template. In addition, Figure 3.39-a, which corresponds to the silica monolith produced from a non-crosslinked hydrogel in the swollen state, reveals the presence of some spheres similar to those identified in alkyl-PAEI-mediated precipitates. Those spheres can not be observed in Figures 3.39-b and -c, which correspond to alkyl-PEI-based hydrogels crosslinked with glutaraldehyde, in the swollen state (3.39-b) and freeze-dried (3.39-c), respectively. The reason for this difference in the structural morphology of the silica monoliths result from the preparation procedure of the hydrogels acting as template. As remarked previously, the silica monolith depicted in Figure 3.39-a has been produced from a non-crosslinked alkyl-PEI hydrogel. The production of this monolith starts with the generation of the hydrogel, i.e. heating up to 80 °C and cooling down to room temperature of an alkyl-PEI suspension in water with $c>c_G$ (Figure 3.24). A mixture of TMOS/EtOH is subsequently poured over the hydrogel allowing reactant diffusion and condensation. On the contrary, the silica monoliths shown in Figures 3.39-b and 3.39-c have been produced from alkyl-PEI hydrogels crosslinked with glutaraldehyde, in the swollen state and freeze-dried, respectively. Here, the alkyl-PEI hydrogels produced as already described are crosslinked in an aqueous solution of glutaraldehyde (see experimental section) and soaked in water in order to remove glutaraldehyde from their voids. Finally, slices of both, crosslinked alkyl-PEI hydrogel in the swollen state and freeze dried are immersed in TMOS/EtOH for silification.

Thus, taking the preparation processes of these silica monoliths into account, the presence of spheres in the silica monolith shown in Figure 3.39-a arises from the fact that the non-crossliked alkyl-PEI hydrogel used as template has not been soaked in pure water before being immersed in TMOS/EtOH. As a consequence, the slices of hydrogel contain an aqueous solution of alkyl-PEI within its fibrous structure. In spite of the low solubility of alkyl-PEI in pure water, the solution within the voids of the hydrogel may contain alkyl-PEI spherical aggregates, which act as template in the subsequent silification process. For this reason, the silica hybrid monolith shown in Figure 3.39-a possesses such a dense morphology, composed of a network-like structure templated by the alkyl-PEI fibrous aggregates, along with fused spheres similar to those observed in alkyl-PAEI silica precipitates and which are templated by spherical alkyl-PEI aggregates. Yet, the silica monoliths depicted in Figures 3.39-b and 3.39-c do not show any fused spheres because of the fact that the hydrogels have been immersed in a gluraldehyde-containing aqueous solution and subsequently in pure water prior to the immersion in TMOS/EtOH. The soaking allows to remove the alkyl-PEI aqueous solution that remains in the voids of the hydrogel after the thermal production process. In the absence of that aqueous solution containing alkyl-PEI aggregates, silification can take place only around the fibrous aggregates of the hydrogel, yielding a network-like structure for the silica monoliths as can be observed in Figures 3.39-a and 3.39-b.

3.3.4 Hydrothermal synthesis

As already described in section 2.1.1, the hydrothermal synthesis or sol-gel process, which leads to the formation of porous structures, is based on the combination of appropriate amounts of a silica source (TMOS, TEOS, dispersions of small silica particles (e.g. Ludox®), fumed silica, sodium silicate), a surfactant (e.g. cetyltrimethylammonium bromide (CTAB)), a base or an acid (e.g. NaOH or HCl) and water. This mixture is then kept at elevated temperatures and pressures (T ~ 100 °C, p ~ 1 bar) for 24 to 144 hours and results in a solid precipitate. Within this work, a similar silification synthetic process has been carried out in the presence of alkyl-PAEI, alkyl-PEI and the triblock copolymer PEG_{20}-PPG_{70}-PEG_{20}. Here, the polymer, water and HCl have been mixed at different ratios and, after complete dissolution, TEOS has been added. Subsequently, the mixture has been kept for 48 hours at 90 °C in an autoclave. Finally, the resulting precipitates have been centrifuged, washed and dried in vacuo. Figure 3.40 shows SEM images of the silica precipitates produced via hydrothermal synthesis with alkyl-PAEI as template. As can be observed, the silica precipitates prepared with solutions containing 0.5 wt % of alkyl-PAEI with $P_n = 10$ and 20 (Figures 3.40-a and 3.40-c respectively) show a morphology composed of fused spheres with diameters around 4 μm. Furthermore, the structure of these silica precipitates resemble that of those prepared with the triblock copolymer PEG_{20}-PPG_{70}-PEG_{20} as template under the same conditions, one of which is depicted in Figure 3.41-c. Yet, the silica precipitates prepared with solutions containing 1.2 wt % of alkyl-PAEI with $P_n = 10$, and 1.9 wt% of the same polymer with $P_n = 20$ (Figures 3.40-b and 3.40-d, respectively) seem to show a similar morphology of fused μ-spheres but together with non-structured silica coating their surface.

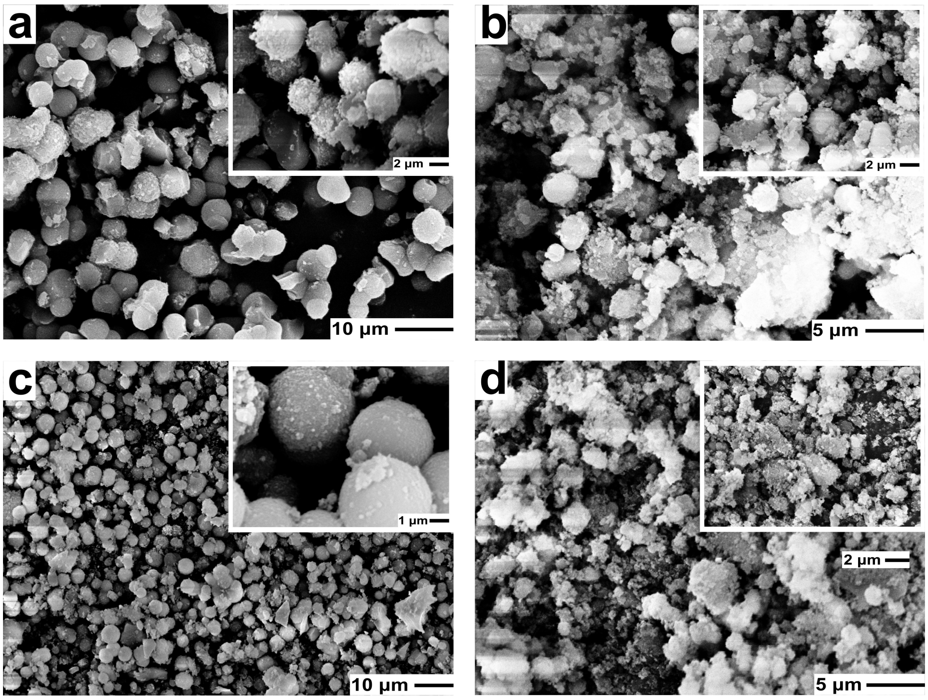

Figure 3.40. SEM images of the silica precipitates produced via hydrothermal synthesis in the presence of alkyl-PAEI with: (a) $P_n = 10$, c = 0.5 wt%; (b) $P_n = 10$, c = 1.2 wt%; (c) $P_n = 20$, c = 0.5 wt%; and (d) $P_n = 20$, c = 1.9 wt%. In all samples, TEOS was used as silica source.

The reason for the higher structured character of the silica precipitates prepared with the less concentrated polymer solutions may result from the fact that, as commented in sections 3.2.1.5 and 3.2.1.6, the features of the aggregates built by alkyl-PAEI in aqueous solutions strongly depend on the polymer concentration. In fact, DLS, SAXS and cryo-TEM experiments revealed that, at low polymer concentrations, alkyl-PAEI aqueous solutions contain non-interacting spherical micelles. Yet, at higher polymer concentrations, the micelles become closer to each other and weak interaction starts to take place resulting in interpenetration phenomena and hence in a complexer aggregate solution. Moreover, at any concentration, aggregates coexist with single polymer molecules and both elements possess functional groups capable of promoting silicic acid condensation. Since, as remarked previously, surfactant aggregation plays a crucial role in sol-gel processes, it may be expected that all these phenomena exert an important effect in the morphology of the porous structure. That may be the reason why the silica precipitates prepared in alkyl-PAEI solutions containing the higher concentrations appear less structured than those containing the lower ones.

Silica precipitates produced via hydrothermal synthesis with different templates, and showing a similar μ-sphere-like morphology, have been reported in the literature[276-279]. Furthermore, different formation mechanisms have been reported to be involved in the production of these precipitates. In this regard, ANTONIETTI *et al.*[276] produced mesoporous silica with μ-sphere-like morphology by performing hydrothermal synthesis with latex. Within those, polystyrene is dispersed in an aqueous phase by means of a stabilizer, usually a polymeric surfactant, yielding drops with sizes depending on the stabilizer. Subsequent hydrothermal synthesis under acidic conditions gives silica precipitates with sphere-like morphology. Taking this mechanism into account, alkyl-PAEI micelles could be regarded as organic drops dispersed within an aqueous phase which contains the silica precursor. In addition, N-acetylethyleneimine groups on the surface of those micelles can promote silicic acid condensation as already has been proven. Under the strongly acidic conditions of the reaction medium, silica growing species are nearly neutral. Therefore, repulsions between those growing species do not take place and aggregation into bigger particles may be plausible.

Another approach dealing with the production of porous sphere-like silica precipitates has been reported by QUI[278]. Here, a double-hydrophilic block copolymer, poly(ethylene oxide)-*b*-poly(methacrylic acid) (PEO-*b*-PMAA), has been used as template for hydrothermal synthesis. Under strong acidic conditions, PEO chains can interact with cationic silica species through a combination of hydrogen bonding, and van der Waals interactions. At the same time, the protonated PMAA chains display a certain degree of hydrophobicity inducing the formation of large aggregates of the copolymer in water. Both phenomena favor the solubilization of hydrolyzed silica species and subsequent formation of spherical particles. In a similar way, both alkyl and poly-(N-(acetyl)ethyleneimine) chains may act analogously to PMAA and PEO, respectively. In fact, as proven via DLS and SAXS experiments alkyl-PAEI can undergo self-assembly in water. Furthermore, non-ionic N-acetylethyleneimine groups on the corona of those micelles can interact with the silica precursors and promote their condensation as has already been proven. This formation mechanism may also explain the formation of the μ-sphere-like silica precipitates by alkyl-PAEI via hydrothermal synthesis.

A similar formation mechanism with the surfactant cetyl trimethyl ammonium bromide (CTAB) as template has been reported in other investigations[277, 279]. Here, mesoporous silica precipitates with morphologies similar to that of MCM-41 have been obtained. CTAB, alone[279] or in the presence of organoalkylsiloxanes[277] self-assembles into bulky supramolecular aggregates at low concentration. Interactions between the amino head groups of the surfactant and the silica precursor have been found to play a crucial role in the formation of the structure. Within the experiments in the presence of organoalkylsiloxanes[277], it has been found that the morphology of the resulting materials can be tailored. Along with sphere-like precipitates, tube-like or rod-like ones can be obtained. Furthermore, co-condensation reactions between the organoalkylsiloxanes allow surface functionalization.

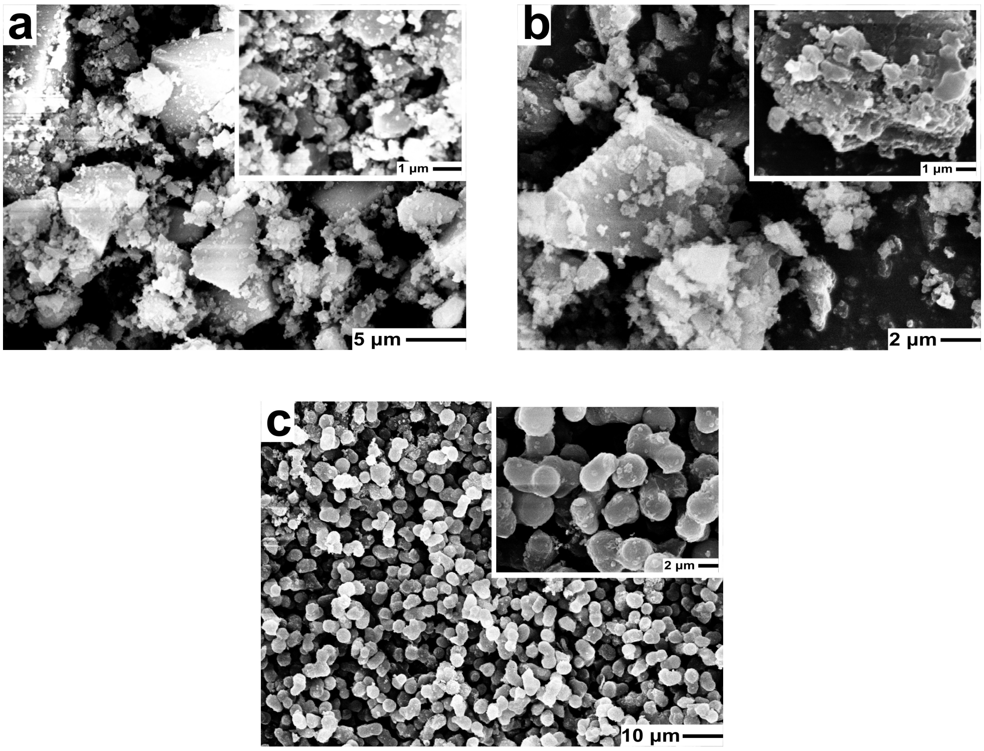

Figure 3.41. SEM images of the silica precipitates produced via hydrothermal synthesis in the presence of: alkyl-PEI ($P_n = 10$) (a) c = 0.28 wt%; and (b) c = 1 wt%; and (c) PEG_{20}-*b*-PPG_{70}-*b*-PEG_{20} with c = 0.28 wt%. In all samples, TEOS was used as silica source.

In a similar way, hydrothermal synthesis in aqueous solutions containing alkyl-PEI has been carried out. Figures 3.41-a and 3.41-b depict SEM images of silica precipitates produced via hydrothermal synthesis with solutions containing 0.28 wt% (3.41-a) and 1 wt% (3.41-b) of alkyl-PEI with $P_n = 10$, respectively. As can be observed, unlike the silica precipitates promoted by alkyl-PAEI (Figure 3.40) or PEG_{20}-*b*-PPG_{70}-*b*-PEG_{20} (Figure 3.41-c), those produced in alkyl-PEI-containing aqueous solutions do not show a sphere-like morphology, but they are non-structured. As commented previously, in the silica precipitates produced in solutions containing the highest alkyl-PAEI concentrations (Figures 3.40-b and 3.40-d) via hydrothermal synthesis, the morphology has been found to be composed of fused spheres coated by non-structured silica. However, as can be observed in Figures 3.41-a and 3-41-b, the morphology of the samples produced in the presence of alkyl-PEI is not structured at all. As remarked in section 2.1.1, the supramolecular aggregation of the template in the aqueous medium plays a crucial role in the morphology of porous structures obtained by sol-gel methods. Thus, such a huge difference between the morphologies of the precipitates produced in the presence of both templates, alkyl-PAEI and alkyl-PEI, via hydrothermal synthesis arises from the different behaviour of both polymers in aqueous solution. Alkyl-PAEI has been proven to be soluble in water and to undergo self-assembly into supramolecular aggregates (section 3.2.1). A similar behaviour has been described for the triblock copolymer PEG_{20}-*b*-PPG_{70}-*b*-PEG_{20}[280]. However, alkyl-PEI has shown a lower solubility in the aqueous medium making it difficult to produce clear solutions of this polymer. Furthermore, as remarked in section 3.2.2, this polymer has shown a higher tendency to undergo thermoreversible gelation rather than micellization in water. Therefore, those polymers possessing better micellization ability in water, i.e. alkyl-PAEI and the triblock copolymer PEG_{20}-*b*-PPG_{70}-*b*-PEG_{20}, promote silica precipitates with a higher structured morphology than those produced in the presence of polymers which do not show such good aggregation behaviour as is the case of alkyl-PEI.

3.3.5 Silicic acid condensation in polymer solvent-modulated media

As has already been reported in the literature[222] and also proven in section 3.2.2.6, poly(ethyleneimine)-based macromolecular structures are capable to undergo thermoreversible hydrogelation in water by simply cooling hot aqueous solutions of the polymer to room temperature resulting in a nanofiber-based three-dimensional network. In addition, those nanofiber-based polymeric networks are highly efficient as template for silica deposition acting as catalyst and scaffold. As has been shown in section 3.3.3, the shape and morphology of the PEI-based hydrogels are able to be precisely transcribed into the resulting silica monoliths. Another method that has been proven to offer multiple morphologies of the silica precipitates is the media modulation developed by JIN *et al.*[247]. By tuning the media in which the PEI-based macromolecular structures pre-organize, it is possible to produce silica precipitates with multiple morphologies and hierarchical structures by silicification of TMOS under ambient conditions. This approach is based on the same principle as the silification in the presence of PEI-based thermoreversible hydrogels. In fact, the variation of the media compositions, in which the PEI-based macromolecular structure pre-organizes, results in supramolecular aggregates with different shapes. Further silification yields silica precipitates with morphologies resembling those of the supramolecular aggregates used as templates. Thus, under this approach, the shape of the silica precipitates may be tuned by adjusting the solvent composition of the media in which silification takes place. In order to confirm this, TMOS silification has been carried out with alkyl-PEI in solvent mixtures, which include water mixed with methanol, ethanol or acetone at different ratios.

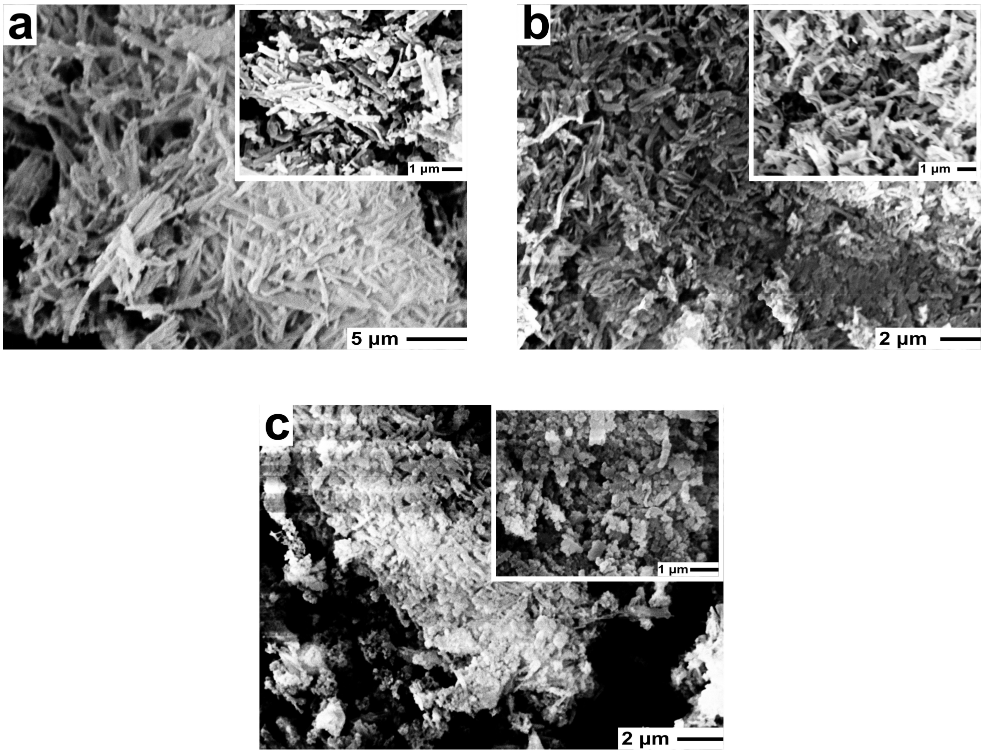

Figure 3.42. SEM images of the silica precipitates produced in the presence of alkyl-PEI ($P_n = 20$) dissolved in methanol and water mixture with volume ratios (MeOH/Water) of: (a) 25/75, (b) 50/50, and (c) 75/25, at room temperature. The polymer concentration in all samples is 1 wt%.

Figure 3.42 depicts SEM images of the silica precipitates produced in the presence of alkyl-PEI ($P_n = 20$) dissolved in a methanol and water mixture with different volume ratios. As can be observed, the silica precipitate obtained in a medium containing a solvent composition MeOH/Water = 25/75 (Figure 3.42-a) possesses a fibrous structure. By increasing the methanol content in the reaction medium, e.g. MeOH/Water = 50/50 (Figure 3.42-b), the fibrous structure becomes less prominent. For higher methanol contents, e.g. MeOH/Water = 75/25 (Figure 3.42-c), the fibrous structure can be hardly observed, but the silica precipitate seems to be composed of non-structured domains. Therefore, as a conclusion it can be established that the structured character of the precipitate decreases by increasing the methanol content of the reaction medium. This is in good agreement with the observations reported by JIN *et al.*[247] concerning TMOS silification within linear-PEI aggregate solutions in media containing MeOH and water at different ratios. According to these investigations, the loss of the fibrous morphology in the silica precipitates results from the high solubility of PEI in methanol. This high solubility hinders the formation of the fibrous aggregates of PEI-based macromolecular structures in reaction media with high methanol contents. In the absence of fibrous PEI aggregates, the resulting silica precipitates become non-structured.

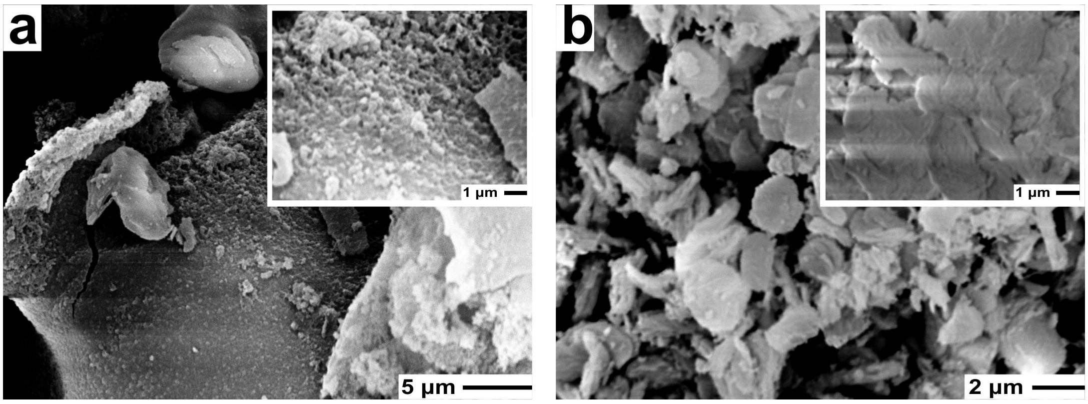

Figure 3.43. SEM images of the silica precipitates produced in the presence of alkyl-PEI (P_n = 20) dissolved (a) in an ethanol and water mixture with a volume ratio EtOH/Water = 50/50, and (b) in an acetone and water mixture with a volume ratio acetone/Water = 50/50, at room temperature. The polymer concentration in all samples is 1 wt%.

In a similar way, silica precipitates have been produced in alkyl-PEI aggregate solutions in which the reaction media are composed of water mixed with ethanol or acetone. Figure 3.43-a shows a SEM image of the silica precipitate produced in the presence of alkyl-PEI (P_n = 20) dissolved in an ethanol and water mixture with volume ratio EtOH/Water = 50/50. As can be appreciated, the silica precipitate does not possess a structured morphology. If comparing the morphology of this silica precipitate with that of the one produced in a reaction medium containing methanol and water at the same ratio (50/50, Figure 3.42-b), it can be recognized that the precipitate produced in methanol seems to possess a more structured character. This observation is not in accordance with those reported by JIN *et al.*[247]. Here, the addition of ethanol has also been proven not to favor the formation of PEI-based fibrous structures. However, compared to the methanol modulation, ethanol is relatively mild in avoiding the aggregation ability of PEI. The reason for this discrepancy between the results expressed by JIN *et al.*[247] and those shown within this work has still not been clarified. It may result from the fact that alkyl-PEI is more hydrophibic than PEI, thus it should have a higher solubility in EtOH than PEI. However, further investigations should be carried out on this topic.

Likewise, Figure 3.43-b shows a SEM image of the silica precipitate produced in the presence of alkyl-PEI ($P_n = 20$) dissolved in an acetone and water mixture with volume ratio acetone/Water = 50/50. As can be observed, in spite of the fact that the morphology of the precipitate does not look like structured, a certain platelet-like structure can be recognized. This observation is in accordance with those expressed by JIN *et al.*[247]. Within that work, silica precipitates have shown nanofiber-like morphology in reaction media with a composition acetone/Water = 25/75. However, by increasing the acetone content to a ratio of acetone/Water = 50/50, the morphology of the silica precipitate becomes disc-like. Moreover, in reaction media with higher acetone contents, e.g. acetone/Water = 75/25, PEI was not soluble even at temperatures around 80 °C. This high insolubility of PEI in acetone may be the reason why this solvent possesses such a strong ability to damage the fibrous morphology of PEI aggregates in comparison to methanol. However, a detailed mechanism of how the solvent can hinder fiber-like aggregation has not been yet proposed. Therefore, further investigations on this interesting topic should be carried out.

3.3.6 Concluding remarks on the production of silica precipitates

Within this section, silica precipitates with different morphologies have been produced by silicic acid condensation in the presence of a wide variety of alkyl-PAEI- and alkyl-PEI-based supramolecular assemblies acting as templates. The precipitates mediated by alkyl-PAEI in clear, aqueous solution are composed of fused spheres with sizes around some hundred nanometers. The size of those spheres has been found to increase with increasing the polymer concentration and the degree of polymerization and by decreasing the pH of the buffer in which the polymer has been dissolved. Furthermore, the spheres become less fused when silicic acid condensation is carried out in phosphate buffer because of the interactions of this multivalent anion with the polymer. Yet, the precipitates produced in the presence of alkyl-PAEI via hydrothermal synthesis also present a morphology composed of fused spheres but with sizes around two micrometers. Unlike the silica precipitates prepared from solutions with low polymer concentration, those produced from solutions containing higher alkyl-PAEI amounts show the presence of non-structured silica coating the fused spheres of the precipitate.

Clear aqueous solutions of alkyl-PEI could be produced in acetate (pH = 4.5) and malonate (pH = 5.5) buffers but only up to concentrations around 0.1 and 0.01 wt%, respectively. Alkyl-PEI dissolved in acetate buffer has been found to favor the formation of silica gels, while in malonate buffer silica precipitation has been observed. Clear solutions containing higher alkyl-PEI concentrations in malonate (pH = 5.5) as well as in phosphate (pH = 5.6) and citrate (pH = 3.5) buffers can be obtained only by heating. Upon subsequently cooling, turbid suspensions of the polymers are obtained. Silicic acid condensation within these turbid suspensions in malonate and phosphate buffers provides precipitates with morphologies consisting of a fibrous network together with fused spheres. Yet, in the turbid suspensions produced in citrate buffer, silicic acid condensation resulted in fused microspheres. In alkyl-PEI-based thermoreversible hydrogels, obtained by dissolving alkyl-PEI in pure hot water and cooling the solution to room temperature, TMOS silification gives silica monoliths with network-like morphology similar to that of the hydrogel used as template. Hydrothermal synthesis in the presence of alkyl-PEI has also been performed yielding non-structured silica precipitates. TMOS silification has been carried out in alkyl-PEI-containing solutions with different solvent composition. Here, the polymer has been dissolved in media containing different ratios of water and another solvent such as methanol, ethanol or acetone. The silification experiments within those solutions have proven that methanol is much more effective than ethanol and acetone in keeping the fibrous morphology of alkyl-PEI aggregates and resulting in also fibrous silica precipitates.

4 Summary and Outlook

Manufactured porous silica is produced via sol-gel processes which require high temperature, high pressure and the presence of harsh reagents. In nature, highly-structured silica-based materials can be found for example in diatom shells. The formation of diatomaceous silica takes place under mild conditions such as near-neutral pH, atmospheric pressure and temperature of the aquatic habitat of the diatom. Within this scope, the aim of this work was the synthesis and characterization of bioinspired, amphiphilic polymers and their application in silica mineralization. For this purpose, a synthetic route for amphiphilic alkyl-polyamines with well-defined degrees of polymerization and different nitrogen-containing functional groups mimicking those found in the biomolecules associated to diatoms has been developed. The cationic ring-opening polymerization of the cyclic iminoethers 2-methyl-2-oxazoline (MeOZO) **4** and 2-methyl-5,6-dihydro-4H-1,3-oxazine (MeOZI) **5** with the alkyl-bearing initiator 1-octadecyltosylate **3**, along with different modification reactions such as alkaline hydrolysis or end-capping has been proven to represent a suitable synthetic route. In fact, alkyl-poly(N-(acetyl)ethyleneimine) (alkyl-PAEI) **9**, alkyl-poly(ethyleneimine) (alkyl-PEI) **11** and their analogous molecular structures with propylene as spacer, alkyl-poly(N-(acetyl)propyleneimine) (alkyl-PAPI) **10** and alkyl-poly(propyleneimine) (alkyl-PPI) **12**, have been successfully synthesized.

The aggregation properties of the template molecules play a crucial role for the final features of the silica structures. For this reason, the aggregation behaviour of the polymers in aqueous solution has been characterized. In this regard, optical polarization microscopy and fluorescence spectroscopy experiments gives clear evidence for the self-assembly ability of alkyl-PAEI **9** in clear, aqueous solutions. The critical micelle concentration (CMC) of alkyl-PAEI in pure water, determined via surface tension measurements, has been found to increase with the degree of polymerization of the hydrophilic segment. Furthermore, investigations on the morphology of the aggregates, performed via scattering methods and electron microscopy, have revealed the presence of spherical core-shell micelles in pure water with sizes depending on the degree of polymerization of the hydrophilic chain. The micelles are monodisperse and non-interacting in the low concentration regime and undergo hard-sphere interactions at higher concentrations. Taking these results into account, alkyl-PAEI fulfils the requirements demanded for a sol-gel template since it can self-assemble in solution and form supramolecular aggregates with well-defined size and dimensions.

Likewise, the aggregation behaviour of alkyl-PEI **11** has been investigated. Because of its low solubility in pure water, alkyl-PEI gives turbid suspensions rather than clear solutions. The acid-base behaviour of alkyl-PEI, investigated via potentiometric titration, is affected by both, the degree of polymerization of the hydrophilic segment, and the hydrophobic interaction that takes place between the alkyl chains. Furthermore, investigations on the solid-state behaviour of alkyl-PEI have revealed that the polymer takes up water from the surrounding atmosphere and forms different hydrates. The ratio of the different hydrates present in the samples is directly related to the water content of the sample. DSC measurements show thermal transitions between the different hydrates, which confirm this complex behaviour. Alkyl-PEI forms opaque, ice-cream-like hydrogels upon cooling down hot aqueous solutions. Electron microscopy images of the hydrogels reveal that they consist of a fibrous network composed of fan-like bundles. DSC measurements have proven the presence of water in different states in the hydrogels namely free (freezing) water and bound (non-freezing) water. The amount of these different types of water in the hydrogels has been found to depend not only on the concentration of hydrophilic amino groups, but also on the total amount of water. For alkyl-PPI **12**, a similar characterization has been performed. Alkyl-PPI is also highly hygroscopic and hence shows a complex, structural and thermal behaviour in the solid state. However, it does not show the formation of hydrogels because of the higher distance between neighbouring amino groups, which hinders interactions with water molecules.

In conclusion, alkyl-PEI does not show such well-defined aggregation properties in water as alkyl-PAEI, but it has a complex behaviour in the solid state and can undergo thermoreversible gelation. It represents a suitable choice as template for sol-gel processes since it provides both, turbid suspensions and hydrogels with well-defined structural properties, which may act successfully as scaffolds in the condensation of silicic acid. However, alkyl-PPI, which possesses a comparable structural and thermal behaviour, can neither undergo thermoreversible gelation nor yield turbid suspensions.

As a final step in the characterization, the synthesized amphiphilic polymers have been tested with regard to their influence on the condensation of silicic acid. For this purpose, the morphology of the silica precipitates produced in the presence of different alkyl-PAEI-, alkyl-PAPI and alkyl-PEI-based supramolecular assemblies as templates have been investigated via scanning electron microscopy (SEM). Within these experiments, it has been found that the morphology and dimensions of the produced silica precipitates strongly depend on both, the polymeric assembly acting as template and the experimental conditions under which the silicic acid condensation takes place. In fact, the combination of the different alkyl-PAEI- and alkyl-PEI-based supramolecular assemblies along with different temperature, pressure, pH and media composition conditions has allowed producing silica precipitates with a wide variety of morphologies like fused spheres or networks. Thus, these results highlight the versatile character of the synthesized polymers towards the production of silica precipitates with tailored shapes and dimensions.

The results obtained within this work for the synthesis of amphiphilic polymers, their aggregation behaviour and their application in silica mineralization may lead to different outlooks. Regarding the development of new polymeric surfactants, a suitable approach could be the replacement of the hydrophobic and hydrophilic segments, alkyl chain and PAEI or PEI, respectively, by others bearing different functional groups. As hydrophobic segment, poly(butadiene) (PBD) or poly(isoprene) (PI), which can be provided via controlled polymerization techniques with adjustable degree of polymerization[281, 282], may be suitable candidates. The hydrophilic block could be produced by controlled radical polymerization of different nitrogen-containing monomers such as 4-vinypyridine, 1-vinylpyrrolidone or N,N-dimethylacrylamide (DMAA). Another possibility could be the combination of those elements in a different architecture. Graft-copolymers with hydrophobic backbone and hydrophilic side chains could represent a suitable choice since they are expected to self-assemble into cylindrical aggregates. Even double hydrophilic block- or graft-copolymers could be produced. That kind of macromolecular structure has already been used in other mineralization processes[283, 284] and could represent a suitable template for silica precipitation.

Regarding the aggregation behaviour, the already synthesized alkyl-PPI should be investigated in more detail in order to elucidate the reasons why this polymer, unlike alkyl-PEI, does not undergo thermoreversible gelation in aqueous solution. Further experiments could be performed in order to develop different self-assemblies based on this polymeric surfactant.

Finally, further characterization of the silica precipitates described in section 3.3, mediated by different alkyl-PEI- and alkyl-PAEI-based supramolecular aggregates, may be performed. Here, classical methods of solid state characterization like XRD, TGA, BET porosimetry or Si-NMR could reveal new aspects on the formation mechanism of the silica precipitates.

5 Experimental Section

5.1 List of chemicals

Acetic acid	Fluka	p.a.
Acetonitrile	Acros	99%
3-Amino-1-propanol	Acros	99%
Benzonitrile (BN)	Fluka	99%
Calcium chloride	Merck	p.a.
Calcium hydride	Aldrich	90-95%
Chloroform	Chem. store	dest.
Citric acid monohydrate	Acros	99.5%
Diethylether	Chem. store	dest.
Dimethylamine (2 M in MeOH)	Aldrich	
Dimethylformamide (DMF)	Fluka	99%
Disodium hydrogen phosphate dihydrate	Fluka	p.a.
2,6-Di-tert.-butyl-4-methylphenol	Aldrich	99%
Glutaraldehyde (aqueous solution)	Acros	25%
Hydranal solvent Karl-Fischer reagent	Riedel-de Haen	
Hydrochloric acid (HCl)	Riedel-de Haen	37%
Imidazole-based Karl-Fischer reagent	Riedel de Haen	
Malonic acid	Fluka	p.a.
Methanol	Chem. store	dest.
Methanol (for Karl-Fischer titration)	Merck	HPLC
2-Methyl-2-oxazoline (MeOZO)	Acros	98%
1-Octadecanol	Aldrich	99%
P123 (PEG_{20}-b-PPG_{70}-PEG_{20})	Aldrich	
Petrolether	Chem. store	dest.
Phosphorous pentoxide	Riedel-de Haen	p.a.
Piperidine	Aldrich	99%
Potassium bromide (for IR)	Aldrich	99%
Potassium carbonate	Merck	p.a.
Potassium dihydrogen phosphate	Riedel-de Haen	p.a.

Pyrene	Acros	98%
Pyridine	Acros	non. Aq. Titr. Grad.
Pyridine-free Karl-Fischer reagent	Merck	
Sodium acetate anhydrate	Acros	p.a.
Sodium chloride	Roth	p.a.
Sodium hydroxide	Roth	p.a.
Sodium sulfate	Roth	p.a.
Tetraethyl orthosilane (TEOS)	Acros	99%
Tetramethyl orthosilane (TMOS)	Acros	99%
p-Toluenesulfonyl chloride	Aldrich	99%
Zinc chloride	Acros	99%

All solvents, monomers and other reagents used in synthesis were dried and distilled using standard procedures[285] and stored under nitrogen atmosphere at -30 °C.

5.2 Synthesis, polymerization and modification reactions

5.2.1 Synthesis of the alkyl-initiator octadecyl tosylate (OcdOTs)

In a 100 mL, three-necked flask 5 g (0.0185 mol) of 1-octadecanol and 3.62 g (0.0190 mol) of p-toluenesulfonyl chloride were dissolved in 50 mL of chloroform under nitrogen atmosphere. 3.10 mL of pyridine were added to this solution dropwise at 0 °C. The mixture was stirred for 16 h at room temperature and hydrolyzed with a solution of 4.4 mL of hydrochloric acid in 12.5 mL of distilled water at 0 °C. The organic phase was separated, washed with distilled water and dried over sodium sulfate. The solvents were evaporated in vacuo and the residue was recrystallized in 90 mL of petrolether to give OcdOTs **3**.

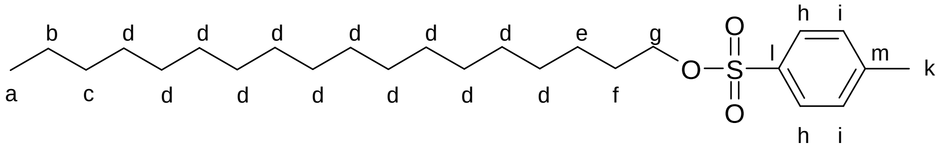

Figure 5.1. Chemical structure of the alkyl-initiator octadecyl tosylate (**OcdOTs**) **3**.

Characterization:

Yield:	44 %
Melting point:	54 °C
^{1}H-NMR (CDCl$_3$) [ppm]:	0,81 (t, $J_{a,b}$ = 6,5 Hz, H-a), 1,16 (m, 30 H, H-b, H-c, H-d, H-e), 1,54 (m, 2 H, H-f), 2,38 (s, 3 H, H-k), 3,95 (t, $J_{f,g}$ = 6,5 Hz, 2 H, H-g), 7,27 (d, $J_{h,I}$ = 7,8 Hz, 2 H, H-i), 7,72 (d, $J_{h,I}$ = 8,3 Hz, 2 H, H-h)
^{13}C-NMR (CDCl$_3$) [ppm]:	14,1 (C-a), 21,6 (C-b), 22,7 (C-k), 25,3 (C-e), 28,9 (C-f), 29,5 (C-d), 31,9 (C-c), 70,7 (C-g), 127,9 (C-h), 129,8 (C-i), 133,3 (C-l), 144,6 (C-m)
IR (KBr) [cm^{-1}]:	812, 838 (1,4-substitution in the aromatic group), 1191, 1360 (tosyl group), 1474 (δ, methyl group), 1598 (aromatic group vibration), 2851, 2916 (ν, methyl and methylene groups)

5.2.2 Synthesis of 2-methyl-5,6-dihydo-4H-1,3-oxazine (MeOZI)

The synthesis of the monomer 2-methyl-5,6-dihydro-*4H*-1,3-oxazine was performed as described by LEE *et al.*[136]. In a 500 mL, three-necked flask 80 mL (1.52 mol) of acetonitrile and 0.05 eq zinc chloride were mixed, resulting in a warm suspension which was subsequently cooled down to 0 °C with ice. At this point, 115 mL (1.50 mol) of 3-amino-1-propanol were added dropwise. Subsequently, 3 spatulatips of the inhibitor 2,6-di-tert.-butyl-4-methylphenol were added. The reaction solution was stirred at 130 °C for 24 h under nitrogen atmosphere. The final product was obtained by vacuum distillation (80 mbar and 90 °C).

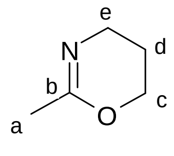

Figure 5.2. Chemical formula of 2-methyl-5,6-dihydo-4H-1,3-oxazine (**MeOZI**) **5**.

Characterization:

Yield:	60 %

^{1}H-NMR ($CDCl_3$) [ppm]: 1.75-1.80 (s und dt, $J_{d,e}$ = 5.3 Hz, $J_{d,c}$ = 5.81 Hz, 5H, H-a, H-d), 3.26 (t, $J_{c,d}$ = 5.81 Hz, 2H, H-c), 4.07 (t, $J_{e,d}$ = 5.5 Hz, 2H, H-e)

^{13}C-NMR ($CDCl_3$) [ppm]: 21.4 (C-d), 21.6 (C-a), 41.9 (C-e), 64.5 (C-c) 157.3 (C-b)

5.2.3 Cationic Ring-Opening Polymerization (CROP)

In a pressure-proof schlenk tube different amounts (see Table 5.1) of initiator, monomer and solvent were placed under nitrogen atmosphere. The tube was then sealed and immersed in an oil bath at the desired temperature. After the polymerization time, the tube was cooled down with ice and then opened. The reaction mixture was diluted with methanol and precipitated in diethylether giving a yellow polymer. After a reprecipitation in methanol/diethylether, the polymer was dried in vacuo.

Table 5.1. CROP of the monomers **MeOZO 4** and **MeOZI 5** with the initiator **OcdOTs 3**.

Sample	P_n[a]	Monomer (M)	V(M), mL	Solvent (S)	V(S), mL	m(OcdTs), g	T, °C	t, h
9.1	20	MeOZO	2	BN	2	0.5	80	22
9.2	20	MeOZO	2	DMF	2	0.5	80	22
9.3	20	MeOZO	2	BN	4	0.5	80	22
9.4	20	MeOZO	2	DMF	4	0.5	90	8
9.5	10	MeOZO	2	DMF	4	1	80	8
9.6	10	MeOZO	2	BN	2	1	80	4
9.7	40	MeOZO	2	DMF	4	0.25	90	16
9.8	40	MeOZO	2	DMF	4	0.25	90	24
10.1	10	MeOZI	4	DMF	4	1.7	80	24
10.2	20	MeOZI	4	DMF	4	0.86	80	24

[a], fixed via the monomer to initiator ratio.

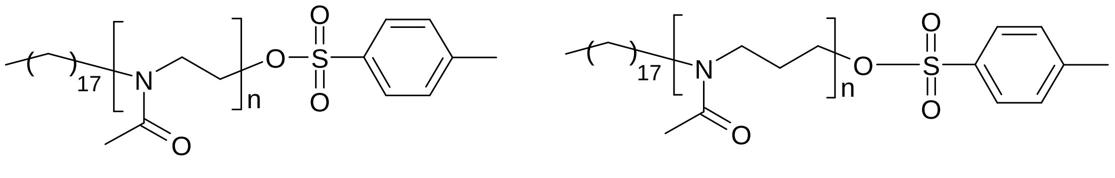

alkyl-PAEI **alkyl-PAPI**

Figure 5.3. Chemical structure of the polymers **alkyl-PAEI 9** and **alkyl-PAPI 10**.

5.2.4 Alkaline hydrolysis

Alkyl-PAEI 9 and alkyl-PAPI 10 were hydrolyzed in an aqueous NaOH solution. Typically, a solution of the polymer in methanol (see amounts in Table 5.2) was prepared in a two-necked flask. NaOH dissolved in distilled water was then added dropwise. The mixture was heated and stirred (temperature and time according to Table 5.2) under reflux and nitrogen atmosphere. After the reaction the solvents were evaporated in vacuo and the mixture was transferred into a dialysis tube (Spectra /Por CE, MWCO: 100, cellulose ester) and dialysed against millipore water for three days. The final product was obtained by freeze-drying.

Table 5.2. Alkaline hydrolysis of **alkyl-PAEI** **9** and **alkyl-PAPI** **10** to **alkyl-PEI** **11** and **alkyl-PPI** **12**, respectively.

Sample	Polymer (P)	P_n[a]	m(P), g	m(NaOH), g	$V(H_2O)/V(MeOH)$, mL,mL	T, °C	t, h
11.1	Alkyl-PAEI	10	1.1	1.7	12/10	85	40
11.2	Alkyl-PAEI	20	1.7	3	25/15	85	40
11.3	Alkyl-PAEI	40	2.1	3.2	25/15	85	70
11.4	Alkyl-PAEI	10	1.5	3	45/15	95	46
11.5	Alkyl-PAEI	10	2.1	4.5	45/15	95	70
11.6	Alkyl-PAEI	20	2.33	4.6	45/15	95	64
11.7	Alkyl-PAEI	20	1.80	4	40/15	95	70
11.8	Alkyl-PAEI	40	2.4	4.5	45/15	95	72
12.1	Alkyl-PAPI	10	2.9	2.6	60/15	95	72
12.2	Alkyl-PAPI	20	2.4	2.1	50/15	95	72
12.3	Alkyl-PAPI	20	2.7	5.3	60/15	95	72

[a], adjusted value. Experimentally is ± 1.

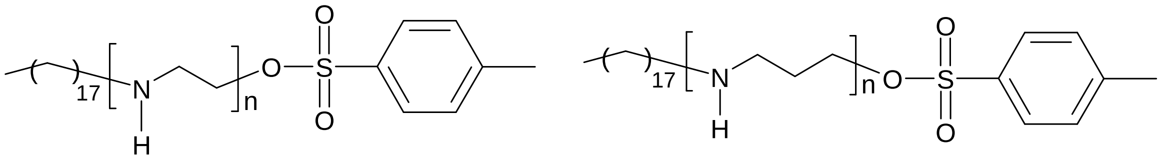

Alkyl-PEI **Alkyl-PPI**

Figure 5.4. Chemical structure of the polymers **alkyl-PEI** **11** and **alkyl-PPI** **12**.

5.2.5 Modification: termination reaction

In a pressure-proof schlenk tube different amounts (see Table 5.3) of initiator (OcdOTs), monomer (MeOZO) and solvent (DMF) were placed under nitrogen atmosphere. The tube was then sealed and immersed in an oil bath at the desired temperature for cationic ring-opening polymerization. After the polymerization time, the reaction solution was cooled down to the desired temperature (according to Table 4.3) and the termination reagent was added under nitrogen atmosphere. After the corresponding reaction time, the tube was cooled down to room temperature and opened. The reaction mixture was diluted with methanol, precipitated twice in diethylether and dried in vacuo. The resulting yellow polymer was solved in water and passed through a column filled with an anionic exchange resin (Dowex 1x2-400, Acros). The final product was obtained by freeze-drying.

Table 5.3. Termination reaction of the CROP of **MeOZO 4** with different reagents.

Sample	P_n^a	Termination reagent	V, mL	T, °C	t, h
17.1	20	dimethylamine 2 M in MeOH	0.6	65	2
17.2	20	dimethylamine 2 M in MeOH	0.6	r.t.	16
17.3	20	dimethylamine 2 M in MeOH	0.6	75	2
17.4	10	dimethylamine 2 M in MeOH	1.2	75	2
18.1	20	piperidine	0.3	r.t.	16
19.1	40	NaOH in water (pH = 10)	0.021	r.t.	24

a, fixed via the monomer to initiator ratio

5.3 Production of polymer-mediated silica precipitates

5.3.1 Polymer-mediated silicic acid condensation

Buffer solutions with different pH values to dissolve the polymers were prepared according to standard procedures[286]. For the production of the polymer solutions, the required amount of polymer (depending on the desired concentration) was dissolved in 50 mL of buffer. Subsequently, 200 µl HCl 0.01 M were mixed with 400 µL tetramethyl orthosilane (TMOS) in centrifuge tubes. 16 mL of the polymer solution were added and the mixture was stirred at room temperature for 40 minutes. The resulting silica precipitates were centrifuged, washed with methanol and distilled water and finally dried in vacuo.

5.3.2 Alkyl-PEI-hydrogel-mediated silicic acid condensation

For the silicic acid condensation with non-cross-linked alkyl-PEI hydrogels, the required amount of alkyl-PEI (depending on c_G, see Figure 3.23) was mixed with 1 mL of distilled water in a screw tube, heated up to 80 °C and cooled down to room temperature. 5 mL of ethanol and 5 mL of TMOS were carefully added over the hydrogel and the mixture was kept under static conditions for 24 h at room temperature to ensure diffusion and subsequent condensation of the silicic acid. The resulting silica monoliths were washed with distilled water and dried in vacuo.

For the silicic acid condensation with cross-linked alkyl-PEI hydrogels, small slices of an alkyl-PEI hydrogel cross-linked with glutaraldehyde and subsequently freeze-dried were dipped into a solution composed of 2 mL of ethanol and 2 mL of TMOS for 24 h at room temperature. The resulting silica composites were washed with methanol and distilled water and dried in vacuo.

5.3.3 Hydrothermal synthesis

Water, HCl and the investigated polymer (alkyl-PAEI, alkyl-PEI and PEG_{20}-b-PPG_{70}-PEG_{20}) were mixed at different ratios. After the polymer was dissolved, Tetraethyl orthosilane (TEOS) was added. The mixture was stirred for 10 min and then transferred into autoclaves where it was kept at 90 °C for 48 h. The resulting silica precipitates were centrifuged, washed with methanol and distilled water and finally dried in vacuo.

5.3.4 Silicic acid condensation in polymer solvent-modulated media

A mixture containing alkyl-PEI, water, and an organic solvent (methanol, ethanol or acetone) with a desired alkyl-PEI concentration and media composition was heated to 80 °C until the alkyl-PEI was completely dissolved. The resulting solution was cooled naturally to room temperature and left for 24 h for alkyl-PEI aggregation. In the alkyl-PEI aggregate solutions, the measured pH values appeared in the range of 10–11.

The silica deposition was performed by adding a silica source into the alkyl-PEI aggregate solution (composed of organic solvent/water in different volume ratios). Typically, 1 mL of the alkyl-PEI aggregate solution was mixed with 0.25 mL of water, 1 mL of TMOS, and 0.75 mL of ethanol. The mixture was left for 40 min at room temperature. The resulting silica composites were centrifuged, washed with methanol and distilled water and finally dried in vacuo.

5.4 Characterization methods

5.4.1 Polymer characterization

^{1}H-NMR and ^{13}C-NMR measurements were conducted on a BRUKER AM400 FT spectrometer (400MHz). Sample concentrations were 15-25 mg/mL for ^{1}H, and 60-80 mg/mL for ^{13}C spectra, respectively. TMS was used as internal standard. IR spectra were recorded on a EQUINOX IFS55 Fourier transform infrared (FTIR) spectrometer. Samples were ground with KBr and pressed into pellets with a hand press. Spectra were recorded at room temperature from 400 to 4000 cm^{-1} with a resolution of 2 cm^{-1} and analyzed with OPUS software. DSC thermograms were measured in thermal analyzer DSC 204 Phoenix (NETZSCH, Germany). The samples were weighted in punched aluminium holding pens and measured with heating and cooling rates of 10 K/min.

5.4.2 Microscope scan of water penetration

Textures of the lyotropic liquid crystalline phases formed by alkyl-poly(N-acetyl-ethyleneimine) (alkyl-PAEI) were observed with an Axiolab ZEISS microscope with crossed polarizers by performing a penetration experiment. The samples for the penetration experiment were prepared by depositing a small amount of polymer and some water drops between a microscope glass slide and a microscope cover glass. By diffusion of water, a concentration gradient was created laterally between the two glass plates.

5.4.3 Fluorescence of pyrene

Stock solutions of alkyl-PAEI in millipore water were prepared. Pyrene (2.4 mg) was dissolved in THF (2 mL) and 100 mL of millipore water were added. Subsequently the THF was removed by evaporation under reduced pressure. The final solutions were prepared by adding 25 μL of the pyrene solution to 5 mL of the polymer stock solution. The concentration of pyrene in these final solutions was $6 \cdot 10^{-7}$ mol/L. Fluorescence excitation and emission spectra at λ_{em} = 392 nm and λ_{ex} = 336 nm, respectively, were obtained employing a KONTRON SFM-25 spectrometer.

5.4.4 Determination of the Critical Micelle Concentration (CMC)

The critical micelle concentration of the polymers was determined via surface tension measurements. Surface tension of aqueous solutions with different polymer concentrations (ranging from 0.003 to 0.25 wt%) were measured in a tensiometer KRÜSS K11 2708 by the ring method at 22 °C.

For the preparation of alkyl-PEI aqueous solutions, the required amount of polymer was suspended in deionized water and the resulting mixture was heated to 80 °C and subsequently cooled down to room temperature.

5.4.5 Dynamic Light Scattering (DLS)

A submicron particle analyzer (PSS Nicomp, PARTICLE SIZING SYSTEMS, Santa Barbara, CA) was used to calculate the photon intensity autocorrelation function[287] of alkyl-PAEI aqueous solutions (concentration range depending on P_n) at different angles (30, 60, 90, 100, 120 and 150°). The solutions were clarified by filtering the solutions through 0.1 μm millipore syringe filters into 6 x 50 mm borosilicate round cells (Kimble) and the measurements were performed at 25 °C. DLS results were subjected to cumulant analysis[287](software ALV-5000), and (assuming small, spherical, non-interacting particles) the hydrodynamic radius R_h was calculated using the Stokes-Einstein equation (see section 2.2.3.1).

5.4.6 Small Angle X-ray Scattering (SAXS)

SAXS measurements of alkyl-PAEI aqueous solutions (c = 5 - 15 wt%) were performed on a NONIUS rotating anode instrument (4 kW, Cu Kα) with pinhole collimation and a MARCCD detector (pixel size: 79). The distance between sample and detector was 74 cm, covering a range of the scattering vector:

$$q = (4\pi n/\lambda)\sin(\theta/2) = 0.2 - 3\ \text{nm}^{-1}$$

$$(\theta = \text{scattering angle},\ \lambda = 0.154\ \text{nm})$$

Two-dimensional (2D) diffraction patterns were transformed into a one-dimensional (1D) radial average of the scattering intensity. Background contributions from capillary and solvent scattering were not subtracted from the sample scattering but modelling of the obtained scattering patterns has been performed. SCATTER version 2.0 has been used in all the simulations for core/shell micelles. This software is based on general expressions and scattering functions derived in previous works[181, 182].

5.4.7 Potentiometric titration

Potentiometric titrations of alkyl-PEI and alkyl-PPI samples were performed on a METTLER-TOLEDO DL 53 titrator with an Inlab 412 combination electrode at 25 °C. 40 mL of a solution containing 0.03 M polyamine (alkyl-PEI, alkyl-PPI), 0.06 M HCl, and 0.5 M NaCl were prepared. During titration, 5 mL of 0.5 M NaOH were delivered in aliquots of 0.1 mL from the titrator. The time interval between additions was 90 s and the temperature was kept at 25 °C by an external thermostat. The titration was carried out under nitrogen. The Inlab 412 combination electrode was calibrated by titrating 45 mL of a mixture with 0.1 M NH_4Ac and 0.1 M HCl before each experiment. The degree of protonation (α) was calculated via

$$\alpha = \frac{NH^+}{N_{tot}} \times 100$$

where NH^+ is the total amount of protonated nitrogen atoms in moles and N_{tot} is the total amount of nitrogen atoms in the solution. NH^+ is calculated after each addition of titrant to the solution by the proton balance

$$\left[NH^+\right] = \frac{C_{HCl} \times V_{HCl} - C_{NaOH} \times V_{NaOH}}{V_{tot}} - 10^{-pH} + \frac{10^{-pKw}}{10^{-pH}}$$

C_{HCl} and C_{NaOH} are the concentrations, and V_{HCl} and V_{NaOH} the volumes of the strong acid and strong base added to the solution of the polymer. V_{tot} is the total volume of the solution and pK_w is the ion product of water.

5.4.8 X-Ray Diffraction (XRD)

X-ray diffraction of the alkyl-PEI samples was done on a StadiP STOE with Cu Kα radiation and position-sensitive detector. Analysis of the XRD patterns was done with WinXPOW STOE software.

5.4.9 Determination of the water content: Karl-Fischer titration

Titrations for water determination in the alkyl-PEI samples were performed On a METTLER TOLEDO DL32 KF coulometer. The one-component pyridine-free KF reagent (equivalent to 1 mg of H_2O/mL), the two component imidazole-based KF reagent (hydranal titrant 2 equiv. to 2 mg of H_2O/mL) and the solvent (hydranal solvent) were stored in brown tightly closed bottles. Dry methanol (measured water content was 0.0137 %) was used to dissolve the polymers.

5.4.10 Thermoreversible gelation

Typically, a given amount of alkyl-PEI (see Figure 3.23) and 0.5 mL of distilled water were poured into a 5-mL screw tube. The mixture was heated to 80 °C until the PEI was completely dissolved. After cooling the hot solution to room temperature, an opaque gel formed. The gel state is confirmed by the vial inversion test.

5.4.11 Chemical cross-linking of polymeric hydrogels

One mL alkyl-PEI hot aqueous solution (concentration depending on P_n, see Figure 3.23) was cast into an alumina column mold with a diameter of 1.0 cm. A column of self-supported alkyl-PEI hydrogel was obtained when the sample was fully cooled down to room temperature. After that, the alumina mold was removed. The cross-linking was carried out by dipping the as-cast physical hydrogel column into 10 mL of glutaraldehyde aqueous solution (1 wt%) for 72 h. The resulting cross-linked gel was washed and soaked in water for 3 days to remove residues of glutaraldehyde trapped in the voids of the gel. The cross-linked gel showed improved mechanical properties, and could be easily cut into thin pieces with various shapes and dimensions.

5.4.12 DSC measurements: types of water in hydrogels

The enthalpy of melting water in the alkyl-PEI hydrogels was measured by differential scanning calorimetry (Netzsch, DSC 204 Phoenix) in the temperature range from -20 °C to 20 °C with a heating rate of 5 K/min under a nitrogen flow. The amounts of free and bound (non-freezing) water were calculated from the melting enthalpies with the following equation[257]:

$$W_b = W_t - \left(W_f - W_{fb}\right) = W_t - \left(\frac{Q_{endo}}{Q_f}\right) \times 100$$

where W_b is the amount of bound water (%); W_f and W_{fb} are the amounts of free water and freezing bound water, respectively; Q_{endo} is the heat of fusion for freezable water in the hydrogel as obtained from the DSC-thermogram (J/g); Q_f is the heat of fusion of pure water (333 J/g) and W_t is the equilibrium water content EWC (%) calculated from the following equation:

$$EWC = \left(\frac{W_s - W_d}{W_s}\right) \times 100$$

where W_s and W_d represent the weight of swollen and freeze dried hydrogel, respectively.

5.4.13 Electron microscopy

Swollen alkyl-PEI hydrogels. The structure of alkyl-PEI hydrogels was examined by cryogenic scanning electron microscopy (S-4800, HITACHI, equipped with a field emission gun). Each sample was cooled by plunging into nitrogen slush at atmospheric pressure. Afterwards, the samples were freeze fractured at -180 °C, etched for 60 s at -98 °C and sputtered with Platinum in the GATAN Alto 2500 cryo-preparation chamber and then transfered into the cryo-SEM.

Alkyl-PAEI aqueous solutions. For cryogenic transmission electron microscopy (cryo-TEM) studies of alkyl-PAEI aqueous solutions, a drop of the sample (aqueous solutions with different polymer concentration) was deposited on an untreated bare copper TEM grid (600 mesh, SCIENCE SERVICES, Munich, Germany), where most of the liquid was removed with blotting paper, leaving a thin film stretched over the grid holes. The specimens were instantly shock vitrified by rapid immersion into liquid ethane and cooled to approximately 90 K by liquid nitrogen in a temperature-controlled freezing unit (Zeiss Cryobox, ZEISS NTS GmbH, Oberkochen, Germany). The temperature was monitored and kept constant in the chamber during all the sample preparation steps. After the sample was frozen, it was inserted into a cryo-transfer holder (CT3500, GATAN, Munich, Germany) and transferred to a Zeiss EM922 EFTEM. Experiments were carried out at temperatures around 90 K at an acceleration voltage of 200 kV. Zero-loss filtered images ($\Delta E = 0$ eV) were taken under reduced dose conditions (100-1000 electrons/nm^2). All images were registered digitally by a bottom-mounted CCD camera system (Ultrascan 1000, Gatan) combined and processed with a digital imaging processing system (Gatan Digital Micrograph 3.10 for GMS 1.5).

Cross-linked, freeze-dried alkyl-PEI hydrogels. SEM investigations of cross-linked and subsequently freeze-dried alkyl-PEI hydrogels, and of silica precipitates were performed employing a JEOL JSM-6400 device.

6 References

[1] Vrieling, E. G.; Sun, Q.; Beelen, T. P. M.; Hazelaar, S.; Gieskes, W. W. C.; Van Santen, R. A.; Sommerdijk, N. A. J. M. *J. Nanosci. Nanotechnol.* **2005**, 5, 68-78.

[2] Morse, D. E. *Trends Biotechnol.* **1999**, 17, 230-232.

[3] Sandhage, K. H.; Dickerson, M. B.; Huseman, P. M.; Caranna, M. A.; Clifton, J. D.; Bull, T. A.; Heibel, T. J.; Overton, W. R.; Schoenwaelder, M. E. A. *Adv. Mater.* **2002**, 14, 429-433.

[4] Hildebrand, M. *Progr. Org. Coat.* **2003**, 47, 256-266.

[5] Falciatore, A; Bowler, C. *Ann. Rev. Plant Biol.* **2002**, 53, 109-130.

[6] Horstmann, S. *Dissertation* **2006**, TU Braunschweig.

[7] Vrieling, E. G.; Beelen, T. P. M.; Van Santen, R. A. *J. Biotechnol.* **1999**, 70, 39-51.

[8] Vrieling, E. G.; Gieskes, W. W. C.; Beelen, T. P. M. *J. Phycol.* **1999**, 35, 548-559.

[9] Vrieling, E. G.; Hazelaar, S.; Gieskes, W. W. C.; Sun, Q.; Beelen, T. P. M.; Van Santen, R. A. *Silicon biomineralization: Biology, Biochemistry, Molecular Biology, Biotechnology*; Müller, W. E. G., Ed.; Springer-Verlag: Berlin/Heidelberg, Germany, **2003**, 301-334.

[10] Kröger, N.; Lorentz, S.; Bruner, E.; Sumper, M. *Science* **2002**, 298, 584.

[11] Mann, S. *Biomineralization*, Oxford University Press, Oxford, UK, **2002**.

[12] Iler, R. K. *The chemistry of silica*, Wiley-Interscience, New York, **1979**.

[13] Göltner, C. G.; Henke, S.; Weissenberger, M.C.; Antonietti, M. *Angew. Chem. Int. Ed.* **1998**, 5, 37.

[14] Galo, J.; Soler-Illia, A.; Sanchez, C.; Lebeau, B.; Patarin, J. *Chem. Rev.* **2002**, 102, 4093-4138.

[15] Hawker, C. J.; Bosman, A. W.; Harth, E. *Chem. Rev.* **2001**, 101, 3661-3688.

[16] Hadjichristidis, N.; Pitsikalis, M.; Pispas, S.; Iatrou, H. *Chem. Rev.* **2001**, 101, 3747-3792.

[17] Van Bommel, K. J. C.; Friggeri, A.; Shinkai, S. *Angew. Chem. Int. Ed.* **2003**, 9, 42.

[18] Sing, K. S. W.; Everett, D. H.; Haul, R. A.; Mosocou, L.; Pierotti, J.; Rouquerol, J.; Siemieniewska, T. *Pure Appl. Chem.* **1985**, 57, 603.

[19] Behrens, P. *Adv. Mater.* **1993**, 5, 127-132.

[20] Kresge, C. T.; Leonowicz, M. E.; Roth, W. J.; Vartuli, J. C.; Beck, J. S. *Nature* **1992**, 359, 710.

[21] Ying, J. Y.; Mehnert, C. P.; Wong, M. S. *Angew. Chem. Int. Ed. Engl.* **1999**, 38, 56.

[22] Leimenstoll, M. *Dissertation* **2005**, TU Braunschweig.

[23] Beck, J. S.; Vartuli, J. C.; Roth, W. J.; Leonowicz, M. E.; Kresge, C. T.; Schmitt, K. D.; Chu, C. T. W.; Olsen, D. H.; Sheppard, E. W.; McCullen, S. B.; Higgins, J. B.; Schlenker, J. L. *J. Am. Chem. Soc.* **1992**, 114, 10834-10843.

[24] Vartuli, J. C.; Kresge, C. T.; Roth, W. J.; McCullen, S. B.; Beck, J. S.; Schmitt, K. D.; Leonowicz, M. E.; Lutner, J. D.; Sheppard, E. W. *Advanced Catalysts and Nanostructured Materials: Modern Synthesis Methods*, Moser, R. W., Ed.; Academic Press, New York, **1996**, 1-19.

[25] Vartuli, J. C.; Kresge, C. T.; Leonowicz, M. E.; Chu, A. S.; McCullen, S. B.; Johnson, I. D.; Sheppard, E. W.; *Chem. Mater.* **1994**, 6, 2070-2077.

[26] Chen, C. Y.; Burkett, S. L.; Li, H. X.; Davis, M. E. *Microporous Mater.* **1993**, 2, 27-34.

[27] Steel, A.; Carr, S. W.; Anderson, M. W. *J. Chem. Soc. Chem. Commun.* **1994**, 1571-1572.

[28] Regev, O. *Langmuir* **1996**, 12, 4940-4944.

[29] Williams, F. R. S. *Phil. Trans. R. Soc. Lond. B* **1984**, 304, 411-424.

[30] Kröger, N. ; Poulsen, N. *Mater. Res. Soc. Symp. Proc.* **2005**, 873, 121-126.

[31] Vrieling, E. G.; Beelen, T. P. M.; Van Santen, R. A.; Gieskes, W. W. C. *J. Phycol.* **2000**, 36, 146-159.

[32] Simpson, T. L.; Volcani, B. E. *Silicon and siliceous structures in biological systems*, Springer Verlag, New York, USA, **1981**.

[33] Round, F. E.; Crawford, R. M.; Mann, D. G. *The diatoms, biology & morphology of the genera*; Cambridge University Press, Cambridge, UK, **1990**.

[34] Pickett-Heaps, J. D.; Schmid, A. M. M.; Edgar, L. A. *Prog. Phycol. Res.* **1990**, 7, 1-168.

[35] Coradin, T. ; Lopez, P. J. ; Gautier, C. ; Livage, J. *C. R. Palevol* **2004**, 3, 443–452.

[36] Hecky, R. E.; Mopper, K.; Kilham, P.; Degens, E. T. *Mar. Biol.* **1973**, 19, 323-331.

[37] Swift, D. M.; Wheeler, A. P. *J. Phycol.* **1992**, 28, 202-209.

[38] Kröger, N.; Bergsdorf, C.; Sumper, M. *Proc. Natl. Acad. Sci. USA* **2000**, 97, 14133-14138.

[39] Van de Poll, W. H. ; Vrieling, E. G. ; Gieskes, W. W. C. *J. Phycol.* **1999**, 35, 1044-105.

[40] Schmid, A. M. M. *Protoplasma* **1994**, 181, 43-60.

[41] Van den Hoek, C.; Mann, D. G.; Jahns, H. M. *Algae, an introduction to phycology*, Cambridge University press, Cambridge, UK, **1995**.

[42] Graham, L. E.; Wilcox, L. W. *Algae*, Prentice Hall, Upper Saddle River, USA, **2000**.

[43] Vrieling, E. G.; Beelen, T. P. M.; Sun, Q.; Hazelaar, S.; Van Santen, R. A.; Gieskes, W. W. C. *J. Mater. Chem.* **2004**, 14, 1970-1975.

[44] Schmid, A. M. M.; Schulze, D. *Protoplasma* **1979**, 100, 267-288.

[45] Darley, W. M.; Sullivan, C. W.; Volcani, B. E. *Planta* **1976**, 130, 159-167.

[46] Darley, W. M.; Volcani, B. E. *Meth. Enzymol.* **1971**, 23, 85-96.

[47] Hildebrand, M.; Volcani, B. E.; Gassmann, W.; Schroeder, J. I. *Nature* **1997**, 385, 688-689.

[48] Hildebrand, M.; Dahlin, K.; Volcani, B. E. *Mol. Gen. Genet.* **1998**, 260, 480-486.

[49] Thamatrakoln, K.; Hildebrand, M. *J. Nanosci. Nanotechnol.* **2005**, 5, 158-166.

[50] Hildebrand, M. *Biomineralization. From biology to biotechnology and medical application*. Bäuerlein, E., Ed.; Wiley-VCH, Weinheim, Germany, **2000**.

[51] Martin-Jézéquel, V.; Hildebrand, M.; Brzezinski, M. A. *J. Phycol.* **2000**, 36, 821-840.

[52] Kröger, N.; Bergsdorf, C.; Sumper, *M. EMBO J.* **1994**, 13, 4676-4683.

[53] Kröger, N.; Bergsdorf, C.; Sumper, M. *Eur. J. Biochem.* **1996**, 239, 259-264.

[54] Kröger, N.; Lehmann, G.; Rachel, R.; Sumper, M. *Eur. J. Biochem.* **1997**, 250, 99-105.

[55] Kröger, N.; Wetherbee, R. *Protist* **2000**, 151, 263-273.

[56] Kröger, N.; Deutzmann, R.; Sumper, M. *Science* **1999**, 286, 1129-1132.

[57] Poulsen, N.; Sumper, M.; Kröger, N. *Proc. Natl. Acad. Sci. USA* **2003**, 100, 12075-12080.

[58] Sumper, M.; Kröger, N. *J. Mater. Chem.* **2004**, 14, 2059-2065.

[59] Wong Po Foo, C.; Huang, J.; Kaplan, D. L. *Trends Biotechnol.* **2004**, 22, 577-585.

[60] Armbrust, E. V.; Berges, J. A.; Bowler, C., *Science* **2004**, 306, 79-86.

[61] Poulsen, N.; Kröger, N. *J. Biol. Chem.* **2004**, 279, 42993-42999.

[62] Wenzl, S.; Deutzmann, R.; Hett, R.; Hochmuth, E.; Sumper, M. *Angew. Chem. Int. Ed.* **2004**, 43, 5933.

[63] Sumper, M. *Science* **2002**, 295, 2430-2433.

[64] Lutz, K.; Gröger, C.; Sumper, M.; Brunner, E. *Chem. Phys.* **2005**, 7, 2812–2815.

[65] Vrieling, E. G.; Beelen, T. P. M.; Van Santen, R. A.; Gieskes, W. W. C. *Angew. Chem. Int. Ed.* **2002**, 41, 1543-1546.

[66] Sun, Q.; Vrieling, E. G.; van Santen, R. A.; Sommerdijk, N. A. J. M. *Curr. Opin. Solid State Mat. Sci.* **2004**, 8, 111-120.

[67] Gill, I.; Ballesteros, A.; *Trends Biotechnol.* **2000**, 18, 282-296.

[68] Mayers, D. *Surfactant Science and Technology*; VCH Publishers, New York, **1988**.

[69] Tanford, C. *The hydrophobic effect*, Wiley, New York, **1980**.

[70] Ringsdorf, H.; Schlarb, B.; Venzmer, J. *Angew. Chem.* **1988**, 100, 117.

[71] Rosen, M. J. *Surfactants and Interfacial Phenomena*, Wiley-Interscience, New Jersey, **2004**.

[72] Stegemeyer, H.; Hiltrop, K.; Engels, T.; Von Rybinski, W.; Kratzat, K.; Müller-Goymann, C. C. *Lyotrope Flüssigkristalle*, Steinkopff, Darmstadt, **1999**.

[73] Schramm, L. L. *Surfactants: Fundamentals and Applications in the Petroleum Industry*, Cambridge University Press, Cambridge, **2000**.

[74] Shinoda, K.; Yamaguchi, N.; Carlsson, A. *J. Phys. Chem.* **1989**, 93, 7216-7218.

[75] Evans, D. F. *The Colloidal Domain: Where Physics, Chemistry, biology, and Technology Meet*, Wiley-VCH, New York, **1999**.

[76] Holmberg, K.; Joensson, B.; Kronberg, B.; Lindman, B. *Surfactants and polymers in aqueous solution*, John Wiley & Sons Ltd., **2002**.

[77] Raman, N.K.; Anderson, M. T. Brinker, C. J. *Chem. Mater.* **1996**, 8, 1682-1701.

[78] Raimondi, M.E.; Seddon, J. M. *Liquid Crystals* **1999**, 26, 305-339.

[79] Mateos, I. G.; Velazquez, M. M.; Rodriguez, L. *Langmuir* **1990**, 6, 1078.

[80] Alheim, M. *Dissertation* **1989**, Universität Hannover.

[81] Zimmerman, S. B.; Murphy, L. D. *Anal. Biochem.* **1996**, 234, 190-193.

[82] Stefansson, M. *Anal. Chem.* **2003**, 75, 281-287.

[83] Wittgren, B.; Stefansson, M.; Porsch, B. *Journal of Chromatography, A* **2005**, 1082, 166-175.

[84] Carlsson, A.; Karlstroem, G.; Lindman, B. *J. Phys. Chem.* **1989**, 93, 3673-3677.

[85] Hammarstroem, A.; Sundeloef, L. O. *Colloid Polym. Sci.* **1993**, 271, 1129-1133.

[86] Nilsson, S.; Thuresson, K.; Lindman, B.; Nystroem, B. *Macromolecules* **2000**, 33, 9641-9649.

[87] Witte, F. M.; Buwalda, P. L.; Engberts, J. B. F. N. *Colloid & Polymer Science* **1987**, 265, 42-44.

[88] Shirahama, K.; Tohdo, M.; Murahashi, M. *J. Colloid Interface Sci.* **1982**, 86, 282-283.

[89] Gradzielski, M.; Langevin, D.; Farago, B.; *Phys. Rev. E* **1996**, 53, 3900.

[90] Glatter, O.; Kratky, O. *Small Angle X-Ray Scattering*, Academic Press, London, **1982**.

[91] Burchard, W.; Richtering, W. *Progr. Coll. Polym. Sci.* **1989**, 80, 151.

[92] Burchard, W. *Adv. Polym. Sci.* **1999**, 143, 113.

[93] Ballauff, M.; Bolze, J.; Dingenouts, N.; Hickl, P.; Pötschke, D., *Makromol. Chem.* **1996**, 197, 3043.

[94] Dingenouts, N.; Ballauff, M., *Macromolecules* **1998**, 31, 7423.

[95] Dingenouts, N.; Bolze, J.; Pötschke, D.; Ballauff, M., *Adv. Polym. Sci.* **1999**, 144, 1.

[96] Hickl, P.; Ballauff; M.; Jada, A., *Macromolecules* **1996**, 29, 4006.

[97] Hickl, P.; Ballauff, M., *Makromol. Chem. Macromol. Symp.* **1997**, 118, 683.

[98] Kholodenko, A.; Ballauff, M.; Granados, M., *Phys. A* **1998**, 260, 267.

[99] Dingenouts, N.; Ballauff, M., *Acta Polym.* **1998**, 49, 178.

[100] Bolze, J.; Peng, B.; Dingenouts, N.; Panine, P.; Narayanan, T.; Ballauff, M.; *Langmuir* **2002**, 18,8364.

[101] Bolze, J.; Pontoni, D.; Ballauff, M.;Narayanan, T.; Cölfen, H., J. *Coll. and Inter. Sci.* **2004**, 277, 84.

[102] Israelachvili, J. N. *Intermolecular and Surface Forces*, Academic Press, New York, **1985**.

[103] Hoeger, S., *Chem. Eur. J.* **2004**, 120, 1320.

[104] Szwarc, M. *Nature* **1956**, 178, 1168.

[105] Matyjaszewski, K.; Davis, T. P. *Handbook of Radical Polymerization*, Wiley Interscience, Hoboken, Canada, **2002**.

[106] Higashimura, T.; Sawamoto, M. *Adv. Polym. Sci.* **1984**, 62, 49.

[107] Otsu, T.; Yoshida, M. *Makromol. Chem., Rapid Commun.* **1982**, 3, 127-132.

[108] Penczek, S.; Kubisa, P.; Matyjaszewski, K. *Cationic ring-opening polymerization of heterocyclic monomers. I., Mechanisms,* Springer Verlag, Berlin/New York, **1980**.

[109] Kobayashi, S. *Prog. Polym. Sci.* **1990**, 15, 751-823.

[110] Kröger, N.; Deutzmann, R.; Bergsdorf, C.; Sumper, M. *Proc. Natl. Acad. Sci.* **2000**, 97, 14133-14138.

[111] Sumper, M. *Angew. Chem.* **2004**, 116, 2301-2304.

[112] Sumper, M.; Lorenz, S.; Brunner, E.; *Angew. Chem.* **2003**, 115, 5350-5353.

[113] Kobayashi, S:, Saegusa, T. *Cyclic 1,3-Oxaza Compounds*, Elsevier Applied Science Publishers, London/New York, **1984**.

[114] Tomalia, D. A.; Sheetz, D. P.; J. *Polym. Sci. Part A* **1966**, 4, 2253-2265.

[115] Saegusa, T.; Kobayashi, S.; Yamada, A. *Macromolecules* **1975**, 8, 390-396.

[116] Kobayashi, S.; Saegusa, T. *Macromol. Chem. Suppl.* **1985**, 12, 11-24.

[117] Volet, G.; Chanthavong, V.; Wintgens, V.; Amiel, C. *Macromolecules* **2005**, 38, 5190-5197.

[118] Saegusa, T.; Yamada, A.; Taoda, H.; Kobayashi, S. *Macromolecules* **1978**, *11,* 435-436.

[119] Tanaka, R.; Koike, M.; Tsutsui, T.; Tanaka, T. *J. Polym. Sci.: Polymer Letters Ed.* **1978**, 16, 13-19.

[120] Saegusa, T.; Nagura, Y.; Kobayashi, S. *Macromolecules* **1973**, 6, 495-498.

[121] Aoi, K.; Miyamoto, M.; Chujo, Y.; Saegusa, T. *Macromol. Symp.* **2002**, 183, 53-64.

[122] Dworak, A. *Macromol. Chem. Phys.* **1998**, 199, 1843-1849.

[123] Saegusa, T.; Kobayashi, S.; Nagura, Y. *Macromolecules* **1974**, 7, 713-716.

[124] R. Hoogenboom, M. W. M. Fijten, C. Brändli, J. Schroer, U. S. Schubert, *Macromol. Rapid Commun.* **24** (2003), 98–103.

[125] Cornelius, F. *Dissertation* **2009**, TU Braunschweig.

[126] Rempp, P. F.; Lutz, P. J. *Comprehensive Polymer Science*, Allen, G.; Bevington, J. G. Ed.; Pergamon Press, Oxford, **1989**.

[127] Pitsilakis, M.; Pispas, S.; Mays, J. W.; Hadjichristidis, N. *Adv. Polym. Sci.* **1998**, 135, 1.

[128] Hadjichristidis, N.; Pitsilakis, M.; Pispas, S.; Iatrou, H. *Chem. Rev.* **2001**, 101, 3747-3792.

[129] Kobayashi, S.; Igarashi, T.; Moriuchi, Y.; Saegusa, T. Macromolecules **1986**,19, 535-541.

[130] Kobayashi, S.; Uyama, H.; Higuchi, N.; Saegusa, T. *Macromolecules* **1990**, 23, 54-59.

[131] Kobayashi, S.; Iijima, S.; Igarashi, T.; Saegusa, T. *Macromolecules* **1987**, 20, 8.

[132] Saegusa, T.; Ikeda, H.; Fujii, H. *Macromolecules* **1972**, 5, 108.

[133] Becker, H. G. O.; Berger, W.; Domschke, G.; *Organikum*, Wiley-VCH, Weinheim, **2001**.

[134] Tanaka, R.; Ueoka, I.; Takaki, Y.; Kataoka, K.; Saito, S. *Macromolecules* **1983**, 16, 849-853.

[135] Ito, Y.; Inubushi, Y.; Zenbayashi, M.; Tomita, S.; Saegusa, T. *J. Am. Chem. Soc.* **1973**, 95, 4447-4448.

[136] Lee, J.; Lee, K.; Kim, H. *Bull. Korean Chem. Soc.* **1996,** 17, 115-116.

[137] Aathimanikandan, S. V.; Savariar, E. N.; Thayumanavan, S. *J. Am. Chem. Soc.* **2005**, 127, 14922-14929.

[138] Nguyen-Misra, M.; Mattice, W. L. *Macromolecules* **1995**, 28, 1444.

[139] Klepinger, R.; Mischenko, N.; Reynaers, H. L.; Koch, M. H. J. *J. Polym. Sci. Polym. Chem. Ed.* **1999**, 37, 1833.

[140] Brandrup, J.; Immergut, E. H. *Polymer Handbook*, John Wiley & Sons, New York/Chichester/Brisbane/Toronto/Singapore, **1989**.

[141] Göltner, C, G.; Henke, S.; Weissenberger, M. C.; Antonietti, M. *Angew. Chem. Int. Ed.* **1998**, 37, 5.

[142] Nuyken, O.; Maier, G.; Groß, A. *Macromol. Chem. Phys.* **1996**, 191, 83-95.

[143] Tuzar, Z.; Kratochvil, P. *Surface and Colloid Science*, Matijevic, E. Ed.; Plenum Press, New York, **1993**.

[144] Won, Y. Y.; Davis, H. T.; Bates, F. S. *Science* **1999**, 283, 960.

[145] Maskos, M.; Harris, J. R. *Macromol. Rapid Commun.* **2001**, 22, 271.

[146] Kwon, G. S.; Suwa, S.; Yokoyama, M.; Okano, T.; Sakurai, Y.; Kataoka, K. *J. Contr. Rel.* **1994**, 29, 17.

[147] Gao, Z.; Varshney, S. K.; Wong, S.; Eisenberg, A. *Macromolecules* **1994**, 27, 7923.

[148] Yu, K.; Eisenberg, A. *Macromolecules* **1996**, 29, 6359.

[149] Calderara, F.; Hruska, Z.; Hurtrez, G.; Lerch, J.; Nugay, T.; Riess, G. *Macromolecules* **1994**, 27, 1210.

[150] Xu, R.; Winnik, M. A.; Riess, G.; Chu, B.; Croucher, M. D. *Macromolecules* **1992**, 25, 644.

[151] Kataoka, K.; Kwon, G. S.; Yokoyama, M.; Okano, T.; Sakurai, Y. *J. Controlled Release* **1993**, 24, 119.

[152] Bokias, G.; Hourdet, D.; Iliopoulos, I. *Macromolecules* **2000,** 33, 2929-2935.

[153] Jimenez-Regalado, E.; Selb, J.; Candau, F. *Langmuir* **2000**, 16, 8611-8621.

[154] Führman, H.; Grassert, I.; Holzhüter, G.; Grüttner, C.; Oehme, G. *New J. Chem.* **2002,** 26, 1675–1681.

[155] Aoi, A.; Takasu, A.; Okada, M.; Imae, T. *Macromol. Chem. Phys.* **1999**, 200**,** 1112–1120.

[156] Aoi, A.; Motoda, A.; Okada, M.; Imae, T. *Macromol. Rapid Commun.* **1997**, 18, 945-952.

[157] Alexandridis, P.; Holzwarth, J.; Hatton, T. *Macromolecules* **1994**, 27, 2414.

[158] Du, J. Z.; Chen, D. P.; Wang, Y. C.; Xiao, C. S.; Lu, Y. J.; Wang, J.; Zhang, G. Z. *Biomacromolecules* **2006,** 7, 1898-1903.

[159] Nakahara, Y.; Kida, T.; Nakatsuji, Y.; Akashi, M. *Langmuir* **2005**, 21, 6688-6695.

[160] Kwon, G.; Naito, M.; Yokoyama, M.; Okano, T.; Sakurai, Y.; Kataokatfs, K. *Langmuir* **1993**, 9, 945-949.

[161] Dai, Z.; Piao, L.; Zhang, X.; Deng, M.; Chen, X.; Jing, X. *Colloid Polym. Sci.* **2004**, 282, 343–350.

[162] A. Cifuentes, A.; Bernal, J. L.; Diez-Masa, J. C. *Anal. Chem.* **1997**, 69, 4271-4274.

[163] Hu, X.; Liu, S.; Chen, X.; Mo, G.; Xie, Z.; Jing, X. *Biomacromolecules* **2008,** 9, 553–560.

[164] Allcock, H. R.; Powell, E. S.; Chang, Y. *Macromolecules* **2004,** 37, 7163-7167.

[165] Kickelbick, G.; Bauer, J.; Hüsing, N.; Andersson, M.; Palmqvist, A. *Langmuir* **2003,** 19, 3198-3201.

[166] Obeid, R.; Maltseva, E.; Thünemann, A. F.; Tanaka, F.; Winnik, F. M. *Macromolecules* **2009**, 42, 2204-2214.

[167] Miguel, M.; Burrows, H. D.; Formosinho, S. J.; Lindman, B. *J. Mol. Struct.* **2001**, 563, 89-98.

[168] Jones, G.; Bullet, V. *Org. letters* **2001**, 3 (16), 2457-2460.

[169] Dong, Y.; Jin, Y.; Wie, D.Q. *J. of Appl. Polym. Sci.* **2006**, 100, 2956–2962.

[170] Lair, V.; Bouguerra, S.; Turmine, M.; Letellier, P. *Langmuir* **2004,** 20, 8490-8495.

[171] Griffiths, P. C.; Paul, A.; Stilbs, P.; Petterson, E. *Macromolecules* **2005,** 38, 3539-3542.

[172] Santos, N. C.; Castanho, M. A. R. B. *Biophysical. J.* **1996**, 71, 1641-1646.

[173] Zhou, Z.; Teraoka, I.; Langley, K.; Karasdst, F. E. *Macromolecules* **1994**, 27, 1759-1765.

[174] Karatzas, A.; Talelli, M.; Vasilakopoulos, T.; Pitsikalis, M.; Hadjichristidis, N. *Macromolecules* **2006**, 39, 8456-8466.

[175] Iijima, M.; Nagasaki, Y.; Okada, T.; Kato, M.; Kataoka, K. *Macromolecules* **1999,** 32, 1140-1146.

[176] Kondo, S.; Mori, H.; Sasai, Y.; Kuyuza, M. *Chem. Pharm. Bull.* **2007,** 55, 389-392.

[177] De Souza Lima, M. M.; Wong, J. T.; Paillet, M.; Borsali, R.; Pecora, R. *Langmuir* **2003,** 19, 24-29.

[178] Ishizu, K.; Mori, A. *Polym. Int.* **2001**, 51, 50-54.

[179] Müller, A.; Burchard, W. *Colloid Polym. Sci.* **1995**, 273, 866-875.

[180] Nyström, B.; Walderhaug, H.; Hansen, F. K. *J. Phys. Chem.* **1993**, 97, 7743-7752.

[181] Förster, S.; Burger, C. *Macromolecules* **1998**, 31, 879.

[182] Förster, S.; Timman, A.; Konrad, M.; Schellbach, C.; Meyer, A.; Funari, S. S.; Mulvaney, P.; Knott, R. *J. Phys. Chem. B* **2005**, 109, 1347.

[183] Ahn, S.; Frisch, H. L. *J. Statis. Phys.* **1974**, 11, 283-289.

[184] Ashcroft, N. W.; Lekner, J. *Phys. Rev.* **1966**, 145, 83-90.

[185] Castelletto, V.; Hamley, I. W.; Yuan, X. F.; Kelarakisc, A.; Booth, C. *Soft Matter* **2005**, 1, 138–145.

[186] Bryant, G.; Williams, S. R.; Qian, L.; Snook, I. Q.; Perez, E.; Pincet, F. *Phys. Rev.* **2002**, 66, 1-4.

[187] Kinning, D.; Thomas, E. *Macromolecules* **1984,** 17, 1712-1718.

[188] Bansil, R.; Nie, H.; Konak, C.; Helmstedt, M.; Lal, J. *J. Polym. Sci. B* **2002**, 40, 2807–2816.

[189] Wang, X.; Dormidontova, E. E.;, Lodge, T. P. *Macromolecules* **2002**, 35, 9687-9697.

[190] Volet, G.; Auvray, L.; Amiel, C. *J. Phys. Chem. B* **2009**, 113, 13537.

[191] Bryant, G.; Williams, S. R.; Qian, L.; Snook, I. K.; Perez, E.; Pincet, F. *Phys. Rev.* **2002**, 66, 60501-60504.

[192] Usyarov, O. G. *Coll. J.* **2007**, 69, 111-116.

[193] Rebolj, N.; Kristl, J.; Kalyuzhnyi, Y. V.; Vlachy, V. *Langmuir* **1997,** 13, 3646-3651.

[194] Amos, D. A.; Markels, J. H.; Lynn, S.; Radke, C. J. *J. Phys. Chem. B* **1998,** 102, 2739-2753.

[195] Rakitin, A.; Pack, G. R.; *J. Phys. Chem. B* **2004,** 108, 2712-2716.

[196] Quirion, F.; Drifford, M. *Langmuir* **1990**, 6, 786-791.

[197] Kelarakis, A.; Crassous, J. J.; Ballauff, M. *Langmuir* **2006,** 22, 6814-6817.

[198] Humpolikova, J.; Panek, M. S.; Prochazka, K.; Hof, M. *J. Phys. Chem. A* **2005,** 109, 10803-10812.

[199] Phillies, G. D. J.; Hunt, R. H.; Strang, K.; Sushkin, N. *Langmuir* **1996**,11, 3408-3416.

[200] Zeng, X.; Liu, Y.; Clerc, M. I. *J. Phys. Chem. B* **2007,** 111, 5174-5179.

[201] Bagchi, B. *Chem. Rev.* **2005**, 105, 3197-3217.

[202] Cochin, D.; Candau, F.; Zana, R.; Talmon, Y. *Macromolecules* **1992**, 25, 4220.

[203] Benjelloun, A.; Brembilla, A.; Lochon, P.; Adrian, M.; Ghanbaja, J. *Langmuir* **1997**, 13, 5770.

[204] Vinson, P. K.; Bellare, J. R.; Davis, H. T.; Miller, W. G.; Scriven, L. E. *J. Colloid Interface Sci.* **1991**, 142, 74-91.

[205] Almgren, M.; Edwards, K.; Gustafsson, J. *Curr. Opin. Colloid Interface Sci.* **1996**, 1, 270-278.

[206] Discher, B. M.; Won, Y. Y.; Ege, D. S.; Lee, J. C. M.; Bates, F. S.; Discher, D. E.; Hammer, D. A. *Science* **1999**, 284, 1143.

[207] Won, Y. Y.; Davis, H. T.; Bates, F. S. *Science* **1999**, 283, 960.

[208] Petersen, H.; Fechner, P.M.; Fischer, D.; Kissel, T. *Macromolecules* **2002**, 35, 6867.

[209] Kobayashi, S.; Kaku, M.; Saegusa, T. *Macromolecules* **1988,** 10, 1921.

[210] Takahashi, T. ; Kimura, T.; Sakurai, K. *Polymer* **1999,** 40, 5939.

[211] Thünemann, A.F. *Langmuir* **2000**, 16, 824.

[212] Kuo, P.L.; Chen, C.C.; Jao, M.W. *J. Phys. Chem. B* **2005,** 109, 9445.

[213] Zhong, Z.; Feijen, J. *Biomacromolecules* **2005,** 6, 3440.

[214] Jin, R.H.; Yuan, J.J. *J. Mater. Chem.* **2005**, 15, 4513.

[215] Xia, X.; Hu, Z.; Gao, J.; Qin, D.; Durst, H.D.; Yin, R. *Langmuir* **2002,** 18, 8302.

[216] Shi, H.; Zhao, Y.; Zhang, X.; Jiang, S.; Wang, D.; Han, C.C.; Xu, D. *Macromolecules* **2004,** 37, 9933.

[217] Wang, W.; Qu, X.; Gray, A.I.; Tetley, L.; Uchegbu, I.F. *Macromolecules* **2004,** 37, 9114.

[218] Shkilnyy, A.; Friedrich, A.; Tiersch, B.; Schöne, S.; Fechner, M.; Koetz, J.; Schläpfer, C.W.; Taubert, A. *Langmuir* **2008**, 24, 2102.

[219] Sedlák, M.; Cölfen, H. *Macromol. Chem. Phys.* **2001,** 4, 202.

[220] Knecht, M.R.; Sewell, S.L.; Wright, D.W. *Langmuir* **2005,** 21, 2058.

[221] Knecht, M.R.; Wright, D.W. *Langmuir* **2004,** 20, 4728.

[222] Yuan, J. J.; Jin, R. H. *Langmuir* **2005,** 21, 3136-3145.

[223] Manzur, M.; Spelzini, D.; Farruggia, B.; Romanini, D.; Pico, G. *J. Chrom. B* **2007**, 860, 63-68.

[224] Patrickios, C.; Sharma, L. R.; Armes, S.; Billingham, N. C. *Langmuir* **1999**, 15, 1613.

[225] Wang, W.; Lu, W.; Jiang, L. *J. Phys. Chem. B* **2008,** 112, 1409-1413.

[226] Kabanov, V. A.; Zezin, A. B.; Rogacheva, V. B.; Gulyaeva, Z. G.; Zansochova, M. F.; Joosten, J. G. H.; Brackman, J. *Macromolecules* **1999,** 32, 1904-1909.

[227] Meszaros, R.; Thompson, L.; Bos, M.; Groot, P. *Langmuir* **2002,** 18, 6164-6169.

[228] Borkovec, M.; Koper, G. J. M. *Macromolecules* **1997**, 30, 2151.

[229] Koper, G. J. M.; Van Duijvenbode, R. C.; Stam, D. D. P. V.; Steuerle, U.; Borkovec, M. *Macromolecules* **2003**, 36, 2500.

[230] Kobayashi, S.; Hiroishi, K.; Tokunoh, M.; Saegusa, T. *Macromolecules* **1987**, 20, 1496.

[231] Chen, C.; Hsu, C.; Kuo, P. *Langmuir* **2007**, 23, 6801.

[232] Chatani, Y.; Kobatake, T.; Tadokoro, H. *Macromolecules* **1983**, 16, 199.

[233] Chatani, Y.; Kobatake, T.; Tadokoro, H.; Tanaka, R. *Macromolecules* **1982**, 15, 170.

[234] Chatani, Y.; Tadokoro, H.; Saegusa, T.; Ikeda, H. *Macromolecules* **1981**, 14, 315.

[235] Hashida, T.; Tashiro, K.; Aoshima, K.; Inaki, Y. *Macromolecules* **2002**, 35, 4330.

[236] Hashida, T.; Tashiro, K. *Polymer* **2007**, 48, 7614.

[237] Scaccia, S. *Talanta* **2005**, 67, 678.

[238] Hashida, T.; Tashiro, K.; Inaki, Y. *J. Polym. Sci., Part B* **2003**, 41, 2937.

[239] Hashida, T.; Tashiro, K. *Macromol. Symp.* **2006**, 242, 262.

[240] Liu, G.; Reinhout, M.; Mainguy, B.; Baker, G. L. *Macromolecules* **2006**, 39, 4726.

[241] Chen, Y.; Baker, G. L. *J. Org. Chem.* **1999**, 64, 6870.

[242] Takeuchi, Y.; Uyama, H.; Tomoshige, N.; Watanabe, E.; Tachibana, Y.; Kobayashi, S. *J. Polym. Sci., Part A* **2006**, 44, 671.

[243] Wang, Q.; Li, L.; Jiang, S. *Langmuir* **2005**, 21, 9068.

[244] Lee, S. C.; Cho, Y. W.; Park, K. *J. Bioact. Compat. Polym.* **2005**, 20, 5.

[245] Li, F.; Li, S.; El Ghzaoui, A.; Nouailhas, H.; Zhuo, R. *Langmuir* **2007**, 23, 2778.

[246] Das, D.; Dasgupta, A.; Roy, S.; Mitra, R. N.; Debnath, S.; Das, P. K. *Chem.;Eur. J.* **2006**, 12, 5068.

[247] Jin, R. H.; Yuan, J. J. *Macromol. Chem. Phys.* **2005**, 206, 2160.

[248] Casillas, N.; Puig, J. E.; Olayo, R.; Hart, T. J.; Frames, E. I. *Langmuir* **1989**, 5, 384.

[249] Kim, S. J.; Shin, S. R.; Lee, Y. M.; Kim, S. Y. *J. Appl. Polym. Sci.* **2003**, 87, 2011.

[250] Bouwstra, J. A.; Salomons-de Vries, M. A.; van Miltenburg, J. C. *Thermochim. Acta* **1995**, 248, 319.

[251] Ahmad, M. B.; Huglin, M. B. *Polym. Int.* **1994**, 33, 273.

[252] Salmeron Sanchez, M.; Monleon Pradas, M.; Gomez Ribelles, J. L. *J. Non- Cryst. Solids* **2002**, 307-310, 750.

[253] Wang, T.; Gunasekaran, S. *J. Appl. Polym. Sci.* **2006**, 101, 3227.

[254] Lopez-Rubio, A.; Flanagan, B. M.; Gilbert, E. P.; Gidley, M. J. *Biopolymers* **2008**, 89, 761-768.

[255] Brott, L. L.; Naik, R. R.; Pikas, D. J.; Kirkpatrick, S. M.; Tomlin, D. W.; Whitlock, P. W.; Clarson, S. J.; Stone, M. O. *Nature* **2001**, 413, 291.

[256] Sundar, V. C.; Yablon, A. D.; Grazul, J. L.; Ilan, M.; Aizenberg, J. *Nature* **2003**, 424, 899.

[257] Sumper, M.; Lorenz, S.; Brunner, E. *Angew. Chem., Int. Ed.* **2003**, 42, 5192.

[258] Knecht, M. R.; Wright, D. W. *Chem. Commun.* **2003**, 3038.

[259] Patwardhan, S. V.; Mukherjee, N.; Clarson, S. J. J. *Inorg. Organomet. Polym.* **2001**, 11, 193.

[260] Brunner, E.; Lutz, K.; Sumper, M. *Phys. Chem. Chem. Phys.* **2004**, 6, 854.

[261] Patwardhan, S. V.; Clarson, S. J. *Mater. Sci. Eng.* **2003**, 23, 495.

[262] Patwardhan, S. V.; Clarson, S. J. *Silicon Chem.* **2002**, 1, 207.

[263] Patwardhan, S. V.; Clarson, S. J. *Polym. Bull.* **2002,** 48, 367-371.

[264] Patwardhan, S. V.; Mukherjee, N.; Clarson, S. J. *Silicon Chem.* **2002,** 1, 47-55.

[265] Jahns, M. *Dissertation* **2007**, Universität Hannover.

[266] Menzel, H.; Horstmann, S.; Behrens, P.; Bärnreuther, P.; Krueger, I.; Jahns, M. *Chem. Comm.* **2003**, 2994.

[267] Welle, F. M.; Beckhaus, H. D.; Rüchardt C. *J. Org. Chem.* **1997,** 62, 552-558.

[268] Ziao, N. ; Laurence, C.; Le Questel, J. Y. *Cryst. Eng. Comm.* **2002**, 4, 326-335.

[269] Patwardhan, S. V.; Clarson, S. J. *J. of Inor. and Org. Polym.* **2002**, 12, 109-116.

[270] Belton, D. J.; Patwardhan, S. V.; Perry, C. C. *J. Mater. Chem.* **2005**, 15, 4629-4638.

[271] Sumper, M.; Brunner, E. *Adv. Funct. Mater.* **2006**, 16, 17–26.

[272] Adamson, D. H.; Dabbs, D. M.; Pacheco, C. R.; Giotto, M. V.; Morse, D. E.; Aksay, I. A. *Macromolecules* **2007,** 40, 5710-5717.

[273] Brinker, A. *J. Non-cryst. Solids* **1988**, 100, 31-50.

[274] Chen, D.; Li, Z.; Yu, C.; Shi, Y.; Zhang, Z.; Tu, B.; Zhao, D. *Chem. Mater.* **2005,** 17, 3228-3234.

[275] Jin, R. H.; Yuan, J. J. J. *Mater. Chem.* **2005**, 15, 4513-4517.

[276] Antonietti, M.; Berton, B.; Göltner, C.; Hentze, H. P. *Adv. Mater.* **1998**, 10, 154-159.

[277] Huh, S.; Wiench, J. W.; Yoo, J. C.; Pruski, M.; Lin, V. S. Y. *Chem. Mater.* **2003,** 15, 4247-4256.

[278] Qui, L. *J. of Mat. Sci. Lett.* **2001**, 20, 2153-2156.

[279] Tjandra, W.; Yao, J.; Tam, K. C. *Langmuir* **2006,** 22, 1493-1499.

[280] Horsky, J.; Walterova, Z. *Coll. Polym. Sci.* **2005**, 283, 1033-1040.

[281] Kongkaew, A.; Wootthikanokkhan, *J. Polym. Bull.* **1999**, 43, 327-332.

[282] Kobatake, S.; Harwood, H. J.; Quirk, R. P. *Macromolecules* **1997,** 30, 4238-4242.

[283] Akiyama, Y.; Harada, A.; Nagasaki, Y.; Kataoka, K. *Macromolecules* **2000,** 33, 5841-5845.

[284] Petersen, H.; Fechner, P. M.; Fischer, D.; Kissel, T. *Macromolecules* **2002,** 35, 6867-6874.

[285] Perrin, D. D.; Armarego, W. L. F. *Purification of laboratory chemicals*, Pergamon Press, Oxford, **1988**.

[286] Rauscher, K.; Voigt, J.; Wilke, I. *Chemische Tabellen und Rechentafeln für die analytische Praxis*, Verlag Harri, Thun/Frankfurt, **2000**.

[287] Schmitz, K. S. *An Introduction to Dynamic Scattering by Macromolecules*, Academic Press, New York, **1990**.

[288] Sasanuma, Y.; Teramae, F.; Yamashita, F.; Hamano, Y.; Hattori, S. *Macromolecules* **2005,** 38, 3519-3532.

Lebenslauf

Persönliche Daten

Name:	Salvador Navarro Navarro
Geburtsdatum und -ort:	28.08.1981 Lorca (Spanien)
Staatsangehörigkeit:	Spanisch
Familienstand:	Ledig

Schulbildung, Studium und Promotion

09.1985 − 06.1995	Alfonso X El Sabio Schule in Lorca (Spanien)
10.1995 − 06.1999	Jose Ibañez Martin Gymnasium in Lorca (Spanien) Abschluß: Selectividad (äquivalent Abitur)
10.1999 − 06.2004	Universidad de Murcia (Spanien), Chemische Verfahrenstechnik
10.2004 − 06.2005	TU Kaiserslautern Erasmus-Sokrates Stipendium, Technische Chemie (Prof. Dr. Stefan Ernst) Masterarbeit, Thema: *Synthese, Charakterisierung und katalytische Eigenschaften von Gold Nanoclustern in Zeolithen*
seit 08.2005	TU Braunschweig Makromolekulare Chemie (Prof. Dr. Henning Menzel), Doktorarbeit im Rahmen des Promotionsprogramms „Neue Materialen mit maßgeschneiderten Eigenschaften“ des ZFM Hannover, Thema: *Amphiphile Polyamine*: *Synthese, Selbstorganisation und Einfluß bei der Mineralisierung von Kieselsäure*

Publikationen

Navarro, S., Shkilnyy, A., Tiersch B., Taubert A., Menzel H., Preparation, characterization and thermal gelation of amphiphilic alkyl-poly(ethyleneimine). Langmuir 25 (18):10558-10566 (2009).

Tagungsbeiträge

Navarro. S., Menzel, H.: From biomineralization to tailored synthesis: nitrogen-containing polymers for the production of porous silica. (Poster) 3. Berichtskolloquium des Schwerpunktprogramms 1117 der Deutschen Forschungs-Gemeinschaft „Prinzipien der Biomineralisation“, Bad Honnef (2006).

Navarro, S., Menzel, H.: Polyamine-based amphiphilic polymers as template for the production of porous silica. (Poster) 10th International conference of the European Ceramic Society, Berlin (2007).

Navarro, S., Cornelius, F., Menzel, H.: Biomimetic model polymers as template for the synthesis of nanostructured silica. (Poster) European Congress on Advanced Materials and Processes, Nürnberg (2007).

Navarro, S., Menzel, H.: Biomimetic model polymers as template for the synthesis of nanostructured silica. (Vortrag) 4. Jungchemikertag des Jungchemikerforum der TU Braunschweig, Braunschweig (2007).